UNIVERSIDAD COMPLUTENSE DE MADRID
FACULTAD DE CIENCIAS FÍSICAS
Departamento de Óptica

TESIS DOCTORAL

Estructura de la polarización en estados cuánticos

Polarization structure of quantum fields

MEMORIA PARA OPTAR AL GRADO DE DOCTOR

PRESENTADA POR

Pablo de la Hoz Iglesias

Director

Luis Lorenzo Sánchez Soto

Madrid 2019

Estructura de la polarización en estados cuánticos

Polarization structure of quantum fields

Memoria presentada para optar al Grado de Doctor por

Pablo de la Hoz Iglesias

Director

Luis Lorenzo Sánchez Soto

Departamento de Optica

Facultad de Físicas

Universidad Complutense de Madrid

Junio de 2018

Publications included in the thesis

1.- L. L. Sánchez-Soto, A. B. Klimov, P. de la Hoz, G. Leuchs:
"Quantum versus classical polarization states: when multipoles count",
Journal of Physics B **46**, 104011 (2013)

2.- L. L. Sánchez-Soto, A. B. Klimov, P. de la Hoz, I. Rigas, J. Rehacek, Z. Hradil, G. Leuchs:
"Orbital angular momentum from marginals of quadrature distributions",
Physical Review A **88**, 053839 (2013)

3.- P. de la Hoz, A. B. Klimov, G. Björk, Y.-H. Kim, C. R. Müller, Ch. Marquardt, G. Leuchs, L. L. Sánchez-Soto:
"Multipolar hierarchy of efficient quantum polarization measures"
Physical Review A **88**, 063803 (2013)

4.- E. Karimi, R. W. Boyd, P. de la Hoz, H. de Guise, Z. Hradil, J. Rehacek, A. Aiello, G. Leuchs, L. L. Sánchez-Soto:
"Radial quantum number of Laguerre-Gauss modes",
Physical Review A **89**, 063813 (2014)

5.- G. Björk, H. de Guise, A.B. Klimov, P. de la Hoz, L.L. Sánchez-Soto:
"Classical distinguishability as an operational measure of polarization",
Physical Review A **90**, 013830

6.- P. de la Hoz, G. Björk, A. B. Klimov, G. Leuchs, L. L. Sánchez-Soto:
"Unpolarized states and hidden polarization",
Physical Review A **90**, 043826 (2014)

7.- Z. Hradil, J. Rehacek, P. de la Hoz, G. Leuchs, L. L. Sánchez-Soto:
"Extremal states for photon number and quadratures as gauges for nonclassicality",
Physical Review A **91**, 042128 (2015)

8.- P. de la Hoz, G. Björk, H. de Guise, A. B. Klimov, G. Leuchs, L. L. Sánchez-Soto:
"Classical polarization multipoles: paraxial versus nonparaxial",
Physica Scripta **90**, 074030 (2015)

9.- G. Björk, M. Grassl, P. de la Hoz, G. Leuchs, L. L. Sánchez-Soto:
"Stars of the quantum universe: extremal constellations on the Poincaré sphere",
Physica Scripta **90**, 108008 (2015)

10.- G. Björk, A. B. Klimov, M. Grassl, P. de la Hoz, G. Leuchs, L. L. Sánchez-Soto:
"Extremal quantum states and their Majorana constellations",
Physical Review A **92**, 031801(R) (2015)

11.- A. Aiello, G. S. Agarwal, M. Paur, B. Stoklasa, Z. Hradil, J. Rehacek, P. de la Hoz, G. Leuchs, L. L. Sánchez Soto:
"Unraveling beam self-healing",
Optics Express **25**, 19147 (2017)

12.- F. Bouchard, P. de la Hoz, G. Björk, R. W. Boyd, M. Grassl, Z. Hradil, E. Karimi, A. Klimov, G. Leuchs, J. Rehacek, L. L. Sánchez-Soto:
"Quantum metrology at the limit with extremal Majorana constellations",
Optica **4**, 1429 (2017)

13.- L. L. Sánchez-Soto, P. de la Hoz, G. Björk, A. B. Klimov, F. Bouchard, E. Karimi, G. Leuchs:
"On the polarization structure of quantum light fields",
Advances in Optics and Photonics [by invitation]

Resumen

Un buen número de experimentos recientes han demostrado que la luz presenta muchas que no se pueden explicar de acuerdo con la teoría clásica y deben tratarse en el contexto de la óptica cuántica. Este es el objetivo básico de la presente memoria.

En el artículo 1, abogamos por una simple expansión multipolar de la matriz de densidad de polarización. Los multipolos resultantes se utilizan para construir distribuciones de cuasiprobabilidad con buenas propiedades, que aparecen como una suma de momentos sucesivos de las variables de Stokes. El primer orden corresponde a la imagen clásica en la esfera de Poincaré. La cuasidistribución que más utilizaremos a lo largo de esta tesis es la función Q que aparece como la proyección en los estados que tienen la polarización más definida de acuerdo a la teoría cuántica. Al observar sus contribuciones multipolares, formulamos una jerarquía completa de medidas que evalúan adecuadamente las correlaciones de polarización de orden superior.

El artículo 2 está dedicado al análisis del momento angular orbital de un campo de radiación. Dicha variable se modeliza mediante la superposición de dos osciladores armónicos independientes a lo largo de dos ejes ortogonales. Derivamos, a través de un cambio de variables consistente, un imagen física completa del momento angular orbital.

En el artículo 3 profundizamos en la caracterización de las correlaciones de polarización de orden superior. Los multipolos resultantes aparecen como momentos sucesivos de las variables de Stokes y se pueden obtener a partir de mediciones realistas. Como resultado, obtenemos una jerarquía de grados de polarización que miden la información de polarización hasta un orden dado. Dichos grados se caracteriza por una distribución acumulativa que definimos en este artículo.

En el artículo 4 presentamos un operador vinculado con el índice radial en los modos Laguerre-Gauss de un oscilador armónico bidimensional en coordenadas cilíndricas. Esto sirve como base para analizar cómo conceptos básicos en óptica cuántica pueden redefinirse en términos de modos radiales.

En el artículo 5 se trata un grado de polarización que puede extenderse de forma natural a campos cuyos frentes de onda no son necesariamente planos. Esta medida aparece como una distancia desde un estado al conjunto de todos los estados obtenidos a partir de éste por una transformación de polarización, que pueden determinarse experimentalmente en una configuración interferométrica. Al final, se llega a una expresión del grado de polarización en términos de los valores propios de la matriz de coherencia.

En el artículo 6 empleamos la noción de expansión multipolar previamente desarrollada. Extendemos la noción de despolarización para incluir estados despolarizados a orden M. La existencia de la polarización oculta emerge de forma natural en este contexto.

En el artículo 7 consideramos que las cuadraturas rotadas contienen la información dependiente de la fase del campo electromagnético. Como resultado del análisis de este par no canónico, obtenemos una relación de incertidumbre exacta, así como un par de desigualdades más débiles. Esto nos permite construir medidas de rendimiento adaptadas para diagnosticar estados gato de Schrödinger, entre otros.

En el artículo 8 discutimos la polarización de los campos de luz clásicos paraxiales y no paraxiales recurriendo a una expansión multipolar de la matriz de polarización correspondiente. Resulta que solo un término dipolar contribuye cuando uno considera SU(2) (paraxial) o SU(3) (no paraxial) como simetrías fundamentales. Pero para la luz no paraxial, la expansión en SU(2) da lugar a una componente dipolar y otra cuadripolar, lo que explica la estructura más rica de este caso.

En el artículo 9 consideramos los estados extremos de la distribución acumulativa introducida en el artículo 3. Encontramos que los estados coherentes SU(2) son máximos para cualquier orden, por lo que son los más polarizados permitidos por la teoría cuántica. El caso inverso de estados puros que minimizan esa distribución, que pueden verse como los más cuánticos. Consideramos la peculiar representación de Majorana de estos estados.

En el artículo 10 profundizamos en la caracterización de estados mínimos de la distribución acumulativa para un rango diverso de la cantidad de fotones. Aprovechando la representación de Majorana, reformulamos el problema como distribuir uniformemente un determinado número de puntos sobre la superficie de la esfera de Poincaré. Presentamos los estados llamados "Reyes cuánticos".

El artículo 11 trata el fenómeno de la autoreconstrucción. Desciframos las matemáticas y la física que subyace al mecanismo de autoreconstrucción y proporcionamos una definición novedosa para la distancia mínima de reconstrucción más allá de la óptica geométrica. Además, proponemos cuantificar la capacidad de auto-reconstrucción de un haz a través de un grado recién creado de autoreconstrucción. Ilustramos este proceso adaptando una innovadora técnica experimental basada en la reconstrucción del frente de onda Shack-Hartmann.

En el documento 12 mostramos que los estados que introducimos, los "Reyes cuánticos" tienen aplicaciones muy importantes en metrología. La estimación de una rotación constituye un ejemplo notable del aumento en la precisión de la medición permitida por la teoría cuántica. Nuestros estados son especialmente pertinentes para esta tarea cuando se desconoce el eje de rotación, ya que tienen una sensibilidad independiente de ese eje y alcanzan el límite de Heisenberg. Aquí, damos cuenta de la realización experimental de estos estados generando estados de momento angular orbital de dimensión hasta 21 generados en fotones individuales, y confirmamos sus altas capacidades metrológicas.

Abstract

As it has been recently demonstrated in a number of recent experiments, light has many properties that cannot be explained in any classical theory and should be treated in the realm of quantum optics. This is the inspiring thread of this Thesis.

In paper 1, we advocate a simple multipole expansion of the polarization density matrix. The resulting multipoles are used to construct bona fide quasiprobability distributions that appear as a sum of successive moments of the Stokes variables. The first order corresponds to the classical picture on the Poincaré sphere. The quasidistribution that we will use the most throughout this Thesis is the Q function. It appears as the projection on the states having the most definite polarization allowed by the quantum theory. Looking at its multipolar contributions, we formulate a whole hierarchy of measures that properly assess higher-order polarization correlations.

Paper 2 is devoted to the analysis of the orbital angular momentum of a light field. We model this variable as a superposition of two independent harmonic oscillators along two orthogonal axes. We derive, via a consistent change of variables, a comprehensive picture of the orbital angular momentum.

In paper 3, we delve into the characterization of higher-order polarization correlations. The resulting multipoles appear as successive moments of the Stokes variables and can be obtained from feasible measurements. As a result, we obtain a hierarchy of degrees of polarization that measure the polarization information up to a given order. Such degrees are characterized by a cumulative distribution we introduce in this paper.

In paper 4, we introduce an operator linked with the radial index in the Laguerre-Gauss modes of a two-dimensional harmonic oscillator in cylindrical coordinates. This serves as a basis for analyzing how basic quantum optical concepts can be recast in terms of radial modes.

In paper 5, we put forward an operational degree of polarization that can be extended in a natural way to fields whose wave fronts are not necessarily planar. This measure appears

as a distance from a state to the set of all of its polarization-transformed counterparts, which can be experimentally determined in an interferometric setup. At the end we come to an expression of the degree of polarization in terms of the eigenvalues of the coherence matrix.

In paper 6, we put to work the multipolar expansion previously developed. We extend the notion of unpolarization to include *M*th-order unpolarized states. The existence of hidden polarization emerges in a natural way in this context.

In paper 7, we consider that rotated quadratures carry the phase-dependent information of the electromagnetic field. As a result of the analysis of this noncanonical pair, we obtain an exact uncertainty relation, as well as a couple of weaker inequalities. This allows us to construct performance measures tailored to diagnose photon-added and Schrödinger-cat-like states, among others.

In paper 8, we discuss the polarization of paraxial and nonparaxial classical light fields by resorting to a multipole expansion of the corresponding polarization matrix. It turns out that only a dipolar term contributes when one considers SU(2) (paraxial) or SU(3) (nonparaxial) as fundamental symmetries. But for nonparaxial light the expansion in SU(2) gives place to both dipolar and quadrupolar components, which explains the richer structure of this instance.

In paper 9, we consider extremal states of the cumulative distribution introduced in paper 3. We find that SU(2) coherent states are maximal to any order, so they are the most polarized allowed by quantum theory. The converse case of pure states minimizing that distribution, which can be seen as the most quantum ones. We consider the peculiar Majorana representation of these states.

In paper 10, we delve into the characterization of the case of minimal states of the cumulative distribution which is investigated for a diverse range of the number of photons. Taking advantage of the Majorana representation, we recast the problem as that of distributing a number of points uniformly over the surface of the Poincaré sphere. We introduce the so called “Kings of quantumness”.

Paper 11 treats the phenomenon of self-healing. We unravel the mathematics and the physics underlying the self-reconstruction mechanism and we provide for a novel definition for the minimum reconstruction distance beyond geometric optics. Moreover, we propose to quantify the self-reconstruction ability of a beam via a newly established degree of self-healing. We illustrate this process by tailoring an innovative experimental technique based upon Shack-Hartmann wave front reconstruction.

In paper 12, we show that the states we introduced, the Kings of quantumness, have very important applications in metrology. The estimation of a rotation constitutes a remarkable example of the boost in the accuracy of measurement allowed by quantum theory. Our state are especially germane for this task when the rotation axis is unknown, as they have a sensitivity independent of that axis and they achieve a Heisenberg-limit scaling. Here, we report the experimental realization of these states by generating up to 21-dimensional orbital angular momentum states of single photons, and confirm their high metrological abilities.

Introducción

Índice

1. Campo de Estudio: La polarización de la luz

La polarización, el aspecto vectorial de la luz, es de suma importancia para una comprensión adecuada del mundo físico y sigue siendo objeto de mucha investigación fundamental hoy en día. Manipular la polarización es crucial para muchas aplicaciones, en muchos casos la polarización es una variable de medición, mientras que en en otros casos, la polarización es una fuente de ruido, cuyo control es decisivo. Éste tema es tan relevante que varias monografías [219, 66, 139, 68, 19, 124, 55, 75, 69, 109, 101, 191] y artículos de revisión [57, 103, 56, 58] están dedicados completamente a a su estudio; el lector interesado puede encontrar allí información extensa, que incluye estudios históricos de nuestra comprensión de la luz polarizada.

En el lado experimental, la polarización de la luz es una característica robusta que puede ser manipulada de manera eficiente utilizando equipos modestos sin introducir más que pérdidas marginales. Por lo tanto, no es sorprendente que esta sea a menudo la variable de elección para codificar la información cuántica, como puede comprobarse mirando a algunos experimentos recientes de vanguardia, incluyendo la distribución de la clave cuántica [184], codificación cuántica densa [178], teleportación cuántica [48], estados rotacionalmente invariantes [196], super-resolución de fase [199], y mediciones débiles [85]. Esto demanda de la existencia de una teoría completa de la polarización en óptica cuántica.

1.1. Desarrollo histórico

Lejos de su fuente, cualquier campo electromagnético que se propaga libremente puede considerarse en una buena aproximación como una onda plana, con su campo eléctrico situado en un plano perpendicular a la dirección de propagación. Esta simple observación es la raíz de la noción de polarización. El extremo del campo eléctrico de una onda describe en el tiempo una curva bien definida ; en general, una elipse.

La elipse de polarización es una simple descripción de la amplitud de la luz polarizada, pero no es directamente accesible a la medición. En 1852, Stokes [222] señaló que la polarización puede ser específicada por cuatro parámetros de intensidad [244, 179, 26] que pueden ser fácilmente medidos [34, 50, 208, 20]. Además, conducen de una manera natural a la esfera de Poincaré [192] en la que el estado de polarización se caracteriza por dos ángulos directamente relacionados con los parámetros de polarización de la elipse. Esto nos proporciona una elegante imagen geométrica en la que analizar el efecto de las transformaciones de polarización.

Estos argumentos se aplican solo a ondas planas ideales. En la práctica, sin embargo, los campos con los que se trabaja en óptica exhiben cierta aleatoriedad. La misma naturaleza caótica del proceso de emisión de la luz requiere entonces una descripción estadística. En realidad, las rápidas fluctuaciones temporales del campo no pueden ser seguidas por ningún detector y uno debe considerar en cambio las correlaciones del campo en diferentes puntos espacio-temporales. Desde este punto de vista, la polarización está cercanamente relacionada a la teoría de la coherencia [246, 198, 177]. En un retrato sencillo podemos considerar que una elipse bien definida representa la polarización total y que la polarización parcial surge por la sucesión rápida y aleatoria de diferentes elipses. En términos más cuantitativos, los parámetros de Stokes se vuelven variables aleatorias y uno debe hacer frente a una distribución de probabilidad en la esfera de Poincaré .

El hecho de que los parámetros de Stokes puedan traducirse inmediatamente al dominio cuántico se puso de manifiesto en el trabajo seminal de Fano [94], y discusiones acerca de los operadores de Stokes resultantes pueden ser encontradas en libros de texto antiguos (ver, por ejemplo, [131, 7]), incluyendo su relación con el espín del fotón [93]. En el nivel cuántico, ningún estado del campo puede tener valores definidos de los tres operadores de Stokes, puesto que estos no conmutan y cualquier medida precisa simultánea de estas cantidades no está permitida. En términos físicos, esto significa que no hay estado con una elipse de polarización bien definida, de la misma manera que uno no puede asignar una trayectoria definida a un partícula cuántica. Las inevitables fluctuaciones implican que los puntos en la esfera de Poincaré pierden su significado. Ésto establece una primera gran diferencia con la descripción clásica y está en el origen de muchas características no clásicas, la más tentadora de las cuales es quizás la compresión de la polarización [62, 151, 165, 170], que ha sido observada en numerosos experimentos [49, 116, 87, 217, 126].

Por otro lado, la polarización clásica a menudo se restringe a los valores promedio de los parámetros de Stokes. Ésto está justificado ya que en su mayoría la luz clásica tiene estadísticas de Gauss. Sin embargo, los estados no gaussianos son de máxima relevancia en óptica cuántica, por lo que los momentos de orden superior de los operadores de Stokes entran en juego.Ésto abre el mundo cuántico a propiedades de polarización que no se han abordado en el dominio clásico. El grado clásico de polarización no puede incluir estos nuevos fenómenos, por lo que debe ser generalizado para incluir estos efectos de polarización de orden superior.

2. Conceptos básicos

2.1. Luz polarizada en óptica clásica

En esta sección proporcionamos una breve descripción de los conceptos básicos de la teoría clásica de la polarización de la luz. El tema se trata en cualquier libro de texto [45] y en las más específicas monografías ya citadas [219, 66, 139, 68, 19, 124, 55, 75, 69, 109, 101, 191]. Ésto nos facilitará la comparación con la versión cuántica de estos mismos conceptos.

2.1.1. Elipse de polarización

Dado un punto en el espacio, el estado de polarización de un haz de luz que se propaga en una dirección fija, digamos z, está dada por la evolución temporal del campo eléctrico de la onda, que se encuentra en un plano perpendicular a la dirección de propagación. Consideramos ondas planas monocromáticas de frecuencia ω y vector de onda $\mathbf{k}$. Sea $\mathbf{E}(z,t)$ el campo eléctrico en un punto z, en el tiempo t, de la onda, las componentes del campo eléctrico són:

$$E_H(z,t) = E_{0H}\exp[-i(\omega t - kz + \delta_H)]\,, \qquad E_V(z,t) = E_{0V}\exp[-i(\omega t - kz + \delta_V)]\,, \tag{1}$$

dónde los subíndices H (horizontal) y V (vertical) se refieren a las dos componentes cartesianas perpendiculares a z. Los coeficientes E_{0H} y E_{0V} denotan las amplitudes reales de las componentes correspondientes y δ_H y δ_V sus fases. Tener en cuenta que los campos medibles vienen dados por la parte real de las expresiones complejas. También se debe señalar que la onda monocromática utilizada en las siguientes discusiones no se puede realizar estrictamente en el experimento; el formalismo, sin embargo, es válido también para campos cuasimonocromáticos en el enfoque paraxial, reemplazando k y ω por sus valores medios respectivos $\bar{k}$ y $\bar{\omega}$. Para obtener la curva que el extremo del vector del campo eléctrico describe en el tiempo, eliminamos el tiempo en la Eq. (1). Después de algunos cálculos simples, obtenemos:

$$\left(\frac{E_H}{E_{0H}}\right)^2 + \left(\frac{E_V}{E_{0V}}\right)^2 - 2\left(\frac{E_H}{E_{0H}}\right)\left(\frac{E_V}{E_{0V}}\right)\cos\delta = \sin^2\delta\,, \tag{2}$$

dónde $\delta = \delta_V - \delta_H$ es la fase relativa entre ambas oscilaciones. Ésta es precisamente la ecuación de la elipse, que degenera en una línea recta o un círculo para algunos valores particulares de la fase relativa. Aunque hemos eliminado la variable temporal , las componentes de los campos E_H y E_V continuan siendo dependientes del espacio-tiempo, pero para la radiación monocromática las amplitudes y las fases son constantes en el tiempo. Esto significa que la elipse de polarización permanece fija mientras el haz polarizado se propaga.

En general, (2) describe una elipse rotada, con los semi-ejes a y b ($a \geqslant b$). El ángulo del semi-eje mayor, medido en sentido antihorario desde el eje horizontal positivo, es el ángulo de orientación ψ ($0 \leqslant \psi \leqslant \pi$). El grado en que la elipse es oval se describe por un parámetro de forma llamado elipticidad χ ($-\pi/4 < \chi \leqslant \pi/4$), definido como $\tan\chi = \mp b/a$, el signo distingue los dos sentidos en los que la elipse puede ser descrita. Estos ángulos dependen de la amplitud y la fase relativa:

$$\tan(2\psi) = \frac{2E_{0H}E_{0V}}{E_{0H}^2 - E_{0V}^2}\cos\delta\,, \qquad \tan(2\chi) = \frac{2E_{0H}E_{0V}}{E_{0H}^2 + E_{0V}^2}\sin\delta\,. \tag{3}$$

El ángulo de orientación es cero cuando el valor de la fase δ es igual a $\pi/2$ o $3\pi/2$. En estas situaciones (2) describe una elipse en su forma estándar. En términos de las amplitudes, la orientación es también cero si E_{0H} (E_{0V}) es cero, en estos casos tenemos luz linealmente polarizada en dirección vertical (horizontal) . Para los casos extremos en los que $b = 0$ tenemos $\chi = 0$ y la luz es linealmente polarizada. En su lugar, cuando $b = a$ tenemos $\chi = \pm\pi/4$ y obtenemos luz circularmente polarizada.

2.1.2. La matriz de coherencia y los parámetros de Stokes

Para nuestros propósitos en lo que sigue es conveniente reformular (1) como:

$$E_H(z,t) = \mathscr{E}_0 a_H \exp[-i(\omega t - kz)]\,, \qquad E_V(z,t) = \mathscr{E}_0\, a_V \exp[-i(\omega t - kz)]\,, \tag{4}$$

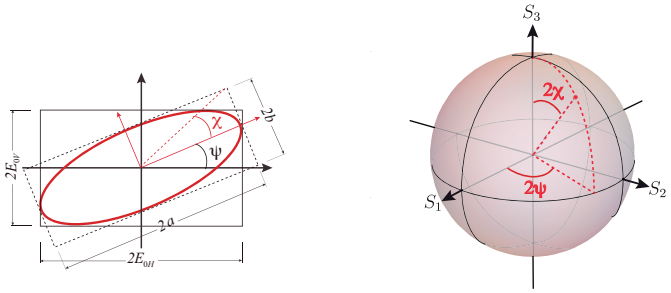

Figura 1: *(Izquierda) Elipse de polarización mostrando los ángulos de orientación ψ y elipticidad χ, que son función del semieje mayor y el semieje menor de la elipse, a y b. (Derecha) Esfera de Poincaré y la parametrización de las variables de Stokes para la luz polarizada en términos de las coordenadas esféricas*

dónde hemos absorbido las fases δ_H y δ_V en las amplitudes complejas adimensionales a_H y a_V. La amplitud del campo $\mathscr{E}_0$, real, puede ser identificada como *campo eléctrico por fotón* en la terminología de la óptica cuántica [214]

Como es sabido, toda la información de la polarización en cualquier plano z está contenida en el vector:

$$\mathbf{A}_{HV} = \begin{pmatrix} a_H \\ a_V \end{pmatrix} \tag{5}$$

al que nos referimos habitualmente como vector de Jones [133]. El subíndice HV destaca la base utilizada para descomponer las amplitudes del campo. Obviamente, este vector se puede expresar en cualquier otra base de polarización, que se obtiene de la base lineal $\{H,V\}$ por una transformación unitaria. En particular, una elección muy conveniente es la base circularmente polarizada $\{+,-\}$ tal que:

$$\mathbf{A}_{\pm} = \frac{1}{\sqrt{2}} \begin{pmatrix} 1 & i \\ 1 & -i \end{pmatrix} \mathbf{A}_{HV} \,. \tag{6}$$

Debido a que sólo las cantidades bilineales en las amplitudes de campo pueden ser detectadas, es ventajoso considerar la matriz

$$\Phi_{\pm} = \mathbf{A}_{\pm} \otimes \mathbf{A}_{\pm}^{\dagger} = \begin{pmatrix} a_+^* a_+ & a_+ a_-^* \\ a_+^* a_- & a_-^* a_- \end{pmatrix} , \tag{7}$$

donde † indica la hermítica conjugada, $\otimes$ representa el producto de Kronecker. En general, para describir el estado de polarización de un campo cuyos componentes pueden fluctuar en el tiempo de una manera complicada, determinista o aleatoria, se toma el promedio temporal de esta matriz, y el resultado es la llamada matriz de coherencia (o polarización) [95, 245, 188, 23, 25]. De esta forma, Φ es una matriz de covarianza de dimensión 2×2 cuyos elementos son los momentos de segundo orden de las amplitudes del campo. Bajo la presunción de que éstas son estacionarias y ergódicas, los brackets pueden ser también entendidos como un promedio del conjunto en diferentes realizaciones.

Los elementos de la diagonal principal de Φ son no-negativos , dado que son las intensidades promedio de las componentes horizontal y vertical de la polarización (en unidades de $\mathscr{E}_0$). En consecuencia, su traza es igual a la intensidad promedio de la onda. Los elementos no diagonales son complejos conjugados entre sí y representan las correlaciones cruzadas de las dos componentes de polarización. Por tanto, Φ es una matriz hermítica. Más aún, una aplicación directa de la desigualdad de Schwarz nos muestra que $|\Phi_{HV}| \leqslant \sqrt{\Phi_{HH}\Phi_{VV}}$, y por consiguiente el determinante de Φ es no-negativo. De hecho, la no-negatividad de sus valores propios constituye un conjunto completo de condiciones necesarias y suficientes para que una matriz hermítica Φ sea una matriz de coherencia, i.e., para que represente el estado de polarización de un campo de luz.

La matriz de coherencia puede expandirse en una base del espacio lineal de las matrices complejas de dimensión 2×2 . Una base natural es la constituida por la identidad ($\sigma_0 = \mathbb{1}$) más las tres matrices de Pauli σ_i (los índices latinos toman valores de 1 a 3). Éstas son hermíticas $\sigma_i = \sigma_i^{\dagger}$, ortogonales $\mathrm{Tr}(\sigma_i \sigma_j) = 2\delta_{ij}$ y satisfacen $\sigma_i^2 = \mathbb{1}$.

Además, son unitarias y de traza nula. La correspondiente expansión da como resultado coeficientes reales [95]:

$$S_\mu = \frac{1}{2}\,\mathrm{Tr}(\Phi\sigma_\mu)\,, \tag{8}$$

donde $\mu = 0,1,2,3$ son conocidos como los parametros de Stokes. Estos pueden ser también expresados como:

$$S_\mu = \frac{1}{2}\mathbf{A}_\pm^\dagger\,\sigma_\mu\,\mathbf{A}_\pm\,. \tag{9}$$

Esta relación puede ser invertida, de modo que podemos escribir los parámetros de Stokes en términos de los elementos de la matriz de polarización:

$$\begin{gathered} S_0 = \tfrac{1}{2}(a_+^* a_+ + a_-^* a_-)\,, \\ S_1 = \tfrac{1}{2}(a_+^* a_- + a_+ a_-^*)\,, \qquad S_2 = \tfrac{i}{2}(a_+ a_-^* - a_+^* a_-)\,, \qquad S_3 = \tfrac{1}{2}(a_+^* a_+ - a_-^* a_-)\,. \end{gathered} \tag{10}$$

Estos cuatro parámetros tienen un perfecto significado operacional. El parámetro S_0 es proporcional a la intensidad total (en unidades de $\mathscr{E}_0^2$), mientras que S_3 representa el exceso en intensidad entre las componentes circularmente polarizadas a izquierda y a derecha. El parámetro S_1 tiene una interpretación similar respecto a las componentes linealmente polarizadas a 45° y 135°. Finalmente, el parámetro S_2 es igual al exceso de la componente horizontal sobre aquella polarizada verticalmente.

En este punto se requiere algo de precaución: nuestra definición contiene un factor 1/2 extra en comparación con la tradicional. Este factor no esencial nos ayudará luego para realizar la conexión con la apropiada definición cuántica. También mencionamos que un cambio de la base utilizada en la definición de la matriz de polarización simplemente conducirá a una reorganización de la definición de los parámetros de Stokes en términos de las amplitudes de los modos, pero la estructura general permanece invariante.

La positividad de $\Phi_\pm$ implica inmediatamente que:

$$S_0^2 \geqslant S_1^2 + S_2^2 + S_3^2\,, \tag{11}$$

y la igualdad se cumple cuando $\det\Phi_\pm = 0$, que es exactamente el caso de la luz monocromática. Esto inmediatamente sugiere introducir el estado de polarización como un punto en una superficie esférica, llamada la esfera de Poincaré, que tiene como ejes las coordenadas (S_1,S_2,S_3). La posición del punto en la esfera de Poincaré está caracterizada por los ángulos de orientación y elipticidad ψ ($0 \leqslant \psi \leqslant \pi$) y χ ($-\pi/4 \leqslant \chi \leqslant \pi/4$) de modo que (ver Fig. 1):

$$S_1 = S_0\cos(2\chi)\sin(2\psi), \qquad S_2 = S_0\cos(2\chi)\cos(2\psi)\,, \qquad S_3 = S_0\sin(2\chi)\,. \tag{12}$$

El vector $\mathbf{S} = (S_1,S_2,S_3)^t$ (donde t es la transpuesta) es conocido como el vector de Stokes. De manera notable, con nuestra elección de la base circular, todos los estados linealmente polarizados se encuentran en el ecuador de la esfera de Poincaré, mientras que los estados circularmente polarizados están en el polo norte y polo sur (circularmente polarizados a la derecha y a la izquierda respectivamente). Los estados polarizados elípticamente están representados en el resto de puntos de la superficie esférica.

Para concluir, mencionamos que una generalización de los parámetros de Stokes de un haz electromagnético aleatorio ha sido introducido por Ellis y Dogariu [91] en el dominio del espacio-tiempo y también ha sido estudiado por Korotkova y Wolf [152] en el dominio espacio-frecuencia. Mientras que los parámetros habituales de Stokes dependen de una variable espacial, estos "parámetros de Stokes de dos puntos", que pueden ser definidos en el dominio espacio-frecuencia a partir del espectro cruzado de la matriz densidad que caracteriza las correlaciones en dos puntos, dependen de dos variables espaciales y contienen información adicional sobre las propiedades de coherencia.

Otro enfoque relevante es el modelo de parámetros de Stokes espacio-angulares que se introducen para rayos generalizados que incluyen dependencia espacial y angular y permiten que su evolución durante la propagación sea considerada.

2.1.3. Transformaciones de polarización

Como se destacó anteriormente, la polarización del campo está determinada por su vector de Jones $\mathbf{A}$ (en adelante, se asume que trabajamos en la base circular, en consecuencia, dejamos de utilizar el subíndice correspondiente). Su norma euclídea:

$$\mathfrak{N} = \|\mathbf{A}\|^2 = \mathbf{A}^\dagger\mathbf{A} = a_+^* a_+ + a_-^* a_- = 2S_0\,. \tag{13}$$

es la intensidad, medida en unidades de $\mathscr{E}_0^2$.

Permítanos ahora considerar las transformaciones lineales del campo, que están representadas por matrices complejas U de dimensión 2×2, tales que $\mathbf{A}' = U\mathbf{A}$. Para transformaciones sin pérdidas de energía, como las producidas por divisores de haz, placas de fase, etc., la intensidad es preservada; es decir: $\mathbf{A}'^{\dagger}\mathbf{A}' = \mathfrak{N}$ y, por tanto U es unitaria. De hecho, imponemos que $U \in \mathrm{SU}(2)$; i.e., el grupo de matrices unitarias complejas 2×2 con determinante unidad. Dado $U \in \mathrm{SU}(2)$, podemos encontrar ángulos de Euler α, β, γ tales que:

$$U(\alpha,\beta,\gamma) = e^{-i\alpha\sigma_3/2}\, e^{-i\beta\sigma_2/2}\, e^{-i\gamma\sigma_3/2} = \begin{pmatrix} e^{-i(\alpha+\gamma)/2}\cos(\beta/2) & -e^{-i(\alpha-\gamma)/2}\sin(\beta/2) \\ e^{+i(\alpha-\gamma)/2}\sin(\beta/2) & e^{+i(\alpha+\gamma)/2}\cos(\beta/2) \end{pmatrix}, \tag{14}$$

donde los angulos de Euler satisfacen: $0 \leqslant \alpha \leqslant 2\pi,\ 0 \leqslant \beta \leqslant \pi,\ 0 \leqslant \gamma \leqslant 4\pi$.

Alternativamente, podemos escribir U en terminos de un vector unidad $\mathfrak{n}$ en la dirección del eje de rotación [específicado por los ángulos esféricos (Θ,Φ)] y un ángulo de rotación ω,

$$U(\mathfrak{n},\omega) = \exp(-i\omega\,\mathfrak{n}\cdot\boldsymbol{\sigma}/2) \quad = \quad \begin{pmatrix} \cos(\omega/2) - i\sin(\omega/2)\cos\Theta & -i\sin(\omega/2)\sin\Theta\, e^{-i\Phi} \\ -i\sin(\omega/2)\sin\Theta\, e^{i\Phi} & \cos(\omega/2) + i\sin(\omega/2)\cos\Theta \end{pmatrix}. \tag{15}$$

Nótese que si las amplitudes complejas experimentan una transformación unitaria $\mathbf{A} \mapsto \mathbf{A}'$ el vector de Stokes $\mathbf{S} \in \mathbb{R}^3$ sufre también una transformación. En realidad, uno puede comprobar que [72]:

$$U\,(\mathbf{S}\cdot\boldsymbol{\sigma})\,U^{\dagger} = (R(U)\mathbf{S}))\cdot\boldsymbol{\sigma}\,, \tag{16}$$

donde la matriz ortogonal $R(U) \in \mathrm{SO}(3)$ es una rotación, y $\boldsymbol{\sigma}$ son las matrices de Pauli. De manera más explícita, $R(U)$ puede ser escogida como:

$$R(U)_{jk} = \frac{1}{2}\,\mathrm{Tr}(\sigma_j\, U\,\sigma_k\, U^{-1})\,. \tag{17}$$

La correspondencia $U \mapsto R(U)$ constituye una representación de SU(2), y toda rotación es imagen de algún elemento U. Nótese que ambas matrices U y $-U$ representan la misma rotación $R(U) = R(-U)$, por lo que la correspondencia anterior produce un doble recubrimiento de SO(3) por SU(2).

Sólo σ_3 y σ_2 son necesarias para generar una transformación SU(2) arbitraria. Utilizando (17), es inmediato mostrar que

$$\begin{aligned} U(\mathbf{e}_3,\phi) = \exp(-i\phi\sigma_3/2) = \begin{pmatrix} e^{-i\phi/2} & 0 \\ 0 & e^{-i\phi/2} \end{pmatrix} \quad &\mapsto \quad R(\mathbf{e}_3,\phi) = \begin{pmatrix} \cos\phi & \sin\phi & 0 \\ -\sin\phi & \cos\phi & 0 \\ 0 & 0 & 1 \end{pmatrix}, \\ U(\mathbf{e}_2,\theta) = \exp(-i\theta\sigma_2/2) = \begin{pmatrix} \cos(\theta/2) & \sin(\theta/2) \\ -\sin(\theta/2) & \cos(\theta/2) \end{pmatrix} \quad &\mapsto \quad R(\mathbf{e}_2,\theta) = \begin{pmatrix} \cos\theta & 0 & \sin\theta \\ 0 & 1 & 0 \\ -\sin\theta & 0 & \cos\theta \end{pmatrix}. \end{aligned} \tag{18}$$

Por lo tanto σ_3 representa cambios de fase diferenciales entre los modos, mientras que σ_2 genera rotaciones alrededor de la dirección de propagación. Resulta entonces que cualquier transformación de polarización se puede realizar con óptica lineal: placas de fase y rotadores.

2.1.4. Grado de polarización

Si la relación entre las componentes del campo E_+ y E_- (o equivalentemente, entre las componentes H y V) es completamente determinista, el campo está completamente polarizado. Para tal estado puro (adoptando la terminología de óptica cuántica) , la matriz de polarización satisface:

$$\mathrm{Tr}^2(\Phi_{\mathrm{pol}}) = \mathrm{Tr}(\Phi_{\mathrm{pol}}^2)\,. \tag{19}$$

Por otra parte, si las componentes del campo están totalmente no-correlacionadas, los elementos fuera de la diagonal son cero. Si, además, la energía está distribuida uniformemente entre las componentes circularmente polarizadas a izquierda y derecha, la matriz de coherencia es proporcional a la matriz identidad:

$$\Phi_{\mathrm{unpol}} = \frac{1}{2}\mathfrak{N}\,\mathbb{1}\,, \tag{20}$$

y podemos decir que el campo está despolarizado. Esto conduce a la importante descomposición de una matriz arbitraria Φ en una parte completamente polarizada y otra completamente despolarizada [245, 188].

$$\Phi = \mathfrak{N}\big[(1-\mathbb{P})\Phi_{\text{unpol}} + \mathbb{P}\Phi_{\text{pol}}\big]\,, \tag{21}$$

donde $\mathbb{P}$, denominado el grado de polarización, aparece como la proporción de la energía de la parte completamente polarizada frente a la energía total, lo que da un claro significado físico a la definición de $\mathbb{P}$.

Alternativamente, $\mathbb{P}$ puede ser escrita de una manera ligeramente distinta pero equivalente:

$$\mathbb{P} = \sqrt{\frac{2\,\text{Tr}(\Phi^2)}{\text{Tr}^2(\Phi)} - 1} = \sqrt{1 - \frac{4\det(\Phi)}{\text{Tr}^2(\Phi)}}\,, \tag{22}$$

como puede ser comprobado a través de un cálculo directo. En la primera expresión, el grado de polarización aparece intimamente relacionado con $\text{Tr}(\Phi^2)$, que, siguiendo de nuevo una notación cuántica, se denomina la pureza. En la segunda expresión, puede ser immediatamente relacionada con los valores propios de Φ: si los denotamos por λ_+ y λ_-, $(\lambda_+ > \lambda_-)$, entonces $(\lambda_+ + \lambda_-)^2 = N^2$ y $\det(\Phi) = \lambda_+\lambda_-$, de manera que

$$\mathbb{P} = \frac{\lambda_+ - \lambda_-}{\lambda_+ + \lambda_-}\,. \tag{23}$$

La acción de cualquier transformación unitaria en Φ deja invariante su traza. De esta manera, podemos siempre considerar la intensidad de un campo parcialmente polarizado como la suma de las componentes de dos campos no-correlacionados con intensidades λ_+ y λ_-. Si la luz es térmica en origen, la falta de correlación implica la independencia estadística de ambas componentes de la polarización y de sus intensidades correspondientes.

Finalmente, otra definición equivalente de el grado de polarización es:

$$\mathbb{P} = \frac{\sqrt{S_1^2 + S_2^2 + S_3^2}}{S_0}\,. \tag{24}$$

En la esfera de Poincaré, los puntos en la superficie representan estados totalmente polarizados (estados puros) y los puntos interiores representan estados parcialmente polarizados (estados mezcla). El estado máximamente mixto se encuentra en el origen y representa luz clásicamente despolarizada.

Para concluir, es oportuno recordar que el concepto de entropía de von Neumann S se puede transladar de forma directa a ondas electromagnéticas [96, 24, 29, 99, 28] como

$$S = -\,\text{Tr}(\Phi \ln \Phi)\,. \tag{25}$$

Esta cantidad es una medida de la diferencia en la cantidad de información entre un estado puro y un estado mezcla (ambos con la misma intensidad). Usando los valores propios de Φ, esta entropía puede ser escrita como

$$S = -\left\{\frac{1}{2}(1+\mathbb{P})\ln\left[\tfrac{1}{2}(1+\mathbb{P})\right] + \frac{1}{2}(1-\mathbb{P})\ln\left[\tfrac{1}{2}(1-\mathbb{P})\right]\right\}. \tag{26}$$

Por lo tanto, S se caracteriza unívocamente por $\mathbb{P}$ y disminuye monótonamente con $\mathbb{P}$. El máximo $S = \ln 2$ corresponde a $\mathbb{P} = 0$, mientras que el mínimo $S = 0$ es alcanzado por $\mathbb{P} = 1$; es decir, cuando la luz está totalmente polarizada.

2.2. Luz polarizada en óptica cuántica

2.2.1. Operadores de Stokes y el sector de polarización

Como hemos advertido, los parámetros Stokes son herramientas analíticas muy adecuadas para el tratamiento de la polarización en el dominio cuántico, porque pueden ser fácilmente convertidas en verdaderos observables cuánticos.

Como antes, consideramos una onda plana monocromática, propagándose en la dirección z. El campo cuántico está ahora caracterizado por dos operadores amplitud complejos, denotados por $\hat{a}_+$ y $\hat{a}_-$, que obedecen las relaciones de commutación bosónicas (donde se toma $\hbar = 1$)

$$[\hat{a}_\lambda, \hat{a}^\dagger_{\lambda'}] = \delta_{\lambda\lambda'}\mathbb{1}\,, \tag{27}$$

donde $\lambda, \lambda' \in \{+,-\}$ y $\delta_{\lambda\lambda'}$ es la función delta de Krönecker.

Los operadores de Stokes se definen entonces como una extensión directa de sus análogos clásicos [94, 67, 136, 218, 166]:

$$\hat{S}_0 = \tfrac{1}{2}(\hat{a}_+^\dagger \hat{a}_+ + \hat{a}_-^\dagger \hat{a}_-)$$
$$\hat{S}_1 = \tfrac{1}{2}(\hat{a}_+^\dagger \hat{a}_- + \hat{a}_+^\dagger \hat{a}_-)\,, \qquad \hat{S}_2 = \tfrac{i}{2}(\hat{a}_+ \hat{a}_-^\dagger - \hat{a}_+^\dagger \hat{a}_-)\,, \qquad \hat{S}_3 = \tfrac{1}{2}(\hat{a}_+^\dagger \hat{a}_+ - \hat{a}_-^\dagger \hat{a}_-)\,. \tag{28}$$

Las componentes del vector $\hat{\mathbf{S}} = (\hat{S}_1, \hat{S}_2, \hat{S}_3)^t$ satisfacen las relaciones de commutación de un momento angular

$$[\hat{S}_k, \hat{S}_\ell] = i\varepsilon_{k\ell m}\hat{S}_m\,, \qquad [\hat{S}_0, \hat{\mathbf{S}}] = 0\,, \tag{29}$$

donde $\varepsilon_{k\ell m}$ es el tensor de Levi-Civita totalmente antisimétrico. Nótese que $\hat{S}_0 = \hat{N}/2$, dónde $\hat{N} = \hat{N}_+ + \hat{N}_-$ es el operador para el número total de excitaciones. Desde el punto de vista matemático los operadores (28) son la representación de Jordan-Schwinger [134, 213] de SU(2) en términos de amplitudes bosónicas. Esta construcción ha sido utilizada en una amplia variedad de contextos y también se ha extendido a simetrías más generales [60].

En la óptica clásica, la intensidad total es una cantidad no fluctuante, por lo que la esfera Poincaré aparece como una superficie lisa con radio igual a la intensidad. En contraposición, en óptica cuántica tenemos que

$$\hat{\mathbf{S}}^2 = \hat{S}_1^2 + \hat{S}_2^2 + \hat{S}_3^2 = S(S+1)\,\hat{\mathbb{1}}\,, \tag{30}$$

con espín $S = S_0 = N/2$, como las fluctuaciones en el número de fotones son inevitables (dejando de lado los estados propios del número de fotones), nos vemos obligados a trabajar en el espacio tridimensional de Poincaré que puede considerarse como un conjunto de esferas anidadas con radios proporcionales a los diferentes números de fotones que contribuyen al estado, y que ha venido siendo denominado como el espacio de Poincaré.

El lado derecho de la ecuación Eq. (29) expresa en el lenguaje cuántico el hecho de que la polarización y la intensidad son conceptos independientes: la forma de la elipse (polarización) no depende de su tamaño (intensidad). Este hecho produce notable simplificaciones. En primer lugar, significa que debemos abordar cada subespacio con un número fijo de fotones N de forma aislada. En otras palabras, en la imagen anterior de cebolla de la esfera de Poincaré, cada capa debe ser abordada de forma independiente. Esto puede ser subrayado si en lugar de los estados de Fock $\{|n_+, n_-\rangle\}$, que son una base ortonormal del espacio de Hilbert de estos campos de dos modos, utilizamos el reetiquetado:

$$|S, m\rangle \equiv |n_+ = S + m, n_- = S - m\rangle\,. \tag{31}$$

Ésta puede ser vista como la base de estados propios comunes a $\{\hat{\mathbf{S}}^2, \hat{S}_3\}$, y estos estados expanden un subespacio de dimensión $(2S+1)$, $\mathscr{H}_S$, en donde actúan de manera estándar:

$$\hat{S}_\pm\,|S, m\rangle = \sqrt{S(S+1) - m(m\pm 1)}\,|S, m\pm 1\rangle\,, \qquad \hat{S}_z\,|S, m\rangle = m|S, m\rangle\,, \tag{32}$$

con $\hat{S}_\pm = \hat{S}_1 \pm i\hat{S}_2$.

En segundo lugar, para cualquier función arbitraria de los operadores de Stokes, $f(\hat{\mathbf{S}})$ tenemos $[f(\hat{\mathbf{S}}), \hat{N}] = 0$, por lo que los elementos de la matriz densidad $\hat{\rho}$ que conectan subespacios con diferente número de fotones no contribuyen a $\langle f(\hat{\mathbf{S}})\rangle$. Entonces, está claro que los momentos de cualquier observable que preserve la energía (como $\hat{S}$) no dependen de las coherencias entre diferentes subespacios. La única información accesible para cualquier estado descrito por la matriz densidad $\hat{\rho}$, viene dado entonces por la forma diagonal en bloques:

$$\hat{\rho}_{\text{pol}} = \bigoplus_S \hat{\rho}^{(S)} = \sum_{S=0}^{\infty} \sum_{m,m'=-S}^{S} \hat{\rho}^{(S)}_{mm'} |S, m\rangle\langle S, m'|\,, \tag{33}$$

y $\hat{\rho}^{(S)}$ es la matriz densidad en el subespacio S (S recorre todo los valores posibles del número de fotones, i.e., $S = \frac{1}{2}, 1, \frac{3}{2}, 2, \ldots$). La forma $\hat{\rho}_{\text{pol}}$ se llama sector de polarización [197, 176, 186] (también la matriz densidad de polarización [137]). Como cualquier $\hat{\rho}$ y su correspondiente forma asociada diagonal por bloques $\hat{\rho}_{\text{pol}}$ no pueden ser distinguidas mediante medidas de polarización, a partir de aquí suprimimos el subíndice pol.

Por último, advertimos que las transformaciones de SU(2) están representadas en el subespacio $\mathscr{H}_S$ por el operador $\hat{U}(\mathbf{n}, \omega) = \exp(-i\omega\hat{\mathbf{S}}\cdot\mathbf{n}/2)$, de modo que los operadores de Stokes son realmente los generadores de estas rotaciones. Como hemos visto anteriormente, la acción de este operador unitario induce una rotación, como indica la Eq. (16).

2.2.2. Relaciones de incertidumbre y compresión de la polarización

Los operadores de Stokes satisfacen las relaciones de incertidumbre estándar del algebra de $SU(2)$;

$$\Delta^2\hat{S}_j\,\Delta^2\hat{S}_k \geqslant \varepsilon_{k\ell m}\,|\langle\hat{S}_\ell\rangle|^2\,, \tag{34}$$

donde $\Delta^2\hat{X} = \langle\hat{X}^2\rangle - \langle\hat{X}\rangle^2$ representa la varianza. La no commutabilidad de estos operadores imposibilita la medida simúltanea precisa de las cantidades físicas que representan. Ésto puede ser mejor cuantificado por la relación:

$$\Delta^2\hat{\mathbf{S}} = \Delta^2\hat{S}_1 + \Delta^2\hat{S}_2 + \Delta^2\hat{S}_3 \geqslant 2\langle\hat{S}_0\rangle\,. \tag{35}$$

Los estados que satisfacen la igualdad $\Delta^2\hat{\mathbf{S}} = 2\langle\hat{S}_0\rangle$ son precisamente los estados coherentes de SU(2) [14, 189, 100], por lo que pueden correctamente ser considerados como los estados más clásicos permitidos por la teoría cuántica. Viven en el subespacio $\mathscr{H}_S$ y se definen en la base estándar de momento angular como

$$|S,\mathbf{n}\rangle = \sum_{m=-S}^{S} c_m(\theta,\phi)\,|S,m\rangle\,, \tag{36}$$

donde los coeficientes $c_m(\mathbf{n})$ siguen una distribución binomial que alcanza su valor máximo en la dirección dada por el vector unidad $\mathbf{n}$ de ángulos esféricos (θ,ϕ):

$$c_m(\mathbf{n}) = \binom{2S}{S+m}^{1/2} [\cos(\theta/2)]^{S-m}\,[\sin(\theta/2)]^{S+m}\,\exp[i(S+m)\phi]\,. \tag{37}$$

Nótese que el límite inferior en (34) depende del estado, y en particular algunas de estas relaciones de incertidumbre pueden volverse triviales, o incluso las tres simultáneamente si $\langle\hat{\mathbf{S}}\rangle = 0$.

Otra cuestión con las relaciones (34) es que no son invariantes SU(2), que es un requisito valioso para evitar realizar conclusiones confusas. Una manera natural de conseguir invarianza SU(2) es usando componentes específicas de los operadores de Stokes. Con esta finalidad, primero definimos la dirección de polarización promedio como (asumiendo $\langle\hat{\mathbf{S}}\rangle \neq 0$)

$$\mathbf{n}_\parallel = \frac{\langle\hat{\mathbf{S}}\rangle}{|\langle\hat{\mathbf{S}}\rangle|}\,. \tag{38}$$

y otros dos vectores ortogonales como $\mathbf{n}_{\perp 1}$ and $\mathbf{n}_{\perp 2}$, que conjuntamente con $\mathbf{n}_\parallel$ definen un sitema de referencia. Si denotamos por $\hat{S}_\mathbf{n} = \hat{\mathbf{S}}\cdot\mathbf{n}$ la proyección de las variables de Stokes en la dirección $\mathbf{n}$, las relaciones de conmutación (29) se convierten ahora en $[\hat{S}_{\perp 1},\hat{S}_{\perp 2}] = i\hat{S}_\parallel$, que sólo proporciona una relación de incertidumbre no trivial, es decir,

$$\Delta^2\hat{S}_{\perp 1}\Delta^2\hat{S}_{\perp 2} \geqslant |\langle\hat{S}_\parallel\rangle| \tag{39}$$

y otras dos triviales $\Delta^2\hat{S}_{\perp 1}\Delta^2\hat{S}_\parallel \geqslant 0$ y $\Delta^2\hat{S}_{\perp 2}\Delta^2\hat{S}_\parallel \geqslant 0$. La igualdad en Eq. (39) es alcanzada por los vectores propios de $\hat{S}_{\perp 1} + i\lambda\hat{S}_{\perp 2}$, para cualquier λ real. Estos han venido siendo denominados estados inteligentes [13, 12]. Los estados coherentes SU(2) son los únicos estados que satisfacen simultáneamente las tres igualdades ya que cumplen que $\Delta^2\hat{S}_\parallel = 0$.

Otra posibilidad para garantizar invarianza SU(2) es usar la matriz de covarianza real y simétrica de dimensión 3×3 para las variables de Stokes [27, 201, 141], definida como

$$\Gamma_{jk} = \frac{1}{2}\langle\{\hat{S}_j,\hat{S}_k\}\rangle - \langle\hat{S}_j\rangle\langle\hat{S}_k\rangle\,, \tag{40}$$

donde $\{\cdot,\cdot\}$ es el anticonmutador. Tenga en cuenta que, si bien los operadores de Stokes son todos hermíticos, la no-conmutabilidad hace que los productos mixtos, no simétricos (tal como $\hat{S}_j\hat{S}_k$) no sean hermíticos, evitando asímismo su medida directa. La simetrización se incluye en la definición (40). En términos de la matriz Γ, tenemos

$$\Delta^2\hat{S}_\mathbf{n} = \mathbf{n}^t\,\Gamma\,\mathbf{n}\,, \tag{41}$$

y como Γ es definida positiva, el mínimo de $\Delta^2\hat{S}_\mathbf{n}$ existe y es único. Si nosotros incorporamos la reestricción $\mathbf{n}^t\cdot\mathbf{n} = 1$ como un multiplicador de Lagrange γ, este mínimo viene dado por $\Gamma\mathbf{n} = \gamma\mathbf{n}$: los valores admisibles de

γ son por tanto los valores propios de Γ y las direcciones que minimizan $\Delta^2\hat{S}_{\mathbf{n}}$ son los correspondientes vectores propios.

También existen relaciones de incertidumbre para la suma de las varianzas de dos operadores de Stokes.

$$\Delta^2\hat{S}_j + \Delta^2\hat{S}_k \geqslant C \tag{42}$$

donde el límite inferior es dependiente del estado. En el caso de número de fotones muy grande, sin embargo, es conocido que $C \simeq \frac{3}{2}\langle\hat{S}_0\rangle^{3/2}$. Éstas se denominan relaciones planas de incertidumbre [115, 195].

Finalmente, mencionemos que las relaciones de incertidumbre pueden ser evaluadas utilizando medidas de incertidumbre distintas de la varianza. La alternativa más popular son medidas entrópicas, según lo revisado recientemente en [238].

El concepto de compresión está estrechamente vínculado con las relaciones de incertidumbre. En el mismo espíritu que para las variables continuas, la compresión se define siempre que las fluctuaciones de uno de los operadores de Stokes están por debajo del nivel "shot-noise", que está establecido por los estados coherentes SU(2). Sin embargo, a diferencia del caso bosónico en el que las varianzas de los estados coherentes son iguales en cualquier dirección, en el caso de un estado coherente SU(2), las varianzas de los operadores de Stokes dependen de la dirección $\mathbf{n}$. En realidad, la componente paralela satisface $\Delta^2 S_{\parallel} = 0$, por lo que la compresión está determinada principalmente por las fluctuaciones de las componentes ortogonales y los criterios de compresión alternativos dependen de las funciones particulares utilizadas.

Para un un estado coherente SU(2) $(\Delta S_{\mathbf{n}_\perp})^2 = S/2$. Es por lo tanto sensato establecer que la compresión se produce cuando la varianza de $S_{\mathbf{n}_\perp}$ es menor que $S/2$, y el valor asociado al parámetro de compresión es [138].

$$\xi_S^2 = \frac{\min \Delta^2 S_{\mathbf{n}_\perp}}{S/2} = \frac{4\min \Delta^2 S_{\mathbf{n}_\perp}}{N} \tag{43}$$

Obviamente $\xi_S^2 = 1$ para los estados coherentes SU(2), mientras podemos obtener compresión siempre que $\xi_S^2 < 1$, esto es, la fluctuación en una dirección está reducida.

En el contexto de espectrometría de Ramsey, Wineland et al. definieron otro grado de compresión como el cociente de la sensibilidad de fase de un estado general frente al estado coherente SU(2) [243, 242] (ver también) [121, 6, 52]). Para un estado coherente SU(2) la sensibilidad de la fase es $\Delta^2\phi_{\mathrm{SU}(2)} = 1/N$ y un cálculo directo da como resultado:

$$\xi_R^2 = \frac{S}{2\left|\langle\mathbf{S}_{\parallel}\rangle\right|^2} \inf_{\mathbf{n}_\perp} \Delta^2 S_{\mathbf{n}_\perp} \tag{44}$$

Hay algunos otros parámetros de compresión que se discuten con detalle en un compendio reciente [168].

La idea de la compresión de la polarización derivada de las relaciones de incertidumbre (42) puede extenderse a las fluctuaciones de dos componentes de Stokes simultáneamente, digamos k y ℓ, como

$$\Delta^2\hat{S}_k + \Delta^2\hat{S}_\ell < \sqrt{\langle\hat{S}_k\rangle^2 + \langle\hat{S}_\ell\rangle^2} \tag{45}$$

que es denominada como compresión plana [115, 195]. Se han obtenido resultados alternativos concernientes a la compresión de dos [194] o de tres [116] operadores de Stokes simultáneamente.

Finalmente, mencionamos que el uso de medidas entrópicas de incertidumbre lleva a la idea de la compresión de espín entrópica, que ha sido considerada por varios autores [2, 65].

Cuando el estado se expande en términos de diferente número de fotones, nos vemos obligados a escudriñar múltiples subespacios con distinta excitación. Cuando esto sucede, llevamos a cabo un promedio del vector de Stokes $\langle\hat{\mathbf{S}}\rangle = \sum_{S=0}^{\infty} P_S \,\mathrm{Tr}(\hat{\rho}^{(S)}\hat{\mathbf{S}})$, donde P_S es la distribución del número de fotones. Como resultado, la compresión del estado puede ser mucho menor que la correspondiente a las capas individuales [185].

2.2.3. El plano oscuro

Es siempre posible establecer una base en la que uno solo de los operadores (28) tiene un valor esperado distinto de cero, pongamos $\langle\hat{S}_j\rangle = \langle\hat{S}_k\rangle = 0$ y $\langle\hat{S}_\ell\rangle \neq 0$. La única relación de incertidumbre no trivial es: $\Delta^2\hat{S}_j\,\Delta^2\hat{S}_k \geqslant |\langle\hat{S}_\ell\rangle|^2$. La compresión de la polarización puede ser sensatamente definida como [151, 49, 210]

$$\Delta^2\hat{S}_j < |\langle\hat{S}_\ell\rangle| < \Delta^2\hat{S}_k\,. \tag{46}$$

La elección de operadores conjugados $\{\hat{S}_j, \hat{S}_k\}$ no es de ningún modo única: existe un conjunto infinito de operadores $\{\hat{S}_\perp(\theta), \hat{S}_\perp(\theta+\pi/2)\}$ que son perpendiculares a la excitación clásica del estado $\hat{S}_\ell$, para los que $\langle \hat{S}_\perp(\theta)\rangle = 0$ para todo θ. Todos estos pares existen en el plano S_j–S_k, que es llamado el "plano oscuro" porque es el plano de intensidad media cero. Podemos expresar un operador genérico $\hat{S}_\perp(\theta)$ como $\hat{S}_\perp(\theta) = \hat{S}_j \cos\theta + \hat{S}_k \sin\theta$, siendo θ un ángulo definido respecto a $\hat{S}_j$. La condición (46) es entonces equivalente a:

$$\Delta^2 \hat{S}_\perp(\theta_{\rm sq}) < |\langle \hat{S}_0 \rangle| < \Delta^2 \hat{S}_\perp(\theta_{\rm sq} + \pi/2), \tag{47}$$

donde $\hat{S}_\perp(\theta_{\rm sq})$ es el parámetro de compresión y $\hat{S}_\perp(\theta_{\rm sq}+\pi/2)$ el parámetro de anticompresión.

Muchos experimentos usan luz circularmente polarizada, que satisface: $\langle \hat{S}_1\rangle = \langle \hat{S}_2\rangle = 0$, $\langle \hat{S}_3\rangle = \alpha^2$. Por lo que el plano oscuro es directamente el plano S_1-S_2 y $\langle \hat{a}_+\rangle = \alpha$ y $\langle \hat{a}_-\rangle = 0$. Expresando las fluctuaciones de $\hat{\mathbf{S}}$ en términos del ruido de los modos circularmente polarizados $\delta\hat{a}_\pm$ y asumiendo $|\langle \delta\hat{a}_\pm\rangle| \ll \alpha$ encontramos [71]

$$\delta\hat{S}_\perp(\theta) = \alpha\delta\hat{X}_-(\theta) = \alpha[\delta\hat{X}_H(\theta) + \delta\hat{X}_V(\theta+\pi/2)], \tag{48}$$

donde $\hat{X}_\lambda = (\hat{a}_\lambda e^{-i\theta} + \hat{a}_\lambda^\dagger e^{i\theta})/\sqrt{2}$ ($\lambda \in \{H,V\}$) son las cuadraturas rotadas para la amplitud λ-ésima. Por otra parte, dado que: $\hat{X}_\lambda = (\hat{a}_\lambda e^{-i\theta} + \hat{a}_\lambda^\dagger e^{i\theta})/\sqrt{2}$ ($\lambda \in \{H,V\}$), la intensidad no exhibe dependencia del modo oscuro. En consecuencia, la condición (47) puede ser reescrita como:

$$\Delta^2 \hat{S}_\perp(\theta) < |\langle \alpha\rangle|^2 \quad \Leftrightarrow \quad \Delta^2 \hat{X}_-(\theta) < 1, \tag{49}$$

esto es, la compresión de la polarización es equivalente a la compresión del vacío en el modo de polarización ortogonal.

En este caso, podemos considerar que la esfera puede ser reemplazada localmente por su plano tangente dado que $S \simeq \alpha^2$, i.e., para estados brillantes, la esfera de Poincaré tiene un gran radio de modo que la curvatura es localmente despreciable y la proyección en el plano oscuro S_1-S_2 es equivalente a un espacio de fase canónico reescalado para la cuadratura x-p.

2.2.4. El conjunto tensorial irreducible

La compresión se refiere exclusivamente al comportamiento de los momentos de segundo orden. Como se destacó anteriormente, las fluctuaciones de orden superior juegan un papel crucial en el dominio cuántico. Para tratar con ellas, es conveniente usar el llamado conjunto tensorial irreducible [97, 220, 41, 233, 172] un concepto básico en el contexto de la teoría cuántica del momento angular. Para un valor fijo del espín S, estos operadores (también llamados operadores de polarización) se definen como:

$$\hat{T}^{(S)}_{Kq} = \sqrt{\frac{2K+1}{2S+1}} \sum_{m,m'=-S}^{S} C^{Sm'}_{Sm,Kq} \, |S,m'\rangle\langle S,m|, \tag{50}$$

con $C^{Sm}_{S_1 m_1, S_2 m_2}$ los coeficientes de Clebsch-Gordan [233] que acoplan un espín S_1 y un espín S_2 a un espín total S y se anulan a menos que las reglas usuales de acoplamiento del momento angular se satisfagan $0 \leqslant K \leqslant 2S$ y $-K \leqslant q \leqslant K$.

De acuerdo con las propiedades de los coficientes de Clebsch-Gordan K toma valores $0, 1, 2, \ldots, 2S$, de manera que hay $(2S+1)^2$ operadores de polarización y ellos constituyen una base del espacio de operadores lineales que actúan sobre $\mathscr{H}_S$, lo cual está garantizado por la propiedad:

$$\mathrm{Tr}\left[\hat{T}^{(S)}_{Kq} \hat{T}^{(S)\dagger}_{K'q'}\right] = \delta_{SS'}\delta_{KK'}\delta_{qq'}. \tag{51}$$

En general, los operadores de polarización no son hermíticos, pero debido a sus propiedades de simetría, para cada S fijo, satisfacen la relación:

$$\hat{T}^{(S)\dagger}_{Kq} = (-1)^q \hat{T}^{(S)}_{K-q}. \tag{52}$$

Aparte, tienen las correctas propiedades de transformación: bajo una transformación de SU(2) parametrizada por los ángulos de Euler $\hat{U}(\alpha,\beta,\gamma)$, tenemos

$$\hat{U}(\alpha,\beta,\gamma)\, \hat{T}^{(S)}_{Kq}\, \hat{U}^\dagger(\alpha,\beta,\gamma) = \sum_{q'} D^S_{q'q}(\alpha,\beta,\gamma)\, \hat{T}^{(S)}_{Kq'}, \tag{53}$$

donde $D^{S}_{q'q}(\alpha,\beta,\gamma)$ son las matrices de rotación de Wigner; esto es, los elementos de matriz de $\hat{U}(\alpha,\beta,\gamma)$ en la base $|S,m\rangle$ [233].

Aunque la definición de $\hat{T}^{(S)}_{Kq}$ pueda parecer poco amigable, la observación esencial para lo que sigue es que $\hat{T}^{(S)}_{Kq}$ puede ser relacionado con la potencia K-ésima de los generadores, por lo que estos operadores están intímamente relacionados con los momentos de las variables de Stokes. De hecho, uno puede reescribir la Eq. (50) como

$$\begin{aligned}
&\hat{T}^{(S)}_{00} = \frac{1}{\sqrt{2S+1}}\hat{\mathbb{1}}\,,\\
&\hat{T}^{(S)}_{10} = \frac{\sqrt{3}}{\sqrt{(2S+1)(S+1)S}}\hat{S}_z\,, \qquad \hat{T}^{(S)}_{1\mp1} = \frac{\sqrt{3}}{\sqrt{(2S+1)(S+1)S}}\hat{S}_\pm\,,\\
&\hat{T}^{(S)}_{20} = \sqrt{\tfrac{C}{6}}(3\hat{S}_z^2-\hat{S}^2)\,, \qquad \hat{T}^{(S)}_{2\mp1} = \sqrt{\tfrac{C}{2}}\{\hat{S}_z,\hat{S}_\pm\}\,, \qquad \hat{T}^{(S)}_{2\mp2} = \sqrt{\tfrac{C}{2}}\hat{S}_\pm^2\,,
\end{aligned} \tag{54}$$

donde $C = 30/[(2S+3)(2S+1)(2S-1)(S+1)]$.

La expansión de la matriz densidad $\rho^{(S)}$ en el conjunto irreducible de tensores se escribe:

$$\hat{\rho}^{(S)} = \sum_{K=0}^{2S}\sum_{q=-K}^{K}\rho^{(S)}_{Kq}\,\hat{T}^{(S)}_{Kq}\,. \tag{55}$$

y los correspondientes coeficientes de la expansión son:

$$\rho^{(S)}_{Kq} = \mathrm{Tr}\left[\hat{\rho}^{(S)}\hat{T}^{(S)\dagger}_{Kq}\right] \tag{56}$$

son conocidos como multipolos del estado y contienen toda la información relativa al estado, agrupada de forma invariante SU(2). Para representar un estado físico el operador densidad debe tener traza unidad, ser hermítico y definido positivo. Estas condiciones se traducen en unas restricciones sobre los valores de los multipolos del estado. La traza unidad fija el valor del monopolo, el único tensor esférico de traza no nula

$$\rho^{(S)}_{00} = \frac{1}{\sqrt{2S+1}}\,, \tag{57}$$

De modo que en cierta manera es trivial. La hermiticidad impone la condición de simetría:

$$\rho^{(S)}_{K-q} = (-1)^q\,\rho^{(S)}_{Kq}\,, \tag{58}$$

y el hecho de que $\hat{\rho}^{(S)}$ sea semidefinida positiva fuerza al límite:

$$\sum_{q=-K}^{K}|\rho^{(S)}_{Kq}|^2 \leqslant C^{(S)}_K\,, \tag{59}$$

para cada $K \geqslant 1$ y $C^{(S)}_K$ una constante positiva.

El dipolo $\rho^{(S)}_{1q}$ es el momento de primer orden de $\hat{\mathbf{S}}$ y proporciona entonces la imagen clásica, en la que el estado es representado por su valor promedio. La caracterización completa del estado requiere el conocimiento de todos los multipolos. Esto implica medir la distribución de probabilidad de $\hat{\mathbf{S}}$ en todas las direcciones, y luego realizar una inversion integral, que resulta ser una ardua labor. Sin embargo, en los casos más realistas sólo se necesitan un número finito de multipolos y entonces la reconstrucción del multipolo K-ésimo implica medir a lo largo de sólo $2K+1$ direcciones independientes, como veremos en la Sección 3.2.

Finalmente, nos referimos a la importante clase de estados axialmente simétricos [42]. Éstos son invariantes bajo rotaciones alrededor de un eje que tomamos como el eje z. Dado que $D^{S}_{qq'}(0,0,\gamma) = \exp(-iq\gamma)\delta_{qq'}$, esto implica

$$\hat{\rho}^{(S)}_{\mathrm{ax}} = \sum_{K=0}^{2S}\rho^{(S)}_{K0}\,\hat{T}^{(S)}_{K0}\,. \tag{60}$$

Entonces, están caracterizados únicamente por las componentes multipolares ρ_{K0}. Cualquier operador densidad que pueda ser obtenido de $\hat{\rho}_{\rm ax}$ por medio de una transformación de SU(2), representa asímismo un estado axialmente simétrico, ya que una rotación sólo cambia la dirección del eje de simetría del estado.

Algunos estados axialmente simétricos son también invariantes ante la inversión del eje de simetría (i.e., $z \to -z$). Como esto se corresponde con una rotación alrededor del eje-y de un ángulo π y $D^S_{qq'}(0,\pi,0) = (-1)^{K+q}\delta_{q\,-q'}$, obtenemos de la Eq. (53)

$$\rho^{(S)}_{K0} = (-1)^K \rho^{(S)}_{K0}\,, \tag{61}$$

por lo que sólo multipolos de rango par K contribuyen.

3. Herramientas básicas

3.1. Espacio de fases

3.1.1. La función de Husimi Q

El enfoque estándar para la óptica cuántica descrito hasta ahora se basa en operadores en el espacio de Hilbert. Para muchos propósitos, resulta muy conveniente usar una formulación del espacio de fases, que se encuentra en varios libros [209, 247, 211] y artículos [122, 112, 158]. La idea es explotar la correspondencia de Weyl entre funciones complejas en el espacio de fase y operadores cuánticos en el espacio de Hilbert.

La simetría SU (2) inherente a la estructura de polarización nos permite simplificar enormemente esta labor. De hecho, Stratonovich [223] y Berezin [33] elaboraron distribuciones de cuasiprobabilidad en la esfera satisfaciendo todos los requerimientos pertinentes. Esta construcción fue generalizada más tarde por otros [5, 53, 118, 142, 145] y ha demostrado ser muy útil en la visualización de las propiedades de sistemas de espín [89, 17, 63, 64, 140]. No necesitamos la maquinaria completa; puesto que para nuestros objetivos es suficiente concentrarnos en la función de Husimi Q [125], definida en completa analogía a su homólogo para variables continuas, a saber [5]:

$$Q(S,\mathbf{n}) = \langle S,\mathbf{n}|\hat{\rho}^{(S)}|S,\mathbf{n}\rangle\,. \tag{62}$$

Donde los estados coherentes SU(2) $|S,\mathbf{n}\rangle$ son los únicos estados que saturan la relación de incertidumbre (34), la definición de $Q(\mathbf{n})$ es bastante atractiva, ya que aparece como la proyección sobre los estados que tienen la polarización más definida permitida por la teoría cuántica. En óptica cuántica la mayoría de los estados implican un sector de polarización completo como en la ecuación Eq.(33). Para la matriz de polarización total $\hat{\rho}$ la función resultante es [205]

$$Q(\mathbf{n}) = \sum_{S=0}^{\infty} (2S+1)\; Q(S,\mathbf{n})\,, \tag{63}$$

que está normalizada de acuerdo a:

$$\frac{1}{4\pi}\int_{\mathscr{S}_2} d\mathbf{n}\, Q(\mathbf{n}) = 1\,, \tag{64}$$

con $d\mathbf{n} = \sin\theta d\theta d\phi$ el elemento diferencial de ángulo sólido.

El punto que queremos destacar aquí es que (63) implica sólo elementos diagonales entre estados con el mismo número de excitaciones. Debido a la falta de contribuciones de la forma $\langle S,\mathbf{n}|\hat{\rho}|S',\mathbf{n}\rangle$ con $S \neq S'$, la función Q toma la forma de un promedio sobre los subespacios con un número total de excitaciones definido . El papel de la suma en S es eliminar la intensidad total de la descripción del estado [143].

Para el caso particular de los estados puros, que se pueden expandir en la base de momento angular con coeficientes Ψ_{Sm}, (i.e., $|\Psi\rangle = \sum_{S=0}^{\infty}\sum_{m=-S}^{S}\Psi_{Sm}\,|S,m\rangle$), la función Q de Husimi toma la forma:

$$Q_{|\Psi\rangle}(\mathbf{n}) = \sum_{S=0}^{\infty}(2S+1)\,|\langle S,\mathbf{n}|\Psi\rangle|^2 = \sum_{S=0}^{\infty}(2S+1)\left|\sum_{m=-S}^{S} c_m(\mathbf{n})\,\Psi_{Sm}\right|^2\,, \tag{65}$$

donde los coeficientes $c_m(\mathbf{n})$ están dados por la Eq. (37).

Permítanos considerar algunos ejemplos ilustrativos. Primero consideramos estados con S fija. Para un estado coherente SU(2) $|S,\mathbf{n}_0\rangle$ se obtiene de manera inmediata:

$$Q_{|S,\mathbf{n}_0\rangle}(S,\mathbf{n}) = \left[\tfrac{1}{2}(1+\mathbf{n}\cdot\mathbf{n}_0)\right]^{2S}\,, \tag{66}$$

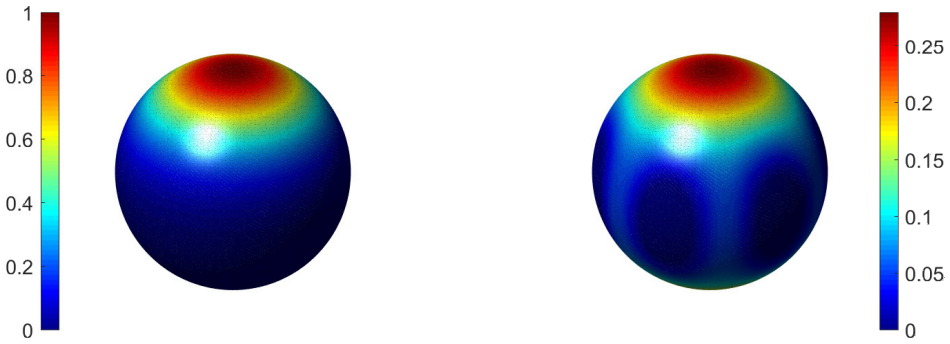

Figura 2: *Gráficos de probabilidad de la función Q para: (izquierda) un estado coherente SU(2) ($S = 3$) centrado en el polo norte, (derecha) un estado N00N con el mismo $S = 3$.*

que, como se esperaba, es una distribución muy pronunciada en la dirección $\mathbf{n}_0$. El segundo ejemplo son los estados N00N [157, 88], que son:

$$|\mathrm{N00N}\rangle = \frac{1}{\sqrt{2}}(|N,0\rangle - |0,N\rangle) = \frac{1}{\sqrt{2}}(|S,S\rangle - |S,-S\rangle)\,. \tag{67}$$

expresados tanto en la base de Fock como en la base de momento angular. Ahora, obtenemos:

$$Q_{|\mathrm{N00N}\rangle}(S,\mathbf{n}) = \frac{1}{2}\left[\sin^{4S}(\theta/2) + \cos^{4S}(\theta/2) - 2\sin^{2S}(\theta/2)\cos^{2S}(\theta/2)\cos(S\phi)\right], \tag{68}$$

que presenta $2S$ mínimos equidistantemente colocados alrededor del ecuador de la esfera de Poincaré. Estas dos funciones de Husimi Q se muestran en la Fig. 2.

Consideremos dos ejemplos extra: el primero es estados coherentes de Glauber en ambos modos $|\alpha_+,\alpha_-\rangle$. Tomamos ambos osciladores con la misma amplitud y fase relativa δ, ya que ésta es quizás la situación más interesante en cuanto a la polarización. Al usar la invarianza de SU (2) podemos considerar, sin pérdida de generalidad, que el estado se obtiene al transformar el estado $|\alpha_H,0_V\rangle$. La descomposición en subespacios invariantes $\mathscr{H}_S$ es:

$$\Psi_{Sm} = e^{-|\alpha|^2}\frac{|\alpha|^{2S}}{\sqrt{(S+m)!(S-m)!}}e^{i(S+m)\delta}. \tag{69}$$

Después de realizar las sumas, el resultado final es:

$$Q_{|\alpha_+,\alpha_-\rangle}(\mathbf{n}) = [1+|\alpha|^2\cos^2(\theta/2)]\exp[-|\alpha^2|\sin^2(\theta/2)]\,. \tag{70}$$

El segundo ejemplo es un estado de vacío comprimido de dos modos [127, 128] $|\mathrm{TMSV}\rangle = \hat{S}(\xi)(|0_+,0_-\rangle)$, donde el operador de compresión de los dos modos es $\hat{S}(\xi) = \exp[r(\hat{a}_+\hat{a}_- - \hat{a}_+^\dagger\hat{a}_-^\dagger)]$ y el parámetro de compresión r se toma real sin pérdida de generalidad. Este estado puede escribirse como

$$|\mathrm{TMSV}\rangle = \sqrt{1-\lambda^2}\sum_N \lambda^N |N,N\rangle = \sqrt{1-\lambda^2}\sum_S \lambda^S |S,0\rangle, \tag{71}$$

otra vez en ambas bases, la de Fock y la de momento angular. Aquí, $\lambda = \tanh r$. Consecuentemente ahora tenemos:

$$\Psi_{Sm} = \delta_{m0}\frac{\tanh^S r}{\cosh r}, \tag{72}$$

y la función de Husimi resultante queda:

$$Q_{|\mathrm{TMSV}\rangle}(\mathbf{n}) = \frac{1}{\cosh^2 r}\frac{1-\tanh^2 r}{[1+\tanh^2 r + 2\tanh r\cos(2\theta)]^{3/2}}\,. \tag{73}$$

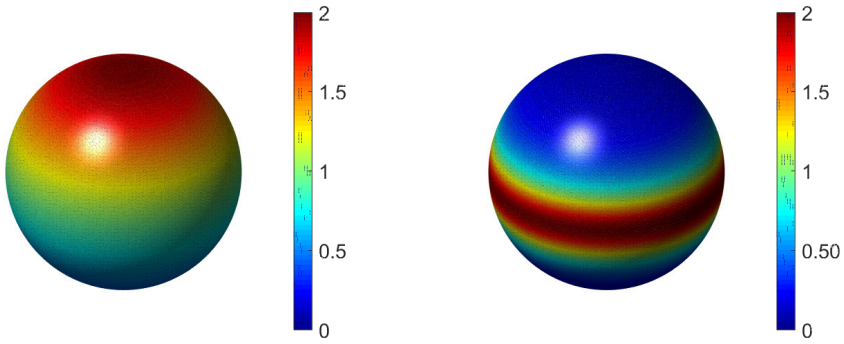

Figura 3: *Gráficos de densidad de la función de Husimi Q de: (izquierda) el estado coherente de dos modos para el caso en que sólo el modo horizontal está excitado, y (derecha) para el estado comprimido de vacío de dos modos con un parámetro de compresión* $r = 0{,}9$.

En la Fig. 3 hemos dibujado los resultados para estos dos últimos estados. Para el estado de vacío comprimido en dos modos tomamos $r = 0{,}9$. Vemos la presencia de un pico gaussiano centrado en $\theta = \pi/2$ e independiente de ϕ. Esto significa que podemos ver este estado como resultado de una superposición de estados con amplitud igual en cada modo de polarización, pero todas las fases relativas posibles ϕ. Estos estados contribuyentes están ubicados en el ecuador y, por lo tanto, vemos un amplio "cinturón" allí.

3.1.2. La función de Husimi y las fluctuaciones de orden superior

La función de Husimi Q contiene información completa sobre el estado. Esto es equivalente a conocer todos los multipolos. Esto puede ser remarcado si reescribimos $Q(S,\mathbf{n})$ como [140]

$$Q(S,\mathbf{n}) = \frac{\sqrt{4\pi}}{\sqrt{2S+1}} \sum_{K=0}^{2S} \sum_{q=-K}^{K} C^{SS}_{SS,K0}\, \rho^{(S)}_{Kq}\, Y^{*}_{Kq}(\mathbf{n})\,, \tag{74}$$

donde $Y^{*}_{Kq}(\mathbf{n})$ son los armónicos esféricos y el coeficiente de Clebsch-Gordan $C^{SS}_{SS,K0}$ tiene una forma analítica muy simple [233]:

$$C^{SS}_{SS,K0} = \frac{\sqrt{2S+1}(2S)!}{\sqrt{(2S-K)!\,(2S+1+K)!}}\,. \tag{75}$$

Insertando la Eq. (74) en la definición general Eq. (63) la función Q del estado aparece como una suma:

$$Q(\mathbf{n}) = \sum_{K=0}^{\infty} Q_K(\mathbf{n})\,, \tag{76}$$

donde cada componente parcial puede ser escrita:

$$Q_K(\mathbf{n}) = \sqrt{4\pi} \sum_{S=\lfloor K/2 \rfloor}^{\infty} \sqrt{2S+1} \sum_{q=-K}^{K} C^{SS}_{SS,K0}\, \rho^{(S)}_{Kq}\, Y^{*}_{Kq}(\mathbf{n})\,. \tag{77}$$

Aquí, la función suelo $\lfloor x \rfloor$ es el entero más grande no mayor que x. Las componentes parciales Q_K heredan las propiedades de Q, pero contienen información exclusiva sobre el K-ésimo momento de las variables de Stokes, así que, la ecuación (76) aparece como una herramienta óptima para organizar los sucesivos momentos.

Ilustramos este punto de vista con el ejemplo simple del estado $|1_{\mathrm{H}}, 1_{\mathrm{V}}\rangle$, que representa a los pares de fotones producidos en conversión paramétrica a la baja del tipo-II [203]. Este estado es $|1,0\rangle$ en la base del momento angular y su función Q puede calcularse de manera immediata:

$$Q(\mathbf{n}) = \frac{3}{4}\sin^2\theta\,. \tag{78}$$

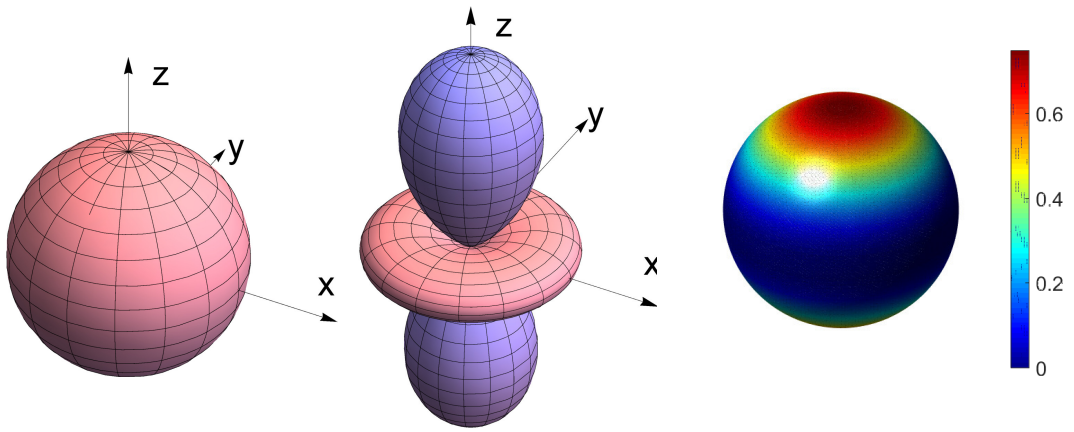

Figura 4: *Gráfico de las componentes monopolar ($K=0$) y cuadrupolar ($K=2$) del estado $|1,0\rangle$, así como la función Q total (derecha). La componente dipolar ($K=1$) se anula, por lo que este estado carece de información de primer orden. Hemos incluido también un gráfico de densidad de la función total de Husimi Q.*

No depende de ϕ y su forma es una barriga ecuatorial, revelando que el estado está altamente deslocalizado en la esfera de Poincaré. Las componentes parciales, conforme a (77),son:

$$Q_0(\mathbf{n}) = \frac{1}{2}, \qquad Q_1(\mathbf{n}) = 0, \qquad Q_2(\mathbf{n}) = \frac{1}{4}\left(1-3\cos^2(\theta)\right). \tag{79}$$

La suma de estos tres términos da, por supuesto, el resultado Eq. (78), pero hay más información codificada en Eq. (79): la contribución dipolar es nula, confirmando que este estado no transmite información de primer orden. Ésta es la razón por la que éste fue el primer estado en el que se detectó la polarización oculta [230]. La Figura 4 muestra las funciones Q_K parciales para este estado, así como la global.

Concluimos observando que, dado que los armónicos esféricos son un conjunto completo de funciones ortonormales en $\mathscr{S}_2$, pueden usarse para expandir la función de Husimi $Q(\mathbf{n})$; los coeficientes resultantes resultan ser los multipolos [47]:

$$\rho_{Kq} = \mathscr{C}_K \int_{\mathscr{S}_2} d^2\mathbf{n}\, Y_{Kq}(\mathbf{n})\, Q(\mathbf{n}), \tag{80}$$

donde la constante de normalización se elige como:

$$\mathscr{C}_K = \sqrt{\frac{4\pi}{2S+1}}\frac{1}{C^{SS}_{SS,K0}}, \tag{81}$$

de acuerdo con las definiciones anteriores.

Cuando se expresan en la base cartesiana estos multipolos aparecen de una manera muy transparente. Por ejemplo, los tres dipolos (ρ_{1q}) y los cinco cuadrupolos (ρ_{2q}) se pueden expresar, respectivamente, como:

$$\wp_i = \langle n_i \rangle, \qquad \mathscr{Q}_{ij} = \langle 3n_i n_j - \delta_{ij} \rangle, \tag{82}$$

donde

$$\langle f(\mathbf{n}) \rangle = \frac{\int_{\mathscr{S}_2} d^2\mathbf{n}\, f(\mathbf{n}) Q(\mathbf{n})}{\int_{\mathscr{S}_2} d^2\mathbf{n}\, Q(\mathbf{n})}. \tag{83}$$

Por lo tanto, estos multipolos aparecen entonces como aquellos estandar en electrostática, pero reemplazando la densidad de carga por $Q(\mathbf{n})$ y las distancias por direcciones [129]. También está claro que son los K-ésimos momentos direccionales del estado y, por tanto, estos términos resuelven rasgos angulares progresivamente más sutiles.

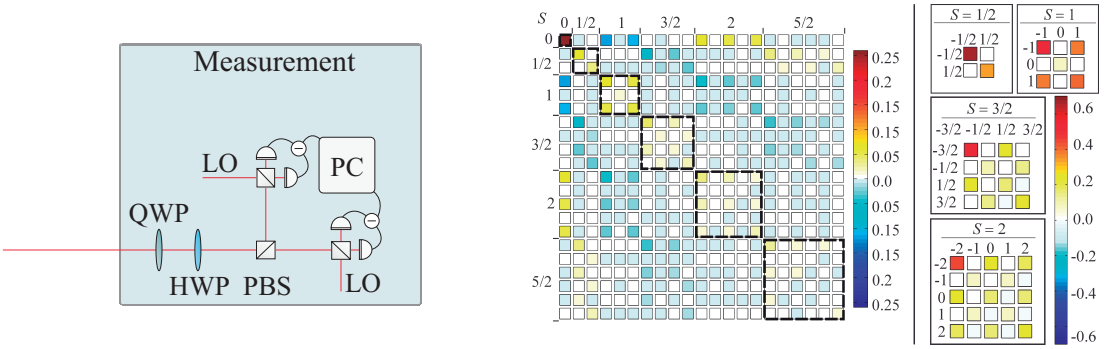

Figura 5: *Izquierda. Configuración experimental para una tomografía de dos modos. Los modos se combinan espacialmente en un divisor de haz polarizante (PBS) y la interferencia entre los modos se puede ajustar con la combinación de una placa de cuarto de onda (QWP) y una placa de media onda (HWP). Los estados de polarización se separan en componentes ortogonales y se realiza tomografía homodina. Derecha. Ilustración del sector de polarización medido (indicatos por bloques negros en línea discontinua) para un estado comprimido de polarización con amplitud coherente* $\alpha = 1{,}13$ *y parámetro de squeezing 0.41. Las subparcelas de la derecha representan diferentes variedades individualmente normalizadas.*

3.2. Tomografía de la polarización

La tomografía cuántica intenta inferir el estado cuántico desconocido a partir de los distintos resultados de una colección de mediciones realizadas en un conjunto finito de copias idénticas del sistema [187, 226]. Lo que hace especial el caso de la polarización es que el operador densidad contiene mucho más que información de la polarización y basta con reconstruir, entonces, el sector de polarización.

3.2.1. Regimen de variable discreta

En el régimen de variables discretas de uno o pocos fotones, el estado de polarización puede determinarse a partir de funciones de correlación de diferentes órdenes [241, 154, 130, 227, 30, 43, 182, 31, 3, 206, 9]. Dada la pequeña dimensionalidad del espacio de Hilbert involucrado, la reconstrucción del estado puede realizarse fácilmente.

En esta situación, es más conveniente trabajar en la base $\{H,V\}$. El caso típico es un estado de la forma $|\Psi\rangle = |\psi_H\rangle \otimes |\psi_V\rangle$. Una configuración típica para la reconstrucción de este tipo de estados se muestra en Fig. 5. Una placa de cuarto de onda (QWP) y una placa de media onda (HWP) permiten verificar la interferencia entre los modos de polarización ortogonales y controlar la base de medición. Para facilitar la de otra forma complicada tomografía de dos modos, los modos de polarización horizontal y vertical están separados por un divisor de haz polarizante y cada uno se caracteriza por tomografía homodina [167]. Las fases del oscilador local (LO) son escaneadas continuamente para adquirir los datos tomográficos y las salidas homodinas se almacenan en un ordenador.

Un ejemplo de la matriz densidad de un estado adquirido experimentalmente se muestra en la Fig. 5, donde se muestran las sub-matrices asociadas con diferentes sectores de polarización [185]. De hecho, ésto corresponde al caso particular de $|\psi_H\rangle = \hat{S}(r)\hat{D}(\alpha_H)|0_H\rangle$ y $|\psi_V\rangle = \hat{S}(r)|0_V\rangle$ con $\alpha_H = 1{,}33$ y $r = 0{,}41$.

También pueden utilizarse de manera eficiente los multipolos para caracterizar el estado. La configuración experimental consiste en una medición general de Stokes , como se muestra en Fig. 6, consistente en una placa de media onda $(\lambda/2,\theta)$, seguido de una placa de cuarto de onda $(\lambda/4,\phi)$ y un divisor de haz polarizante. En términos físicos, las placas de onda transforman la polarización entrante efectuando un desplazamiento del estado que puede ser descrito por el operador $\hat{D}(\mathbf{n})$. Esto permite la medida de los diferentes parametros de Stokes por la proyección en las bases $|S,m\rangle$. Las dos salidas del divisor de haz polarizante son medidas por detectores de fotones: la suma de fotocorriente da directamente el valor propio de $\hat{S}_0$, mientras que la diferencia da el observable $\hat{S}_\mathbf{n}$ [176].

En conjunto, esto indica que el esquema conduce a la distribución de probabilidad para $\hat{S}_\mathbf{n}$, de donde podemos inferir equivalentemente los momentos $\mathfrak{m}_\ell^{(S)}(\mathbf{n}) = \mathrm{Tr}[\hat{S}_\mathbf{n}^\ell \hat{\rho}^{(S)}]$. Para simplificar, nos limitamos a un subespacio con un número fijo de fotones S, pero todo puede extenderse sin problemas a un sector de polarización entero.

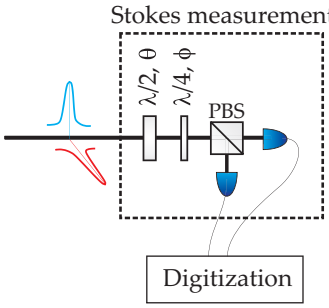

Figura 6: *Configuración para una medida de Stokes eficiente.*

Empezamos observando que los momentos medibles pueden ser expresados en términos de los multipolos como:

$$\mathfrak{m}_\ell^{(S)}(\mathbf{n}) = \mathrm{Tr}[\hat{S}_3^\ell \hat{D}(\mathbf{n})\,\hat{\rho}^{(S)}\,\hat{D}^\dagger(\mathbf{n})] = \mathrm{Tr}\left[\hat{S}_3^\ell \sum_{K=0}^{2S}\sum_{q,q'=-K}^{K} \rho_{Kq}^{(S)}\, D^K_{qq'}(\mathbf{n})\,\hat{T}^{(S)}_{Kq}\right], \tag{84}$$

donde $D^K_{q'q}(\mathbf{n})$ es de nuevo una matriz de rotación de Wigner. Esta traza se puede calcular utilizando la maquinaria del momento angular, y entonces los momentos salen conectados con los multipolos de una manera bastante elegante:

$$\mathfrak{m}_\ell^{(S)}(\mathbf{n}) = \sqrt{\frac{4\pi}{2S+1}} \sum_{K=0}^{\ell}\sum_{q=-K}^{K} \rho_{Kq}^{(S)}\, f_{K\ell}^{(S)}\, Y_{Kq}(\mathbf{n}), \tag{85}$$

donde $f_{K\ell}^{(S)} = \sum_m m^\ell C^{Sm}_{Sm,K0}$ ($K \leqslant \ell$). Dada la ortonormalidad de $Y_{Kq}(\mathbf{n})$, podemos invertir Eq. (85) de modo que obtenemos

$$\rho_{Kq}^{(S)} = \sqrt{\frac{2S+1}{4\pi}} \frac{1}{f_{K\ell}^{(S)}} \int_{\mathscr{S}^2} d\mathbf{n}\, \mathfrak{m}_\ell^{(S)}(\mathbf{n})\, Y^*_{Kq}(\mathbf{n}). \tag{86}$$

La reconstrucción del estado requiere entonces el conocimiento de *todos* los multipolos: esto implica medir *todos* los momentos en *todas* las direcciones, lo que resulta ser muy laborioso [186] .

No obstante, podemos atacar el problema de una manera mucho más económica. La idea central es que para determinar el K-ésimo multipolo, basta con realizar una medición de Stokes en $2K+1$ direcciones independientes. De hecho, la propuesta procede de forma recurrente: primero, medimos los momentos de primer orden en los tres ejes de coordenadas (u otros equivalentes) y reconstruimos $\rho_{1q}^{(S)}$ a través de una inversión lineal. La medición de los segundos momentos nos da:

$$\mathfrak{m}_2(\mathbf{n}) = \frac{1}{2S+1} f_{02}^{(S)} + \sqrt{\frac{4\pi}{2S+1}} f_{22}^{(S)} \sum_{q=-2}^{2} \rho_{2q}^{(S)}\, Y_{2q}(\mathbf{n}), \tag{87}$$

con $f_{02}^{(S)} = \frac{1}{3}S(S+1)(2S+1)$, $f_{22}^{(S)} = \frac{4}{5!}(2S+1)\sqrt{S(2S-1)(S+1)(2S+3)}$, mientras $f_{12}^{(S)} = 0$. Necesitamos fijar cinco direcciones óptimas para invertir ese sistema. Por ejemplo, podemos escoger las direcciones como aquellas que maximizan el ángulo mínimo entre las líneas y así, de alguna manera, separamos las mediciones sobre la esfera de Poincaré tanto como sea posible [70]. El sistema puede entonces ser resuelto, y todo lo que necesitamos para caracterizar el proceso en segundo orden es conocido.

Podemos continuar con el procedimiento de esta manera hasta llegar al orden deseado. La elección de las direcciones apropiadas es, en general, una cuestión difícil si se quiere estar seguro acerca de la independencia lineal, pero se ha estudiado a fondo [123, 98]. En la práctica, métodos tales como el de máxima verosimilitud son mucho más eficientes en el manejo de esa inversión [187]. Esta estrategia ha sido experimentalmente puesta a prueba para pares de fotones generados en conversión paramétrica a la baja espóntanea; estos son, los estados $|1_H, 1_V\rangle$ [38].

3.2.2. Regimen de variable continua

Déjanos reconsiderar la medida de Stokes básica, como se esquematiza brevemente en Fig. 6. El campo a ser caracterizado se analiza utilizando un aparato para la medición general de la polarización que consiste en una placa

de media onda $(\lambda/2,\theta)$ seguido de una placa de cuarto de onda $(\lambda/4,\phi)$ y divisor de haz polarizante (PBS). En términos físicos, las placas de onda transforman la polarización de entrada permitiendo la medición de diferentes parámetros por la proyección sobre la base $|S,m\rangle$. Esta fotodetección puede ser modelada por las proyecciones $\hat{\Pi}_m^{(S)} = |S,m\rangle\langle S,m|$ por lo que para cada dirección $\mathbf{n}$ detectamos las probabilidades tomográficas:

$$w_m^{(S)}(\mathbf{n}) = \mathrm{Tr}[\hat{\rho}\,\hat{\Pi}_m^{(S)}(\mathbf{n})] = \mathrm{Tr}[\hat{\rho}\,\hat{D}(\mathbf{n})\hat{\Pi}_m^{(S)}\,\hat{D}^{\dagger}(\mathbf{n})]\,. \tag{88}$$

que corresponden a la probabilidad de detectar $n_H = S+m$ fotones en el modo horizontal y simultáneamente $n_V = S-m$ fotones en el vertical. Por supuesto, cuando el número total de fotones no se mide y sólo se observa la diferencia m, se reduce a $\hat{\Pi}_m = \sum_{S=|m|}^{\infty} |S,m\rangle\langle S,m|$.

La reconstrucción en cada subespacio invariante $\mathscr{H}_S$ puede llevarse a cabo de manera exacta ya que es esencialmente equivalente a un espín S [54, 10, 77, 144]. Uno puede proceder de diferentes maneras, pero quizás la más simple es buscar una representación integral de los tomogramas[176];

$$w_m^{(S)}(\mathbf{n}) = \frac{1}{2\pi}\int_0^{2\pi} d\omega\ \mathrm{Tr}[\hat{\rho}^{(S)}\,\exp(i\omega\hat{\mathbf{S}}\cdot\mathbf{n})]\,e^{-im\omega}\,, \tag{89}$$

Esto es, aparecen como la transformada de Fourier de la función característica para el observable $\hat{\mathbf{S}}\cdot\mathbf{n}$. Después de algunas manipulaciones directas, encontramos que:

$$\hat{\rho}^{(S)} = \frac{1}{4\pi}\sum_{m=-S}^{S}\int_{\mathscr{S}_2} d\mathbf{n}'\ w_m^{(S)}(\mathbf{n}')\,\mathscr{K}(\hat{\mathbf{S}}\cdot\mathbf{n}'-m)\,, \tag{90}$$

donde el kernel $\mathscr{K}(x)$ es:

$$\mathscr{K}(x) = \frac{2S+1}{4\pi^2}\int_0^{2\pi} d\omega\ \sin^2(\omega/2)\,e^{-i\omega x}\,. \tag{91}$$

Aunque Eq. (90) es una solución formal, es más práctico asignar esta matriz de densidad a la correspondiente función de Husimi Q. Para este propósito, sólo necesitamos calcular los elementos de matriz del kernel $\mathscr{K}_S(x)$. La forma más directa de proceder es notar que:

$$\langle S,\mathbf{n}|\mathscr{K}(\mathbf{n}'\cdot\hat{\mathbf{S}}-n)|S,\mathbf{n}\rangle = \frac{2S+1}{4\pi^2}\int_0^{2\pi} d\omega\ \sin^2(\omega/2)\,e^{-im\omega}\,[\cos(\omega/2)-i\sin(\omega/2)\cos\chi]^{2S}\,, \tag{92}$$

donde $\cos\chi = \mathbf{n}\cdot\mathbf{n}'$. En el límite de $S\gg 1$ la integral en Eq. (92) se reduce a $d^2\delta(x)/dx^2$ evaluado en $x = S\mathbf{n}\cdot\mathbf{n}'-m$. Dado que m puede tomarse como una variable cuasicontinua, integramos por partes para obtener

$$Q(S,\mathbf{n}) = \frac{2S+1}{4\pi^2}\int_{-\infty}^{\infty} dm\int_{\mathscr{S}_2} d\mathbf{n}'\,\frac{d^2 w_m^{(S)}(\mathbf{n})}{dm^2}\,\delta(S\mathbf{n}\cdot\mathbf{n}'-m)\,. \tag{93}$$

Esto significa que, en el límite de un gran números de fotones, se reduce a una transformada de Radón inversa [80] de los tomogramas medidos de manera que el cálculo de $Q(S,\mathbf{n})$ se simplifica en gran manera.

En la Fig. 7, mostramos una superficie de contorno de $Q(S,\mathbf{n}) =$ constante en el espacio de Poincaré con S_1, S_2 y S_3 como los ejes ortogonales para estados comprimidos como los descritos en Ref. [176]. La forma elipsoidal del estado es claramente visible. La dirección anticomprimida del elipsoide está dominada por el exceso de ruido. También dibujamos gráficos de densidad de las proyecciones en los planos de coordenadas de la función Q anterior. El contorno elíptico en el plano S_1 - S_3 está ligeramente girado, lo cual está relacionado con el ángulo de compresión [117]. Las proyecciones en los planos S_1 - S_2 y S_2 - S_3 muestra una expansión adicional del estado comprimido en la dirección S_3 causada por el imperfecto contraste de polarización en la configuración de medición que mezcla algo de la anticompresión en la dirección S_3. Como la excitación clásica del estado se produce en la dirección S_3, se espera alcanzar el límite "shot-noise" en esta proyección.

Sumando sobre todos los valores de S obtendremos la función $Q(\mathbf{n})$ total, que es una distribución de probabilidad sobre la esfera unidad de Poincaré y está correctamente normalizada.

La reconstrucción de Radón requiere medir un gran conjunto de datos para obtener una representación razonablemente precisa del estado. Hay dos razones principales para esto: las integrales se aproximan por sumas finitas y el kernel (91) es singular, por lo que algún filtrado *ad hoc* de los datos sin procesar es necesario. Adquirir conjuntos de

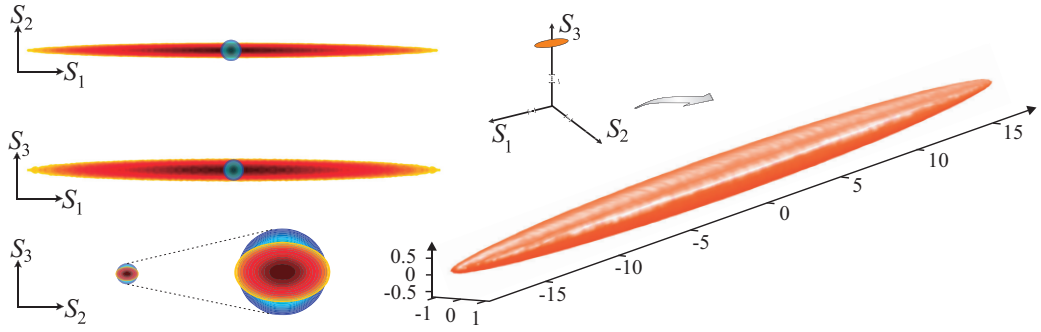

Figura 7: *(Derecha) Superficie de contorno de nivel $1/e$ (desde el máximo) de la función de Husimi $Q(S,\mathbf{n})$ para el estado de polarización comprimida. (Izquierda) Secciones de la función Q a través de los tres planos de coordenadas. En azul mostramos la sección isotrópica para un estado coherente, que usamos como unidad para todas las gráficas.*

datos tan grandes puede ser imprudente, porque exige largos tiempos de medición. Asegurar la estabilidad adecuada de la configuración es esencial y podría ser difícil dependiendo del estado cuántico medido. Esta limitación puede ser evitada adoptando un método estadísticamente motivado, como el de máxima verosimilitud [187].

Para un amplio tipo de estados, los tomogramas registrados son gaussianos, lo que parece requerir una reconstrucción de máxima verosimilitud gaussiana [236]. La gaussianidad se usa como información a priori sobre la señal, que nos ayuda a reducir drásticamente el número de parámetros libres, tal como se comprobó experimentalmente en Ref. [186].

4. Propuestas para la medida de la polarización

En la óptica clásica, los parámetros de Stokes y el grado clásico de polarización definido en (24) son suficientes para caracterizar la mayoría de los haces, ya que son estados de luz gaussiana. Tal descripción en términos de momentos de primer orden de las variables de Stokes puede extenderse ingenuamente al dominio cuántico como:

$$\mathbb{P}_S = \frac{|\langle\hat{\mathbf{S}}\rangle|}{\langle\hat{S}_0\rangle} = \frac{\sqrt{\langle\hat{S}_1\rangle^2+\langle\hat{S}_2\rangle^2+\langle\hat{S}_3\rangle^2}}{\langle\hat{S}_0\rangle}. \tag{94}$$

Nos referimos a esta definición como el grado semiclásico de polarización. Sin embargo, podemos esperar que $\mathbb{P}_S$ sea un grado incompleto. Esto se confirma cuando se examinan las dos situaciones extremas $\mathbb{P}_S = 1,0$, representando la luz completamente polarizada y completamente despolarizada, respectivamente. Por ejemplo, todos los estados coherentes SU (2) tienen $\mathbb{P}_S = 1$ y esto es válido para cualquier combinación de ellos en diferentes sectores de polarización, como, por ejemplo, los estados coherentes de Glauber $|\alpha_H,\alpha_V\rangle$. Pero esto significa que $\mathbb{P}_S = 1$ para estados arbitrariamente próximos al estado de vacío de dos modos $|0_H,0_V\rangle$, lo cual es un resultado extraño.

Por otro lado, hay estados de luz con $\mathbb{P}_S = 0$ que difícilmente pueden ser considerados como no polarizados. Esto da lugar al fenómeno de polarización oculta. Como se mencionó antes, un ejemplo de polarización oculta es el estado $|1_H,1_V\rangle$, que es $|1,0\rangle$ en la base de momento angular. Una rotación de 45° grados alrededor de su eje de propagación transforma este estado en $[(\sqrt{2}+i)|1,-1\rangle+(\sqrt{2}-i)|1,1\rangle]/\sqrt{6}$, que es ortogonal al estado $|1,0\rangle$, luego perfectamente distinguible del estado sin girar. Sin embargo, según el grado semiclásico de polarización, este estado no está polarizado. Esto se debe al hecho de que este cambio no puede ser detectado por ninguna combinación lineal de los operadores de Stokes, ya que requiere medidas de correlación de campo de orden superior. Por esta razón, tal vez sería mejor decir que tales estados tienen una polarización de orden superior.

4.1. Condiciones para las medidas de polarización

De la discusión anterior se puede concluir que una medida apropiada de polarización que asigna un número $\mathbb{P}(\hat{\rho})$ al operador de densidad $\hat{\rho}$ debe satisfacer algunos requisitos que capturan las propiedades de los operadores de Stokes y las transformaciones de polarización. Por lo tanto, requerimos [39]:

C.1 $\mathbb{P}(\hat{\rho}) = 0$ sii $\hat{\rho}$ es no polarizado

C.2 $\mathbb{P}(\hat{\rho}) = \mathbb{P}(\hat{U}\,\hat{\rho}\,\hat{U}^{\dagger})$ para cualquier transformación de polarización unitaria U.

C.3 $\mathbb{P}(\hat{\rho})$ no debe de depender de las coherencias entre diferentes subespacios.

La condición C1 excluye varias posibilidades como el grado semi-clásico de polarización, porque este grado considera como no polarizados, estados que tienen correlaciones de polarización de orden superior. Este requisito también impide la definición del grado de polarización en términos de la pureza de un estado $\mathscr{P} = \mathrm{Tr}(\hat{\rho}^2)$, ya que los estados cuánticos no polarizados abarcan toda la escala de pureza. Hay ejemplos de estados no polarizados entre los estados puros (el vacío de dos modos), y también hay estados no polarizados que están parcial o máximamente mezclados.

Condición C2 es simplemente invarianza SU(2), que es una característica obvia de cualquier medida.

La C3 también es razonable, ya que las transformaciones de polarización no producen coherencias entre diferentes subespacios, dado que los operadores de Stokes preservan el número de fotones y cualquier medida de una combinación lineal de estos operadores será independiente de cualquier coherencia entre las variedades. Podemos reformular C3 de una manera más cuantitativa. Con este fin, vamos a introducir el canal cuántico

$$\Lambda[\hat{\rho}] \to \sum_{S=0}^{\infty} \hat{\mathbb{1}}_S \hat{\rho}\, \hat{\mathbb{1}}_S \tag{95}$$

que puede ser visto como aleatorización de las fases entre superposiciones entre estados en diferentes variedades de excitación. Por lo tanto, el estado $\hat{\rho}$ y el $\hat{\rho}_{\mathrm{pol}} = \Lambda[\hat{\rho}]$ no pueden ser distinguidos en mediciones de polarización. Por ello, podemos reformular C.3 en la forma equivalente

C.3′ $\mathbb{P}(\hat{\rho}) = \mathbb{P}(\Lambda[\hat{\rho}]) = \mathbb{P}(\hat{\rho}_{\mathrm{pol}})$.

Una condición habitual para las medidas de polarización es también $0 \leqslant \mathbb{P}(\hat{\rho}) \leqslant 1$. Sin embargo, algunas candidatas a medidas de polarización, como la entropía, son sólo definidas positivas ($0 \leqslant \mathbb{S} < \infty$). En este caso, suele ser más importante el ordenamiento de los estados que el valor numérico de la medida. Por esta razón, un remedio común es la normalización $\mathbb{P} = \mathbb{S}/(1+\mathbb{S})$, que es una reescala de la medida que mantiene intacto el ordenamiento de los estados.

Aparte de las condiciones básicas C1–C3, la medida debe ser operativa, fácilmente mesurable y fácil de calcular. Sin embargo, estas condiciones son difíciles de cumplir al mismo tiempo.

En esta subsección, exploraremos varias propuestas para la definición de un grado cuántico de polarización. Es importante recalcar, sin embargo, que estas medidas inducen ordenamientos diferentes entre los estados, ya que parten de diferentes conceptos.

Antes de proceder mas allá, enfatizamos que una referencia físicamente significativa para cualquier grado de polarización es la proporcionada por la luz no polarizada. De hecho, los estados de luz completamente despolarizados pueden definirse adecuadamente como los estados invariantes bajo cualquier transformación de polarización. Esto exige que toda la distribución de probabilidad sea invariante SU(2) [193, 4]; esto es,

$$[\hat{\rho}, \hat{\mathbf{S}}] = 0\,, \tag{96}$$

De donde se deduce que en cada subespacio invariante el estado es completamente mixto [221]

$$\hat{\rho}^{(S)}_{\mathrm{unpol}} = \frac{1}{2S+1}\,\hat{\mathbb{1}}_{2S+1}\,. \tag{97}$$

4.2. Medidas basadas en distancias

El concepto de polarización en la óptica cuántica puede ser cuantificado en términos de medidas de distancia. La idea principal es definir el grado de polarización como la distancia más corta entre el estado y el conjunto $\mathscr{U}$ de estados despolarizados dados por Eq. (97). Otras nociones tales como no clasicalidad [120, 86, 175], entrelazamiento [234] localización [169, 11, 108] e información cuántica [212, 59, 207, 61, 104] han sido formulados sistemáticamente en términos de distancias a un conjunto dado de estados. La distancia determina la distinguisibilidad de un estado con respecto a dicho conjunto.

Por lo tanto, parece razonable cuantificar el grado de polarización como

$$\mathbb{P}(\hat{\rho}) \propto \inf_{\hat{\sigma}\in\mathscr{U}} D(\hat{\rho}, \hat{\sigma})\,, \tag{98}$$

Donde $D(\hat{\rho},\hat{\sigma})$ es cualquier medida de distancia (no necesariamente una métrica) entre las matrices densidad $\hat{\rho}$ y $\hat{\sigma}$ de tal forma que $\mathbb{P}(\hat{\rho})$ satisface los requisitos C1–C3.

Hay muchas opciones no triviales para $D(\hat{\rho},\hat{\sigma})$ (por no trivial queremos decir que la elección no es una simple transformación de escala de ninguna otra distancia). Ninguna de ellas podría decirse que sea más importante que cualquier otra *a priori*, sino que el significado de cada candidata tendría que ser visto a través de suposiciones físicas. Para el caso de la polarización pueden considerarse varias distancias [146], como la distancia de Hilbert-Schmidt, Bures y Chernoff [102]:

$$\mathbb{P}_{\rm HS}(\hat{\rho}) = \inf_{\sigma\in\mathscr{U}} {\rm Tr}[(\hat{\rho}-\hat{\sigma})^2] \qquad \mathbb{P}_{\rm B}(\hat{\rho}) = 1-\sup_{\sigma\in\mathscr{U}}\sqrt{F(\hat{\rho},\hat{\sigma})} \qquad \mathbb{P}_{\rm C}(\hat{\rho}) = 1-\sup_{\sigma\in\mathscr{U}}\left[\inf_{t\in[0,1]}{\rm Tr}(\hat{\rho}^t\hat{\sigma}^{1-t})\right] \tag{99}$$

donde el ínfimo en Eq. (99) se toma sobre una función que es continua con respecto a t, y la fidelidad es [229, 135, 8]:

$$F(\hat{\rho},\hat{\sigma}) = \{{\rm Tr}[(\hat{\sigma}^{1/2}\hat{\rho}\hat{\sigma}^{1/2})^{1/2}]\}^2 \tag{100}$$

En su estado actual, estos grados no cumplen con el requisito C.3; es decir, estas medidas son sensibles a las coherencias entre los diferentes subespacios. Pero es muy fácil evitar este inconveniente si simplemente definimos la distancia no al estado, sino a su forma diagonal en bloques o sector de polarización; es decir, $\mathbb{P}_X(\hat{\rho}) = \mathbb{P}_X(\Lambda[\hat{\rho}])$ para $X\in\{{\rm HS},{\rm B},{\rm C}\}$.

Usando el hecho de que $\Lambda[\hat{\rho}]$ y $\hat{\sigma}$ conmutan, encontramos las siguientes fórmulas generales:

$$\mathbb{P}_{\rm HS}(\hat{\rho}) = \sum_{S=0}^{\infty} P_S^2\left(\xi_S^{(2)}-\frac{1}{2S+1}\right), \qquad \mathbb{P}_{\rm B}(\hat{\rho}) = 1-\left[\sum_{S=0}^{\infty}\frac{P_S}{2S+1}\left(\xi_S^{(1/2)}\right)^2\right]^{1/2},$$
$$\mathbb{P}_{\rm C}(\hat{\rho}) = 1-\inf_{t\in[0,1]}\left[\sum_{S=0}^{\infty}P_S(2S+1)^{1-1/t}(\xi_S^{(t)})^{1/t}\right]^t, \tag{101}$$

donde $\lambda_{S,n}$ son los valores propios de $\hat{\rho}^{(S)}$ y $\xi_S^{(t)} = \sum_{n=0}^{2S}\lambda_{S,n}^t$.

4.3. Medidas en el espacio de fases

Las ideas discutidas en la subsección anterior 4.2 pueden ser traducidas directamente al espacio de fases. El grado de polarización puede definirse naturalmente como la distancia entre la función de Husimi Q y la función correspondiente a la luz no polarizada. En este contexto, la luz no polarizada se define por una distribución uniforme,

$$Q_{\rm unpol}(\mathbf{n}) = \frac{1}{4\pi} \tag{102}$$

lo que concuerda con (97). Entonces definimos la distancia como [163, 164]:

$$D_Q(\hat{\rho}) = \frac{1}{4\pi}\int_{\mathscr{S}_2} d\mathbf{n}\ [Q(\mathbf{n})-1]^2 = \frac{1}{4\pi}\left[\int_{\mathscr{S}_2} d\mathbf{n}\, Q^2(\mathbf{n})\right]-1\,. \tag{103}$$

El término relevante en el miembro derecho de (103) puede ser considerado como un caso particular de una clase general de medidas de localización [169, 108]

$$M_r = \left[\int_{\mathscr{S}_2} d\mathbf{n}\, Q^{1+r}(\mathbf{n})\right]^{1/r}, \tag{104}$$

cuyas propiedades matemáticas han sido estudiadas en detalle [114]. Dado que:

$$\lim_{r\to 0} M_r = \int_{\mathscr{S}_2} d\mathbf{n}\, Q(\mathbf{n})\ln Q(\mathbf{n})\,, \tag{105}$$

éstas incluyen la entropía de Wehrl [239, 240] como caso límite.

En términos físicos, la extensión de la función Q nos da una indicación del grado de polarización del estado. Para los estados que están muy dispersos sobre la esfera unidad el grado de polarización es pequeño, como en el caso del estado no polarizado. Para los estados que tienen un pico máximo pronunciado alrededor de algún valor de las coordenadas esféricas, se espera que el grado de polarización sea alto.

Mencionamos que la función de Wigner ya se utilizó como medida del área ocupada por un estado cuántico en el caso de variables continuas [119]. Sin embargo, en el caso de la esfera, la integral de $W^2(\mathbf{n})$ da como resultado la pureza [232]. Esta es una de las razones convincentes por las que utilizamos la función de Husimi Q a lo largo de esta tesis.

Dado que D_Q oscila de 0 a ∞, el grado de polarización asociado, de acuerdo con nuestra argumentación anterior, es:

$$\mathbb{P}_Q(\hat{\rho}) = \frac{D_Q(\hat{\rho})}{D_Q(\hat{\rho})+1}\,. \tag{106}$$

Los únicos estados con $\mathbb{P}_Q = 0$ son los estados no polarizados. En contraste con la definición clásica, hay estados con $\langle\hat{\mathbf{S}}\rangle = 0$ y $\mathbb{P}_Q \neq 0$. Esto ocurre porque $\mathbb{P}_Q$ es una función de todos los momentos de los operadores de Stokes y no sólo del primero. Además, la definición de $\mathbb{P}_Q$ es invariante bajo transformaciones SU(2) aplicadas al estado del campo. Ésto significa que el grado de polarización depende de la forma de la función Q, pero no de su posición u orientación en la esfera de Poincaré.

Para los estados coherentes de SU(2) $|S,\mathbf{n}\rangle$ la función Q viene dada por Eq. (66). El grado de polarización asociado es:

$$\mathbb{P}_Q(|S;\mathbf{n}\rangle) = \left(\frac{2S}{2S+1}\right)^2. \tag{107}$$

De hecho, los estados máximamente polarizados, según este grado de polarización, son los estados coherentes SU(2). Esto se debe a que como estos estados tienen un pico muy pronunciado en algún punto de la esfera, son los estados de polarización de mínima incertidumbre y los estados que maximizan la diferencia con una distribución uniforme de estados de polarización.

4.4. Enfoque operacional

Está claro que un estado que no es invariante bajo todas las posibles transformaciones lineales de polarización tiene un grado finito de polarización cuántica. Por lo tanto, podemos utilizar la distinguibilidad de un estado bajo todas las posibles transformaciones de polarización como un grado de polarización. Si usamos $\mathrm{Tr}(\hat{\rho}_1\hat{\rho}_2)$ como la distinguibilidad para los estados mixtos, se podría definir [36, 40]

$$\mathbb{P}_{\mathrm{d}}(\hat{\rho}) = \left[1 - \inf_{\hat{U}\in \mathrm{SU}(2)} \sum_{S=0}^{\infty} P_S\ \mathrm{Tr}(\hat{\rho}^{(S)}\,\hat{U}\,\hat{\rho}^{(S)}\,\hat{U}^{\dagger})\right]^{1/2}. \tag{108}$$

Esta es la superposición mínima promedio entre un estado y todos sus estados transformados SU (2). Por lo tanto, da la visibilidad máxima que se puede lograr utilizando un interferómetro de polarización. El inconveniente de esta definición es que no es trivial determinar el grado de polarización para un estado dado, ya que, en general, no existe una manera obvia de encontrar el $\hat{U}_{pol}$ que maximiza la visibilidad polarimétrica. Esta medida de polarización es diferente a las anteriores porque asigna grado de polarización uno para estados con un número finito de excitaciones. Se ha demostrado [215] que todos los estados puros con un número impar de excitaciones alcanzan grado uno de polarización bajo esta definición. También es cierto que para $N = 1$, es decir, estados de un solo fotón, la definición implica que cualquier estado puro está completamente polarizado, ya que una transformación U puede transformar el estado en su ortogonal, situado diametralmente opuesto en la esfera. Se puede conjeturar que los estados puros con un número par de excitaciones N, excepto el vacío de dos modos, también están completamente polarizados de acuerdo con esta medida de polarización, pero todavía no hay una prueba de ello.

La última especulación hace que sea tentador definir un grado de polarización tal que los estado puros con un número determinado de excitaciones estén polarizados al máximo, es un grado de polarización en términos de las purezas de los estados en cada subespacio de excitación [39]:

$$\mathbb{P}_{\mathrm{p}}(\hat{\rho}) = \sum_{S=\frac{1}{2}}^{\infty} \frac{1}{2S}[(2S+1)\ \mathrm{Tr}(\hat{\rho}_S^2) - 1]\,, \tag{109}$$

Donde necesitamos la definición adicional $\mathbb{P}_{\rm p}|0,0\rangle = 0$. Nuevamente, los estados máximamente polarizados son los estados puros en cada subespacio de excitación. La única propiedad de los operadores de Stokes que utiliza esta medida consiste en su definición como suma directa sobre los subespacios de excitación con un número distinto de fotones. Como consecuencia, esta medida cuantifica la distinguibilidad bajo las transformaciones unitarias generales que preservan la energía y no la distinguibilidad en el caso más concreto de transformaciones de polarización. Esta medida también se basa en la conjetura crítica de que los estados puros en cada subespacio de excitación están completamente polarizados. Al igual que muchos de los otros grados de polarización, una medida de $\mathbb{P}_{\rm p}$ es difícil ya que determinar las purezas requiere que se realice una tomografía de la polarización.

4.5. Grados de polarización de orden superior

En este punto, debe de haber quedado claro que muchas de las dificultades al definir un grado apropiado de polarización se pueden remontar al hecho de que la polarización clásica se construye sobre todo en función de los momentos de primer orden de las variables de Stokes, mientras que los momentos de orden más alto pueden jugar un mayor papel en los campos cuánticos. Una comprensión completa de los sutiles efectos de polarización que surgen en el mundo cuántico requeriere una caracterización de las fluctuaciones de polarización de orden superior, como sucede en la teoría de la coherencia, donde se necesita, en general, una jerarquía de funciones de correlación [173].

Hemos visto que los multipolos contienen la información de las fluctuaciones de orden superior, ordenadas de la manera apropiada. Esto sugiere considerar la distribución acumulativa [79]

$$\mathscr{A}_M^{(S)} = \sum_{K=1}^{M} \sum_{m=-K}^{K} |\rho_{Kq}^{(S)}|^2 , \tag{110}$$

que contiene toda la información hasta el orden M. Sabemos, por la teoría de probabilidad, que tiene propiedades notables [132]. Por otra parte, nuestra reconstrucción anterior en la Sección 3.2 deja en clara evidencia que para obtener el multipolo de orden K-ésimo, se necesita determinar todos los multipolos anteriores. Como con cualquier distribución acumulativa, $\mathscr{A}_M^{(S)}$ es una función monótona no decreciente del orden multipolar, con $\mathscr{A}_{2S}^{(S)}$ siendo proporcional a la pureza del estado [excepto por la contribución monopolar, que no está incluida en (110)].

Para los estados coherentes de SU (2), obtenemos

$$\mathscr{A}_{M,\mathrm{SU}(2)}^{(S)} = \frac{2S}{2S+1} - \frac{[\Gamma(2S+1)]^2}{\Gamma(2S-M)\Gamma(2S+M+2)} , \tag{111}$$

ha sido demostrado [37] que este valor es realmente máximo para cada M entre todos los estados en el subespacio con S fijo. Esto sugiere la definición de una jerarquía de grados de polarización que mide la información de la polarización cuando se miden los operadores de Stokes hasta el orden M:

$$\mathbb{P}_M = \sum_S P_S \left(\frac{\mathscr{A}_M^{(S)}}{\mathscr{A}_{M,\mathrm{SU}(2)}^{(S)}} \right)^{1/2} . \tag{112}$$

De acuerdo con (112), $\mathbb{P}_M = 1$ (para cada M) para estados coherentes SU(2), lo que es compatible con la idea de que son los estados más localizados sobre la esfera.

Para el caso particular pero significativo del dipolo ($M = 1$), Eq. (112) se reduce a:

$$\mathbb{P}_1 = \sum_S^{\infty} P_S \frac{\sqrt{\langle \hat{S}_1 \rangle^2 + \langle \hat{S}_2 \rangle^2 + \langle \hat{S}_3 \rangle^2}}{\langle \hat{S}_0 \rangle} , \tag{113}$$

y los valores medios se calculan en cada subespacio S. Curiosamente, esta definición se ha propuesto recientemente como una forma de eludir las deficiencias del grado estándar de polarización [153]; en nuestro enfoque, emerge de una manera bastante natural.

Para los estados coherentes en cuadratura, el resultado es:

$$\mathbb{P}_M(|\alpha_+, \alpha_-\rangle) = \sum_{S=M/2}^{\infty} \frac{e^{-\bar{N}} \bar{N}^{2S}}{(2S)!} \simeq \frac{1}{2} \mathrm{erfc} \left(\frac{M - \bar{N}}{\sqrt{2\bar{N}}} \right) , \tag{114}$$

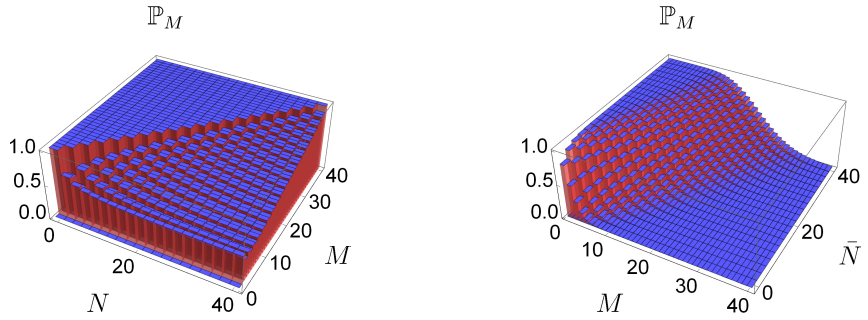

Figura 8: *(Color online) Grado de polarización $\mathbb{P}_M$ como función del orden multipolar M para el estado $|S,0\rangle$ (izquierda) y un estado coherente en cuadraturas $|\alpha_+,\alpha_-\rangle$ con un número promedio de fotones $\bar{N} = |\alpha_+|^2 + |\alpha_-|^2$ (derecha).*

Aquí, $\bar{N}$ es el número medio de fotones y la segunda igualdad, en términos de la función de error complementaria, es válida para $\bar{N} \gg 1$. A partir de las propiedades de esta función, podemos estimar que los multipolos que contribuyen efectivamente son, a grosso modo, de 1 a $\bar{N}$. En la Fig. 8 representamos $\mathbb{P}_M$ para los estados $|S,0\rangle$ y $|\alpha_+,\alpha_-\rangle$. Para $M = 2$, esto da:

$$\mathbb{P}_2(|\alpha_+,\alpha_-\rangle) = 1 - (1+\bar{N})\exp(-\bar{N})\,, \tag{115}$$

Que tiende a la unidad cuando el número medio de fotones $\bar{N}$ es suficientemente grande, de acuerdo con los enfoques de segundo orden anteriores [141].

5. Resultados

La constitución de la luz no polarizada fue investigada desde el principio de la óptica moderna. De hecho, Verdet [235] propusó una caracterización lúcida de lo que ellos llamaban luz "natural" usando las proyecciones de la intensidad sobre los ejes de un sistema de coordenadas cartesianas girado. Los estados no polarizados son aquellos que permanecen invariables bajo cualquier rotación de ese sistema de coordenadas y bajo cualquier cambio de fase entre sus componentes rectangulares.

En la óptica clásica, las componentes de un campo de luz no polarizada están bien modeladas por un proceso aleatorio gaussiano estacionario, no correlacionado y con cero promedio [231]. Las condiciones de invariancia anteriores determinan así toda la estructura probabilística de las intensidades proyectadas [27]. Sin embargo, como la teoría estándar está limitada a los momentos de primer orden, la luz no polarizada se presenta como aquella con un vector Stokes promedio cero, que en términos geométricos significa que es sólo el origen de la esfera de Poincaré.

5.1. Estados despolarizados a orden M

A nivel cuántico, el requisito de invariancia fija de una vez por todas la estructura de la matriz densidad, así que especifica la distribución de probabilidad y, como resultado, todos los momentos de las variables de Stokes, como ya hemos argumentado. Sin embergo, uno podría pensar en extender esta noción: cuando todos los multipolos hasta un orden dado (digamos M) desaparecen, el estado carece de información de polarización hasta ese orden y por lo tanto se llamará despolarizado a orden M. La imagen clásica coincide con la teoría de primer orden, mientras que la condición cuántica implica que todos los multipolos son idénticamente nulos.

En consecuencia, vamos a decir que un estado es despolarizado a orden M cuando $\mathbb{P}_M^{(S)} = 0$, esto obviamente implica $\mathscr{A}_M^{(S)} = 0$; i.e., todos los multipolos hasta el orden M se anulan. Vamos a denotar estos estados como: $\hat{\rho}^{(S)}_{\text{unpol},K}$. En términos más físicos, la condición de despolarización de orden M equivale a imponer que los momentos $\langle \hat{\mathbf{S}}_{\mathbf{n}}^{\ell} \rangle$ son independientes de la dirección $\mathbf{n}$ para $\ell = 1,\ldots,M$ (i.e., son isotrópicos). Por lo tanto, todos los momentos hasta el orden M no muestran ninguna estructura angular, mientras que los de orden superior sí. Tenga en cuenta,

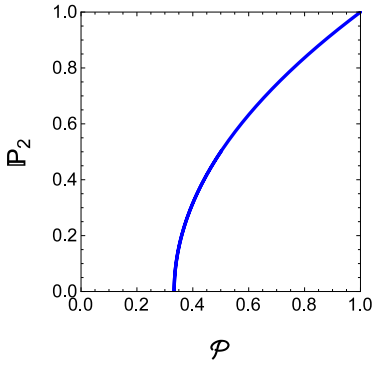

Figura 9: *El grado de polarización de segundo orden en función de la pureza, para los estados despolarizados de primer orden* (120).

sin embargo, que los estados despolarizados a orden M llevan información de polarización cuando uno mira a momentos de orden superior.

Esto se ha conocido como polarización oculta, de acuerdo con la terminología acuñada por Klyshko [148, 147, 149], aunque sería mejor decir que tales estados muestran una polarización de orden superior [111].

Ilustramos este punto con algunos ejemplos relevantes: empezamos con estados de un solo fotón ($S = 1/2$). La expansión multipolar de un estado general de un solo fotón es

$$\hat{\rho}^{(1/2)} = \rho_{00}^{(1/2)}\,\hat{T}_{00}^{(1/2)} + \sum_q \rho_{1q}^{(1/2)}\,\hat{T}_{1q}^{(1/2)}\,. \tag{116}$$

Puesto que el estado tiene solamente componente dipolar, las descripciones cuánticas y clásicas coinciden y estos estados pueden ser despolarizados solamente a primer orden. La positividad limita los posibles valores del dipolo al rango $0 \leqslant \mathscr{A}_1^{(1/2)} \leqslant 1/2$. La condición $\mathscr{A}_1^{(1/2)} = 0$, fija los estados no polarizados; viz

$$\rho_{\text{unpol},1}^{(1/2)} = \frac{1}{2}\,\mathbb{1}_2\,. \tag{117}$$

Enfatizamos, no obstante, que como todos los objetos cuánticos, estos estados sólo pueden ser considerados como elementos de un conjunto [190].

Para estados de dos fotones, hay estados despolarizados a primer orden (o clásicamente) y a segundo orden (o cuánticamente) . La condición general para la despolarización de primer orden es que el término dipolar se anule; i.e.,

$$\hat{\rho}_{\text{unpol},1}^{(1)} = \rho_{00}^{(1)}\,\hat{T}_{00}^{(1)} + \sum_q \rho_{2q}^{(1)}\,\hat{T}_{2q}^{(1)}\,, \tag{118}$$

Con la restricción adicional de la positividad. El caso de los estados axialmente simétricos, ya considerados en la Eq. (60) merece una atención especial ya que siempre se pueden diagonalizar a través de las rotaciones SU (2); viz, $\hat{\rho}_{\text{ax}}^{(1)} = \hat{U}(\alpha,\beta,\gamma)\,\hat{\rho}_d^{(1)}\,\hat{U}^\dagger(\alpha,\beta,\gamma)$ con

$$\hat{\rho}_d^{(1)} = \text{diag}(\lambda_1,\lambda_2,\lambda_3) = \frac{1}{\sqrt{3}}\hat{T}_{00}^{(1)} + \frac{\lambda_1-\lambda_3}{\sqrt{2}}\hat{T}_{10}^{(1)} + \frac{1-3\lambda_2}{\sqrt{6}}\hat{T}_{20}^{(1)}\,. \tag{119}$$

Aquí, $\text{diag}(d_1,\ldots,d_n)$ representa una matriz diagonal cuyos elementos diagonales son aquellos en el argumento.

El estado es despolarizado a primer orden cuando $\lambda_1 = \lambda_3$. Como $\text{Tr}(\hat{\rho}_d) = 1$, podemos escribir

$$\hat{\rho}_{\text{unpol},1}^{(1)} = \text{diag}(\lambda, 1-2\lambda, \lambda) \tag{120}$$

y la positividad fuerza a que $0 \leqslant \lambda \leqslant 1/2$, i.e., $0 \leqslant \mathscr{A}_2^{(1)} \leqslant 2/3$. Ambas pureza $\mathscr{P}^{(1)} = \text{Tr}\{[\hat{\rho}_d^{(1)}]^2\}$ y grado de polarización de segundo orden $\mathbb{P}_2^{(1)}$ dependen de λ:

$$\mathscr{P}^{(1)} = 6\lambda^2 - 4\lambda + 1\,, \qquad \mathbb{P}_2^{(1)} = \sqrt{(3\lambda-1)^2}\,, \tag{121}$$

mientras $\mathbb{P}_1 = 0$ como anticipamos. Ésto puede ser reescrito como

$$\mathbb{P}_2 = \sqrt{[3\mathscr{P} - 1]/2}, \tag{122}$$

Como se representa en la Fig. 9 . El grado máximo de $\mathbb{P}_2$ se alcanza para los estados puros

$$|\Psi^{(1)}_{\text{unpol},1}\rangle = \frac{1}{\sqrt{2}} \sin\beta[e^{i\alpha}|1,1\rangle - e^{-i\alpha}|1,-1\rangle] + \cos\beta|1,0\rangle, \tag{123}$$

y son la transformación del estado $|1,0\rangle$ bajo transformaciones SU(2) $\hat{U}(\alpha,\beta,\gamma)$. Estos estados han servido como la muestra para verificar experimentalmente la existencia de polarización oculta [230, 215]. Para un análisis más detallado de estos estados, el lector es referido a Ref. [78].

5.2. Reyes cuánticos

5.2.1. Representación de Majorana

Los estados coherentes SU(2) se pueden identificar con un punto en la esfera, y se dice que son los estados más clásicos. Además, tienen propiedades extremas ventajosas, tales como la varianza total mínima de $\hat{\mathbf{S}}$ [82] o entropía mínima de Wehrl [160, 156, 161]. En nuestro contexto, es notable que tengan máxima potencia multipolar acumulativa $\mathscr{A}_M^{(S)}$ para cualquier orden M [79]. Resulta irresistible preguntar que estados alcanzan el mínimo de esta magnitud, ya que pueden considerarse en cierto sentido como "lo opuesto" de los estados coherentes de SU(2) y por tanto los más no clásicos.

Para investigar este punto es ventajoso usar la representación estelar de Majorana [171], que nos permite representar un estado de espín en $\mathscr{H}_S$ como $2S$ puntos en la esfera unidad. Varias décadas después de su concepción, esta representación ha atraído recientemente una gran atención en varios campos [200, 155, 159, 84, 74, 162].

El método es una generalización directa de la esfera de Bloch para una partícula de espín-1/2 y utiliza la función de onda en la representación de estados coherentes; esto es, $\Psi(\mathbf{n}) = \langle \mathbf{n}|\Psi\rangle$ (para aligerar la notación, obviaremos la etiqueta S, ya que nos estamos restringiendo siempre a un espín fijo). Una vez que insertamos la unidad en términos de los estados $|S,m\rangle$, y tomamos en cuenta el valor de la superposición $\langle \mathbf{n}|S,m\rangle$, obtenemos

$$\Psi(\mathbf{n}) = \sum_{m=-S}^{S} \sqrt{\frac{(2S)!}{(S-m)!(S+m)!}} \Psi_m \, \zeta^{S+m}, \tag{124}$$

donde $\zeta = \tan(\theta/2)e^{i\phi}$, que es sólo la proyección estereográfica de un punto de la esfera unitaria con el ángulo (θ,ϕ). Aparte del factor positivo no esencial, este es un polinomio de orden $2S$; por lo tanto, $|\Psi\rangle$ se determina por el conjunto $\{z_i\}$ de los $2S$ ceros complejos de $\Psi(\mathbf{n})$, adecuadamente completados por puntos en el infinito si el grado del polinomio es menor que $2S$. La configuración de puntos resultante en la esfera unidad se llama la constelación de Majorana asociada al estado $|\Psi\rangle$.

Hay una manera complementaria de introducir el polinomio de Majorana, que proporciona una interpretación perspicaz de la representación de Majorana.

Cualquier estado puro $|\Psi\rangle \in \mathscr{H}_S$ puede ser factorizado en términos de los operadores bosónicos $\hat{a}_\pm$ como:

$$|\Psi\rangle = \frac{1}{\sqrt{\mathscr{N}}} \prod_{m=1}^{2S} \left[\cos\left(\frac{\theta_m}{2}\right) \hat{a}_+^\dagger + e^{i\phi_m} \sin\left(\frac{\theta_m}{2}\right) \hat{a}_-^\dagger \right] |0_+, 0_-\rangle, \tag{125}$$

Donde $\mathscr{N}$ es un factor de normalización, $|0_+,0_-\rangle$ es el vacio de dos modos y los ángulos θ_m y ϕ_m satisfacen las restricciones naturales $0 \leqslant \theta_m \leqslant \pi$ y $0 \leqslant \phi_m < 2\pi$. Así, cada factor en (125) se puede representar como un punto en la esfera unidad de Poincaré . Puesto que los operadores $\hat{a}_+^\dagger$ y $\hat{a}_-^\dagger$ crean una excitación en modos circularmente polarizados en sentido derecha e izquierda respectivamente, cada uno de los factores de (125) también se puede interpretar como creando una "componente de excitación" en un estado de polarización correspondiente a su posición en la esfera [32].

Una rotación de SU(2) simplemente corresponde a una rotación sólida de la constelación de Majorana. Por lo tanto, una transformación de SU(2) no afecta el grado de polarización del estado: los estados con la misma constelación, independientemente de su orientación relativa, tienen los mismos invariantes de polarización. Para los estados coherentes de SU(2), la constelación de Majorana colapsa a un solo punto de la esfera unidad. Intuitivamente, se podría adivinar que los estados con polarización tan isotrópica como sea posible tendrán una constelación tan simétrica como sea posible.

Cuadro 1: *Estados que anulan $\mathscr{A}_M$ para los valores indicados de S. En la segunda columna, indicamos el orden M, que conjeturamos es el más alto posible. Damos las componentes no nulas del estado Ψ_m ($m=-S,\ldots,S$) y la constelación de Majorana.*

S	M	Estado	Constelación
1	1	$\Psi_0=1$	línea radial
$\frac{3}{2}$	1	$\Psi_{\pm\frac{3}{2}}=\frac{1}{\sqrt{2}}$	triángulo ecuatorial
2	2	$\Psi_{-1}=\frac{2}{\sqrt{3}},\quad \Psi_2=\sqrt{\frac{1}{3}}$	tetraedro
$\frac{5}{2}$	1	$\Psi_{\pm\frac{3}{2}}=\frac{1}{\sqrt{2}}$	triangulo ecuatorial + polos
3	3	$\Psi_{\pm 2}=\frac{1}{\sqrt{2}}$	octaedro
$\frac{7}{2}$	2	$\Psi_{-\frac{5}{2}}=\Psi_{\frac{1}{2}}=\sqrt{\frac{7}{18}},\quad \Psi_{\frac{7}{2}}=\sqrt{\frac{2}{9}}$	dos triangulos + polo
4	3	$\Psi_{\pm 4}=\sqrt{\frac{5}{24}},\quad \Psi_0=\sqrt{\frac{7}{12}}$	cubo
$\frac{9}{2}$	2	$\Psi_{\pm\frac{9}{2}}=\frac{1}{\sqrt{6}},\quad \Psi_{\pm\frac{3}{2}}==\frac{1}{\sqrt{3}}$	tres triángulos
5	3	$\Psi_{\pm 5}=\frac{1}{\sqrt{5}},\quad \Psi_0=\frac{3}{\sqrt{5}}$	prisma pentagonal
$\frac{11}{2}$	3	$\Psi_{\pm\frac{11}{2}}=\frac{\sqrt{17}}{12},\quad \Psi_{\pm\frac{5}{2}}=i\frac{\sqrt{55}}{12}$	pentágono + dos triángulos
6	5	$\Psi_{\pm 5}=\pm\frac{\sqrt{7}}{5},\quad \Psi_0=-\frac{\sqrt{11}}{5}$	icosaedro
7	4	$\Psi_{\pm 6}=\sqrt{\frac{854}{3645}},\quad \Psi_{\pm 3}=\sqrt{\frac{637}{13420}}+i\sqrt{\frac{512603}{9783180}}$ $\Psi_0=\sqrt{\frac{12561757}{163053000}}-i\sqrt{\frac{512603}{2013000}}$	tres cuadrados + polos
10	5	$\Psi_{\pm 10}=\sqrt{\frac{187}{1875}},\quad \Psi_{\pm 5}=\pm\sqrt{\frac{209}{625}},\quad \Psi_0=\sqrt{\frac{247}{1875}}$	dodecaedro deformado

5.2.2. Estados extremos de la distribución acumulativa: los Reyes cuánticos

La distribución $\mathscr{A}_M^{(S)}$ puede considerarse como un funcional no lineal de la matriz de densidad $\hat{\rho}^{(S)}$. Por ese motivo, se puede tratar de determinar los estados extremos de $\mathscr{A}_M^{(S)}$ para cada orden M. Consideraremos solamente estados puros, que expandiremos como $|\Psi\rangle=\sum_{m=-S}^{S}\Psi_m|S,m\rangle$, con coeficientes $\Psi_m=\langle S,m|\Psi\rangle$. Obtenemos fácilmente que

$$\mathscr{A}_M=\sum_{K=1}^{M}\sum_{q=-K}^{K}\frac{2K+1}{2S+1}\left|\sum_{m,m'=-S}^{S}C_{Sm,Kq}^{Sm'}\Psi_{m'}\Psi_m^*\right|^2. \tag{126}$$

Como hemos mencionado, los estados coherentes de SU(2) $|S,\theta,\phi\rangle$ maximizan $\mathscr{A}_M^{(S)}$ para todos los órdenes M.

A continuación, nos concentramos en minimizar $\mathscr{A}_M$. La estrategia que adoptamos es, por lo tanto, muy simple de explicar: partiendo de un conjunto de amplitudes de estado desconocidas pero normalizadas en Eq. (126), las cuales escribimos como $\Psi_m=a_m+ib_m$ ($a_m,b_m\in\mathbb{R}$), tratamos de obtener $\mathscr{A}_M=0$ para el valor máximo posible de M. Esto conduce un sistema de ecuaciones polinómicas de grado dos para a_m y b_m, que se resuelven usando las bases de Gröbner implementadas en el sistema de álgebra computacional MAGMA [46]. Como la orientación de la constelación es irrelevante, el número de variables se puede reducir fijando uno de los puntos, por ejemplo, en el polo norte y otro en el plano S_2 - S_3. De esta manera, obtenemos expresiones algebraicas exactas y podemos detectar cuando no hay solución factible.

La Tabla 1 enumera los estados resultantes (que, en algunos casos, no son únicos) para una selección de valores diferentes de S. También indicamos las constelaciones de Majorana asociadas. Por completitud, en la Fig. 10 también se dibujan las constelaciones, así como las funciones Q para algunos de estos estados. Una lista completa se encuentra en [1], una discusión detallada de los estados resultantes, que se han llamado los Reyes cuánticos, se pueden encontrar en[37, 35].

Intuitivamente, se podría esperar que estas constelaciones tengan los puntos colocados tan simétricamente en la esfera unidad como sea posible. Esto encaja bien con la noción de estados de máxima entropía de Wehrl-Lieb [21]. Para algunos valores de S, como 4, 6, 8, 12 y 20, uno puede adivinar que la constelación máximamente despolarizada corresponde en cada caso a los vértices de un sólido platónico. Para otros números como $S=17/2$ no es fácil

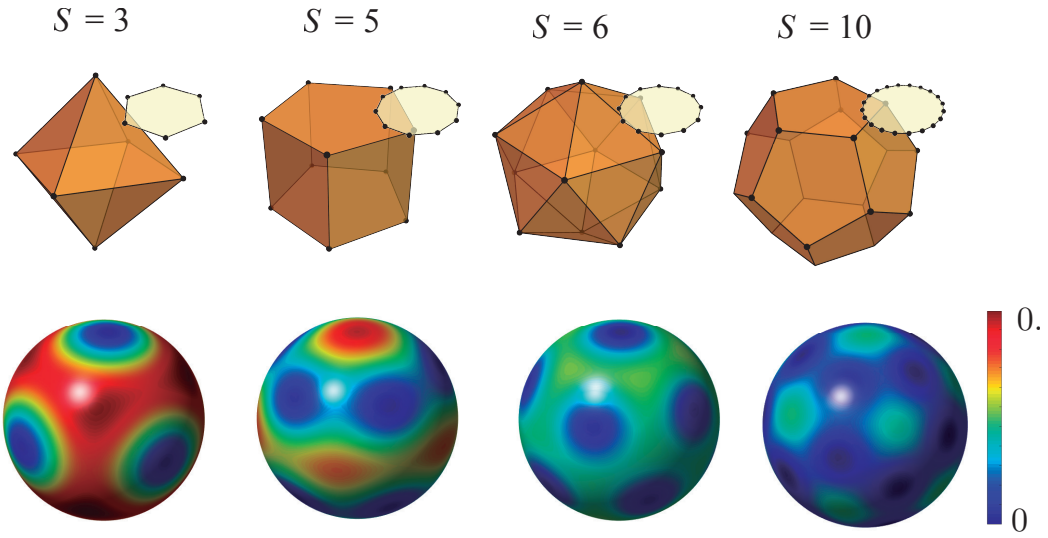

Figura 10: *(Color en línea) Gráficos de densidad de las funciones Q para los estados óptimos de la Tabla I para los casos* $S = 5/2, 3, 7/2, 9/2, 5$ *y* 7 *(de izquierda a derecha, azul indica valor cero y el valor máximo se representa rojo). En la parte superior, bosquejamos la constelación de Majorana para cada uno de ellos.*

adivinar una constelación "exacta" óptima, pero resolviendo el sistema de ecuaciones polinómicas, como se describe al comienzo de esta sección, se llega a expresiones algebraicas exactas para los coeficientes Ψ_m, a partir de las cuales uno puede calcular fácilmente los puntos de la constelación de Majorana con precisión numérica arbitraria.

Ésto parece estar estrechamente relacionado con la propuesta reciente de estados anti-coherentes [248, 73, 22]. Los estados anticoherentes son en cierto sentido "lo opuesto" a los estados coherentes de SU(2): mientras éste último corresponde lo más fielmente posible a un vector de espín clásico señalando en una dirección dada, el anterior "apunta a ninguna parte", es decir, el vector promedio de Stokes se cancela y las fluctuaciones hasta orden M son isotrópicas. Para el caso de dimensiones reducidas, estos estados coinciden con nuestros estados óptimos. Sin embargo, hacemos hincapié en que esta teoría está construida a partir de primeros principios y proporciona un criterio algebraico, éste es, la anulación de la distribución multipolar acumulada, que se puede manejar de una manera clara y compacta.

El problema de distribuir N puntos en una esfera de la manera "más simétrica" tiene una larga historia y muchas soluciones diferentes dependiendo de la función que se intenta optimizar [70, 204, 51]. Aquí, sólo discutiremos algunas de las formulaciones: t diseños esféricos [83], el problema de Thomson [228, 16, 90, 180] y las Reinas cuánticas [107].

Los t-diseños esféricos son configuraciones de N puntos en una esfera tal que el valor promedio de cualquier polinomio de grado como máximo t, es el mismo sobre los N puntos que sobre la esfera. Así, se puede considerar que los N puntos dan un valor promedio representativo de cualquier polinomio de grado t o inferior. Dichos diseños se pueden encontrar para (hiper)esferas de dimensiones superiores, pero para ver la relación con los estados máximamente despolarizados sólo consideraremos t-diseños en la esfera tridimensional. Se ha conjeturado que un estado es despolarizado a orden t si y sólamente si su constelación de Majorana es un t-diseño esférico [73]. Sin embargo, aunque la afirmación es verdadera para algunos t-diseños, como los representados por los sólidos platónicos, la conjetura no es verdadera en general [22].

Está claro que debe haber alguna conexión entre el número de puntos que uno tiene a su disposición N y el grado máximo t para el que una configuración de N puntos permite un diseño esférico de orden t. Las configuraciones que maximizan t para un determinado N se llaman diseños óptimos, y en lo prosiguiente t denotará el grado de un diseño óptimo de N puntos. No se conoce ninguna expresión analítica entre N y t: se sabe que para un t -diseño en el espacio tridimensional, el número de puntos N es al menos proporcional a t^2, mientras que para algunos órdenes t sólo se conocen construcciones para las cuales N escala proporcionalmente a t^3. Como una función de N, el orden t no es monotónico. El estado actual del conocimiento se resume para $1 \leqslant N \leqslant 100$ en [113].

De los datos numéricos obtenidos hasta el momento uno puede concluir que el máximo de M y t coinciden. Por lo tanto, conjeturamos que si un diseño esférico óptimo de orden t existe para un N, entonces uno puede encontrar un estado despolarizado a M orden con N fotones y con $M = t$. Este estado es máximamente despolarizado.

Lo siguiente que se puede apreciar es que un diseño óptimo de grado t no necesariamente corresponde a un estado despolarizado a orden t . Muy a menudo las configuraciones son similares, e.g. polígonos regulares con la normal a su superficie a lo largo del eje polar, pero desplazados unos de otros a lo largo del eje por ciertas distancias. Sin embargo, estas distancias necesitan a menudo ser ajustadas para que un t-diseño óptimo se convierta en un estado máximamente despolarizado. Los sólidos platónicos son excepciones a esta observación. Que las configuraciones óptimas de los t-diseños y los estados máximamente despolarizados no coincidan, acentúa el "misterio" de que el t óptimo y el máximo M siempre parecen ser iguales para cualquier N (o equivalentemente, para cualquier S).

Otra similitud entre los t-diseños esféricos óptimos y los Reyes cuánticos es que las configuraciones típicamente no son únicas, a excepción de las dimensiones más pequeñas.

El problema de Thomson consiste en disponer N cargas puntuales idénticas en la superficie de una esfera para que se minimice la energía potencial electrostática de la configuración. Para $N = 2$ la solución se visualiza fácilmente: la fuerza repelente tiende a situar las cargas en puntos antipodales de la esfera, maximizando así la distancia entre ellos. El problema puede generalizarse a energías potenciales de la forma r^{-d}, donde r es la distancia euclidia entre las cargas. La elección $d = 1$ es el problema de Thomson, que corresponde al potencial habitual de Coulomb y es en el que nos centraremos en este trabajo. El caso $d \to \infty$ se llama problema de Tammes [225].

Vemos que para S pequeños, hasta 3, las configuraciones son idénticas al t-diseño esférico óptimo y al estado máximamente despolarizado. Para S mayores, difieren en general y el grado de despolarización de los estados de "Thomson" es menor que el máximo. A diferencia de los dos casos anteriores, la solución del problema de Thomson parece ser única por cada S [92].

Las Reinas cuánticas son los estados que maximizan la distancia de Hilbert-Schmidt al punto más cercano de la envolvente convexa de la mezcla de estados coherentes SU(2) [107]. Esta envolvente convexa define el subespacio de los estados clásicos. Por lo tanto, los estados que maximizan la distancia al punto más cercano de esta envolvente pueden considerarse como los poseedores de características máximamente cuánticas. En [107] se afirma que las Reinas pueden ser vistas como los menos clásicos (o más cuánticos) de todos los estados dada esta métrica. Aunque hemos utilizado otra figura de mérito, nuestro enfoque y el de [107] comparten la consideración de que los estados "más diferentes" de los estados coherentes de SU(2) son los más no clásicos.

No es de extrañar que las Reinas resulten anticoherentes (despolarizadas a segundo orden) cuando sea posible, ya que deberían estar lo más "lejos posible" del estado coherente de SU(2). Estas configuraciones también parecen ser únicas, contrariamente a los estados máximamente despolarizados y a los diseños esféricos óptimos.

En casos particulares de baja dimensión, estos dos casos coinciden con nuestros estados óptimos. Sin embargo, enfatizamos que nuestra teoría se construye comenzando por primeros principios, a partir de magnitudes que se determinan rutinariamente en el laboratorio.

Cuando interpretamos nuestro subespacio $\mathscr{H}_S$ como el subespacio simétrico de un sistema de S qubits, los Reyes aparecen también conectados con otros problemas intrigantes, como estados simétricos máximamente entrelazados [18, 106] y estados k-máximamente mezclados [15, 110].

5.2.3. Aplicaciones metrológicas

En el último párrafo hemos derivado los estados extremales desde la perpectiva de la polarización. Sin embargo, las propiedades notables de tales estados los convierten en candidatos potenciales para superar a los estados clásicos en ciertas tareas.

El objetivo principal de la metrología cuántica es medir una magnitud física con una precisión sorprendente mediante la explotación de recursos cuánticos [105]. En particular, adaptar los estados de polarización para detectar mejor las rotaciones de SU(2) es un problema bastante relevante con aplicaciones directas a magnetometría [237, 216, 183], polarimetría [181, 76] y metrología en general [202].

La característica más destacada de los estados máximamente despolarizados es su capacidad de detectar pequeñas pero arbitrarias transformaciones SU(2) con resolución óptima. Esto ya se ha anticipado en [150], donde los autores hallaron específicamente que para un número de fotones 4, 6, 8, 12 y 20, los estados correspondientes a constelaciones de Majorana correspondientes a poliedros regulares mejoran la detección de los desalineamientos entre dos marcos de referencia cartesianos. Para entender esto, es instructivo observar estados relacionados, por ejemplo, los estados N00N.

Se sabe que tales estados N00N tienen la más alta sensibilidad para una excitación fija S a pequeñas rotaciones sobre el eje $\hat{S}_3$ [44]. Esto se puede entender fácilmente mirando a su constelación de Majorana, que ha sido incluida en Fig. 10 y que consiste simplemente en $2S$ puntos equidistantes colocados alrededor del ecuador de la esfera de Poincaré.

Una rotación alrededor del eje $\hat{S}_3$ está descrita por el operador unitario $\hat{U}(\vartheta) = \exp(-i\vartheta\hat{S}_3/2)$. Tenemos que para $\vartheta = \pi/(2S)$ los estados $|\text{N00N}\rangle$ y $\hat{U}(\vartheta)|\text{N00N}\rangle$ son ortogonales, Mientras que para $\vartheta = q\pi/S$ son paralelos, donde q es un entero. Por lo tanto, no debería sorprender que los estados N00N sean óptimos para detectar pequeñas rotaciones alrededor del eje $\hat{S}_3$, en el intervalo $0 \leqslant \vartheta \leqslant \pi/(2S)$. Sin embargo, tan pronto como la rotación exceda el límite superior en esta desigualdad, se tendrá dificultades para resolver el ángulo de rotación, ya que dos o más ángulos de rotación darán como resultado el mismo estado rotado. Si el eje de rotación se encuentra en el plano ecuatorial, entonces se necesita una rotación de π para obtener un estado paralelo, independientemente de S. Esto sucede sólo si el eje intersecta uno de los puntos de Majorana cuando S es un medio entero o si el eje interseca un punto o es el intersector entre dos puntos si S es un entero. Por lo tanto, la resolución de la rotación es altamente direccional para un estado N00N.

Ésta es precisamente la ventaja de los estados máximamente despolarizados: ya que tienen un alto grado de simetría esférica, resuelven las rotaciones alrededor de cualquier eje aproximadamente igual de bien. Puede no ser obvio por su apariencia que tienen alta sensibilidad a pequeñas rotaciones alrededor de un eje arbitrario. Para sustanciar esta afirmación, recuerde que la acción τ necesaria para hacer que un estado $|\Psi\rangle$ evolucione de manera que $|\langle\Psi|\exp(i\hat{A}\tau)|\psi\rangle|^2 = 1-\varepsilon$ donde ε es un número pequeño, positivo, real, y $\hat{A}$ es hermítica, es inversamente proporcional a la varianza del estado $\langle(\hat{A}-\langle\hat{A}\rangle)^2\rangle = \langle\Delta^2\hat{A}\rangle$ [174]. La relación que conecta la velocidad de evolución $d\varepsilon/d\tau$ y la varianza a veces se llama el "límite de velocidad cuántica" [224, 81]. Un estado N00N en la base $\hat{S}_3$ tiene maxima varianza $\langle\Delta^2\hat{S}_3\rangle = S^2$ para un S fijo y por lo tanto es el estado con máxima sensibilidad para una rotación alrededor del eje $\hat{S}_3$. Sin embargo, las varianzas $\hat{S}_1$ y $\hat{S}_2$ del estado son sólo $S/2$ y por lo tanto el estado es bastante insensible a las rotaciones alrededor de esos ejes (o a cualquier eje de rotación en el plano $\hat{S}_1$ - $\hat{S}_2$). Sin embargo, todos los Reyes cuánticos tienen varianzas isotrópicas iguales a $S(S+1)/3$, es decir, cerca del máximo. La prueba de esta afirmación es la siguiente:

$$\langle\Delta^2\hat{S}_1\rangle + \langle\Delta^2\hat{S}_2\rangle + \langle\Delta^2\hat{S}_3\rangle = \langle\hat{S}_1^2\rangle + \langle\hat{S}_2^2\rangle + \langle\hat{S}_3^2\rangle = \langle\hat{S}_0^2\rangle = S(S+1) \tag{127}$$

La segunda expresión de la izquierda se deriva del hecho de que los estados Reyes tienen momentos de primer orden nulos $\langle\hat{S}_{\mathbf{n}}\rangle$. Dado que su varianza por definición es isotrópica, también tenemos que $\langle\hat{S}_{\mathbf{n}}^2\rangle = \langle\hat{S}_1^2\rangle = \langle\hat{S}_2^2\rangle = \langle\hat{S}_3^2\rangle$. Al tener una varianza grande e isotrópica del operador de Stokes, el teorema del límite de velocidad cuántico afirma que estos estados son bastante sensibles a las rotaciones alrededor de cualquier eje $\hat{S}_{\mathbf{n}}$.

Otra forma de explicar la sensibilidad de los estados Reyes a una rotación alrededor de un eje arbitrario es observar que, dado que estos estados tienen simetría esférica "máxima", se vuelven paralelos o casi paralelos para rotaciones relativamente pequeñas alrededor de varios ejes. Por ejemplo, para los sólidos platónicos, las rotaciones alrededor de todos los ejes normales a sus caras transforman la constelación de Majorana en sí misma (resultando en un estado paralelo) para rotaciones de $2\pi/3$ (tetraedro, octaedro y icosaedro), $\pi/2$ (cubo), o $2\pi/5$ (dodecaedro). Para otras constelaciones y otros ejes de rotación la constelación de Majorana sólo se hará aproximadamente idéntica, pero el problema con la resolución de grandes rotaciones predominantemente permanecerá. Sin embargo, teniendo un alto grado de simetría esférica, los estados máximamente despolarizados resolverán las rotaciones alrededor de cualquier eje aproximadamente igual de bien. Para cuantificar esta afirmación se podría utilizar la información de Fisher y el límite de Cramér-Rao para evaluar la incertidumbre en la estimación de la dirección de rotación y el ángulo de rotación[224, 81].

En otro apunte, llamamos la atención sobre la similitud estructural entre los Reyes cuánticos y los códigos de corrección de errores cuánticos: en ambos casos se requiere que los términos de orden inferior en la expansión de la matriz densidad tengan que anularse.

6. Artículos de la tesis

La labor realizada durante el período de investigación de la tesis ha dado lugar a la publicación de diversos artículos en revistas científicas del área de óptica. Si bien gran parte de los artículos publicados siguen una misma línea de investigación, ésta es, *la estructura de la polarización en los estados cuánticos*, que da nombre a esta tesis, también se han escrito artículos sobre otros temas relativos a nociones de óptica cuántica y óptica clásica que han surgido a lo largo de este tiempo y que también nos han resultado de interés científico puesto que amplían las fronteras de conocimiento en este área. A continuación, realizaremos una enumeración de los artículos que componen esta tesis y detallaremos brevemente su contenido y la relación entre los diversos artículos.

1.- Quantum versus classical polarization states: when multipoles count
En este artículo exponemos que los problemas que hemos identificado al extender la definición del grado de polarización al dominio cuántico se deben al hecho de que su definición está planteada en términos de los momentos de primer orden de las variables de Stokes. En óptica cuántica es imprescindible ir más allá de una descripción de primer orden y analizar las fluctuaciones de polarización de orden superior. Para este propósito, tomamos prestadas ideas básicas procedentes de las distribuciones de cuasiprobabilidad estándar para el caso de SU(2), pero las reinterpretamos en términos de multipolos que contienen los momentos sucesivos de las variables de Stokes. Finalmente, ilustramos como el caso particular de la función de Husimi Q puede ser utilizada como una medida eficiente para la evaluación cuantitativa de esas fluctuaciones, como se vió en Eq. (74).

2.- Orbital angular momentum from marginals of quadrature distributions
Este artículo propone una forma alternativa para derivar distribuciones en el espacio de fases a través de marginales adecuados de las distribuciones para las cuadraturas del campo, una vez que hemos eliminado los grados de libertad que son irrelevantes en la descripción del problema. En este caso aplicamos estas ideas a vórtices que transportan momento angular orbital, pero las mismas ideas también han sido utilizadas para estudiar las propiedades de la polarización cuántica, como se ha puesto de manifiesto en la Sección 3.1.

3.- Multipolar hierarchy of efficient quantum polarization measures
En este artículo profundizamos en el desarrollo teórico del Art.**1**. Recurrimos a la expansión multipolar de la matriz densidad. La distribución de probabilidad para estos multipolos proporciona la información completa acerca de las propiedades de polarización de cualquier estado; en términos de ésta proponemos una medida adecuada para la evaluación cuantitativa de las fluctuaciones de polarización, que se corresponde con la Eq. (112).

4.- Radial quantum number of Laguerre-Gauss modes
Este artículo presta atención al índice radial de los modos de Laguerre-Gauss. Nuestro propósito en este artículo es presentar un análisis simple y comprensivo de esta variable. Este artículo viene a complementar al Art.**2** en el que se introdujeron los vórtices que transportan momento orbital.

5.- Classical distinguishability as an operational measure of polarization
En este artículo ampliamos los conceptos básicos de la polarización en óptica clásica tratados en la Sección 2.1 a campos completamente tridimensionales (3D). En este artículo retomamos una medida operacional que fue introducida hace algunos años en el contexto de la óptica cuántica[40] y que en este texto se desarrolla en la Sección 4.4. Pasar de la situación 2D a la 3D consiste en extender el conjunto de los estados rotados SU(2) a su análogo para SU(3), y los grados de polarización resultantes tienen una clara interpretación física.

6.- Unpolarized states and hidden polarization
En este artículo partimos de las nociones teóricas desarrolladas en los Arts. **1** y **3**. La idea de los estados despolarizados puede ser interpretada en este marco teórico. Cuándo todos los multipolos hasta un cierto orden (M) se anulan, el estado carece de información de polarización a ese orden dado y denominamos a estos estados despolarizados a M orden. Esta noción esta relacionada con la llamada polarización *oculta*, introducida por Klyschko [147, 148]

7.- Extremal states for photon number and quadratures as gauges for nonclassicality
En este artículo, al igual que en el Art. **2** adoptamos un enfoque que considera que la fase está codificada en las cuadraturas del campo. Buscamos estados extremos para estas variables y exploramos como estos estados extremos pueden ser utilizados para diagnosticar la no clasicidad de un estado.

8.- Classical polarization multipoles: paraxial versus nonparaxial
En este artículo empleamos la expansión multipolar Eq. (55) para indagar en las propiedades de la polarización para el caso de campos clásicos en la aproximación paraxial y no paraxial. Para el caso paraxial, SU(2) es el grupo de simetría natural del problema y la matriz de polarización contiene únicamente el término dipolar. Para el caso no paraxial, la expansión en términos de multipolos de SU(2) da lugar a una componente dipolar y a una componente cuadrupolar, que explica la más compleja estructura que se da en este caso.

9.- Stars of the quantum Universe: extremal constellations on the Poincaré sphere
Este artículo parte de la definición de estados despolarizados a M orden introducida en el Art.**6**. Hacemos uso de la representación de Majorana [171] que establece una correspondencia entre estados de polarización de N fotones y configuraciones de N puntos en la esfera de Poincaré. Vemos, a continuación, que el problema que estamos considerando (obtener estados despolarizados a M orden) está relacionado con otros varios problemas sin aparente relación que aparecen en física y en ciencia computacional. Todos ellos se reducen a un problema geométrico, éste es, el de encontrar la configuración óptima para disponer N puntos en la esfera "de la manera más simétrica" posible.

10.- Extremal quantum states and their Majorana constellations
Al igual que en el Art.**9** anterior, en este artículo se buscan los estados extremos para la mencionada distribución multipolar que utilizamos recurrentemente en esta tesis. Encontramos que los estados coherentes de SU(2) maximizan la distribución dada por Eq. (110) para cualquier orden y, por tanto, son los más polarizados permitidos por la teoría cuántica. Determinamos también cuales son los estados que anulan esta distribución hasta un orden dado M. Estos estados son lo opuesto a los estados coherentes SU(2) y pueden ser considerados los Reyes cuánticos, según nuestra denominación. Estamos interesados en calcular las expresiones de los estados puros despolarizados a M orden. Estos resultados se resumen en el cuadro 1 y más ejemplos pueden encontrarse en la Ref. [1].

11.- Unraveling beam self-healing
Este artículo es en realidad un estudio clásico de auto-reconstrucción. Introduccimos un grado adecuado que cuantifica la similitud entre el campo del haz no perturbado y el campo del haz tras la perturbación. De esta forma, ponemos de manifiesto que la auto-reconstrucción es un propiedad de la distribución espacial de tanto la intensidad como la fase del haz.

12.- Quantum metrology at the limit with extremal Majorana constellations
En este artículo investigamos la utilidad de los Reyes cuánticos, estados de polarización definidos en el Art. **10**. En esta publicación demostramos experimentalmente la generación de estos estados y certificamos su potencial para la metrología cuántica, como se resume en la Sección 5.2.3.

7. Conclusiones

La polarización cuántica proporciona un escenario adecuado para mostrar características no clásicas. Ésto es porque este grado de libertad es de fácil acceso tanto teórica como experimentalmente. Además, hemos demostrado que esta variable en realidad encuentra semejanzas con muchos temas diferentes de física cuántica. Por ejemplo, la evolución del campo eléctrico es equivalente a la dinámica de partículas estándar. Los operadores de Stokes abarcan, entre otras situaciones físicas, la dinámica de espín, la interferometría, conjuntos de átomos de dos niveles y la metrología cuántica.

La luz ha sido un excelente laboratorio para la investigación en la teoría cuántica. Esperamos que los resultados contenidos en esta tesis muestren que éste es también el caso de la polarización de la luz.

A continuación enumeraremos algunas conclusiones que se han obtenido en la elaboración de esta tesis:

1.- Las expansiones multipolares son una herramienta muy poderosa en muchas ramas de la física. Hemos aplicado una expansión multipolar a la matriz densidad de polarización, que muestra cómo los correspondientes multipolos del estado representan correlaciones de orden más elevado en las variables de Stokes. Estos multipolos pueden ser obtenidos a partir de mediciones factibles.

2.- Los multipolos resultantes pueden ser utilizados para construir distribuciones de cuasiprobabilidad que corresponden a la suma de los momentos de las variables de Stokes. De esta forma, el primer término coincide con la imagen clásica de la esfera de Poincaré.

3.- La expansión multipolar proporciona, por tanto, una caracterización sistemática de las fluctuaciones cuánticas de la polarización que, paradójicamente, no existía en el contexto de la óptica cuántica.

4.- La funcion Q de Husimi es un caso particular de distribución de cuasiprobabilidad que es especialmente útil al ser definida positiva y corresponde a la projección sobre los estados coherentes. Utilizamos esta función Q para formular una jerarquía completa de medidas que evalúan de manera adecuada las correlaciones de polarización de orden superior.

5.- Este formalismo puede ser ampliado a otros sístemas en los que la simetría SU(2) juega un papel crucial (tal puede ser el caso de los condensados de Bose-Einstein o las cadenas de espín) mientras que las extensiones a otras simetrías, como SU(3) (que es esencial en el entendimiento de las propiedades de polarización del campo cercano), son objeto actual de investigación.

6.- Hemos utilizado la función de Wigner para representar el comportamiento de la polarización en dos y tres dimensiones. A pesar de que ésta ha venido siendo considerada como una herramienta cuántica, tambien ha demostrado ser útil al tratar con campos clásicos. Especialmente en el caso tridimensional, hemos diseñado un procedimiento eficiente para representar el estado en la esfera.

7.- La expansión multipolar nos permite una caracterización sistemática de los estados despolarizados, como aquellos estados cuyos multipolos se anulan hasta un cierto orden. Se introduce, así, el concepto de estados despolarizados a orden M, descubriendo que la polarización escondida no es más que un caso particular de estos estados.

8.- La distribución acumulativa $\mathscr{A}_M^{(S)}$ 110 contiene la información de polarización hasta orden M. Puede ser considerada como un funcional no lineal de la matriz densidad. Tiene notables propiedades y es una magnitud razonable y experimentalmente realizable.

9.- Hemos demostrado que entre los estados puros los estados coherentes SU(2) maximizan esta distribución acumulativa a todos los órdenes: de esta forma, estos estados manifiestan sus virtudes clásicas. En el caso opuesto están los estados que minimizan esta cantidad, hemos denominado a dichos estados los Reyes cuánticos para los que los momentos de las variables de Stokes son isotrópicos para $1 \leqslant \ell \leqslant M$.

10.- Hemos derivado los Reyes cuánticos para un variado rango de dimensiones, sobre todo cuando el número de fotones N satisface $1 \leqslant N < 100$.

11.- La representación de Majorana constituye una herramienta muy útil para representar los estados de polarización como puntos en la esfera de Poincaré, y está constituida por los ceros de la función Q de Husimi. Para

estados coherentes SU(2) todos estos puntos coinciden (están degenerados), mientras que para los Reyes cuánticos los puntos tienden a distribuirse de la manera más simétrica posible alrededor de la esfera de Poincaré.

12.- Un problema interestante consiste en averiguar el orden M de despolarización máximo permitido para un estado puro de N fotones. No se conoce una relación analítica entre M y N. Pero hemos encontrado, en todas las dimensiones analizadas, que para un estado puro de N fotones, el grado de despolarización más alto posible es $M = t$, donde t es el grado óptimo para un t-diseño esférico con N puntos. Sin embargo, las constelaciones de puntos que se obtienen para los Reyes cuánticos y los correspondientes diseños esféricos no siempre coinciden.

13.- Hemos discutido las posibles conexiones entre las costelaciones correspondientes a nuestros estados mínimos de polarización y algunos otros problemas que implican la distribución simétrica de puntos en la esfera, como, por ejemplo, el problema de Thomson y las Reinas cuánticas, y hemos concluido que aunque estos problemas están relacionados, las soluciones sólo coinciden para las dimensiones más pequeñas. Una excepción a este caso se produce cuando una simetría exacta es posible como en el caso de las costelaciones correspondientes a los sólidos platónicos.

14.- Los Reyes cuánticos son una curiosidad académica en tanto en cuanto pueden considerarse los estados de polarización menos clásicos. En un sentido más práctico, estos parecen ser también los estados óptimos para detectar pequeñas rotaciones de SU(2) alrededor de un eje arbitrario desconocido. Ésto es debido a que su sensibilidad es independiente del eje de rotación y a que alcanza una resolución en el límite de Heisenberg.

15.- Informamos de la realización experimental de estos estados generando estados de un sólo fotón de momento orbital angular de dimensión hasta 21 y confirmamos sus buenas habilidades metrológicas.

Referencias

[1] http://polarization.markus-grassl.de.

[2] ABDEL-ATY, M., ABDALLA, M. S., AND OBADA, A.-S. F. Entropy squeezing of a two-mode multiphoton jaynes-cummings model in the presence of a nonlinear medium. *J. Opt. B 4*, 2 (2002), 134.

[3] ADAMSON, R. B. A., AND STEINBERG, A. M. Improving quantum state estimation with mutually unbiased bases. *Phys. Rev. Lett. 105* (2010), 030406.

[4] AGARWAL, G. S. On the state of unpolarized radiation. *Lett. Nuovo Cimento 1*, 2 (1971), 53–56.

[5] AGARWAL, G. S. Relation between atomic coherent-state representation, state multipoles, and generalized phase-space distributions. *Phys. Rev. A 24* (1981), 2889–2896.

[6] AGARWAL, G. S., AND PURI, R. R. Atomic states with spectroscopic squeezing. *Phys. Rev. A 49*, 6 (06 1994), 4968–4971.

[7] AKHIEZER, A. I., AND BERESTETSKII, V. B. *Quantum Electrodynamics*. Wiley, Neq York, 1965.

[8] ALBERTI, P. M. Playing with fidelities. *Rep. Math. Phys. 51*, 1 (2003), 87–125.

[9] ALTEPETER, J. B., OZA, N. N., MEDI, M., JEFFREY, E. R., AND KUMAR, P. Entangled photon polarimetry. *Opt. Express 19* (2011), 26011–26016.

[10] AMIET, J.-P., AND WEIGERT, S. Reconstructing the density matrix of a spin s through stern-gerlach measurements: Ii. *J. Phys. A 32* (1999), L269–L274.

[11] ANDERSON, A., AND HALLIWELL, J. J. Information-theoretic measure of uncertainty due to quantum and thermal fluctuations. *Phys. Rev. D 48* (1993), 2753–2765.

[12] ARAGONE, C., CHALBAUD, E., AND SALAMÓ, S. On intelligent spin states. *J. Math. Phys. 17*, 11 (2018/04/16 1976), 1963–1971.

[13] ARAGONE, C., GUERRI, G., SALAMO, S., AND TANI, J. L. Intelligent spin states. *J. Phys. A 7*, 15 (1974), L149–L152.

[14] ARECCHI, F. T., COURTENS, E., GILMORE, R., AND THOMAS, H. Atomic coherent states in quantum optics. *Phys. Rev. A 6* (1972), 2211–2237.

[15] ARNAUD, L., AND CERF, N. J. Exploring pure quantum states with maximally mixed reductions. *Phys. Rev. A 87* (2013), 012319.

[16] ASHBY, N., AND BRITTIN, W. E. Thomson's problem. *Am. J. Phys. 54* (1986), 776–777.

[17] ATAKISHIYEV, N. M., CHUMAKOV, S. M., AND WOLF, K. B. Wigner distribution function for finite systems. *J. Math. Phys. 39* (1998), 6247–6261.

[18] AULBACH, M., MARKHAM, D., AND MURAO, M. The maximally entangled symmetric state in terms of the geometric measure. *New J. Phys 12* (2010), 073025.

[19] AZZAM, R. M., AND BASHARA, N. M. *Ellipsometry and Polarized Light*. Elsevier, Amsterdam, 1996.

[20] AZZAM, R. M. A. Stokes-vector and mueller-matrix polarimetry. *J. Opt. Soc. Am. A 33*, 7 (2016), 1396–1408.

[21] BAECKLUND, A., AND BENGTSSON, I. Four remarks on spin coherent states. *Phys. Scr. T163*, T163 (2014), 014012.

[22] BANNAI, E., AND TAGAMI, M. A note on anticoherent spin states. *J. Phys. A 44* (2011), 342002.

[23] BARAKAT, R. Theory of the coherency matrix for light of arbitrary spectral bandwidth. *Journal of the Optical Society of America 53*, 3 (1963), 317–323.

[24] BARAKAT, R. *n*-fold polarization measures and associated thermodynamic entropy of *n* partially coherent pencils of radiation. *Opt. Acta 30*, 8 (08 1983), 1171–1182.

[25] BARAKAT, R. The statistical properties of partially polarized light. *Opt. Acta 32* (1985), 295–312.

[26] BARAKAT, R. Statistics of the stokes parameters. *J. Opt. Soc. Am. A 4*, 7 (1987), 1256–1263.

[27] BARAKAT, R. Natural light, generalized Verdet-Stokes conditions, and the covariance matrix of the Stokes parameters. *J. Opt. Soc. Am. A 6* (1989), 649–659.

[28] BARAKAT, R. Polarization entropy transfer and relative polarization entropy. *Opt. Commun. 123*, 4 (1996), 443–448.

[29] BARAKAT, R., AND BROSSEAU, C. Von neumann entropy of *n* interacting pencils of radiation. *J. Opt. Soc. Am. A 10*, 3 (1993), 529–532.

[30] BARBIERI, M., DE MARTINI, F., DI NEPI, G., MATALONI, P., D'ARIANO, G. M., AND MACCHIAVELLO, C. Detection of entanglement with polarized photons: Experimental realization of an entanglement witness. *Phys. Rev. Lett. 91* (2003), 227901.

[31] BARBIERI, M., VALLONE, G., MATALONI, P., AND DE MARTINI, F. Complete and deterministic discrimination of polarization bell states assisted by momentum entanglement. *Phys. Rev. A 75* (2007), 042317.

[32] BENGTSSON, I., AND ŻYCZKOWSKI, K. *Geometry of Quantum States*. Cambridge University Press, Cambridge, 2006.

[33] BEREZIN, F. A. General concept of quantization. *Commun. Math. Phys. 40* (1975), 153–174.

[34] BERRY, H. G., GABRIELSE, G., AND LIVINGSTON, A. E. Measurement of the stokes parameters of light. *Appl. Opt. 16*, 12 (1977), 3200–3205.

[35] BJÖRK, G., GRASSL, M., DE LA HOZ, P., LEUCHS, G., AND SÁNCHEZ-SOTO, L. L. Stars of the quantum universe: extremal constellations on the Poincaré sphere. *Physica Scripta 90*, 10 (2015), 108008.

[36] BJÖRK, G., INOUE, S., AND SÖDERHOLM, J. Visibility is not a good measure of a well-defined relative phase. *Physical Review A 62*, 2 (07 2000), 023817–.

[37] BJÖRK, G., KLIMOV, A. B., DE LA HOZ, P., GRASSL, M., LEUCHS, G., AND SÁNCHEZ-SOTO, L. L. Extremal quantum states and their Majorana constellations. *Phys. Rev. A 92*, 3 (09 2015), 031801.

[38] BJÖRK, G., SÖDERHOLM, J., KIM, Y. S., RA, Y. S., LIM, H. T., KOTHE, C., KIM, Y. H., SÁNCHEZ-SOTO, L. L., AND KLIMOV, A. B. Central-moment description of polarization for quantum states of light. *Phys. Rev. A 85* (2012), 053835.

[39] BJÖRK, G., SÖDERHOLM, J., SÁNCHEZ-SOTO, L. L., KLIMOV, A. B., GHIU, I., MARIAN, P., AND MARIAN, T. A. Quantum degrees of polarization. *Opt. Commun. 283* (2010), 4440–4447.

[40] BJÖRK, G., SÖDERHOLM, J., TRIFONOV, A., USACHEV, P. A., SÁNCHEZ-SOTO, L. L., AND KLIMOV, A. B. Applications of entangled-state interference. *Proc. SPIE 4750* (2002), 1–12.

[41] BLUM, K. *Density Matrix Theory and Applications*. Plenum, New York, 1981.

[42] BLUM, K. *Density Matrix Theory and Applications*. Plenum, New York, 1981.

[43] BOGDANOV, Y. I., CHEKHOVA, M. V., KULIK, S. P., MASLENNIKOV, G. A., ZHUKOV., A. A., OH, C. H., AND TEY, M. K. Qutrit state engineering with biphotons. *Phys. Rev. Lett. 93* (2004), 230503.

[44] BOLLINGER, J. J., ITANO, W. M., WINELAND, D. J., AND HEINZEN, D. J. Optimal frequency measurements with maximally correlated states. *Phys. Rev. A 54* (1996), R4649–R4652.

[45] BORN, M., AND WOLF, E. *Principles of Optics*, 7 ed. Cambridge University Press, Cambridge, 1999.

[46] BOSMA, W., CANNON, J., AND PLAYOUST, C. The Magma algebra system. i. the user language. *J. Symbolic Comput. 24* (1997), 235–265.

[47] BOUCHARD, F., DE LA HOZ, P., BJÖRK, G., BOYD, R. W., GRASSL, M., HRADIL, Z., KARIMI, E., KLIMOV, A. B., LEUCHS, G., ŘEHÁČEK, J., AND SÁNCHEZ-SOTO, L. L. Quantum metrology at the limit with extremal majorana constellations. *Optica 4*, 11 (2017), 1429–1432.

[48] BOUWMEESTER, D., PAN, J.-W., MATTLE, K., EIBL, M., WEINFURTER, H., AND ZEILINGER, A. Experimental quantum teleportation. *Nature 390* (1997), 575–579.

[49] BOWEN, W. P., SCHNABEL, R., BACHOR, H.-A., AND LAM, P. K. Polarization squeezing of continuous variable Stokes parameters. *Phys. Rev. Lett. 88* (2002), 093601.

[50] BOYER, G. R., LAMOUROUX, B. F., AND PRADE, B. S. Automatic measurement of the stokes vector of light. *Appl. Opt. 18*, 8 (1979), 1217–1219.

[51] BRAUCHART, J. S., AND GRABNER, P. J. Distributing many points on spheres: Minimal energy and designs. *J. Complexity 31*, 3 (6 2015), 293–326.

[52] BRIF, C., AND MANN, A. Nonclassical interferometry with intelligent light. *Phys. Rev. A 54*, 5 (11 1996), 4505–4518.

[53] BRIF, C., AND MANN, A. A general theory of phase-space quasiprobability distributions. *J. Phys. A 31* (1998), L9–L17.

[54] BRIF, C., AND MANN, A. Phase-space formulation of quantum mechanics and quantum-state reconstruction for physical systems with lie-group symmetries. *Phys. Rev. A 59* (1999), 971–987.

[55] BROSSEAU, C. *Fundamentals of Polarized Light: A Statistical Optics Approach*. Wiley, New York, 1998.

[56] BROSSEAU, C. Polarization and coherence optics: Historical perspective, status, and future directions. *Prog. Opt. 54* (2010), 149–208.

[57] BROSSEAU, C., AND DOGARIU, A. Symmetry properties and polarization descriptors for an arbitrary electromagnetic wavefield. *Prog. Opt. 49* (2006), 315–380.

[58] BROWN, T. G. Unconventional polarization states: Beam propagation, focusing, and imaging. *Prog. Opt. 56* (2011), 81–129.

[59] BRUKNER, Č., AND ZEILINGER, A. Operationally invariant information in quantum measurements. *Phys. Rev. Lett. 83*, 17 (10 1999), 3354–3357.

[60] CHATURVEDI, S., MARMO, G., AND MUKUNDA, N. The Schwinger representation of a group: concept and applications. *Rev. Math. Phys. 18*, 08 (2017/01/24 2006), 887–912.

[61] CHILDS, A. M., PRESKILL, J., AND RENES, J. Quantum information and precision measurement. *J. Mod. Opt. 47* (02 2000), 155–176.

[62] CHIRKIN, A. S., ORLOV, A. A., AND PARASHCHUK, D. Y. Quantum theory of two-mode interactions in optically anisotropic media with cubic nonlinearities: Generation of quadrature- and polarization-squeezed light. *Quantum Electron. 23* (1993), 870–874.

[63] CHUMAKOV, S. M., FRANK, A., AND WOLF, K. B. Finite kerr medium: macroscopic quantum superposition states and wigner functions on the sphere. *Phys. Rev. A 60* (1999), 1817–1822.

[64] CHUMAKOV, S. M., KLIMOV, A. B., AND WOLF, K. B. Connection between two wigner functions for spin systems. *Phys. Rev. A 61* (2000), 034101.

[65] CIVITARESE, O., REBOIRO, M., AND TIELAS, D. Spin observables in an atomic cqe system. *J. Phys. B 46*, 6 (2013), 065502.

[66] CLARKE, D., AND GRAINGER, J. F. *Polarized Light and Optical Measurement*. Pergamon, New York, 1971.

[67] COLLETT, E. Stokes parameters for quantum systems. *Am. J. Phys. 38* (1970), 563–574.

[68] COLLETT, E. *Polarized Light: Fundamentals and Applications*. Marcel Dekker, New York, 1993.

[69] COLLETT, E. *Field Guide to Polarization*. SPIE Press, Bellingham, 2005.

[70] CONWAY, J. H., HARDIN, R. H., AND SLOANE, N. J. A. Packing lines, planes, etc.: Packings in Grassmannian spaces. *Exp. Math. 5* (1996), 139–159.

[71] CORNEY, J. F., HEERSINK, J., DONG, R., JOSSE, V., DRUMMOND, P. D., LEUCHS, G., AND ANDERSEN, U. L. Simulations and experiments on polarization squeezing in optical fiber. *Phys. Rev. A 78* (2008), 023831.

[72] CORNWELL, J. F. *Group Theory in Physics*, vol. II. Academic, London, 1984.

[73] CRANN, J., PEREIRA, R., AND KRIBS, D. W. Spherical designs and anticoherent spin states. *J. Phys. A 43* (2010), 255307.

[74] CUI, X., LIAN, B.AND HO, T.-L., LEV, B. L., AND ZHAI, H. Synthetic gauge field with highly magnetic lanthanide atoms. *Phys. Rev. A 88*, 1 (07 2013), 011601.

[75] DAMASK, J. N. *Polarization Optics in Telecommunications*. Springer, New York, 2004.

[76] D'AMBROSIO, V., SPAGNOLO, N., DEL RE, L., SLUSSARENKO, S., LI, Y., KWEK, L. C., MARRUCCI, L., WALBORN, S. P., AOLITA, L., AND SCIARRINO, F. Photonic polarization gears for ultra-sensitive angular measurements. *Nat. Commun. 4* (09 2013), 2432 EP –.

[77] D'ARIANO, G. M., MACCONE, L., AND PAINI, M. Spin tomography. *J. Opt. B 5* (2003), 77–84.

[78] DE LA HOZ, P., BJÖRK, G., KLIMOV, A. B., LEUCHS, G., AND SÁNCHEZ-SOTO, L. L. Unpolarized states and hidden polarization. *Phys. Rev. A 90* (2014), 043826.

[79] DE LA HOZ, P., KLIMOV, A. B., BJÖRK, G., KIM, Y. H., MÜLLER, C., MARQUARDT, C., LEUCHS, G., AND SÁNCHEZ-SOTO, L. L. Multipolar hierarchy of efficient quantum polarization measures. *Phys. Rev. A 88*, 6 (12 2013), 063803.

[80] DEANS, S. R. *The Radon Transform and Some of its Applications*. Wiley, New York, 1983.

[81] DEL CAMPO, A., EGUSQUIZA, I. L., PLENIO, M. B., AND HUELGA, S. F. Quantum speed limits in open system dynamics. *Phys. Rev. Lett. 110*, 5 (01 2013), 050403.

[82] DELBOURGO, R. Minimal uncertainty states for the rotation and allied groups. *J. Phys. A: Math. Gen. 10*, 11 (1977), 1837–1841.

[83] DELSARTE, P., GOETHALS, J. M., AND SEIDEL, J. J. Spherical codes and designs. *Geom. Dedicata 6*, 3 (1977), 363–388.

[84] DEVI, A. R. U., SUDHA, AND RAJAGOPAL, A. K. Majorana representation of symmetric multiqubit states. *Quantum Inf. Process. 11*, 3 (2012), 685–710.

[85] DIXON, P. B., STARLING, D. J., JORDAN, A. N., AND HOWELL, J. C. Ultrasensitive beam deflection measurement via interferometric weak value amplification. *Phys. Rev. Lett. 102* (2009), 173601.

[86] DODONOV, V. V., MAN'KO, O. V., MAN'KO, V. I., AND WÜNSCHE, A. Hilbert-schmidt distance and non-classicality of states in quantum optics. *J. Mod. Opt. 47*, 4 (03 2000), 633–654.

[87] DONG, R., HEERSINK, J., YOSHIKAWA, J.-I., GLÖCKL, O., ANDERSEN, U. L., AND LEUCHS, G. An efficient source of continuous variable polarization entanglement. *New J. Phys. 9* (2007), 410.

[88] DOWLING, J. P. Quantum optical metrology–the lowdown on high-N00N states. *Contemp. Phys. 49*, 2 (03 2008), 125–143.

[89] DOWLING, J. P., AGARWAL, G. S., AND SCHLEICH, W. P. Wigner distribution of a general angular momentum state: application to a collection of two-level atoms. *Phys. Rev. A 49* (1994), 4101–4109.

[90] EDMUNDSON, J. R. The distribution of point charges on the surface of a sphere. *Acta Cryst. A48* (1992), 46–60.

[91] ELLIS, J., AND DOGARIU, A. Complex degree of mutual polarization. *Opt. Lett. 29*, 6 (2004), 536–538.

[92] ERBER, T., AND HOCKNEY, G. M. Equilibrium configurations of *n* equal charges on a sphere. *J. Phys. A: Math. Gen. 24* (1991), L1369–L1374.

[93] FALKOFF, D. L., AND MACDONALD, J. E. On the stokes parameters for polarized radiation. *J. Opt. Soc. Am. 41*, 11 (1951), 861–862.

[94] FANO, U. Remarks on the classical and quantum-mechanical treatment of partial polarization*. *J. Opt. Soc. Am. 39*, 10 (1949), 859–863.

[95] FANO, U. A stokes-parameter technique for the treatment of polarization in quantum mechanics. *Phys. Rev. 93*, 1 (01 1954), 121–123.

[96] FANO, U. Description of states in quantum mechanics by density matrix and operator techniques. *Rev. Mod. Phys. 29*, 1 (01 1957), 74–93.

[97] FANO, U., AND RACAH, G. *Irreducible Tensorial Sets*. Academic Press, New York, 1959).

[98] FILIPPOV, S. N., AND MAN'KO, V. I. Inverse spin-s portrait and representation of qudit states by single probability vectors. *J. Russ. Las. Res. 31* (2010), 32–54.

[99] GASE, R. Methods of quantum mechanics applied to partially coherent light beams. *J. Opt. Soc. Am. A 11*, 7 (1994), 2121–2129.

[100] GAZEAU, J. P. *Coherent States in Quantum Physics*. Wiley-VCH, Berlin, 2009.

[101] GHATAK, A., AND KUMAR, A. *Polarization of Light*. Tata McGraw Hill, New Delhi, 2012.

[102] GHIU, I., BJÖRK, G., MARIAN, P., AND MARIAN, T. A. Probing light polarization with the quantum chernoff bound. *Phys. Rev. A 82*, 2 (08 2010), 023803.

[103] GIL, J. J. Polarimetric characterization of light and media. *Eur. Phys. J. Appl. Phys. 40*, 1 (10 2007), 1–47.

[104] GILCHRIST, A., LANGFORD, N. K., AND NIELSEN, M. A. Distance measures to compare real and ideal quantum processes. *Phys. Rev. A 71*, 6 (06 2005), 062310.

[105] GIOVANNETTI, V., LLOYD, S., AND MACCONE, L. Advances in quantum metrology. *Nat. Photon. 5*, 4 (04 2011), 222–229.

[106] GIRAUD, O., BRAUN, D., BAGUETTE, D., BASTIN, T., AND MARTIN, J. Tensor representation of spin states. *Phys. Rev. Lett. 114* (2015), 080401.

[107] GIRAUD, O., BRAUN, P., AND BRAUN, D. Quantifying quantumness and the quest for queens of quantumness. *New J. Phys. 12*, 6 (2010), 063005.

[108] GNUTZMANN, S., AND ŻYCZKOWSKI, K. Rényi-Wehrl entropies as measures of localization in phase space. *J. Phys. A: Math. Theor. 34*, 47 (2001), 10123.

[109] GOLDSTEIN, D. H. *Polarized Light*, third ed. CRC, Boca Raton, 2011.

[110] GOYENECHE, D., AND ŻYCZKOWSKI, K. Genuinely multipartite entangled states and orthogonal arrays. *Phys. Rev. A 90* (2014), 022316.

[111] GUPTA, G. K., KUMAR, A., AND SINGH, R. S. Generation of hidden optical-polarization: Squeezing and non-classicality. *Opt. Commun. 284* (2011), 4951–4956.

[112] HANSEN, F. Quantum mechanics in phase space. *Rep. Math. Phys. 19*, 3 (1984), 361–381.

[113] HARDIN, R. H., AND SLOANE, N. J. A. Mclaren's improved snub cube and other new spherical designs in three dimensions. *Discrete Comp. Geom. 15* (1996), 429–441.

[114] HARDY, G. H., LITTLEWOOD, J. E., AND POLYA, G. *Inequalities*. Cambridge University Press, Cambridge, 1952.

[115] HE, Q. Y., PENG, S.-G., DRUMMOND, P. D., AND REID, M. D. Planar quantum squeezing and atom interferometry. *Phys. Rev. A 84*, 2 (08 2011), 022107.

[116] HEERSINK, J., GABER, T., LORENZ, S., GLÖCKL, O., KOROLKOVA, N., AND LEUCHS, G. Polarization squeezing of intense pulses with a fiber-optic sagnac interferometer. *Physical Review A 68*, 1 (07 2003), 013815–.

[117] HEERSINK, J., JOSSE, V., LEUCHS, G., AND ANDERSEN, U. L. Efficient polarization squeezing in optical fibers. *Opt. Lett. 30* (2005), 1192–1194.

[118] HEISS, S., AND WEIGERT, S. Discrete moyal-type representations for a spin. *Phys. Rev. A 63* (2000), 012105.

[119] HELLER, E. J. Quantum localization and the rate of exploration of phase space. *Phys. Rev. A 35* (1987), 1360–1370.

[120] HILLERY, M. Nonclassical distance in quantum optics. *Phys. Rev. A 35*, 2 (01 1987), 725–732.

[121] HILLERY, M., AND MLODINOW, L. Interferometers and minimum-uncertainty states. *Physical Review A 48*, 2 (08 1993), 1548–1558.

[122] HILLERY, M., O'CONNELL, R. F., SCULLY, M. O., AND WIGNER, E. P. Distribution functions in physics: Fundamentals. *Phys. Rep. 106* (1984), 121–167.

[123] HOFMANN, H. F., AND TAKEUCHI, S. Quantum-state tomography for spin-l systems. *Physical Review A 69*, 4 (04 2004), 042108–.

[124] HUARD, S. *Polarization of Light*. Wiley, New York, 1997.

[125] HUSIMI, K. Some formal properties of the density matrix. *roc. Phys. Math. Soc. Jpn. 22* (1940), 264–314.

[126] ISKHAKOV, T., CHEKHOVA, M. V., AND LEUCHS, G. Generation and direct detection of broadband mesoscopic polarization-squeezed vacuum. *Phys. Rev. Lett. 102* (2009), 183602.

[127] ISSUE, S. Squeezed light. *J. Mod. Opt. 34* (1987).

[128] ISSUE, S. Squeezed light. *J. Opt. Soc. Am. B 4* (1987).

[129] JACKSON, J. D. *Classical Electrodynamics*, 3rd ed. John Wiley, New York, 1999.

[130] JAMES, D. F. V., KWIAT, P. G., MUNRO, W. J., AND WHITE, A. G. Measurement of qubits. *Phys. Rev. A 64* (2001), 052312.

[131] JAUCH, J. M., AND ROHRLICH, F. *Theory of Photons and Electrons*. Addison-Wesley, New York, 1955.

[132] JAYNES, E. T. *Probability Theory: The Logic of Science*. Cambridge University Press, Cambridge, 2003.

[133] JONES, R. C. A new calculus for the treatment of optical systemsi. description and discussion of the calculus. *J. Opt. Soc. Am. 31*, 7 (1941), 488–493.

[134] JORDAN, P. Der zusammenhang der symmetrischen und linearen gruppen und das mehrkörperproblem. *Z. Phys. 94* (1935), 531–535.

[135] JOZSA, R. Fidelity for mixed quantum states. *J. Mod. Opt. 41*, 12 (12 1994), 2315–2323.

[136] KARASSIOV, V. P. Polarization structure of quantum light fields: a new insight. i. general outlook. *J. Phys. A 26* (1993), 4345–4354.

[137] KARASSIOV, V. P., AND MASALOV, A. V. The method of polarization tomography of radiation in quantum optics. *JETP 99* (2004), 51–60.

[138] KITAGAWA, M., AND UEDA, M. Squeezed spin states. *Phys. Rev. A 47*, 6 (06 1993), 5138–5143.

[139] KLIGER, D. S. *Polarized Light in Optics and Spectroscopy*. Academic, London, 1990.

[140] KLIMOV, A. B. Exact evolution equations for su(2) quasidistribution functions. *J. Math. Phys. 43* (2002), 2202–2213.

[141] KLIMOV, A. B., BJÖRK, G., SÖDERHOLM, J., MADSEN, L. S., LASSEN, M., ANDERSEN, U. L., HEERSINK, J., DONG, R., MARQUARDT, C., LEUCHS, G., AND SÁNCHEZ-SOTO, L. L. Assessing the polarization of a quantum field from Stokes fluctuations. *Phys. Rev. Lett. 105*, 15 (10 2010), 153602.

[142] KLIMOV, A. B., AND CHUMAKOV, S. M. Quasi-probability distributions for the simplest dynamical groups. *J. Opt. Soc. Am. A 17* (2000), 2315–2318.

[143] KLIMOV, A. B., DELGADO, J., AND SÁNCHEZ-SOTO, L. L. Quantum phase-space description of light polarization. *Opt. Commun. 258*, 2 (2006), 210–218.

[144] KLIMOV, A. B., MAN'KO, O. V., MAN'KO, V. I., SMIRNOV, Y. F., AND TOLSTOY, V. N. Tomographic representation of spin and quark states. *J. Phys. A 35*, 29 (2002), 6101–6123.

[145] KLIMOV, A. B., AND ROMERO, J. L. A generalized wigner function for quantum systems with the su (2) dynamical symmetry group. *J. Phys. A 41* (2008), 055303.

[146] KLIMOV, A. B., SÁNCHEZ-SOTO, L. L., YUSTAS, E. C., SÖDERHOLM, J., AND BJÖRK, G. Distance-based degrees of polarization for a quantum field. *Physical Review A 72*, 3 (09 2005), 033813–.

[147] KLYSHKO, D. M. Polarization of light: fourth-order effects and polarization-squeezed states. *JETP 84* (1997), 1065–1079.

[148] KLYSHKO, D. N. Multiphoton interference and polarization effects. *Phys. Lett. A 163* (1992), 349–355.

[149] KLYSHKO, D. N. Basic quantum mechanical concepts from the operational viewpoint. *Phys. Usp. 41* (1998), 885–922.

[150] KOLENDERSKI, P., AND DEMKOWICZ-DOBRZANSKI, R. Optimal state for keeping reference frames aligned and the platonic solids. *Phys. Rev. A 78*, 5 (11 2008), 052333.

[151] KOROLKOVA, N., LEUCHS, G., LOUDON, R., RALPH, T. C., AND SILBERHORN, C. Polarization squeezing and continuous-variable polarization entanglement. *Phys. Rev. A 65* (04 2002), 052306.

[152] KOROTKOVA, O., AND WOLF, E. Generalized stokes parameters of random electromagnetic beams. *Opt. Lett. 30*, 2 (2005), 198–200.

[153] KOTHE, C., MADSEN, L., ANDERSEN, U. L., AND BJÖRK, G. Experimental determination of the degree of polarization of quantum states. *Phys. Rev. A 87*, 4 (04 2013), 043814.

[154] KWIAT, P. G., BERGLUND, A. J., ALTEPETER, J. B., AND WHITE, A. G. Experimental verification of decoherence-free subspaces. *Science 290* (2000), 498–501.

[155] LAMACRAFT, A. Low-energy dynamics of spinor condensates. *Phys. Rev. B 81*, 18 (05 2010), 184526.

[156] LEE, C. T. Wehrl's entropy of spin states and lieb's conjecture. *J. Phys. A: Math. Gen. 21*, 19 (1988), 3749.

[157] LEE, H., KOK, P., AND DOWLING, J. P. A quantum Rosetta stone for interferometry. *J. Mod. Opt. 49*, 14-15 (11 2002), 2325–2338.

[158] LEE, H.-W. Theory and application of the quantum phase-space distribution functions. *Phys. Rep. 259* (1995), 147–211.

[159] LIAN, B., HO, T.-L., AND ZHAI, H. Searching for non-Abelian phases in the Bose-Einstein condensate of dysprosium. *Phys. Rev. A 85*, 5 (05 2012), 051606.

[160] LIEB, E. H. Proof of an entropy conjecture of wehrl. *Commun. Math. Phys. 62*, 1 (1978), 35–41.

[161] LIEB, E. H., AND SOLOVEJ, J. P. Proof of an entropy conjecture for bloch coherent spin states and its generalizations. *Acta Math. 212*, 2 (2014), 379–398.

[162] LIU, H. D., AND FU, L. B. Berry phase and quantum entanglement in Majorana's stellar representation. *Phys. Rev. A 94*, 2 (08 2016), 022123.

[163] LUIS, A. Degree of polarization in quantum optics. *Phys. Rev. A 66* (2002), 013806.

[164] LUIS, A. Polarization distributions and degree of polarization for quantum gaussian light fields. *Opt. Commun. 273* (2007), 173–181.

[165] LUIS, A., AND KOROLKOVA, N. Polarization squeezing and nonclassical properties of light. *Phys. Rev. A 74* (2006), 043817.

[166] LUIS, A., AND SÁNCHEZ-SOTO, L. L. Quantum phase difference, phase measurements and Stokes operators. *Prog. Opt. 41* (2000), 421–481.

[167] LVOVSKY, A. I., AND RAYMER, M. G. Continuous-variable optical quantum-state tomography. *Rev. Mod. Phys. 81*, 1 (03 2009), 299–322.

[168] MA, J., WANG, X., SUN, C. P., AND NORI, F. Quantum spin squeezing. *Phys. Rep. 509*, 2 (2011), 89–165.

[169] MAASSEN, H., AND UFFINK, J. B. M. Generalized entropic uncertainty relations. *Phys. Rev. Lett. 60* (1988), 1103–1106.

[170] MAHLER, D., JOANIS, P., VILIM, R., AND DE GUISE, H. Squeezing in su(2) intelligent states. *New J. Phys. 12* (2010), 033037.

[171] MAJORANA, E. Atomi orientati in campo magnetico variabile. *Nuovo Cimento 9*, 2 (1932), 43–50.

[172] MANAKOV, N. L., MEREMIANIN, A. V., AND STARACE, A. F. Multipole expansions of irreducible tensor sets and some applications. *J. Phys. B 35*, 1 (2002), 77.

[173] MANDEL, L., AND WOLF, E. *Optical Coherence and Quantum Optics*. Cambridge University Press, Cambridge, 1995.

[174] MANDELSHTAM, L. I., AND TAMM, I. E. The uncertainty relation between energy and time in nonrelativistic quantum mechanics. *J. Phys. (USSR) 9* (1945), 249–254.

[175] MARIAN, P., MARIAN, T. A., AND SCUTARU, H. Quantifying nonclassicality of one-mode gaussian states of the radiation field. *Phys. Rev. Lett. 88*, 15 (03 2002), 153601.

[176] MARQUARDT, C., HEERSINK, J., DONG, R., CHEKHOVA, M. V., KLIMOV, A. B., SÁNCHEZ-SOTO, L. L., ANDERSEN, U. L., AND LEUCHS, G. Quantum reconstruction of an intense polarization squeezed optical state. *Phys. Rev. Lett. 99* (2007), 220401.

[177] MARTÍNEZ-HERRERO, R., MEJÍAS, P. M., AND PIQUERO, G. *Characterization of Partially Polarized Light Fields*. Springer, Berlin, 2009.

[178] MATTLE, K., WEINFURTER, H., KWIAT, P. G., AND ZEILINGER, A. Dense coding in experimental quantum communication. *Phys. Rev. Lett. 76* (1996), 4656–4659.

[179] MCMASTER, W. H. Polarization and the Stokes parameters. *Am. J. Phys. 22* (1954), 351–362.

[180] MELNYK, T. H., KNOP, O., AND SMITH, W. R. Extremal arrangements of points and unit charges on a sphere: equi librium configurations revisited. *Can. J. Chem. 55* (1977), 1745–1761.

[181] MEYER, V., ROWE, M. A., KIELPINSKI, D., SACKETT, C. A., ITANO, W. M., MONROE, C., AND WINELAND, D. J. Experimental demonstration of entanglement-enhanced rotation angle estimation using trapped ions. *Phys. Rev. Lett. 86*, 26 (06 2001), 5870–5873.

[182] MOREVA, E. V., MASLENNIKOV, G. A., STRAUPE, S. S., AND KULIK, S. P. Realization of four-level qudits using biphotons. *Phys. Rev. Lett. 97* (2006), 023602.

[183] MUESSEL, W., STROBEL, H., LINNEMANN, D., HUME, D. B., AND OBERTHALER, M. K. Scalable spin squeezing for quantum-enhanced magnetometry with bose-einstein condensates. *Phys. Rev. Lett. 113*, 10 (09 2014), 103004.

[184] MULLER, A., BREGUET, J., AND GISIN, N. Experimental demonstration of quantum cryptography using polarized photons in optical fibre over more than 1 km. *EPL 23*, 6 (1993), 383.

[185] MÜLLER, C. R., MADSEN, L. S., KLIMOV, A. B., SÁNCHEZ-SOTO, L. L., LEUCHS, G., MARQUARDT, C., AND ANDERSEN, U. L. Parsing polarization squeezing into fock layers. *Phys. Rev. A 93*, 3 (03 2016), 033816.

[186] MÜLLER, C. R., STOKLASA, B., PEUNTINGER, C., GABRIEL, C., ŘEHÁČEK, J., HRADIL, Z., KLIMOV, A. B., LEUCHS, G., MARQUARDT, C., AND SÁNCHEZ-SOTO, L. L. Quantum polarization tomography of bright squeezed light. *New J. Phys. 14* (2012), 085002.

[187] PARIS, M. G. A., AND ŘEHÁČEK, J., Eds. *Quantum State Estimation*, vol. 649 of *Lect. Not. Phys.* Springer, Berlin, 2004.

[188] PARRENT, G. B., AND ROMAN, P. On the matrix formulation of the theory of partial polarization in terms of observables. *Il Nuovo Cimento 15*, 3 (1960), 370–382.

[189] PERELOMOV, A. *Generalized Coherent States and their Applications*. Springer, Berlin, 1986.

[190] PERES, A. *Quantum Theory: Concepts and Methods*. Kluwer, New York, 2002.

[191] PÉREZ, J. J. G., AND OSSIKOVSKI, R. *Polarized Light and the Mueller Matrix Approach*. CRC, Boca Raton, 2016.

[192] POINCARÉ, H. *Théorie Mathématique de la Lumière*. Georges Carré, Paris, 1889.

[193] PRAKASH, H., AND CHANDRA, N. Density operator of unpolarized radiation. *Phys. Rev. A 4*, 2 (08 1971), 796–799.

[194] PRAKASH, R., AND SHUKLA, N. Polarization squeezing in polarized light. *Opt. Commun. 284*, 14 (2011), 3568–3570.

[195] PUENTES, G., COLANGELO, G., SEWELL, R. J., AND MITCHELL, M. W. Planar squeezing by quantum non-demolition measurement in cold atomic ensembles. *New J. Phys. 15*, 10 (2013), 103031.

[196] RÅDMARK, M., ŻUKOWSKI, M., AND BOURENNANE, M. Experimental high fidelity six-photon entangled state for telecloning protocols. *New J. Phys. 11* (2009), 103016.

[197] RAYMER, M. G., MCALISTER, D. F., AND FUNK, A. Measuring the quantum polarization state of light. In *Quantum Communication, Computing, and Measurement 2* (New York, 2000), P. Kumar, Ed., Plenum.

[198] RÉFRÉGIER, P., AND ROUEFF, A. Intrinsic coherence: A new concept in polarization and coherence theory. *Opt. Photon. News 18*, 2 (2007), 30–35.

[199] RESCH, K. J., PREGNELL, K. L., PREVEDEL, R., GILCHRIST, A., PRYDE, G. J., O'BRIEN, J. L., AND WHITE, A. G. Time-reversal and super-resolving phase measurements. *Phys. Rev. Lett. 98* (2007), 223601.

[200] RIBEIRO, P., VIDAL, J., AND MOSSERI, R. Thermodynamical limit of the Lipkin-Meshkov-Glick model. *Phys. Rev. Lett. 99*, 5 (08 2007), 050402.

[201] RIVAS, A., AND LUIS, A. Characterization of quantum angular-momentum fluctuations via principal components. *Phys. Rev. A 77* (2008), 022105.

[202] ROZEMA, L. A., MAHLER, D. H., BLUME-KOHOUT, R., AND STEINBERG, A. M. Optimizing the choice of spin-squeezed states for detecting and characterizing quantum processes. *Phys. Rev. X 4*, 4 (11 2014), 041025.

[203] RUBIN, M. H., KLYSHKO, D. N., SHIH, Y. H., AND SERGIENKO, A. V. Theory of two-photon entanglement in type-ii optical parametric down-conversion. *phys. Rev. A 50*, 6 (12 1994), 5122–5133.

[204] SAFF, E. B., AND KUIJLAARS, A. B. J. Distributing many points on a sphere. *Math. Intell. 19*, 1 (1997), 5–11.

[205] SÁNCHEZ-SOTO, L. L., KLIMOV, A. B., DE LA HOZ, P., AND LEUCHS, G. Quantum versus classical polarization states: when multipoles count. *J. Phys. B 46* (2013), 104011.

[206] SANSONI, L., SCIARRINO, F., VALLONE, G., MATALONI, P., CRESPI, A., RAMPONI, R., AND OSELLAME, R. Polarization entangled state measurement on a chip. *Phys. Rev. Lett. 105* (2010), 200503.

[207] SCHACK, R., AND CAVES, C. M. Classical model for bulk-ensemble nmr quantum computation. *Phys. Rev. A 60*, 6 (12 1999), 4354–4362.

[208] SCHAEFER, B., COLLETT, E., SMYTH, R., BARRETT, D., AND FRAHER, B. Measuring the Stokes polarization parameters. *Am. J. Phys. 75* (2007), 163–168.

[209] SCHLEICH, W. P. *Quantum Optics in Phase Space*. Wiley-VCH, Berlin, 2001.

[210] SCHNABEL, R., BOWEN, W. P., TREPS, N., RALPH, T. C., BACHOR, H.-A., AND LAM, P. K. Stokes-operator-squeezed continuous-variable polarization states. *Phys. Rev. A 67* (2003), 012316.

[211] SCHROEK, F. E. *Quantum Mechanics on Phase Space*. Kluwer, Dordrecht, 1996.

[212] SCHUMACHER, B. Quantum coding. *Phys. Rev. A 51*, 4 (04 1995), 2738–2747.

[213] SCHWINGER, J. On angular momentum. In *Quantum Theory of Angular Momentum*, L. C. Biedenharn and H. Dam, Eds. Academic, New York, 1965.

[214] SCULLY, M. O., AND ZUBAIRY, M. S. *Quantum Optics*. Cambridge University Press, Cambridge, 2012.

[215] SEHAT, A., SÖDERHOLM, J., BJÖRK, G., ESPINOZA, P., KLIMOV, A. B., AND SÁNCHEZ-SOTO, L. L. Quantum polarization properties of two-mode energy eigenstates. *Phys. Rev. A 71* (2005), 033818.

[216] SEWELL, R. J., KOSCHORRECK, M., NAPOLITANO, M., DUBOST, B., BEHBOOD, N., AND MITCHELL, M. W. Magnetic sensitivity beyond the projection noise limit by spin squeezing. *Phys. Rev. Lett. 109*, 25 (12 2012), 253605–.

[217] SHALM, L. K., A., A. R. B., AND STEINBERG, A. M. Squeezing and over-squeezing of triphotons. *Nature 457* (2009), 67–70.

[218] SHUMOVSKY, A. S., AND MÜSTECAPLIOĞLU, Ö. E. Stokes operators, angular momentum and radiation phase. *J. Mod. Opt. 45*, 3 (03 1998), 619–628.

[219] SHURCLIFF, W. A. *Polarized Light: Production and Use*. Harvard University Press, Cambridge, MA, 1962.

[220] SILVER, B. L. *Irreducible Tensor Methods*. Academic, New York, 1976.

[221] SÖDERHOLM, J., BJÖRK, G., AND TRIFONOV, A. Unpolarized light in quantum optics. *Opt. Spectrosc. 91* (2001), 532—534.

[222] STOKES, G. G. On the composition and resolution of streams of polarized light from different sources. *Trans. Cambridge Phil. Soc. 9* (1852), 399–416.

[223] STRATONOVICH, R. L. On distributions in representation space. *JETP 31* (1956), 1012—1020.

[224] TADDEI, M. M., ESCHER, B. M., DAVIDOVICH, L., AND DE MATOS FILHO, R. L. Quantum speed limit for physical processes. *Phys. Rev. Lett. 110*, 5 (01 2013), 050402.

[225] TAMMES, P. M. L. On the origin of number and arrangement of places of exit on the surface of pollen grains,. *Recueil Trav. Bot. Néerl. 27* (1930), 1–84.

[226] TEO, Y. S. *Introduction to Quantum State Estimation*. World Scientific, Singapore, 2015.

[227] THEW, R. T., NEMOTO, K., WHITE, A. G., AND MUNRO, W. J. Qudit quantum-state tomography. *Phys. Rev. A 66* (2002), 012303.

[228] THOMSON, J. J. On the structure of the atom: an investigation of the stability and periods of oscillation of a number of corpuscles arranged at equal intervals around the circumference of a circle; with application of the results to the theory of atomic structure. *Philos. Mag. Ser. 6 7*, 39 (03 1904), 37265.

[229] UHLMANN, A. The "transition probability" in the state space of a *-algebra. *Rep. Math. Phys. 9*, 2 (1976), 273–279.

[230] USACHEV, P., SÖDERHOLM, J., BJÖRK, G., AND TRIFONOV, A. Experimental verification of differences between classical and quantum polarization properties. *Opt. Commun. 193* (2001), 161–173.

[231] VAN KAMPEN, N. G. *Stochastic Processes in Physics and Chemistry*, 2nd ed. Elsevier, Amsterdam, 2007.

[232] VARILLY, J. C., AND GRACIA-BONDÍA, J. M. The moyal representation for spin. *Ann. Phys. 190* (1989), 107–148.

[233] VARSHALOVICH, D. A., MOSKALEV, A. N., AND KHERSONSKII, V. K. *Quantum Theory of Angular Momentum*. World Scientific, Singapore, 1988.

[234] VEDRAL, V., PLENIO, M. B., RIPPIN, M. A., AND KNIGHT, P. L. Quantifying entanglement. *Phys. Rev. Lett. 78*, 12 (03 1997), 2275–2279.

[235] VERDET, E. *Leçons d' Optique Physique*, vol. 2. Imprimerie Impériale, Paris, 1869.

[236] ŘEHÁČEK, J., OLIVARES, S., MOGILEVTSEV, D., HRADIL, Z., PARIS, M. G. A., FORNARO, S., D'AURIA, V., PORZIO, A., AND SOLIMENO, S. Effective method to estimate multidimensional Gaussian states. *Phys. Rev. A 79*, 3 (03 2009), 032111.

[237] WASILEWSKI, W., JENSEN, K., KRAUTER, H., RENEMA, J. J., BALABAS, M. V., AND POLZIK, E. S. Quantum noise limited and entanglement-assisted magnetometry. *Phys. Rev. Lett. 104*, 13 (03 2010), 133601.

[238] WEHNER, S., AND WINTER, A. Entropic uncertainty relations—a survey. *New. J. Phys. 12*, 2 (2010), 025009.

[239] WEHRL, A. General properties of entropy. *Rev. Mod. Phys. 50*, 2 (04 1978), 221–260.

[240] WEHRL, A. The many facets of entropy. *Rep. Math. Phys. 30*, 1 (1991), 119–129.

[241] WHITE, A. G., JAMES, D. F. V., EBERHARD, P. H., AND KWIAT, P. G. Nonmaximally entangled states: Production, characterization, and utilization. *Phys. Rev. Lett. 83*, 16 (1999), 3103–3107.

[242] WINELAND, D. J., BOLLINGER, J. J., ITANO, W. M., AND HEINZEN, D. J. Squeezed atomic states and projection noise in spectroscopy. *Phys. Rev. A 50*, 1 (07 1994), 67–88.

[243] WINELAND, D. J., BOLLINGER, J. J., ITANO, W. M., MOORE, F. L., AND HEINZEN, D. J. Spin squeezing and reduced quantum noise in spectroscopy. *Physical Review A 46*, 11 (12 1992), R6797–R6800.

[244] WOLF, E. Optics in terms of observable quantities. *Il Nuovo Cimento 12*, 6 (1954), 884–888.

[245] WOLF, E. Coherence properties of partially polarized electromagnetic radiation. *Il Nuvo Cimento 13*, 6 (1959), 1165–1181.

[246] WOLF, E. *Introduction to the Theory of Coherence and Polarization of Light*. Cambridge University Press, Cambridge, 2007.

[247] ZACHOS, C. K., FAIRLIE, D. B., AND CURTRIGHT, T. L., Eds. *Quantum mechanics in phase space*. World Scientific, Singapore, 2005.

[248] ZIMBA, J. "Anticoherent" spin states via the Majorana representation. *EJTP 3* (2006), 143–156.

Paper 1

L. L. Sánchez-Soto, A. B. Klimov, P. de la Hoz, G. Leuchs:

"Quantum versus classical polarization states: when multipoles count",

Journal of Physics B **46**, 104011 (2013)

J. Phys. B: At. Mol. Opt. Phys. **46** (2013) 104011 (5pp) doi:10.1088/0953-4075/46/10/104011

Quantum versus classical polarization states: when multipoles count

L L Sánchez-Soto[1,2,3], A B Klimov[4], P de la Hoz[3] and G Leuchs[1,2]

[1] Max-Planck-Institut für die Physik des Lichts, Günther-Scharowsky-Straße 1, Bau 24, D-91058 Erlangen, Germany
[2] Department für Physik, Universität Erlanger-Nürnberg, Staudtstraße 7, D-91058 Erlangen, Germany
[3] Departamento de Óptica, Facultad de Física, Universidad Complutense, E-28040 Madrid, Spain
[4] Departamento de Física, Universidad de Guadalajara, 44420 Guadalajara, Jalisco, Mexico

E-mail: lsanchez@fis.ucm.es

Received 4 December 2012, in final form 30 January 2013
Published 9 May 2013
Online at stacks.iop.org/JPhysB/46/104011

Abstract
We advocate a simple multipole expansion of the polarization density matrix. The resulting multipoles are used to construct *bona fide* quasiprobability distributions that appear as a sum of successive moments of the Stokes variables, the first one corresponding to the classical picture on the Poincaré sphere. We employ the particular case of the Q function to formulate a whole hierarchy of measures that properly assess higher-order polarization correlations.

(Some figures may appear in colour only in the online journal)

1. Introduction

Polarization is a fundamental property of light that has received a lot of attention over the years [1]. As polarization is a robust characteristic, relatively simple to manipulate without inducing more than marginal losses, it is not surprising that many experiments at the forefront of quantum optics involve this observable [2].

In classical optics, polarization is elegantly visualized using the Poincaré sphere and is determined by the Stokes parameters. These are measurable quantities that allow for a classification of the states according to a degree of polarization. Furthermore, the formalism can be extended to the quantum domain, where the Stokes parameters become the mean values of the Stokes operators [3].

The classical degree of polarization is just the length of the Stokes vector. This provides a very intuitive picture, but for intricate fields it has serious drawbacks. Indeed, this classical quantity does not distinguish between states having remarkably different polarization properties [4]. In particular, it can be zero for light that cannot be regarded as unpolarized, giving rise to the so-called *hidden polarization* [5]. All these flaws have prompted some alternative measures [6–19].

We adhere to the viewpoint that the Stokes measurements ought to be the basic building blocks for any practical approach to polarization. Actually, the aforesaid problems with the classical degree are due to its definition in terms exclusively of first-order moments of the Stokes variables. This may be sufficient for most classical situations, but for quantum fields higher-order correlations might be crucial.

Our goal in this paper is to advance a practical solution to these hurdles. From coherence theory, we learn that a complete description of interference phenomena involves a hierarchy of correlation functions, with classical behaviour represented by the first one of those. In the same spirit, we propose to go beyond the first-order description and look for a way to systematically assess higher-order polarization correlations.

For that purpose, we borrow basic ideas from the standard SU(2) quasidistributions [20], but we reinterpret them in terms of multipoles that contain sequential moments of the Stokes variables. The dipole, being just the first-order moment, can be identified with the classical picture, whereas the other multipoles account for higher-order correlations. Finally, we illustrate how the particular instance of the SU(2) Q function can be used as an efficient measure for the quantitative assessment of those fluctuations.

2. Polarization structure of quantum fields

We start with a brief survey of the basic ingredients involved in a proper description of quantum polarization. We assume a monochromatic plane wave, propagating in the z direction, so its electric field lies in the xy plane. We are thus effectively

dealing with a two-mode field that can be characterized by two complex amplitude operators, denoted by $\hat{a}_{\rm H}$ and $\hat{a}_{\rm V}$, where the subscripts H and V label horizontal and vertical polarization modes. These operators obey the commutation rules $[\hat{a}_\lambda, \hat{a}_\mu^\dagger] = \delta_{\lambda\mu}$, with $\lambda, \mu \in \{\rm H, V\}$.

The use of the Schwinger representation [21]

$$\hat{S}_1 = \frac{1}{2}(\hat{a}_{\rm H}^\dagger \hat{a}_{\rm V} + \hat{a}_{\rm V}^\dagger \hat{a}_{\rm H})\,, \qquad \hat{S}_2 = \frac{i}{2}(\hat{a}_{\rm H}\hat{a}_{\rm V}^\dagger - \hat{a}_{\rm H}^\dagger \hat{a}_{\rm V})\,,$$
$$\hat{S}_3 = \frac{1}{2}(\hat{a}_{\rm H}^\dagger \hat{a}_{\rm H} - \hat{a}_{\rm V}^\dagger \hat{a}_{\rm V})\,, \tag{2.1}$$

together with the total number operator $\hat{N} = \hat{a}_{\rm H}^\dagger \hat{a}_{\rm H} + \hat{a}_{\rm V}^\dagger \hat{a}_{\rm V}$, will prove very convenient in what follows. In fact, the average of $\hat{\mathbf{S}} = (\hat{S}_1, \hat{S}_2, \hat{S}_3)$ coincides (except for an unimportant factor 1/2) with the classical Stokes vector [3]. Such a numerical factor is inserted to guarantee that $\{\hat{S}_k\}$ satisfy the commutation relations of the su(2) algebra

$$[\hat{S}_k, \hat{S}_\ell] = {\rm i}\epsilon_{k\ell m}\hat{S}_m\,, \qquad [\hat{N}, \hat{S}_k] = 0\,, \tag{2.2}$$

where the Latin indices run over {1, 2, 3} and $\epsilon_{k\ell m}$ is the Levi-Civita fully antisymmetric tensor. This noncommutability precludes the simultaneous sharp measurement of the physical quantities they represent, which is expressed by the uncertainty relation

$$\Delta^2\hat{\mathbf{S}} = \Delta^2\hat{S}_1 + \Delta^2\hat{S}_2 + \Delta^2\hat{S}_3 \geqslant \langle\hat{N}\rangle/2\,, \tag{2.3}$$

$\Delta^2\hat{S}_k = \langle\hat{S}_k^2\rangle - \langle\hat{S}_k\rangle^2$ standing for the variance.

In classical optics, the states of definite polarization are specified by the constraint $\langle\hat{\mathbf{S}}\rangle^2 = \langle\hat{N}/2\rangle^2$. Since the intensity there is a nonfluctuating quantity, in the three-dimensional space of the Stokes parameters this defines a sphere with radius equal to the intensity: the Poincaré sphere. In contradistinction, in quantum optics we have that $\hat{\mathbf{S}}^2 = S(S+1)\mathbb{1}$, with the angular momentum being $S = N/2$ and, as fluctuations in the number of photons are unavoidable, we are forced to work in the three-dimensional Poincaré space that can be regarded as a set of nested spheres with radii proportional to the different photon numbers that contribute to the state.

As our final remark, we stress that the second equation in (2.2) prompts us to address each subspace with a fixed number of photons N separately. To bring this point out more clearly, it is advantageous to relabel the standard two-mode Fock basis $|n_{\rm H}, n_{\rm V}\rangle$ in the form

$$|S, m\rangle = |n_{\rm H} = S + m, n_{\rm V} = S - m\rangle\,, \tag{2.4}$$

so that $S = N/2$ and $m = (n_H - n_V)/2$. For each fixed S, m runs from $-S$ to S and the states (2.4) span a $(2S+1)$-dimensional subspace wherein $\hat{\mathbf{S}}$ acts in the standard way.

3. The polarization sector

For any arbitrary function of the Stokes operators $f(\hat{\mathbf{S}})$, we have $[f(\hat{\mathbf{S}}), \hat{N}] = 0$ as well, so the matrix elements of the density matrix $\hat{\rho}$ connecting subspaces with different photon numbers do not contribute to $\langle f(\hat{\mathbf{S}})\rangle$. This translates the fact that polarization and intensity are, in principle, independent concepts: in classical optics the form of the ellipse traced out by the electric field (polarization) does not depend on its size (intensity).

In other words, the only accessible information from $\hat{\rho}$ is its polarization sector [22–26], which is specified by the block-diagonal form

$$\hat{\rho}_{\rm pol} = \bigoplus_S \hat{\rho}^{(S)}, \tag{3.1}$$

where $\hat{\rho}^{(S)}$ is the reduced density matrix in the Sth subspace (S runs over all the possible photon numbers, i.e. $S = 1/2, 1, \ldots$). Any $\hat{\rho}$ and its associated block-diagonal form $\hat{\rho}_{\rm pol}$ cannot be distinguished in polarization measurements; accordingly, we drop henceforth the subscript pol.

To proceed, we resort to the standard SU(2) machinery [27] and expand each $\hat{\rho}^{(S)}$ as

$$\hat{\rho}^{(S)} = \sum_{K=0}^{2S}\sum_{q=-K}^{K} \rho_{Kq}^{(S)}\,\hat{T}_{Kq}^{(S)}\,, \tag{3.2}$$

where the irreducible tensor operators $\hat{T}_{Kq}^{(S)}$ (note carefully that the index K takes only integer values) read [28]

$$\hat{T}_{Kq}^{(S)} = \sqrt{\frac{2K+1}{2S+1}}\sum_{m,m'=-S}^{S} C_{Sm,Kq}^{Sm'}\,|S, m'\rangle\langle S, m|\,, \tag{3.3}$$

and the expansion coefficients

$$\rho_{Kq}^{(S)} = {\rm Tr}\left[\hat{\rho}^{(S)}\,T_{Kq}^{(S)\,\dagger}\right] \tag{3.4}$$

are known as state multipoles and contain all the information about the state. The quantities $C_{Sm,Kq}^{Sm'}$ are the Clebsch–Gordan coefficients that couple a spin S and a spin K to a total spin S and vanish unless the usual angular momentum coupling rules are satisfied, namely

$$0 \leqslant K \leqslant 2S\,, \qquad -K \leqslant q \leqslant K\,. \tag{3.5}$$

The operators $\hat{T}_{Kq}^{(S)}$ are quite a convenient tool for they have the proper transformation properties under rotations and besides fulfil

$${\rm Tr}\left[T_{Kq}^{(S)\,\dagger}\,T_{K'q'}^{(S)}\right] = \delta_{KK'}\delta_{qq'}\,, \tag{3.6}$$

so, they indeed constitute the most suitable orthonormal basis for the problem at hand. Although the definition of $\hat{T}_{Kq}^{(S)}$ in (3.3) might look a bit unfriendly, the essential observation for what follows is that $\hat{T}_{Kq}^{(S)}$ can be related to the Kth power of the generators (2.1), so they are intimately linked to the moments of the Stokes variables, precisely our main objective in this work. In particular, the monopole $\rho_{00}^{(S)}$ being proportional to the identity is always trivial, while the dipole $\rho_{1q}^{(S)}$ is the first-order moment of $\hat{\mathbf{S}}$ and thus gives the classical picture, in which the state is represented by its average value.

The complete characterization of the state demands the knowledge of all the multipoles. This implies measuring the probability distribution of $\hat{\mathbf{S}}$ in all directions, and then performing an integral inversion (put in another way, a whole tomography), which turns out to be a hard task [24–26]. However, in most realistic cases, only a finite number of multipoles are needed and then the reconstruction of the Kth multipole entails measuring along just $2K+1$ independent directions [29, 30].

4. Polarization quasidistributions

The discussion thus far suggests that polarization must be specified by a probability distribution of polarization states. As a matter of fact, such a probabilistic description is unavoidable in quantum optics from the very beginning, since $\{\hat{S}_k\}$ do not commute and thus no state can have a definite value of all of them simultaneously.

The SU(2) symmetry inherent in the polarization structure, as discussed in the previous sections, allows us to take advantage of the pioneering work of Stratonovich [31] and Berezin [32], who worked out quasiprobability distributions on the sphere satisfying all the pertinent requirements. This construction was later generalized by others [33–37] and has proved to be very useful in visualizing the properties of spinlike systems [38–42].

For each partial $\hat{\rho}^{(S)}$, one can define the SU(2) Q function as

$$Q^{(S)}(\theta,\phi) = \langle S;\theta,\phi|\hat{\rho}^{(S)}|S;\theta,\phi\rangle\,, \tag{4.1}$$

where $|S;\theta,\phi\rangle$ are the SU(2) coherent states (also known as spin or atomic coherent states), given by [43, 44]

$$|S;\theta,\phi\rangle = \hat{D}(\theta,\phi)|S,-S\rangle\,. \tag{4.2}$$

Here $\hat{D}(\theta,\phi) = \exp(\xi\hat{S}_+ - \xi^*\hat{S}_-)$ (with $\xi = (\theta/2)\exp(-\mathrm{i}\phi)$ and (θ,ϕ) being spherical angular coordinates) plays the role of a displacement on the Poincaré sphere of radius S. The ladder operators $\hat{S}_\pm = \hat{S}_1 \pm \mathrm{i}\hat{S}_2$ select the fiducial state $|S,-S\rangle$ as usual: $\hat{S}_-|S,-S\rangle = 0$. As we can appreciate, both the definition of the Q function and the coherent states for SU(2) closely mimic their standard counterparts for position momentum.

While for spins, S is typically a fixed number, in quantum optics most of the states involve a full polarization sector as in equation (3.1) and for the total polarization matrix $\hat{\rho}$ we have

$$Q(\theta,\phi) = \sum_S \frac{2S+1}{4\pi} Q^{(S)}(\theta,\phi)\,. \tag{4.3}$$

The sum extends over the subspaces contributing to the state. Since the SU(2) coherent states are eigenstates of the total number $\hat{N}$, the sum over S in (4.3) attempts to remove the total intensity of the field in such a way that $Q(\theta,\phi)$ contains only relevant polarization information. Furthermore, since $|S;\theta,\phi\rangle$ are the only states saturating the uncertainty relation (2.3), the definition of $Q(\theta,\phi)$ is quite appealing, for it appears as the projection on the states having the most definite polarization allowed by the quantum theory.

On the other hand, as Q contains the whole information about the state, its knowledge is tantamount to determining all the state multipoles. Actually, the Q function (and, more generally, any s-parametrized quasidistribution) can also be written in terms of $\rho_{Kq}^{(S)}$ [45]:

$$Q^{(S)}(\theta,\phi) = \frac{\sqrt{4\pi}}{\sqrt{2S+1}} \sum_{K=0}^{2S}\sum_{q=-K}^{K} C_{SS,K0}^{SS}\,\rho_{Kq}^{(S)}\,Y_{Kq}^*(\theta,\phi)\,, \tag{4.4}$$

with $Y_{Kq}(\theta,\phi)$ being the spherical harmonics, which constitute a complete set of orthonormal functions on the sphere. This definition can be shown to be fully equivalent to (4.1). Note also that the Clebsch–Gordan coefficient $C_{SS,K0}^{SS}$ has a very simple analytical form [28]:

$$C_{SS,K0}^{SS} = \frac{\sqrt{2S+1}\,(2S)!}{\sqrt{(2S-K)!\,(2S+1+K)!}}\,. \tag{4.5}$$

By plugging (4.4) in the general definition (4.3), we can express the Q function as a sum over multipoles:

$$Q(\theta,\phi) = \sum_{K=0}^{\infty} Q_K(\theta,\phi)\,, \tag{4.6}$$

where each partial component can be written as

$$Q_K(\theta,\phi) = \sum_{S=K/2}^{\infty} \sqrt{\frac{2S+1}{4\pi}} \sum_{q=-K}^{K} C_{SS,K0}^{SS}\,\rho_{Kq}^{(S)}\,Y_{Kq}^*(\theta,\phi)\,. \tag{4.7}$$

For the particular case of single S (fixed number of photons), the sum over S has to be ignored.

The partial components Q_K inherit the properties of Q, but they contain exclusively the relevant information of the Kth moment of the Stokes variables. So, (4.6) appears as an optimum tool to arrange the successive moments and thus achieves our goals in this paper.

Let us illustrate our viewpoint with the simple example of the state $|1_\mathrm{H}, 1_\mathrm{V}\rangle$, produced in parametric down-conversion. In the $|S,m\rangle$ notation, the state is $|1,0\rangle$ and its Q function can be easily computed according to (4.6) and (4.7); the final result is

$$Q(\theta,\phi) = \frac{3}{4}\sqrt{\frac{1}{3\pi}}\sin^2\theta\,. \tag{4.8}$$

It does not depend on ϕ and its shape is an equatorial belly, revealing that the state is highly delocalized. The partial components are

$$\begin{aligned} Q_0(\theta,\phi) &= \frac{1}{2}\sqrt{\frac{1}{3\pi}}\,, \qquad Q_1(\theta,\phi) = 0,\\ Q_2(\theta,\phi) &= \frac{1}{2}\sqrt{\frac{1}{3\pi}}\left(\frac{3}{2}\cos^2\theta - \frac{1}{2}\right)\,. \end{aligned} \tag{4.9}$$

The sum of these three terms gives, of course, the result (4.8), but anyway there is more information encoded in (4.9): the dipole contribution is absent, confirming that this state conveys no first-order information (i.e. it is *unpolarized* to that order). This is the reason why this is the first state in which hidden polarization was detected. Figure 1 shows the partial Q_K functions for this state, as well as the global one.

5. Assessing higher-order polarization moments

Let us consider the following quantity:

$$\mathscr{A} = \int \mathrm{d}\Omega\,[Q(\theta,\phi)]^2\,, \tag{5.1}$$

where the integral extends over the whole sphere and $\mathrm{d}\Omega = \sin\theta\mathrm{d}\theta\mathrm{d}\phi$ is the solid angle. This function can be interpreted as the effective area where the Q function is different from zero. Similar proposals have already been used as measures of localization and uncertainty in different contexts [46–51]. In polarization, (5.1) has also been used as an essential ingredient in formalizing an alternative degree arising as the

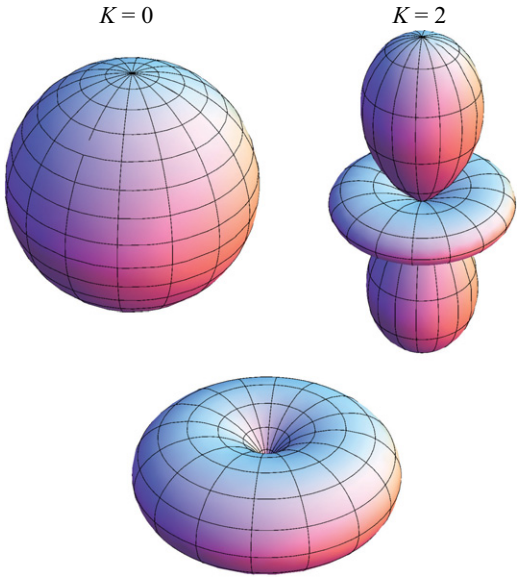

Figure 1. Plot of the monopolar ($K = 0$) and quadrupolar ($K = 2$) components of the state $|1, 0\rangle$ (top), as well as the total Q function (bottom). The dipolar component ($K = 1$) vanishes, so this state lacks any first-order information, which translates in the presence of *hidden polarization*.

distance between the state's Q function and the Q function for unpolarized light [6].

One might think the use of the Wigner function preferable as a measure of the area occupied by a quantum state in phase space. However, for SU(2), $\int \mathrm{d}\Omega[W(\theta,\phi)]^2$ takes exactly the same value for all pure states, so that this provides a measure of purity of quantum states rather than a measure of polarization. For this compelling reason, we have instead employed the Q function so far.

Note that (5.1) is invariant under SU(2) transformations: this means that such an effective area depends on the form of the Q function, but not on its position or orientation on the Poincaré sphere.

Of course, the decomposition in multipoles (4.6) is of straightforward application here. Consequently, we can define the magnitude

$$\mathscr{A}_K = \int \mathrm{d}\Omega\,[Q_K(\theta,\phi)]^2\,, \tag{5.2}$$

with an analogous interpretation to that $\mathscr{A}$, but restricted to the Kth multipole. When the explicit form of Q_K in (4.7) is used, $\mathscr{A}_K$ reduces to

$$\mathscr{A}_K = \sum_{S=K/2}^{\infty} \frac{2S+1}{4\pi}\left(C^{SS}_{SS,K0}\right)^2 \sum_{q=-K}^{K} \left|\rho^{(S)}_{Kq}\right|^2. \tag{5.3}$$

In this way, $\mathscr{A}_K$ can be reinterpreted as a measure of the strength of the corresponding multipole, confirming that it provides full information about the state Kth moment.

As an appealing illustration of our method, we analyse the outstanding example of SU(2) coherent states. Without loss of generality, we deal with the south pole $|S, -S\rangle$, since from (4.2) any other coherent state can be obtained by the application of a displacement to that state. The associated multipoles turn out to be $\rho^{(S)}_{Kq} = \sqrt{(2K+1)/(2S+1)}\,C^{SS}_{SS,K0}$, so that

$$\mathscr{A}_K = \frac{2K+1}{4\pi}\left(C^{SS}_{SS,K0}\right)^4. \tag{5.4}$$

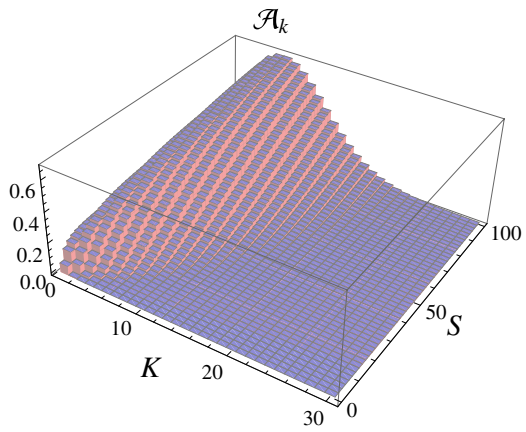

Figure 2. Function $\mathscr{A}_K$ as a function of the multipole-order K for an SU(2) coherent state for different values of S.

In figure 2 we have plotted $\mathscr{A}_K$ as a function of K and S. The first multipoles always contribute the most to the state localization, something that one could expect from physical intuition. However, as S gets larger, the number of multipoles to be taken into account also increases.

6. Concluding remarks

Multipolar expansions are a commonplace and a powerful tool in many branches of physics. We have applied such an expansion to the polarization density matrix, showing how the corresponding state multipoles represent higher-order correlations in the Stokes variables. This paves the way to a systematic characterization of quantum polarization fluctuations that, paradoxically, is still missing in the realm of quantum optics. Such a complete programme is currently in progress in our group.

Acknowledgments

We thank G S Agarwal, G Björk, J H Eberly, W P Schleich, T H Seligman and K B Wolf for useful discussions. Financial support from the EU FP7 (Grant Q-ESSENCE), the Spanish DGI (Grant FIS2011-26786), the UCM-BSCH program (Grant GR-920992) and the Mexican CONACyT (Grant 106525) is acknowledged.

References

[1] Brosseau C 1998 *Fundamentals of Polarized Light: A Statistical Optics Approach* (New York: Wiley)
[2] Mandel L and Wolf E 1995 *Optical Coherence and Quantum Optics* (Cambridge: Cambridge University Press)
[3] Luis A and Sánchez-Soto L L 2000 *Quantum Phase Difference, Phase Measurements and Stokes Operators (Progress in Optics* vol 41*)* (Amsterdam: Elsevier) pp 421–81

[4] Tsegaye T, Söderholm J, Atatüre M, Trifonov A, Björk G, Sergienko A V, Saleh B E A and Teich M C 2000 *Phys. Rev. Lett.* **85** 5013–7
[5] Klyshko D N 1992 *Phys. Lett.* A **163** 349–55
[6] Luis A 2002 *Phys. Rev.* A **66** 013806
[7] Legré M, Wegmüller M and Gisin N 2003 *Phys. Rev. Lett.* **91** 167902
[8] Saastamoinen T and Tervo J 2004 *J. Mod. Opt.* **51** 2039–45
[9] Picozzi A 2004 *Opt. Lett.* **29** 1653–5
[10] Ellis J, Dogariu A, Ponomarenko S and Wolf E 2005 *Opt. Commun.* **248** 333–7
[11] Luis A 2005 *Phys. Rev.* A **71** 053801
[12] Sehat A, Söderholm J, Björk G, Espinoza P, Klimov A B and Sánchez-Soto L L 2005 *Phys. Rev.* A **71** 033818
[13] Klimov A B, Sánchez-Soto L L, Yustas E C, Söderholm J and Björk G 2005 *Phys. Rev.* A **72** 033813
[14] Réfrégier P 2005 *Opt. Lett.* **30** 1090–2
[15] Réfrégier P and Goudail F 2006 *J. Opt. Soc. Am.* A **23** 671–8
[16] Luis A 2007 *Opt. Commun.* **273** 173–81
[17] Björk G, Söderholm J, Sánchez-Soto L L, Klimov A B, Ghiu I, Marian P and Marian T A 2010 *Opt. Commun.* **283** 4440–7
[18] Klimov A B *et al* 2010 *Phys. Rev. Lett.* **105** 153602
[19] Qian X F and Eberly J H 2011 *Opt. Lett.* **36** 4110–2
[20] Varilly J C and Gracia-Bondía J M 1989 *Ann. Phys.* **190** 107–48
[21] Schwinger J 1965 On angular momentum *Quantum Theory of Angular Momentum* ed L C Biedenharn and H Dam (New York: Academic) pp 229–79
[22] Karassiov V P 1993 *J. Phys. A: Math. Gen.* **26** 4345–54
[23] Raymer M G, McAlister D F and Funk A 2000 Measuring the quantum polarization state of light *Quantum Communication, Computing, and Measurement* vol 2, ed P Kumar (New York: Plenum) pp 235–95
[24] Karassiov V P and Masalov A V 2004 *J. Exp. Theor. Phys.* **99** 51–60
[25] Marquardt C, Heersink J, Dong R, Chekhova M V, Klimov A B, Sánchez-Soto L L, Andersen U L and Leuchs G 2007 *Phys. Rev. Lett.* **99** 220401
[26] Müller C R, Stoklasa B, Peuntinger C, Gabriel C, Řeháček J, Hradil Z, Klimov A B, Leuchs G, Marquardt C and Sánchez-Soto L L 2012 *New J. Phys.* **14** 085002
[27] Blum K 1981 *Density Matrix Theory and Applications* (New York: Plenum)
[28] Varshalovich D A, Moskalev A N and Khersonskii V K 1988 *Quantum Theory of Angular Momentum* (Singapore: World Scientific)
[29] Newton R G and Young B l 1968 *Ann. Phys.* **49** 393–402
[30] Klimov A B, de la Hoz P, Björk G, Müller C, Leuchs G and Sánchez-Soto L L 2013 in preparation
[31] Stratonovich R L 1956 *J. Exp. Theor. Phys.* **31** 1012–20
[32] Berezin F A 1975 *Commun. Math. Phys.* **40** 153–74
[33] Agarwal G S 1981 *Phys. Rev.* A **24** 2889–96
[34] Brif C and Mann A 1998 *J. Phys. A: Math. Gen.* **31** L9–17
[35] Heiss S and Weigert S 2000 *Phys. Rev.* A **63** 012105
[36] Klimov A B and Chumakov S M 2000 *J. Opt. Soc. Am.* A **17** 2315–8
[37] Klimov A B and Romero J L 2008 *J. Phys. A: Math. Theor.* **41** 055303
[38] Dowling J P, Agarwal G S and Schleich W P 1994 *Phys. Rev.* A **49** 4101–9
[39] Atakishiyev N M, Chumakov S M and Wolf K B 1998 *J. Math. Phys.* **39** 6247–61
[40] Chumakov S M, Frank A and Wolf K B 1999 *Phys. Rev.* A **60** 1817–22
[41] Chumakov S M, Klimov A B and Wolf K B 2000 *Phys. Rev.* A **61** 034101
[42] Klimov A B 2002 *J. Math. Phys.* **43** 2202–13
[43] Arecchi F T, Courtens E, Gilmore R and Thomas H 1972 *Phys. Rev.* A **6** 2211–37
[44] Perelomov A 1986 *Generalized Coherent States and Their Applications* (Berlin: Springer)
[45] Agarwal G S 1981 *Phys. Rev.* A **24** 2889–96
[46] Heller E J 1987 *Phys. Rev.* A **35** 1360–70
[47] Maassen H and Uffink J B M 1988 *Phys. Rev. Lett.* **60** 1103–6
[48] Anderson A and Halliwell J J 1993 *Phys. Rev.* D **48** 2753–65
[49] Hall M J W 1999 *Phys. Rev.* A **59** 2602–15
[50] Gnutzmann S and Zyczkowski K 2001 *J. Phys. A: Math. Gen.* **34** 10123–40
[51] Muñoz C, Klimov A B and Sánchez-Soto L L 2012 *J. Phys. A: Math. Theor.* **45** 244014

Paper 2

P. de la Hoz, I. Rigas, J. Rehacek, Z. Hradil, G. Leuchs:

"Orbital angular momentum from marginals of quadrature distributions",

Physical Review A **88**, 053839 (2013)

Orbital angular momentum from marginals of quadrature distributions

L. L. Sánchez-Soto,[1,2,3] A. B. Klimov,[4] P. de la Hoz,[1] I. Rigas,[1,2] J. Řeháček,[5] Z. Hradil,[5] and G. Leuchs[2,3]

[1]*Departamento de Óptica, Facultad de Física, Universidad Complutense, 28040 Madrid, Spain*

[2]*Max-Planck-Institut für die Physik des Lichts, Günther-Scharowsky-Straße 1, Bau 24, 91058 Erlangen, Germany*

[3]*Department für Physik, Universität Erlangen-Nürnberg, Staudtstraße 7, Bau 2, 91058 Erlangen, Germany*

[4]*Departamento de Física, Universidad de Guadalajara, 44420 Guadalajara, Jalisco, Mexico*

[5]*Department of Optics, Palacký University, 17. listopadu 12, 746 01 Olomouc, Czech Republic*

(Received 7 June 2013; published 25 November 2013)

We set forth a method to analyze the orbital angular momentum of a light field. Instead of using the canonical formalism for the conjugate pair angle-angular momentum, we model this latter variable by the superposition of two independent harmonic oscillators along two orthogonal axes. By describing each oscillator by a standard Wigner function, we derive, via a consistent change of variables, a comprehensive picture of the orbital angular momentum. We compare this with previous approaches and show how this method works in some relevant examples.

DOI: 10.1103/PhysRevA.88.053839 PACS number(s): 42.25.Bs, 03.30.+p, 78.67.Pt, 78.20.Ci

I. INTRODUCTION

The term vortex is commonly used to designate a region of concentrated rotation in a flow, such as an eddy, a whirlpool, or the depression at the center of a whirling body of air or water. Naturally occurring vortices include hurricanes, tornadoes, waterspouts, and dust devils [1]. Yet vortices can also be created in many different media: they manifest in plasmas [2], superfluids [3], ferromagnets [4], acoustical waves [5], quantum Hall fluids [6], Bose-Einstein condensates [7], and electron wave packets [8], to cite only a few relevant examples. This points to the ubiquity of this phenomenon and reveals a growing interest in these singularities.

The case of optical vortices deserves a special mention [9]. An optical vortex is a beam of light exhibiting a pure screw phase dislocation along the propagation axis, i.e., an azimuthal phase dependence $\exp(i\ell\varphi)$. The number ℓ plays the role of a topological charge: the phase changes its value in ℓ cycles of 2π in any closed circuit about the axis, while the amplitude is zero there.

One of the most interesting properties of vortices is that they carry orbital angular momentum (OAM): the integer ℓ can be seen as the eigenvalue of the OAM operator and its sign defines the helicity or direction of rotation. Indeed, the OAM of such a field can be easily manipulated and transferred, which opens many experimental perspectives, such as optical tweezers and spanners [10], as well as potential astronomical [11] and communication applications [12].

The fact that individual photons also carry OAM presents the most exciting possibilities for using this variable in the quantum domain, and a number of uses has already been demonstrated [13–17].

In quantum theory, the operator representing the OAM has an unbounded spectrum that includes positive and negative integers. Accordingly, its conjugate variable, the azimuthal angle, might be expected to be represented by a bona fide operator. Periodicity, however, brings out subtleties that have triggered long and heated discussions [18–20].

Here, we look at this issue from a phase-space perspective. Such an approach was introduced in the very early days of quantum theory to avoid some of the troubles arising in the abstract Hilbert-space formulation. The pioneering works of Weyl [21], Wigner [22], and Moyal [23] paved the way to formally picturing the quantum world as a statistical theory on phase space [24–26].

In a few words, the key idea is to look for a mapping that relates operators (in Hilbert space) to functions (in phase space). For the conjugate pair angle-OAM, the phase space is the discrete cylinder $\mathscr{S}\times\mathbb{Z}$ ($\mathscr{S}$ denotes the unit circle associated with the angle, while $\mathbb{Z}$ are the integers labeling OAM). It seems natural to work out a Wigner function (or any other quasiprobability) therein. A pioneer attempt in that direction was made by Mukunda [27]; his work was subsequently elaborated and developed in a variety of directions by other authors [28–40].

However, one might properly argue that in such a (correct) way of proceeding one is overlooking significant information about the transverse distribution. This means, for example, that using cylindrical coordinates all the states $\Psi_\ell(r,\varphi) = A_\ell(r)\exp(i\ell\varphi)$ represent eigenstates of the angular momentum, irrespective of the form of the amplitudes $A_\ell(r)$. A similar problem arises in the description of spinlike systems over the Bloch sphere: one disregards in this way fluctuations in the number of particles, because a sphere of fixed radius cannot accommodate those fluctuations. To bypass this drawback one needs to include the whole Bloch space that can be envisioned as foliated in a set of nested spheres with radii proportional to the different number of particules that contribute to the state.

Below, we propose an alternative road and derive phase-space distributions via suitable marginals of distributions for field quadratures, once we remove the degrees of freedom irrelevant for the specification of the problem. The same ideas have been used also to study quantum polarization properties [41,42]. Perhaps this provides the most down-to-earth approach to the problem at hand, since the quadrature distributions can be determined by very simple experimental procedures [43]. This widespread measurability does not hold for the Wigner functions on the cylinder: the proposals for their practical reconstruction are rather cumbersome [44] and lack the simple and intuitive picture provided by schemes measuring quadrature distributions.

The plan of this paper is as follows. In Sec. II we concisely sketch the phase-space fundamentals for a single harmonic oscillator. In Sec. III we start from two kinematical independent orthogonal oscillators and express the resulting Wigner function in cylindrical coordinates. By eliminating an inessential variable (the radial momentum), we get a well-behaved distribution that gives complete information not only on the pair angle-OAM but also on the radial distribution. We apply the resulting Wigner function to some relevant states in Sec. IV, and conclude that it constitutes a most suitable tool to deal with this problem.

II. PHASE-SPACE PICTURE OF A ONE-DIMENSIONAL HARMONIC OSCILLATOR

To keep the discussion as self-contained as possible, we first boil down the rudiments of the phase-space formalism for a harmonic oscillator that we shall need later on.

The relevant dynamical observables are the conjugate coordinate and momentum operators $\hat{x}$ and $\hat{p}$, with canonical commutation relation (with $\hbar = 1$ throughout)

$$[\hat{x},\hat{p}] = i\,\hat{\mathbb{1}}\,, \tag{2.1}$$

so that they are the generators of the Heisenberg-Weyl algebra [45]. Ubiquitous and profound, this algebra has become the hallmark of noncommutativity in quantum theory. The classical phase space is here the plane $\mathbb{R}^2$.

Sometimes, it is advantageous to use instead complex amplitudes represented by the annihilation and creation operators

$$\hat{a} = \frac{1}{\sqrt{2}}(\hat{x} + i\,\hat{p})\,, \quad \hat{a}^\dagger = \frac{1}{\sqrt{2}}(\hat{x} - i\,\hat{p})\,, \tag{2.2}$$

in terms of which the commutation relation (2.1) turns out to be $[\hat{a},\hat{a}^\dagger] = \hat{\mathbb{1}}$.

A pivotal role will be played in what follows by the unitary

$$\hat{D}(x,p) = \exp[i(p\hat{x} - x\hat{p})]\,, \tag{2.3}$$

which is called the displacement operator for it displaces a localized state by $(x,p) \in \mathbb{R}^2$. The Fourier transform of $\hat{D}(x,p)$,

$$\hat{w}(x,p) = \frac{1}{(2\pi)^2}\int_{\mathbb{R}^2} \exp[-i(px' - xp')]\,\hat{D}(x',p')\,dx'dp'\,, \tag{2.4}$$

is an instance of a Stratonovich-Weyl quantizer [46]. One can check that the operators $\hat{w}(x,p)$ are a complete trace-orthonormal set that transforms properly under displacements

$$\hat{w}(x,p) = \hat{D}(x,p)\,\hat{w}(0,0)\,\hat{D}^\dagger(x,p)\,, \tag{2.5}$$

where $\hat{w}(0,0) = \int_{\mathbb{R}^2}\hat{D}(x,p)\,dxdp = 2\hat{P}$, and

$$\hat{P} = \int_{\mathbb{R}} |x\rangle\langle -x|\,dx = \int_{\mathbb{R}} |p\rangle\langle -p|\,dp = (-1)^{\hat{a}^\dagger\hat{a}} \tag{2.6}$$

is the parity operator.

Let $\hat{A}$ be an arbitrary operator acting on the Hilbert space of the system. Using the Stratonovich-Weyl quantizer we can associate to $\hat{A}$ a function $a(x,p)$ representing the action of the corresponding dynamical variable in phase space. In fact, this is known as the Wigner-Weyl map and is given by [47]

$$a(x,p) = \mathrm{Tr}[\hat{A}\,\hat{w}(x,p)]\,. \tag{2.7}$$

The function $a(x,p)$ is the symbol of the operator $\hat{A}$. Conversely, we can reconstruct the operator from its symbol through

$$\hat{A} = \frac{1}{(2\pi)^2}\int_{\mathbb{R}^2} a(x,p)\,\hat{w}(x,p)\,dxdp\,. \tag{2.8}$$

In this context, the Wigner function is nothing but the symbol of the density matrix $\hat{\rho}$, and therefore

$$\begin{aligned} W_{\hat{\rho}}(x,p) &= \mathrm{Tr}[\hat{\rho}\,\hat{w}(x,p)]\,,\\ \hat{\rho} &= \frac{1}{(2\pi)^2}\int_{\mathbb{R}^2}\hat{w}(x,p)W_{\hat{\rho}}(x,p)\,dxdp\,. \end{aligned} \tag{2.9}$$

For a pure state $|\Psi\rangle$, it simplifies

$$W_{|\Psi\rangle}(x,p) = \frac{1}{4\pi}\int_{\mathbb{R}} \Psi^*(x-x')\,\Psi(x+x')\,\exp(i2px')\,dx'\,, \tag{2.10}$$

which is, perhaps, the most convenient form for actual calculations.

The Wigner function defined in Eq. (2.9) fulfills all the basic properties required for any good probabilistic description. First, due to the Hermiticity of $\hat{w}(x,p)$, it is real for Hermitian operators. Second, the probability distributions for the canonical variables can be obtained as the marginals

$$\int_{\mathbb{R}} W_{\hat{\rho}}(x,p)\,dp = \langle x|\hat{\rho}|x\rangle\,, \quad \int_{\mathbb{R}} W_{\hat{\rho}}(x,p)\,dx = \langle p|\hat{\rho}|p\rangle\,. \tag{2.11}$$

Third, $W_{\hat{\rho}}(x,p)$ is translationally covariant, which means that for the displaced state $\hat{\rho}' = \hat{D}(x',p')\,\hat{\rho}\,\hat{D}^\dagger(x',p')$, one has

$$W_{\hat{\rho}'}(x,p) = W_{\hat{\rho}}(x-x',p-p')\,, \tag{2.12}$$

so that it follows displacements rigidly without changing its form, reflecting the fact that physics should not depend on a certain choice of the origin.

Finally, the overlap of two density operators is proportional to the integral of the associated Wigner functions:

$$\mathrm{Tr}(\hat{\rho}\,\hat{\rho}') \propto \int_{\mathbb{R}^2} W_{\hat{\rho}}(x,p)W_{\hat{\rho}'}(x,p)\,dxdp\,. \tag{2.13}$$

This property (known as traciality) offers practical advantages, since it allows one to predict the statistics of any outcome, once the Wigner function of the measured state is known.

The displacements constitute also a basic ingredient in the concept of coherent states. If we choose a fixed normalized reference state $|\Psi_0\rangle$, we have [48]

$$|x,p\rangle = \hat{D}(x,p)\,|\Psi_0\rangle\,, \tag{2.14}$$

so they are parametrized by phase-space points. These states have a number of remarkable properties inherited from those of $\hat{D}(x,p)$. In particular, $\hat{D}(x,p)$ transforms any coherent state in another coherent state:

$$\hat{D}(x',p')\,|x,p\rangle = \exp[i(x'p - p'x)/2]\,|x+x',p+p'\rangle\,. \tag{2.15}$$

The standard choice for the fiducial vector $|\Psi_0\rangle$ is the vacuum $|0\rangle$, which has quite a number of relevant properties.

III. PHASE-SPACE PICTURE OF A TWO-DIMENSIONAL HARMONIC OSCILLATOR

Next, we analyze the superposition of two oscillators in orthogonal directions, say x and y, with momenta $\hat{p}_x$ and $\hat{p}_y$, respectively. The corresponding complex amplitudes $\hat{a}_x$ and $\hat{a}_y$ fulfill $[\hat{a}_j,\hat{a}_k^\dagger]=\delta_{jk}\hat{\mathbb{1}}$ $(j,k\in\{x,y\})$. Since these oscillators are kinematically independent (i.e., they play the role of modes for the problem), the total system is represented by the product of the corresponding kernels

$$\hat{w}(x,p_x;y,p_y)=\hat{w}(x,p_x)\,\hat{w}(y,p_y)\,. \tag{3.1}$$

The information is thus encoded in the four real variables (x,p_x) and (y,p_y). The resulting Wigner function $W(x,p_x;y,p_y)$ is informationally complete, but it is hard to grasp any physical flavor from it. In particular, it cannot be plotted (which is always a major advantage when depicting complex phenomena) and one must content oneself with sections of $W(x,p_x;y,p_y)$, which illustrate only partial aspects [49].

Because we are interested in elaborating on the behavior of OAM, which mostly appears when cylindrical symmetry is present, we make the change from Cartesian (x,y) to polar (r,φ) coordinates:

$$r=\sqrt{x^2+y^2}\,,\quad \varphi=\arctan(y/x)\,. \tag{3.2}$$

Simultaneously, we change from (p_x,p_y) to

$$p_r=\frac{1}{r}(xp_x+yp_y)\,,\quad \ell=xp_y-yp_x\,, \tag{3.3}$$

where p_r is the radial momentum and ℓ is the OAM. This transition from Cartesian to polar coordinates is not smooth at the origin and needs qualification because it takes from a contractible space to one which is not contractible. This lies at the root of the problems appearing when dealing with angle variables [50–57]. In quantum optics there are, however, a number of ways to bypass this drawback [58–65]. In the same vein, the radial momentum p_r is singular at the origin, which reflects a classical symptom of quantum illness [66], for such an operator is not self-adjoint (nor has self-adjoint extensions) [67–69]. Precisely, the use of Wigner-Weyl kernels alleviates these problems arising in a direct quantization. However, we brush aside these mathematical subtleties and move on to find a suitable solution for our problem.

Using the explicit form (2.5) for each orthogonal oscillator and after disentangling the exponentials, we can rewrite (3.1) in the equivalent way,

$$\begin{aligned}\hat{w}(r,p_r;\varphi,\ell)=4(-1)^{\hat{N}}&\exp[-2\cos\varphi(\alpha_r\hat{a}_x^\dagger-\alpha_r^*\hat{a}_x)]\\&\times\exp[2i\lambda_r\sin\varphi(\hat{a}_x^\dagger+\hat{a}_x)]\\&\times\exp[-2\sin\varphi(\alpha_r\hat{a}_y^\dagger-\alpha_r^*\hat{a}_y)]\\&\times\exp[-2i\lambda_r\cos\varphi(\hat{a}_y^\dagger+\hat{a}_y)]\,,\end{aligned} \tag{3.4}$$

where

$$\hat{N}=\hat{a}_x^\dagger\hat{a}_x+\hat{a}_y^\dagger\hat{a}_y \tag{3.5}$$

is the total number of excitations and we have denoted $\alpha_r=(r+ip_r)/\sqrt{2}$ and $\lambda_r=\ell/(\sqrt{2}r)$.

The structure of this kernel suggests the use of the rotated operators

$$\hat{a}_+=\frac{1}{\sqrt{2}}(\hat{a}_x-i\hat{a}_y)\,,\quad \hat{a}_-=\frac{1}{\sqrt{2}}(\hat{a}_x+i\hat{a}_y)\,, \tag{3.6}$$

in terms of which the OAM operator reads as

$$\hat{L}=\hat{a}_+^\dagger\hat{a}_+-\hat{a}_-^\dagger\hat{a}_-\,. \tag{3.7}$$

In this way, we can interpret ℓ as the difference of quanta with opposite chirality. Note that the form of $\hat{N}$ and $\hat{L}$ suggests that the boson operators $\hat{a}_x$ and $\hat{a}_y$ furnish a Jordan-Schwinger representation for the problem at hand [much in the same way as the original oscillator construction for SU(2)], which can be justified on very general grounds [70]. On the other hand, such a representation should not come as a surprise, for it is well known that any three-dimensional Lie algebra (as the one we are dealing with here) can be realized in terms of creation and annihilation operators of two orthogonal oscillators [71].

By noticing that $e^{-i\varphi\hat{L}}\,\hat{a}_\pm\,e^{i\varphi\hat{L}}=\hat{a}_\pm e^{\pm i\varphi}$, we can recast the Wigner kernel (3.4) as the displaced version

$$\hat{w}(r,p_r;\varphi,\ell)=e^{-i\varphi\hat{L}}\,\hat{w}(r,p_r;\ell)\,e^{i\varphi\hat{L}}\,, \tag{3.8}$$

with

$$\begin{aligned}\hat{w}(r,p_r,\ell)=4(-1)^{\hat{N}}&\exp[2i\lambda_r(\hat{p}_+-\hat{p}_-)]\\&\times\exp[-\sqrt{2}ip_r(\hat{x}_++\hat{x}_-)]\\&\times\exp[\sqrt{2}ir(\hat{p}_++\hat{p}_-)]e^{-2ip_rr}\,,\end{aligned} \tag{3.9}$$

and we have introduced the corresponding quadratures for the rotated amplitudes

$$\hat{x}_\pm=\frac{1}{\sqrt{2}}(\hat{a}_\pm+\hat{a}_\pm^\dagger)\,,\quad \hat{p}_\pm=\frac{1}{\sqrt{2}i}(\hat{a}_\pm-\hat{a}_\pm^\dagger)\,. \tag{3.10}$$

The radial momentum p_r plays no relevant role in the dynamics, so it seems entirely reasonable to integrate over this variable. To evaluate the resulting kernel we use an entangled state basis $|\xi\rangle$ (the properties of these states are briefly reviewed in Appendix A), such that

$$(\hat{a}_++\hat{a}_-^\dagger)|\xi\rangle=\xi\,|\xi\rangle\,,\quad (\hat{a}_+^\dagger+\hat{a}_-)|\xi\rangle=\xi^*|\xi\rangle\,. \tag{3.11}$$

The calculations are lengthy and the details are sketched in Appendix B. The final result for the Wigner function for a pure state $|\Psi\rangle$ turns out to be remarkably simple:

$$\begin{aligned}W_{|\Psi\rangle}(r,\varphi,\ell)=4\int_{\mathbb{R}}&\Psi^*(r-ir',\varphi)\,\Psi(r+ir',\varphi)\\&\times\exp(i2\ell r'/r)\,dr'\,,\end{aligned} \tag{3.12}$$

which is the central result of this work. Here $\Psi(r,\varphi)$ denotes the wave function of $|\Psi\rangle$ in the entangled representation; i.e.,

$$\Psi(r,\varphi)=\langle\xi|e^{i\varphi\hat{L}}|\Psi\rangle=\langle\xi\,e^{-i\varphi}|\Psi\rangle\,. \tag{3.13}$$

Notice that the similarity with the single-mode Wigner function (2.10) is manifest. Obviously, the marginal over the radial variable

$$W(\varphi,\ell)=\int_0^\infty W(r,\varphi,\ell)\,dr \tag{3.14}$$

contains complete information about the pair angle-OAM and can be constructed from first principles [39].

IV. EXAMPLES

To gain further insight into this formalism, we work out Eq. (3.12) for several states of interest. First, we look for the case of a simultaneous eigenstate of both the total number of particles and the orbital angular momenta $|N,\ell_0\rangle$, viz.,

$$\hat{N}|N,\ell_0\rangle = N|N,\ell_0\rangle\,, \quad \hat{L}|N,\ell_0\rangle = \ell_0|N,\ell_0\rangle\,. \tag{4.1}$$

Using the entangled representation, it is easy to check that

$$\Psi_{|N,\ell_0\rangle}(r,\varphi) = \frac{e^{-|\xi|^2/2}}{\sqrt{\left(\frac{N-\ell_0}{2}\right)!\left(\frac{N+\ell_0}{2}\right)!}} \times H_{\frac{N-\ell_0}{2},\frac{N+\ell_0}{2}}(\xi e^{-i\varphi},\xi^* e^{i\varphi}), \tag{4.2}$$

where $H_{m,n}(\lambda,\lambda^*)$ stands for the two-variable Hermite polynomial. In terms of the generalized Laguerre polynomials $L_p^{\ell}(x)$, this reduces to

$$\Psi_{|N,\ell_0\rangle}(r,\varphi) = C_{N,\ell_0} e^{-\frac{1}{2}r^2} r^{|\ell_0|} L^{|\ell_0|}_{\frac{N-|\ell_0|}{2}}(r^2) e^{-i\ell_0\varphi}\,, \tag{4.3}$$

where C_{N,ℓ_0} is a normalization constant. This wave function is very reminiscent of the standard Laguerre-Gauss modes employed in classical optics. The associated Wigner function is

$$W_{|N,\ell_0\rangle}(r,\varphi,\ell) = 4|C_{N,\ell_0}|^2 \int_{\mathbb{R}} (r+ir')^{2|\ell_0|}\left[L^{\ell_0}_{\frac{N-|\ell_0|}{2}}(r^2+r'^2)\right]^2 \times \exp[-(r^2+r'^2+2i\ell r'/r)]\,dr'\,. \tag{4.4}$$

This integral can be computed in a closed way, although the expression is involved enough to be of practical use. If we sum over N, we get the state

$$|\ell_0\rangle = \sum_N \frac{1}{\sqrt{N+1}}|N,\ell_0\rangle\,. \tag{4.5}$$

In Fig. 1 we have plotted an isocontour surface corresponding to $W_{|\ell_0\rangle}(r,\ell,\phi) = \text{constant}$, for $\ell_0 = 0$. We clearly appreciate quite a rich radial structure. At the top of the surface, we also include a density plot of a section by the plane $\ell = 0$, displaying the characteristic rings of the Laguerre modes. We recall that the standard Wigner function for the pair angle-OAM simplifies in this case to

$$W_{|\ell_0\rangle}(\ell,\varphi) = \frac{1}{2\pi}\delta_{\ell,\ell_0}\,, \tag{4.6}$$

which is flat in φ and the integral over the whole phase space gives the unity, reflecting the normalization of $|\ell_0\rangle$. We can recognize the amount of information lost in this approach when compared with $W(r,\varphi,\ell)$. A similar procedure can be used for the case of the eigenstates of the angle $|\varphi_0\rangle$.

As our second example, we address the superposition

$$|\Psi\rangle = \frac{1}{\sqrt{2}}(|\ell_1\rangle + e^{i\phi_0}|\ell_2\rangle) \tag{4.7}$$

of two angular-momentum eigenstates with a relative phase $e^{i\phi_0}$. The resulting features are nicely illustrated in Fig. 2. The state $|\Psi\rangle$ is plotted for $\ell_2 = -3$ and $\ell_1 = 3$. Changing the relative phase ϕ_0 results in a global rotation of the cylinder.

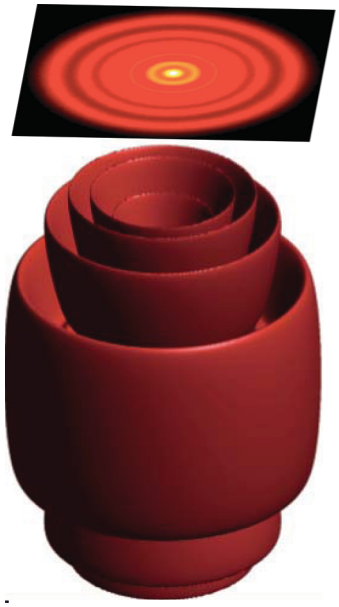

FIG. 1. (Color online) Isocontour surface of the level $1/e$ from the maximum of the Wigner function $W(r,\varphi,\ell)$ for an eigenstate of the OAM $|\ell_0\rangle$. At the top, we show a density plot of a section of that surface by the plane $\ell = 0$.

Again a rich radial structure can be appreciated. The "holes" in the isosurface correspond to points for which the Wigner function takes on negative values [72], as can be appreciated in the inset, where we draft the corresponding Wigner function $W(\ell,\varphi)$ for this state.

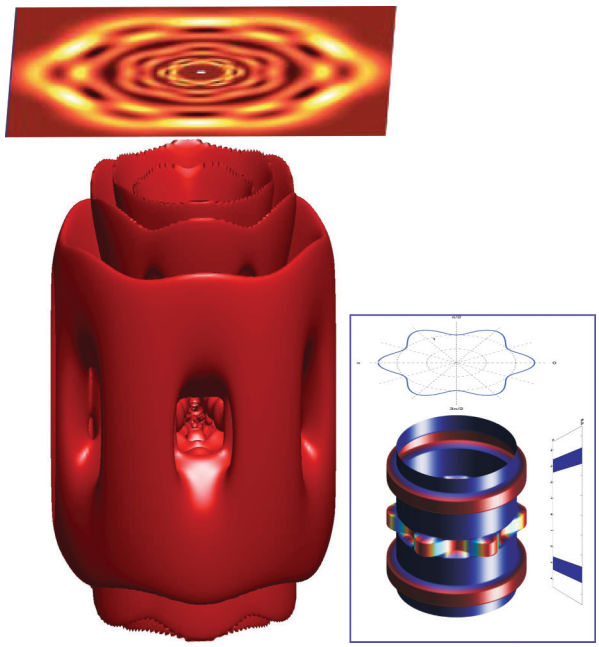

FIG. 2. (Color online) Isocontour surface of the level $1/e$ from the maximum of the Wigner function $W(r,\varphi,\ell)$ for the superposition state in Eq. (4.7), with $\ell_2 = -3$ and $\ell_1 = 3$. At the top, we show a density plot of a section of that surface by the plane $\ell = 0$. In the inset we show the standard Wigner function $W(\ell,\varphi)$ for this state, as well as the associated marginals.

V. CONCLUDING REMARKS

In summary, we have shown how to extend in a consistent way all the techniques developed for a continuous-variable phase space to the case of angle and angular momentum, including significant information about the radial variable. While we have not left aside the mathematical details, our main emphasis has been on presenting a simple and useful toolkit that any practitioner in the field should master. In our view, far from being an academic curiosity, the ideas expressed here have a wide range of potential applications in numerous hot topics in which OAM plays a key role.

ACKNOWLEDGMENTS

The inspiring ideas in this paper originated after many discussions with Prof. W. Schleich. Over the years, they have been further developed and completed with questions, suggestions, criticism, and advice from many colleagues. Particular thanks for help in various ways go to A. G. Barriuso, B.-G. Englert, J. C. Gallego, H. de Guise, and H. Kastrup. The work was supported by the EU FP7 (Grant Q-ESSENCE), the Spanish DGI (Grant FIS2011-26786), the Mexican CONACyT (Grant 106525), the Czech Ministry of Education (Project MSM6198959213), and the Czech Ministry of Industry and Trade (Project FR-TI1/364).

APPENDIX A: ENTANGLED-STATE REPRESENTATION

For the two modes $\pm$ defined in Eq. (3.6), the Fock space is spanned by

$$|n_+,n_-\rangle = \frac{(\hat{a}_+^\dagger)^{n_+}(\hat{a}_-^\dagger)^{n_-}}{\sqrt{n_+!n_-!}}|0,0\rangle\,, \tag{A1}$$

where $|0,0\rangle$ is the two-mode vacuum. Then one can immediately check that the vectors [73,74]

$$\begin{aligned} |\xi\rangle &= \exp\left[-\frac{1}{2}|\xi|^2 + \xi\hat{a}_+^\dagger + \xi^*\hat{a}_-^\dagger - \hat{a}_+^\dagger\hat{a}_-^\dagger\right]|0,0\rangle\,, \\ |\eta\rangle &= \exp\left[-\frac{1}{2}|\eta|^2 + \eta\hat{a}_+^\dagger - \eta^*\hat{a}_-^\dagger + \hat{a}_+^\dagger\hat{a}_-^\dagger\right]|0,0\rangle \end{aligned} \tag{A2}$$

are indeed eigenstates of the following operators:

$$\begin{aligned} \hat{x}_+ - \hat{x}_-|\eta\rangle &= \sqrt{2}\,\mathrm{Re}(\eta)|\eta\rangle\,, \quad \hat{p}_+ + \hat{p}_-|\eta\rangle = \sqrt{2}\,\mathrm{Im}(\eta)|\eta\rangle\,, \\ \hat{x}_+ + \hat{x}_-|\xi\rangle &= \sqrt{2}\,\mathrm{Re}(\xi)|\xi\rangle\,, \quad \hat{p}_+ - \hat{p}_-|\xi\rangle = \sqrt{2}\,\mathrm{Im}(\xi)|\xi\rangle\,, \end{aligned} \tag{A3}$$

where $\hat{x}_\pm$ and $\hat{p}_\pm$ are the quadrature operators associated to the modes $\pm$. This shows that these states are the continuous-variable versions of the original Einstein-Podolsky-Rosen states [75].

Using the technique of integration within an ordered product of operators [76], we can prove the orthogonal property and completeness relation

$$\langle\eta'|\eta\rangle = \pi\delta^{(2)}(\eta-\eta')\,, \quad \frac{1}{\pi}\int d^2\eta\,|\eta\rangle\langle\eta| = \hat{\mathbb{1}}\,, \tag{A4}$$

and an analogous one for ξ. In fact, one can also check that

$$\langle\xi|\eta\rangle = \tfrac{1}{2}\exp[(\xi\eta^* - \xi^*\eta)/2]\,. \tag{A5}$$

We observe also that if we use the Shapiro-Wagner angle operator [60]

$$\hat{E} = \sqrt{\frac{\hat{a}_+ + \hat{a}_-^\dagger}{\hat{a}_+^\dagger + \hat{a}_-}}\,, \tag{A6}$$

then

$$\hat{E}|\xi\rangle = \sqrt{\frac{\hat{a}_+ + \hat{a}_-^\dagger}{\hat{a}_+^\dagger + \hat{a}_-}}|\xi\rangle = \sqrt{\frac{\xi}{\xi^*}}|\xi\rangle = e^{i\varphi}|\xi\rangle\,, \tag{A7}$$

so these states have a well-defined angle.

If we recall that the two-variable Hermite polynomials, defined as [77]

$$H_{m,n}(\lambda,\lambda^*) = \sum_{\ell=0}^{\min(m,n)} \frac{m!n!}{\ell!(m-\ell)!(n-\ell)!}(-1)^\ell\lambda^{m-\ell}\lambda^{*n-\ell}\,, \tag{A8}$$

have the generating function

$$\sum_{m,n}^{\infty}\frac{t^m t'^n}{m!n!}H_{m,n}(\lambda,\lambda^*) = \exp(-tt' + t\lambda + t'\lambda^*)\,, \tag{A9}$$

by simple inspection we note that

$$\begin{aligned} |\eta\rangle &= \exp(-|\eta|^2/2)\sum_{n_+,n_-}\frac{(-1)^{n_-}}{\sqrt{n_+!n_-!}}H_{n_+,n_-}(\eta,\eta^*)|n_+,n_-\rangle\,, \\ |\xi\rangle &= \exp(-|\xi|^2/2)\sum_{n_+,n_-}\frac{1}{\sqrt{n_+!n_-!}}H_{n_+,n_-}(\xi,\xi^*)|n_+,n_-\rangle\,, \end{aligned} \tag{A10}$$

which constitute a compact expression of these entangled vectors in the Fock basis.

APPENDIX B: EVALUATING THE WIGNER-WEYL KERNEL

Our task here is to evaluate the kernel [Eq. (3.8)] and then integrate over the variable p_r. Using the properties of the entangled states in the previous appendix, we can write

$$\begin{aligned} \hat{w}(r,\ell) &= \int dp_r\ \hat{w}(r,p_r,\ell) \\ &= \frac{1}{\pi}(-1)^{\hat{N}}\int d^2\eta d^2\xi\ |\eta\rangle\langle\xi|\exp[(\xi\eta^* - \xi^*\eta)/2] \\ &\quad\times\exp[\sqrt{2}\lambda_r(\xi-\xi^*)]\exp[r(\eta-\eta^*)]\delta[r-\mathrm{Re}(\xi)]\,. \end{aligned} \tag{B1}$$

To simplify as much as possible what follows, we assume pure states, for which

$$W(r,\varphi,\ell) = \langle\Psi|\hat{w}(r,\varphi,\ell)|\Psi\rangle = \langle\Psi|e^{-i\varphi\hat{L}}\hat{w}(r,\ell)e^{i\varphi\hat{L}}|\Psi\rangle\,. \tag{B2}$$

This is in fact a marginal of the Wigner function of the problem. Next, we choose to expand $e^{i\varphi\hat{L}}|\Psi\rangle$ in the $|\xi\rangle$ basis. Taking

into account the properties of these states, we have

$$\Psi(\xi,\varphi) = \langle \xi | e^{i\varphi \hat{L}} | \Psi \rangle = \langle \xi e^{-i\varphi} | \Psi \rangle \,. \tag{B3}$$

Therefore, we get

$$W(r,\varphi,\ell) = \frac{1}{\pi^2} \int d^2\xi' d^2\eta d^2\xi \, \langle \xi' | (-1)^{\hat{N}} | \eta \rangle \, \delta[r - \mathrm{Re}(\xi)] \times \Psi^*(\xi',\varphi)\Psi(\xi,\varphi) \exp[(\xi\eta^* - \xi^*\eta)/2] \times \exp[\sqrt{2}\lambda_r(\xi - \xi^*)] \exp[r(\eta - \eta^*)] \,. \tag{B4}$$

If we use the decomposition of these entangled states in terms of double-variable Hermite polynomials in Eq. (A10), and we recall that $H_{m,n}(\xi,\xi^*) = H^*_{n,m}(\xi,\xi^*)$, then it is easy to check that $\langle \xi' | (-1)^{\hat{N}} | \eta \rangle = \langle \eta | \xi' \rangle$. Consequently, we have

$$\int d^2\eta \langle \eta | \xi' \rangle \, \exp[(\xi\eta^* - \xi^*\eta)/2 + r(\eta - \eta^*)] = 4\pi^2 \delta^{(2)}(\xi + \xi' - 2r) \,. \tag{B5}$$

Finally, if we perform the integral over ξ' using this result we get

$$W(r,\varphi,\ell) = 4 \int d^2\xi \, \Psi^*(2r - \xi,\varphi)\Psi(\xi,\varphi) \times \exp[\sqrt{2}\lambda_r(\xi - \xi^*)] \, \delta[r - \mathrm{Re}(\xi)] \,. \tag{B6}$$

By separating the differential $d^2\xi$ in real and imaginary parts, after integrating over the real part $\mathrm{Re}(\xi)$ we get the result (3.12).

[1] P. R. N. Childs, *Rotating Flow* (Butterworth-Heinemann, Oxford, 2011).
[2] A. B. Mikhailovskii, V. P. Lakhin, G. D. Aburdzhaniya, L. A. Mikhailovskaya, O. G. Onishchenko, and A. I. Smolyakov, Plasma Phys. Controlled Fusion **29**, 1 (1987).
[3] M. M. Salomaa and G. E. Volovik, Rev. Mod. Phys. **59**, 533 (1987).
[4] A. Hubert and R. Schäfer, *Magnetic Domains* (Springer, New York, 1998).
[5] B. T. Hefner and P. M. Marston, J. Acoust. Soc. Am. **106**, 3313 (1999).
[6] Z. F. Ezawa, *Quantum Hall Effects* (World Scientific, Singapore, 2000).
[7] L. Pitaevskii and S. Stringari, *Bose-Einstein Condensation* (Oxford University Press, Oxford, 2003).
[8] K. Y. Bliokh, Y. P. Bliokh, S. Savel'ev, and F. Nori, Phys. Rev. Lett. **99**, 190404 (2007).
[9] J. Torres and L. Torner (eds.), *Twisted Photons: Applications of Light with Orbital Angular Momentum* (Wiley-VCH, Weinheim, 2011).
[10] M. J. Padgett, J. Molloy, and D. McGloin (eds.), *Optical Tweezers* (Chapman and Hall, London, 2010).
[11] N. M. Elias, Astron. Astrophys. **492**, 883 (2008).
[12] J. Wang, J.-Y. Yang, I. M. Fazal, N. Ahmed, Y. Yan, H. Huang, Y. Ren, Y. Yue, S. Dolinar, M. Tur, and A. E. Willner, Nat. Photon. **6**, 488 (2012).
[13] A. Mair, A. Vaziri, G. Weihs, and A. Zeilinger, Nature (London) **412**, 313 (2001).
[14] G. Molina-Terriza, A. Vaziri, J. Řeháček, Z. Hradil, and A. Zeilinger, Phys. Rev. Lett. **92**, 167903 (2004).
[15] S. S. R. Oemrawsingh, A. Aiello, E. R. Eliel, G. Nienhuis, and J. P. Woerdman, Phys. Rev. Lett. **92**, 217901 (2004).
[16] L. Marrucci, C. Manzo, and D. Paparo, Phys. Rev. Lett. **96**, 163905 (2006).
[17] G. Molina-Terriza, L. Rebane, J. P. Torres, L. Torner, and S. Carrasco, J. Eur. Opt. Soc. **2**, 07014 (2007).
[18] R. Lynch, Phys. Rep. **256**, 367 (1995).
[19] V. Peřinova, A. Lukš, and J. Peřina, *Phase in Optics* (World Scientific, Singapore, 1998).
[20] A. Luis and L. L. Sánchez-Soto, Prog. Opt. **44**, 421 (2000).
[21] H. Weyl, *Gruppentheorie und Quantemechanik* (Hirzel-Verlag, Leipzig, 1928).
[22] E. P. Wigner, Phys. Rev. **40**, 749 (1932).
[23] J. E. Moyal, Proc. Cambridge Philos. Soc. **45**, 99 (1949).
[24] F. E. Schroek, *Quantum Mechanics on Phase Space* (Kluwer, Dordrecht, 1996).
[25] W. P. Schleich, *Quantum Optics in Phase Space* (Wiley-VCH, Berlin, 2001).
[26] C. K. Zachos, D. B. Fairlie, and T. L. Curtright (eds.), *Quantum Mechanics in Phase Space* (World Scientific, Singapore, 2005).
[27] N. Mukunda, Am. J. Phys. **47**, 182 (1979); N. Mukunda, G. Marmo, A. Zampini, S. Chaturvedi, and R. Simon, J. Math. Phys. **46**, 012106 (2005).
[28] J. P. Bizarro, Phys. Rev. A **49**, 3255 (1994).
[29] A. Vourdas, J. Phys. A **29**, 4275 (1996).
[30] L. M. Nieto, N. M. Atakishiyev, S. M. Chumakov, and K. B. Wolf, J. Phys. A **31**, 3875 (1998).
[31] M. Ruzzi and D. Galetti, J. Phys. A **35**, 4633 (2002).
[32] S. Zhang and A. Vourdas, J. Math. Phys. **44**, 5084 (2003).
[33] K. Kakazu and E. Sakai, Prog. Theor. Phys. **115**, 1027 (2006).
[34] K. Kowalski, J. Rembieliński, and L. C. Papaloucas, J. Phys. A **29**, 4149 (1996).
[35] J. A. González and M. A. del Olmo, J. Phys. A **31**, 8841 (1998).
[36] Y. Ohnuki and S. Kitakado, J. Math. Phys. **34**, 2827 (1993).
[37] B. C. Hall and J. J. Mitchell, J. Math. Phys. **43**, 1211 (2002).
[38] M. Ruzzi, M. A. Marchiolli, E. C. da Silva, and D. Galetti, J. Phys. A **39**, 9881 (2006).
[39] I. Rigas, L. L. Sánchez-Soto, A. B. Klimov, J. Řeháček, and Z. Hradil, Opt. Spectrosc. **108**, 206 (2010).
[40] I. Rigas, L. L. Sánchez-Soto, A. B. Klimov, J. Řeháček, and Z. Hradil, Ann. Phys. **326**, 426 (2011).
[41] A. Luis, Phys. Rev. A **71**, 053801 (2005).
[42] A. B. Klimov, J. Delgado, and L. L. Sánchez-Soto, Opt. Commun. **258**, 210 (2006).
[43] A. I. Lvovsky and M. G. Raymer, Rev. Mod. Phys. **81**, 299 (2009).
[44] I. Rigas, L. L. Sánchez-Soto, A. B. Klimov, J. Řeháček, and Z. Hradil, Phys. Rev. A **78**, 060101 (2008); J. Řeháček, Z. Hradil, Z. Bouchal, A. B. Klimov, I. Rigas, and L. L. Sánchez-Soto, Opt. Lett. **35**, 2064 (2010).

[45] E. Binz and S. Pods, *The Geometry of Heisenberg Groups* (American Mathematical Society, Providence, 2008).
[46] R. L. Stratonovich, JETP **31**, 1012 (1956) [Sov. Phys. JETP **4**, 891 (1957)].
[47] C. Brif and A. Mann, J. Phys. A **31**, L9 (1998).
[48] A. Perelomov, *Generalized Coherent States and their Applications* (Springer, Berlin, 1986).
[49] R. P. Singh, S. Roychowdhury, and V. K. Jaiswal, Opt. Commun. **274**, 281 (2007).
[50] P. Carruthers and M. M. Nieto, Rev. Mod. Phys. **40**, 411 (1968).
[51] J. C. Garrison and J. Wong, J. Math. Phys. **11**, 2242 (1970).
[52] E. C. Lerner, H. W. Huang, and G. E. Walters, J. Math. Phys. **11**, 1679 (1970).
[53] R. G. Newton, Ann. Phys. **124**, 327 (1980).
[54] R. A. Leacock, Found. Phys. **17**, 799 (1987).
[55] D. Ellinas, J. Math. Phys. **32**, 135 (1991).
[56] X. Ma and W. Rhodes, Phys. Rev. A **43**, 2576 (1991).
[57] A. Luis and L. L. Sánchez-Soto, Phys. Rev. A **48**, 752 (1993).
[58] L. Susskind and J. Glogower, Physics **1**, 49 (1964).
[59] H. Paul, Fortschr. Phys. **22**, 657 (1974).
[60] J. H. Shapiro and S. S. Wagner, IEEE J. Quantum Electron. **QE-20**, 803 (1984).
[61] S. M. Barnett and D. T. Pegg, J. Mod. Opt. **36**, 7 (1989).
[62] V. N. Popov, Theor. Math. Phys. **89**, 1292 (1991).
[63] J. W. Noh, A. Fougères, and L. Mandel, Phys. Rev. A **45**, 424 (1992).
[64] Z. Hradil, Quantum Opt. **4**, 93 (1992).
[65] M. Freyberger, K. Vogel, and W. Schleich, Quantum Opt. **5**, 65 (1993).
[66] C. Zhu and J. R. Klauder, Am. J. Phys. **61**, 605 (1993).
[67] R. L. Liboff, *Introductory Quantum Mechanics*, 3rd ed. (Addison, Reading, 1998).
[68] A. Galindo and P. Pascual, *Quantum Mechanics* (Springer, Berlin, 1991).
[69] G. Paz, Eur. J. Phys. **22**, 337 (2001).
[70] S. Chaturvedi, G. Marmo, N. Mukunda, R. Simon, and A. Zampini, Rev. Math. Phys. **18**, 887 (2006).
[71] J. M. Gracia-Bondía, F. Lizzi, G. Marmo, and P. Vitale, J. High Energy Phys. 04 (2002) 026.
[72] I. Rigas, L. L. Sánchez-Soto, A. B. Klimov, J. Řeháček, and Z. Hradil, Phys. Rev. A **81**, 012101 (2010).
[73] H. Fan, Phys. Rev. A **65**, 064102 (2002).
[74] H.-Y. Fan, Commun. Theor. Phys. **54**, 241 (2010).
[75] A. Einstein, B. Podolsky, and N. Rosen, Phys. Rev. **47**, 777 (1935).
[76] Fan Hong-Yi, H. R. Zaidi, and J. R. Klauder, Phys. Rev. D **35**, 1831 (1987).
[77] V. V. Dodonov, J. Phys. A **27**, 6191 (1994).

Paper 3

P. de la Hoz, A. B. Klimov, G. Björk, Y.-H. Kim, C. R. Müller, Ch. Marquardt, G. Leuchs, L. L. Sánchez-Soto:

"Multipolar hierarchy of efficient quantum polarization measures",

Physical Review A **88**, 063803 (2013)

Multipolar hierarchy of efficient quantum polarization measures

P. de la Hoz,[1] A. B. Klimov,[2] G. Björk,[3] Y.-H. Kim,[4] C. Müller,[5,6] Ch. Marquardt,[5,6] G. Leuchs,[5,6] and L. L. Sánchez-Soto[1,5,6]

[1]*Departamento de Óptica, Facultad de Física, Universidad Complutense, 28040 Madrid, Spain*

[2]*Departamento de Física, Universidad de Guadalajara, 44420 Guadalajara, Jalisco, Mexico*

[3]*Department of Applied Physics, Royal Institute of Technology, AlbaNova University Center, SE-106 91 Stockholm, Sweden*

[4]*Department of Physics, Pohang University of Science and Technology, Pohang 790-784, Korea*

[5]*Max-Planck-Institut für die Physik des Lichts, Günther-Scharowsky-Straße 1, Bau 24, 91058 Erlangen, Germany*

[6]*Department für Physik, Universität Erlangen-Nürnberg, Staudtstraße 7, Bau 2, 91058 Erlangen, Germany*

(Received 9 July 2013; published 2 December 2013)

We advocate a simple multipole expansion of the polarization density matrix. The resulting multipoles appear as successive moments of the Stokes variables and can be obtained from feasible measurements. In terms of these multipoles we construct a whole hierarchy of measures that accurately assess higher-order polarization fluctuations.

DOI: 10.1103/PhysRevA.88.063803 PACS number(s): 42.25.Ja, 42.50.Ar, 42.50.Dv, 42.50.Lc

I. INTRODUCTION

The standard notion of polarization comes from the treatment of light as a beam. This hints at a well-defined direction of propagation, and thus at a specific transverse plane, wherein the tip of the electric field describes an ellipse. This polarization ellipse can be elegantly visualized by using the Poincaré sphere and is determined by the Stokes parameters, the degree of polarization being simply the length of the Stokes vector [1].

This geometric representation not only provides remarkable insight but also greatly simplifies otherwise complex problems and, as a result, has become an indisputable tool to deal with polarization phenomena. However, the necessity of addressing new issues, such as highly nonparaxial fields [2], narrow-band imaging systems [3], and the recognition of associated propagation questions [4], has brought about significant modifications of this simple classical picture [5–13].

In the quantum domain, the classical setting can be immediately mimicked in terms of the Stokes operators, which can be obtained from the Stokes parameters by quantizing the field amplitudes [14]. However, the appearance of hurdles such as hidden polarization [15], the fact that the Poincaré sphere cannot accommodate photon-number fluctuations [16], and the difficulties in defining polarization properties of two-photon entangled fields [17], to cite only a few examples, show that the resulting theory is insufficient.

The root of these difficulties can be traced to the fact that classical polarization is chiefly built on first-order moments of the Stokes variables, whereas higher-order moments can play a major role for quantum fields. Polarization squeezing [18], a nonclassical effect that is actually defined only by the variances of the Stokes operators, illustrates that point in the most clear way.

Nowadays, there is a general consensus in that a full understanding of the subtle polarization effects arising in the realm of the quantum world would require a characterization of higher-order polarization fluctuations, as it happens in coherence theory, where one needs, in general, a hierarchy of correlation functions. Some results along these lines have already been reported, but either they use magnitudes difficult to determine in practice, such as distances [19], generalized visibilities [20–23], and central moments [24], or they go only up to second order [25,26], and the pertinent extensions are difficult to discern.

In this paper, we propose a systematic and feasible solution to such a fundamental and longstanding problem. To that end, we resort to a multipole expansion of the density matrix that naturally sorts successive moments of the Stokes variables. The dipole term, being just the first-order moment, can be identified with the classical picture, while the other multipoles account for higher-order moments. The probability distribution for these multipoles provides thus a complete information about the polarization properties of any state; in terms of it we propose a suitable measure for the quantitative assessment of those fluctuations.

II. SETTING THE SCENARIO

Throughout, we assume a monochromatic quantum field specified by two operators, $\hat{a}_H$ and $\hat{a}_V$, representing the complex amplitudes in two linearly polarized orthogonal modes, which we denote as horizontal (H) and vertical (V), respectively. The Stokes operators can be concisely defined as

$$\hat{S}_\mu = \frac{1}{2}(\hat{a}_H^\dagger \ \hat{a}_V^\dagger)\,\sigma_\mu \begin{pmatrix} \hat{a}_H \\ \hat{a}_V \end{pmatrix}, \tag{2.1}$$

the subscript $\dagger$ denoting the Hermitian adjoint. The Greek index μ runs from 0 to 3, where $\sigma_0 = \mathbb{1}$ and $\{\sigma_k\}$ $(k = 1,2,3)$ are the Pauli matrices.

Note carefully that $\hat{S}_0 = \hat{N}/2$, where $\hat{N} = \hat{a}_H^\dagger \hat{a}_H + \hat{a}_V^\dagger \hat{a}_V$ is the operator for the total number of photons. On the other hand, with our definition the average of $\hat{\mathbf{S}} = (\hat{S}_1, \hat{S}_2, \hat{S}_3)$ differs by a factor of $1/2$ from the classical Stokes vector [14]. However, in this way $\{\hat{S}_k\}$ satisfy the commutation relations of the SU(2) algebra

$$[\hat{S}_k, \hat{S}_\ell] = i\epsilon_{k\ell m}\,\hat{S}_m, \tag{2.2}$$

where $\epsilon_{k\ell m}$ is the Levi-Civita fully antisymmetric tensor. This noncommutability precludes the simultaneous exact measurement of the physical quantities they represent, which can be formulated quantitatively by the uncertainty relation

$$\Delta^2\hat{\mathbf{S}} = \Delta^2\hat{S}_1 + \Delta^2\hat{S}_2 + \Delta^2\hat{S}_3 \geqslant \tfrac{1}{2}\langle\hat{N}\rangle, \tag{2.3}$$

where the variances are given by $\Delta^2\hat{S}_i = \langle\hat{S}_i^2\rangle - \langle\hat{S}_i\rangle^2$. In other words, the electric vector of a monochromatic quantum field never traces a definite ellipse.

In classical optics, the states of definite polarization are specified by $\langle\hat{\mathbf{S}}\rangle^2 = \langle\hat{S}_0\rangle^2$ and the average intensity is a well-defined quantity. In the three-dimensional space of the Stokes parameters this defines a sphere with radius equal to the intensity: the Poincaré sphere. In contradistinction, in quantum optics we have that $\hat{\mathbf{S}}^2 = \hat{S}_0(\hat{S}_0 + \hat{\mathbb{1}})$. As fluctuations in the number of photons are, in general, unavoidable, we are forced to work with a full three-dimensional Poincaré space that can be regarded as a set of nested spheres with radii proportional to the different photon numbers that contribute to the state.

The Hilbert space $\mathscr{H}$ of these fields is spanned by the Fock states $\{|n_H,n_V\rangle\}$ for both polarization modes. However, since $[\hat{N},\hat{\mathbf{S}}] = 0$, each subspace with a fixed number of photons N (i.e., fixed spin $S \equiv S_0 = N/2$) must be handled separately. In other words, in the previous onionlike picture of the Poincaré space, each shell has to be addressed independently. This can be underlined if we employ the relabeling

$$|S,m\rangle \equiv |n_H = S+m, n_V = S-m\rangle. \tag{2.4}$$

In this angular momentum basis, $S = N/2, m = (n_H - n_V)/2$, and, for each S, m runs from $-S$ to S. This can be seen as the basis of common eigenstates of $\{\hat{\mathbf{S}}^2,\hat{S}_3\}$, and these states span a $(2S+1)$-dimensional subspace wherein $\hat{\mathbf{S}}$ acts in the standard way.

III. THE POLARIZATION SECTOR AND THE MULTIPOLE EXPANSION

From the previous discussion, it is clear that the moments of any energy-preserving observable (such as $\hat{\mathbf{S}}$) do not depend on the coherences between different subspaces. The only accessible information from any state described by the density matrix $\hat{\varrho}$ is thus its polarization sector [27], which is given by the block-diagonal form

$$\hat{\varrho}_{\rm pol} = \bigoplus_S P_S\,\hat{\varrho}^{(S)}, \tag{3.1}$$

where P_S is the photon-number distribution (S takes on the values $0, 1/2, 1, \ldots$) and $P_S\,\hat{\varrho}^{(S)}$ is the reduced density matrix in the subspace with spin S. Any $\hat{\varrho}$ and its associated block-diagonal form $\hat{\varrho}_{\rm pol}$ cannot be distinguished in polarization measurements, and so, accordingly, we drop henceforth the subscript *pol*. This is consistent with the fact that polarization and intensity are, in principle, separate concepts: in classical optics the form of the ellipse described by the electric field (polarization) does not depend on its size (intensity).

To proceed further we need to represent every component $\hat{\varrho}^{(S)}$ in a polarization basis. Instead of using directly the states $\{|S,m\rangle\}$, it is more convenient to write such an expansion as

$$\hat{\varrho}^{(S)} = \sum_{K=0}^{2S}\sum_{q=-K}^{K} \varrho_{Kq}^{(S)}\,\hat{T}_{Kq}^{(S)}, \tag{3.2}$$

TABLE I. Values of $\mathscr{W}_K$ and the degree $\mathbb{P}_K$ for three different quantum polarization states. $|S;\theta,\phi\rangle$ stands for an SU(2) coherent state in the S subspace, and $|\alpha_H,\alpha_V\rangle$ is a two-mode quadrature coherent state with $\bar{N} = |\alpha_H|^2 + |\alpha_V|^2$ the average number of photons.

State	$\mathscr{W}_K$	$\mathbb{P}_K$
$\lvert S,m\rangle$	$\frac{2K+1}{2S+1}(C^{Sm}_{Sm,K0})^2$	$\left[\frac{\sum_{\ell=1}^{K}\frac{2\ell+1}{2S+1}(C^{Sm}_{Sm,\ell 0})^2}{\sum_{\ell=1}^{K}\frac{2\ell+1}{2S+1}(C^{SS}_{SS,\ell 0})^2}\right]^{1/2}$
$\lvert S;\theta,\phi\rangle$	$\frac{2K+1}{2S+1}(C^{SS}_{SS,K0})^2$	1
$\lvert\alpha_H,\alpha_V\rangle$	$\sum_{S=K/2}^{\infty}\frac{\bar{N}^{2S}e^{-\bar{N}}}{(2S)!}\frac{2K+1}{2S+1}(C^{SS}_{SS,K0})^2$	$\sum_{S=K/2}^{\infty}\frac{\bar{N}^{2S}e^{-\bar{N}}}{(2S)!}$

where the irreducible tensor operators $\hat{T}_{Kq}^{(S)}$ are [28]

$$\hat{T}_{Kq}^{(S)} = \sqrt{\frac{2K+1}{2S+1}}\sum_{m,m'=-S}^{S} C^{Sm'}_{Sm,Kq}\,|S,m'\rangle\langle S,m|, \tag{3.3}$$

with $C^{Sm'}_{Sm,Kq}$ being the Clebsch-Gordan coefficients that couple a spin S and a spin K ($0 \leqslant K \leqslant 2S$) to a total spin S.

Although at first sight Eq. (3.3) might look a bit intricate, $\hat{T}_{Kq}^{(S)}$ is related to the Kth power of the Stokes operators, a simple observation that will turn out crucial in the following. In particular, the monopole $\hat{T}_{00}^{(S)}$, being proportional to the identity, is always trivial, while the dipole $\hat{T}_{1q}^{(S)}$ is proportional to $\hat{S}_q$ and thus renders the classical picture, in which the state is depicted by its average value. Therefore, higher-order multipoles embody the polarization fluctuations we wish to appraise [29].

The expansion coefficients $\varrho_{Kq}^{(S)} = {\rm Tr}[\hat{\varrho}^{(S)}\,T_{Kq}^{(S)\dagger}]$ are known as state multipoles, and they contain complete information, but sorted in a manifestly SU(2)-invariant form.

Alternatively, one can look at

$$\mathscr{W}_K^{(S)} = \sum_{q=-K}^{K}\left|\varrho_{Kq}^{(S)}\right|^2, \tag{3.4}$$

which is just the square of the state overlapping with the Kth multipole patterns in the Sth subspace. When there is a distribution of photon numbers, we sum over all of them: $\mathscr{W}_K = \sum_S P_S\,\mathscr{W}_K^{(S)}$. One can easily find out that

$$\sum_K \mathscr{W}_K = {\rm Tr}(\hat{\varrho}^2), \tag{3.5}$$

so it is just the purity. Actually, as shown in the Appendix, $\mathscr{W}_K$ can be interpreted as a measure of the localization of the state in phase space.

In Table I we have worked out the values of $\mathscr{W}_K$ for three outstanding examples of quantum states that will serve as a guide: the state $|S,0\rangle$ (which reads $|N,N\rangle$, with $N = S$, in the basis $|n_H,n_V\rangle$), the SU(2) coherent state $|S;\theta,\phi\rangle$ (defined in the Appendix), and a two-mode quadrature coherent state $|\alpha_H,\alpha_V\rangle$, summing up over the Poissonian photon-number distribution (with $\bar{N} = |\alpha_H|^2 + |\alpha_V|^2$). In Fig. 1 we also plot these cases in point; as we can see, for the classical quadrature

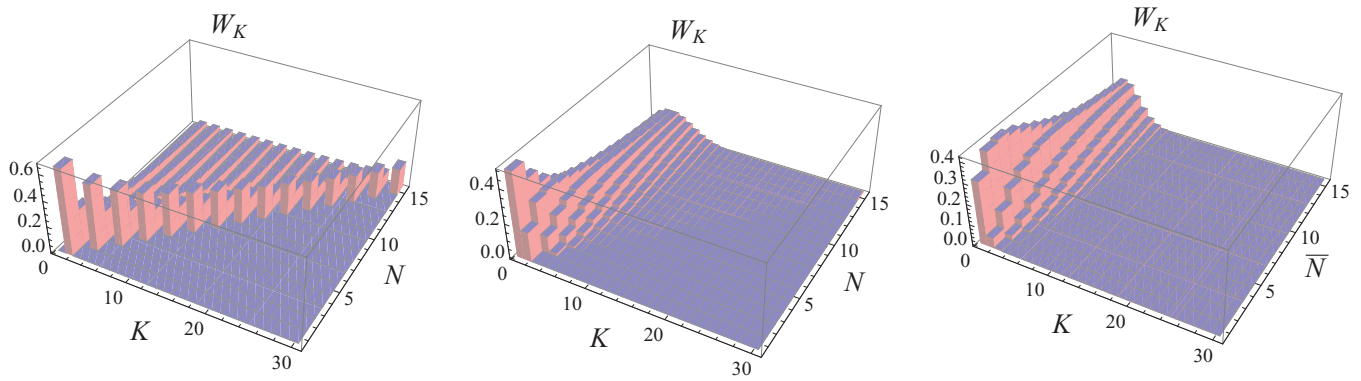

FIG. 1. (Color online) Distribution $\mathscr{W}_K$ as a function of the multipole order K for the examples in Table I. From left to right, the state $|S,0\rangle$ ($|N,N\rangle$, with $S=N$, in the basis $|n_H,n_V\rangle$), the SU(2) coherent state $|S;\theta,\phi\rangle$, and a two-mode quadrature coherent state with average number of photons $\bar{N}=|\alpha_H|^2+|\alpha_V|^2$.

coherent state the first multipoles contribute the most, whereas for the nonclassical $|S,0\rangle$ state the converse holds.

IV. RECONSTRUCTING THE MULTIPOLES

The analysis thus far confirms that multipoles constitute a natural tool to deal with polarization properties. We will show next that, in addition, they can be experimentally determined.

The polarization state is customarily analyzed with a Stokes measurement setup (see Fig. 2), consisting of a quater-wave plate (QWP) with the axis at angle ϕ, followed by a half-wave plate (HWP) at angle θ and a polarizing beam splitter (PBS) that separates the H and V modes. The wave plates effectively perform a displacement of the state that can be described by the operator $\hat{D}(\theta,\phi)=e^{i\theta\hat{S}_2}e^{i\phi\hat{S}_3}$, and (θ,ϕ) are angular coordinates on the sphere. Each of the two outputs of the PBS are measured by photon detectors: the photocurrent sum gives directly the eigenvalue of $\hat{N}$, while the difference gives the observable $\hat{S}_{\mathbf{n}}=\mathbf{n}\cdot\hat{\mathbf{S}}$, where $\mathbf{n}$ is the unit vector in the direction (θ,ϕ) [30].

Altogether, this indicates that the scheme yields the probability distribution for $\hat{S}_{\mathbf{n}}$, from which we can equivalently infer the moments

$$\mu_\ell^{(S)}(\theta,\phi)=\mathrm{Tr}\left[\hat{S}_{\mathbf{n}}^\ell\,\hat{\varrho}^{(S)}\right]. \tag{4.1}$$

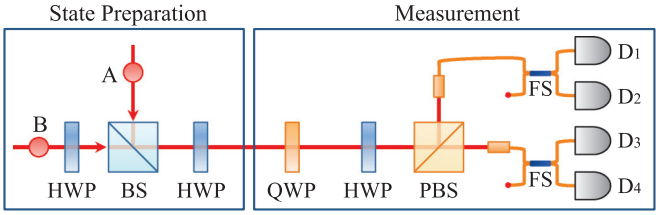

FIG. 2. (Color online) Experimental setup. Single photons A and B, both horizontally polarized, are prepared by spontaneous parametric down-conversion. (P)BS denotes a (polarization) beam splitter. HWP and QWP denote half-wave and quarter-wave plates, respectively. FS denotes a 50:50 fiber splitter, and D1–D4 denote single-photon avalanche photodiodes.

For simplicity, we restrict ourselves to a subspace with a fixed number of photons S, but everything can be smoothly extended to the whole polarization sector.

We start by noticing that the measurable moments can be expressed in terms of the state multipoles as

$$\begin{aligned}\mu_\ell^{(S)}(\theta,\phi)&=\mathrm{Tr}\left[\hat{S}_3^\ell\,\hat{D}(\theta,\phi)\,\hat{\varrho}^{(S)}\,\hat{D}^\dagger(\theta,\phi)\right]\\&=\mathrm{Tr}\left[\hat{S}_3^\ell\sum_{K=0}^{2S}\sum_{q,q'=-K}^{K}\varrho_{Kq}^{(S)}\,D_{qq'}^K(\theta,\phi)\,\hat{T}_{Kq}^{(S)}\right],\end{aligned} \tag{4.2}$$

where $D_{mm'}^S(\theta,\phi)=\langle S,m|\hat{D}(\theta,\phi)|S,m'\rangle$ is the Wigner D function [28]. To proceed further we need to compute

$$\begin{aligned}\mathrm{Tr}\left[\hat{S}_3^\ell\,\hat{T}_{Kq}^{(S)}\right]=\delta_{q0}\left[\frac{S(S+1)(2S+1)}{3}\right]^{\ell/2}\frac{3^{\ell/2}\sqrt{2K+1}}{(2S+1)^{(\ell+1)/2}}\\\times\sum_{m=-S}^{S}\left(C_{Sm,10}^{Sm}\right)^\ell C_{Sm,K0}^{Sm}.\end{aligned} \tag{4.3}$$

Interestingly, we have that $C_{Sm,10}^{Sm}=m/\sqrt{S(S+1)}$ and

$$\sum_{m=-S}^{S}m^\ell C_{Sm,K0}^{Sm}=i^{\ell-K}\,\partial_\omega^\ell\chi_K^S(\omega)\big|_{\omega=0}\equiv f_{K\ell}^{(S)}\qquad K\leqslant\ell, \tag{4.4}$$

with $\chi_S^m(\omega)$ the generalized SU(2) character [28]. Collecting all those results together, the moments come out connected with the multipoles in quite an elegant way:

$$\mu_\ell^{(S)}(\theta,\phi)=\sqrt{\frac{4\pi}{2S+1}}\sum_{K=0}^{\ell}\sum_{q=-K}^{K}\varrho_{Kq}^{(S)}\,f_{K\ell}^{(S)}\,Y_{Kq}(\theta,\phi), \tag{4.5}$$

$Y_{Kq}(\theta,\phi)$ being the spherical harmonics.

We can benefit from the orthonormality of $Y_{Kq}(\theta,\phi)$ to integrate Eq. (4.5) so as to obtain

$$\varrho_{Kq}^{(S)}=\frac{1}{f_{K\ell}^{(S)}}\sqrt{\frac{2S+1}{4\pi}}\int_{\mathscr{S}^2}d\Omega\,\mu_\ell^{(S)}(\theta,\phi)\,Y_{Kq}^*(\theta,\phi), \tag{4.6}$$

where $K\leqslant\ell$ and the integral extends over the whole unit sphere $\mathscr{S}^2$ with $d\Omega=\sin\theta d\theta d\phi$ being the solid angle. The

reconstruction of the state requires the knowledge of *all* the multipoles: this implies measuring *all* the moments in *all* the directions, which proves to be very demanding [16].

Nonetheless, we can attack the problem in a much more economic way. The central idea is that to determine the Kth multipole it is enough to perform a Stokes measurement in $2K+1$ independent directions. As a matter of fact, the proposal proceeds in a recurrent way: first, we measure the first-order moments in the three coordinate axis (or other equivalent ones) and reconstruct $\varrho_{1q}^{(S)}$. That is, from the values of $\mu_1^{(S)}(\theta,\phi)$, which can write down as

$$\mu_1^{(S)}(\theta,\phi) = f_{11}^{(S)}\sqrt{\frac{4\pi}{2S+1}}\sum_{q=-1}^{1}\varrho_{1q}^{(S)}Y_{1q}(\theta,\phi), \tag{4.7}$$

we need to know $\varrho_{1q}^{(S)}$. By taking into account that $f_{11}^{(S)} = (2S+1)\sqrt{S(S+1)}/3$, we can solve the resulting linear system, getting

$$\begin{pmatrix}\varrho_{11}^{(S)}\\ \varrho_{10}^{(S)}\\ \varrho_{1-1}^{(S)}\end{pmatrix} = \sqrt{\frac{3}{2S(S+1)(2S+1)}}\begin{pmatrix}-1 & i & 0\\ 0 & 0 & \sqrt{2}\\ 1 & i & 0\end{pmatrix}\begin{pmatrix}\mu_{1,1}^{(S)}\\ \mu_{1,2}^{(S)}\\ \mu_{1,3}^{(S)}\end{pmatrix}, \tag{4.8}$$

from which we infer all the first-order properties. Here $\mu_{1,k}^{(S)}$ indicate the first-order moment in the kth direction.

The measurement of the second moments gives us

$$\mu_2^{(S)}(\theta,\phi) = \frac{1}{2S+1}f_{02}^{(S)} + f_{22}^{(S)}\sqrt{\frac{4\pi}{2S+1}}\sum_{q=-2}^{2}\varrho_{2q}^{(S)}Y_{2q}(\theta,\phi), \tag{4.9}$$

with

$$\begin{aligned} f_{02}^{(S)} &= \tfrac{1}{3}S(S+1)(2S+1),\\ f_{22}^{(S)} &= \frac{4(2S+1)}{5!}\sqrt{S(2S-1)(S+1)(2S+3)}, \end{aligned} \tag{4.10}$$

while $f_{12}^{(S)} = 0$. We need to fix five optimal directions to invert that system. For example, thinking of the measurements as lines, we can choose the directions as

$$\mathbf{n}_{1,2} \propto \begin{pmatrix}0\\ \pm 2\\ 1+\sqrt{5}\end{pmatrix}, \quad \mathbf{n}_{3,4} \propto \begin{pmatrix}\pm 2\\ 1+\sqrt{5}\\ 0\end{pmatrix}, \quad \mathbf{n}_5 \propto \begin{pmatrix}1+\sqrt{5}\\ 0\\ 2\end{pmatrix}, \tag{4.11}$$

which maximizes the minimum angle between the lines and thus in some sense spreads out the measurements over the Poincaré sphere as much as possible [31]. The system can be then solved, and all we need to characterize the process at second order is known.

For the Lth moment, we have

$$\boldsymbol{\mu}_L^{(S)} = \sqrt{\frac{4\pi}{2S+1}}f_{KL}^{(S)}\mathbf{Y}_K\,\boldsymbol{\varrho}_K^{(S)}, \tag{4.12}$$

where $\boldsymbol{\mu}_L^{(S)} = (\mu_L^{(S)}(\theta_1,\phi_1),\ldots,\mu_L^{(S)}(\theta_{2L+1},\phi_{2L+1}))$ and similarly for $\boldsymbol{\varrho}_K^{(S)}$ and $[\mathbf{Y}_L]_{ij} = Y_{Lj}(\theta_i,\phi_i)$. Observe that, in general, the right-hand side hinges on the results of lowest-order measurements. The linear inversion of that equation can be formally written down as

$$\boldsymbol{\varrho}_K^{(S)} = \frac{1}{f_{KL}^{(S)}}\sqrt{\frac{2S+1}{4\pi}}\frac{4\pi}{2L+1}\mathbf{P}_L^{-1}\mathbf{Y}_L^{\dagger}\boldsymbol{\mu}_L^{(S)}, \tag{4.13}$$

where $\mathbf{P}_L = 4\pi/(2L+1)\mathbf{Y}_L\mathbf{Y}_L^{\dagger}$, with $[\mathbf{P}_L]_{ij} = P_L(\omega_{ij})$, $\cos\omega_{ij} = \cos\theta_i\cos\theta_j + \sin\theta_i\sin\theta_j\sin(\phi_i-\phi_j)$, and $P_L(\omega_{ij})$ is the Legendre polynomial. The choosing of the appropriate directions is, in general, a tricky question if one wants to be sure about the linear independence, but it has been thoroughly studied [32]. In practice, methods such as maximum likelihood are much more efficient in handling that inversion [33].

To check the proposed strategy, we have performed an experiment using spontaneous parametric down-conversion. The photon pairs centered at 780 nm were generated in a 2-mm-thick type-I β-barium-borate (BBO) crystal pumped by a femtosecond laser pulse centered at 390 nm and subsequently filtered by an interference filter with a 4-nm bandwidth and brought to the inputs of a Hong-Ou-Mandel interferometer. After the interferometer, either the state $|1_H,1_V\rangle$ or the state $|2_H,0_V\rangle$ can be postselected, depending on the relative polarizations of the incident photons.

The setup is sketched in Fig. 2. At each output of the PBS, a two-photon detector is simulated by a 50:50 fiber beam splitter (FS) and two single-photon detectors (PerkinElmer, SPCM-AQRH). The photon detection efficiency of each single-photon detector channel is used to calibrate the measurement of the Stokes parameters. To achieve full information about the first- and second-order moments, we have measured these coincidences in five distinct measurement bases and then reconstructed the multipoles via linear inversion. Each measurement is done for 3 s and repeated three times to improve the precision.

In Table II we summarize the results obtained for the state $|2_H,0_V\rangle$ (which is $|1,1\rangle$ in the angular momentum basis). The agreement with the theory is pretty good. Although this instance might look a bit naive, it constitutes quite a conclusive proof of principle of our method.

V. ASSESSING HIGHER-ORDER POLARIZATION CORRELATIONS

Even though the polarization information is encoded in the set $\{\mathscr{W}_K^{(S)}\}$, for most of the states only a limited number of multipoles play a substantive role and the rest of them have an exceedingly small contribution, so that gaining a good feeling of the corresponding behavior may be tricky.

A possible way to bypass this disadvantage is to look at the cumulative distribution

$$\mathscr{A}_K^{(S)} = \sum_{\ell=1}^{K}\mathscr{W}_\ell^{(S)}, \tag{5.1}$$

TABLE II. Experimental and theoretical results obtained for the state $|2_H,0_V\rangle$ (which is the $|1,1\rangle$ state in the angular momentum basis). The number in parentheses indicates the error in the last figure. The directions of measurement are the three coordinate axes for μ_1 and (4.11) for μ_2.

	Experiment		Theory			Experiment		Theory	
Direction	μ_1	μ_2	μ_1	μ_2	Multipole	$K=1$	$K=2$	$K=1$	$K=2$
1	−0.10 (3)	0.84 (7)	0	0.8618	ϱ_{K-2}		−0.01 (7) −0.01 (1) i		0
2	0.06 (2)	0.87 (1)	0	0.8618	ϱ_{K-1}	−0.05 (2) + 0.03 (1)i	0.07 (6) −0.02 (2) i	0	0
3	0.99 (3)	0.50 (2)	1	0.5000	ϱ_{K0}	0.70 (1)	0.39 (4)	0.7071	0.4082
4		0.52 (1)		0.5000	ϱ_{K1}	0.05 (2) + 0.03 (1) i	−0.07 (7) −0.02 (1) i	0	0
5		0.70 (2)		0.6382	ϱ_{K2}		−0.01 (1) +0.01 (1) i		0

which conveys the whole information *up* to order K. We know from probability that it has remarkable properties [34]. Moreover, our previous reconstruction puts in clear evidence that to obtain the Kth multipole one needs to determine all the previous moments.

As with any cumulative distribution, $\mathscr{A}_K^{(S)}$ is a monotone nondecreasing function of the multipole order, with $\mathscr{A}_{2S}^{(S)}$ being proportional to the state purity [except by the monopole contribution, $K=0$, which is not included in Eq. (5.1)]. One might be interested in dealing instead with magnitudes satisfying $0 \leqslant \mathbb{P}_K \leqslant 1$ for every K, as any sensible degree of polarization [35]. To that end, we note that for SU(2) coherent states we have

$$\mathscr{A}_{K,\mathrm{SU}(2)}^{(S)} = \frac{2S}{2S+1} - \frac{[\Gamma(2S+1)]^2}{\Gamma(2S-K)\Gamma(2S+K+2)}. \tag{5.2}$$

We conjecture that $\mathscr{A}_{K,\mathrm{SU}(2)}^{(S)}$ is indeed maximal for any K in each subspace S. This seems to suggest a degree of polarization up to the Kth order as

$$\mathbb{P}_K = \sum_S P_S \sqrt{\frac{\mathscr{A}_K^{(S)}}{\mathscr{A}_{K,\mathrm{SU}(2)}^{(S)}}}. \tag{5.3}$$

According to the definition Eq. (5.3), $\mathbb{P}_K = 1$ (for every K) for SU(2) coherent states, which is compatible with the idea that they are the most localized states over the sphere. On the other hand, for quadrature coherent states, which constitute an acid test for any new proposal in polarization, the result, as indicated in Table I, reads

$$\mathbb{P}_K = \sum_{S=K/2}^{\infty} \frac{e^{-\bar{N}}\bar{N}^{2S}}{(2S)!} \simeq \frac{1}{2}\mathrm{erfc}\left(\frac{K-\bar{N}}{\sqrt{2\bar{N}}}\right). \tag{5.4}$$

Here, $\bar{N}$ is the average number of photons, and the second equality, in terms of the complementary error function, holds true for $\bar{N} \gg 1$. From the properties of this function, we can estimate that the multipoles that contribute effectively are, roughly speaking, from 1 to $\bar{N}$. In Fig. 3 we plot $\mathbb{P}_K$ for the states $|S,0\rangle$ and $|\alpha_H,\alpha_V\rangle$.

To round off our understanding of $\mathbb{P}_K$, in Fig. 4 we have depicted $\mathbb{P}_K$ for two other relevant quantum states routinely treated in this context: NOON and two-mode squeezed vacuum states, defined as

$$\begin{aligned} |\mathrm{NOON}\rangle &= \frac{1}{\sqrt{2}}(|N,0\rangle + |0,N\rangle), \\ |\mathrm{TMSV}\rangle &= \sqrt{1-\lambda^2}\sum_N \lambda^N |N,N\rangle. \end{aligned} \tag{5.5}$$

To follow the standard notation, in both cases we have employed the $\{|n_H,n_V\rangle\}$ basis and $\lambda = \tanh r$, with r the squeezing parameter.

For the particular yet significant case of the dipole ($K=1$), Eq. (5.3) reduces to

$$\mathbb{P}_1 = \sum_S^{\infty} P_S \frac{\sqrt{\langle\hat{S}_1\rangle^2 + \langle\hat{S}_2\rangle^2 + \langle\hat{S}_3\rangle^2}}{\langle\hat{S}_0\rangle}, \tag{5.6}$$

and the average values are calculated in every subspace S. Interestingly, this definition has been recently proposed as a way to circumvent the shortcomings of the standard degree of

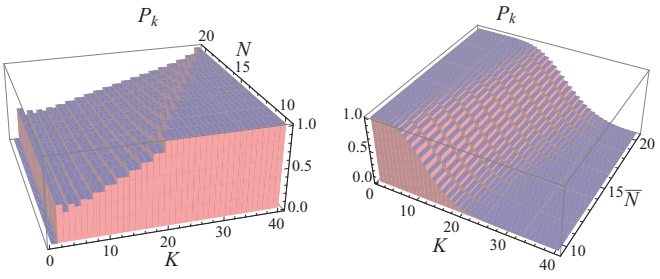

FIG. 3. (Color online) Degree of polarization $\mathbb{P}_K$ as a function of the multipole order K for the state $|S,0\rangle$ (left panel) and a quadrature coherent state $|\alpha_H,\alpha_V\rangle$ with average number of photons $\bar{N} = |\alpha_H|^2 + |\alpha_V|^2$ (right panel).

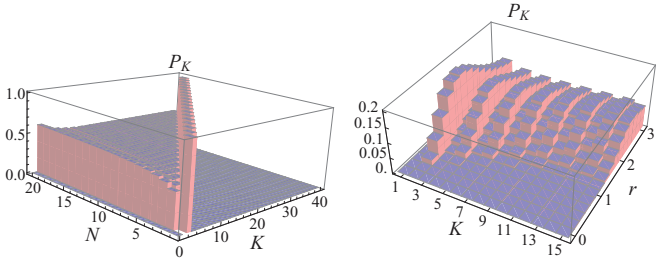

FIG. 4. (Color online) Degree of polarization $\mathbb{P}_K$ for the NOON (left panel) and two-mode squeezed vacuum (right panel) using the squeezing parameter r as a measure of the average number of photons.

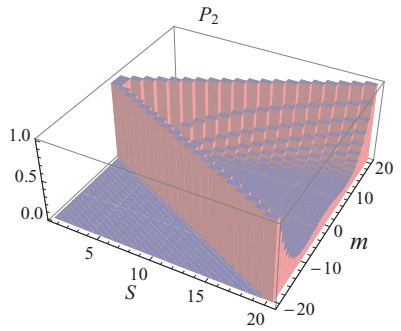

FIG. 5. (Color online) Second-order degree of polarization $\mathbb{P}_2$ for the state $|S,m\rangle$.

polarization [36]; in our approach, it emerges quite in a natural way.

To close our paper, we briefly consider the instance of $\mathbb{P}_2$. For two-mode quadrature coherent states $|\alpha_H,\alpha_V\rangle$ we immediately get

$$\mathbb{P}_2(|\alpha_H,\alpha_V\rangle) = 1-(1+\bar{N})\exp(-\bar{N}), \tag{5.7}$$

which tends to the unity when the average number of photons $\bar{N}$ becomes large enough, in agreement with previous second-order approaches [25]. For the states $|S,m\rangle$, we have

$$\mathbb{P}_2(|S,m\rangle) = \sqrt{\frac{45m^4+5S^2(S+1)^2-9m^2[2S(S+1)+1]}{4S^2(2S-1)(4S+1)}}. \tag{5.8}$$

This expression is exactly unity whenever $m=\pm S$ or $\pm\sqrt{1+2S-3S^2}/\sqrt{5}$ (this equality is valid only when m is an integer). This latter condition is only met when $S=1$ with $m=0$.

On the other hand, $\mathbb{P}_2$ attains its minimum value

$$\mathbb{P}_{2,\min}(|S,m\rangle) = \sqrt{\frac{9+18S+8S^2}{80S^2}} \simeq \frac{1}{\sqrt{10}}, \tag{5.9}$$

whenever $m=\pm\sqrt{1+2S+2S^2}/\sqrt{10}$. In Fig. 5 we outline these facts.

VI. CONCLUDING REMARKS

Multipolar expansions are a commonplace and a formidable tool in many branches of physics. We have applied such an expansion to the polarization density matrix, showing how the corresponding state multipoles quantify higher-order fluctuations in the Stokes variables. In this way we have provided a systematic characterization of quantum polarization fluctuations that, paradoxically, was missing in the realm of quantum optics.

Moreover, the formalism can be manifestly extended to other systems in which SU(2) symmetry plays a crucial role (such as in Bose-Einstein condensates and spin chains) and to other unitary symmetries, such as SU(3) (which is pivotal to understanding the polarization properties of the near field). This is more than an academic curiosity, and work in this direction is ongoing in our group.

ACKNOWLEDGMENTS

Financial support from the Swedish Foundation for International Cooperation in Research and Higher Education (STINT), the Swedish Research Council (VR) through its Linnæus Center of Excellence ADOPT and Contract No. 621-2011-4575, the CONACyT (Grant No. 106525), the European Union FP7 (Grant Q-ESSENCE), and the Spanish Dirección General de Investigación (Grant No. FIS2011-26786) is gratefully acknowledged. It is also a pleasure to thank H. de Guise for stimulating discussions.

APPENDIX: POLARIZATION QUASIDISTRIBUTIONS

The discussion in this paper suggests that polarization must be specified by a probability distribution of polarization states. As a matter of fact, such a probabilistic description is unavoidable in quantum optics from the very beginning, since $\{\hat{S}_k\}$ do not commute and thus no state can have a definite value of all of them simultaneously.

The SU(2) symmetry inherent in the polarization structure of quantum fields allows us to take advantage of the pioneering work of Stratonovich [37] and Berezin [38], who worked out quasiprobability distributions on the sphere satisfying all the pertinent requirements. This construction was later generalized by others [39–43] and has proved to be very useful in visualizing properties of spinlike systems [44–46].

For each partial $\hat{\varrho}^{(S)}$, one can define r-parametrized SU(2) quasidistributions as

$$W_r^{(S)}(\theta,\phi) = \frac{\sqrt{4\pi}}{\sqrt{2S+1}} \sum_{K=0}^{2S} \sum_{q=-K}^{K} \left(C_{SS,K0}^{SS}\right)^{-r} \varrho_{Kq}^{(S)}\, Y_{Kq}^{*}(\theta,\phi). \tag{A1}$$

For $r=0$ this is the Wigner function, while $r=+1$ and -1 lead to the P and Q functions, respectively. Note also that the Clebsch-Gordan coefficient $C_{SS,K0}^{SS}$ has a very simple analytical form [28]:

$$C_{SS,K0}^{SS} = \frac{\sqrt{2S+1}(2S)!}{\sqrt{(2S-K)!\,(2S+1+K)!}}. \tag{A2}$$

While, for spins, S is typically a fixed number, in quantum optics most of the states involve a full polarization sector and one should sum over the subspaces contributing to the state.

The integral

$$\Sigma = \frac{1}{\int d\Omega \left[W_r^{(S)}(\theta,\phi)\right]^2}, \tag{A3}$$

extended to the whole sphere, can be interpreted as the effective area where the corresponding quasidistribution is different from zero. In other words, Σ is a measure of the number of polarization states contained in a given field state. This and similar definitions have already been used as measures of localization and uncertainty in different contexts [47].

Using the explicit form of Eq. (A1) we immediately get

$$\int d\Omega \left[W_r^{(S)}(\theta,\phi)\right]^2 = \frac{4\pi}{2S+1} \sum_{K=0}^{2S} \left(C_{SS,K0}^{SS}\right)^{-2r} \mathscr{W}_K^{(S)}. \tag{A4}$$

We can appreciate a deep connection (except for the unessential Clebsch-Gordan coefficient) between the distribution $\{\mathscr{W}_K^{(S)}\}$ and the notion of localization in phase space. In particular, for the Wigner function $r = 0$, the right-hand side of Eq. (A4) is giving information about the measured $\{\mathscr{W}_K^{(S)}\}$.

For the sake of completeness, we briefly recall the definition of the SU(2) coherent states (also known as spin or atomic coherent states), which reads [48,49]

$$|S;\theta,\phi\rangle = \hat{D}(\theta,\phi)|S,-S\rangle. \tag{A5}$$

Here $\hat{D}(\theta,\phi) = \exp(\xi\hat{S}_+ - \xi^*\hat{S}_-)$ [with $\xi = (\theta/2)\exp(-i\phi)$ and (θ,ϕ) being spherical angular coordinates] plays the role of a displacement on the Poincaré sphere of radius S.

The ladder operators $\hat{S}_\pm = \hat{S}_1 \pm i\hat{S}_2$ select the fiducial state $|S,-S\rangle$ as usual: $\hat{S}_-|S,-S\rangle = 0$. This definition closely mimics its standard counterpart for position and momentum.

Note that these coherent states are eigenstates of the measured operator $\hat{S}_\mathbf{n} = \mathbf{n}\cdot\hat{\mathbf{S}}$,

$$\hat{S}_\mathbf{n}|S;\theta,\phi\rangle = S|S;\theta,\phi\rangle, \tag{A6}$$

and they saturate the uncertainty relation Eq. (2.3), so they are the minimum uncertainty states in polarization optics.

The two-mode quadrature coherent states $|\alpha_H,\alpha_V\rangle$ can be expressed as a Poissonian superposition of SU(2) coherent states:

$$|\alpha_H,\alpha_V\rangle = \sum_S \frac{\bar{N}^{2S}e^{-\bar{N}}}{(2S)!}|2S,\theta,\phi\rangle, \tag{A7}$$

where $\bar{N} = |\alpha_H|^2 + |\alpha_V|^2$ is the average number of photons.

[1] C. Brosseau, *Fundamentals of Polarized Light: A Statistical Optics Approach* (Wiley, New York, 1998).
[2] E. A. Ash and G. Nicholls, Nature (London) **237**, 510 (1972).
[3] D. W. Pohl, W. Denk, and M. Lanz, Appl. Phys. Lett. **44**, 651 (1984).
[4] J. C. Petruccelli, N. J. Moore, and M. A. Alonso, Opt. Commun. **283**, 4457 (2010).
[5] J. C. Samson, Geophys. J. R. Astron. Soc. **34**, 403 (1973).
[6] R. Barakat, Opt. Commun. **23**, 147 (1977).
[7] T. Setälä, A. Shevchenko, M. Kaivola, and A. T. Friberg, Phys. Rev. E **66**, 016615 (2002).
[8] A. Luis, Opt. Commun. **253**, 10 (2005).
[9] J. Ellis, A. Dogariu, S. Ponomarenko, and E. Wolf, Opt. Commun. **248**, 333 (2005).
[10] P. Réfrégier and F. Goudail, J. Opt. Soc. Am. A **23**, 671 (2006).
[11] M. R. Dennis, J. Opt. Soc. Am. A **24**, 2065 (2007).
[12] C. J. R. Sheppard, J. Opt. Soc. Am. A **28**, 2655 (2011).
[13] X.-F. Qian and J. H. Eberly, Opt. Lett. **36**, 4110 (2011).
[14] A. Luis and L. L. Sánchez-Soto, *Quantum Phase Difference, Phase Measurements and Stokes Operators* (Elsevier, Amsterdam, 2000), pp. 421–481.
[15] D. N. Klyshko, Phys. Lett. A **163**, 349 (1992).
[16] C. R. Müller, B. Stoklasa, C. Peuntinger, C. Gabriel, J. Řeháček, Z. Hradil, A. B. Klimov, G. Leuchs, C. Marquardt, and L. L. Sánchez-Soto, New J. Phys. **14**, 085002 (2012).
[17] G. Jaeger, M. Teodorescu-Frumosu, A. Sergienko, B. E. A. Saleh, and M. C. Teich, Phys. Rev. A **67**, 032307 (2003).
[18] A. S. Chirkin, A. A. Orlov, and D. Y. Parashchuk, Quantum Electron. **23**, 870 (1993). N. Korolkova, G. Leuchs, R. Loudon, T. C. Ralph, and C. Silberhorn, Phys. Rev. A **65**, 052306 (2002).
[19] A. B. Klimov, L. L. Sánchez-Soto, E. C. Yustas, J. Söderholm, and G. Björk, Phys. Rev. A **72**, 033813 (2005).
[20] G. Björk, S. Inoue, and J. Söderholm, Phys. Rev. A **62**, 023817 (2000).
[21] A. Sehat, J. Söderholm, G. Björk, P. Espinoza, A. B. Klimov, and L. L. Sánchez-Soto, Phys. Rev. A **71**, 033818 (2005).
[22] T. S. Iskhakov, I. N. Agafonov, M. V. Chekhova, G. O. Rytikov, and G. Leuchs, Phys. Rev. A **84**, 045804 (2011).
[23] R. S. Singh and H. Prakash, Ann. Phys. **333**, 198 (2013).
[24] G. Björk, J. Söderholm, Y.-S. Kim, Y.-S. Ra, H.-T. Lim, C. Kothe, Y.-H. Kim, L. L. Sánchez-Soto, and A. B. Klimov, Phys. Rev. A **85**, 053835 (2012).
[25] A. B. Klimov, G. Björk, J. Söderholm, L. S. Madsen, M. Lassen, U. L. Andersen, J. Heersink, R. Dong, C. Marquardt, G. Leuchs, and L. L. Sánchez-Soto, Phys. Rev. Lett. **105**, 153602 (2010).
[26] R. S. Singh and H. Prakash, Phys. Rev. A **87**, 025802 (2013).
[27] M. G. Raymer, D. F. McAlister, and A. Funk, in *Quantum Communication, Computing, and Measurement 2*, edited by P. Kumar (Plenum, New York, 2000).
[28] D. A. Varshalovich, A. N. Moskalev, and V. K. Khersonskii, *Quantum Theory of Angular Momentum* (World Scientific, Singapore, 1988).
[29] L. L. Sánchez-Soto, A. B. Klimov, P. de la Hoz, and G. Leuchs, J. Phys. B **46**, 104011 (2013).
[30] C. Marquardt, J. Heersink, R. Dong, M. V. Chekhova, A. B. Klimov, L. L. Sánchez-Soto, U. L. Andersen, and G. Leuchs, Phys. Rev. Lett. **99**, 220401 (2007).
[31] J. H. Conway, R. H. Hardin, and N. J. A. Sloane, Exp. Math. **5**, 139 (1996).
[32] S. N. Filippov and V. I. Man'ko, J. Russ. Laser Res. **31**, 32 (2010).
[33] *Quantum State Estimation*, edited by M. G. A. Paris and J. Řeháček, Lecture Notes in Physics Vol. 649 (Springer, Berlin, 2004).
[34] E. T. Jaynes, *Probability Theory: The Logic of Science* (Cambridge University Press, Cambridge, 2003).
[35] G. Björk, J. Söderholm, L. L. Sánchez-Soto, A. B. Klimov, I. Ghiu, P. Marian, and T. A. Marian, Opt. Commun. **283**, 4440 (2010).
[36] C. Kothe, L. S. Madsen, U. L. Andersen, and G. Björk, Phys. Rev. A **87**, 043814 (2013).
[37] R. L. Stratonovich, JETP **31**, 1012 (1956).
[38] F. A. Berezin, Commun. Math. Phys. **40**, 153 (1975).
[39] G. S. Agarwal, Phys. Rev. A **24**, 2889 (1981).

[40] C. Brif and A. Mann, J. Phys. A **31**, L9 (1998).
[41] S. Heiss and S. Weigert, Phys. Rev. A **63**, 012105 (2000).
[42] A. B. Klimov and S. M. Chumakov, J. Opt. Soc. Am. A **17**, 2315 (2000).
[43] A. B. Klimov and J. L. Romero, J. Phys. A **41**, 055303 (2008).
[44] J. P. Dowling, G. S. Agarwal, and W. P. Schleich, Phys. Rev. A **49**, 4101 (1994).
[45] S. M. Chumakov, A. Frank, and K. B. Wolf, Phys. Rev. A **60**, 1817 (1999).
[46] A. B. Klimov, J. Math. Phys. **43**, 2202 (2002).
[47] M. J. W. Hall, Phys. Rev. A **59**, 2602 (1999).
[48] F. T. Arecchi, E. Courtens, R. Gilmore, and H. Thomas, Phys. Rev. A **6**, 2211 (1972).
[49] A. Perelomov, *Generalized Coherent States and Their Applications* (Springer, Berlin, 1986).

Paper 4

E. Karimi, R. W. Boyd, P. de la Hoz, H. de Guise, Z. Hradil, J. Rehacek, A. Aiello, G. Leuchs, L. L. Sánchez-Soto:

"Radial quantum number of Laguerre-Gauss modes"

Physical Review A **89**, 063813 (2014)

Radial quantum number of Laguerre-Gauss modes

E. Karimi,[1] R. W. Boyd,[1] P. de la Hoz,[2] H. de Guise,[3] J. Řeháček,[4] Z. Hradil,[4] A. Aiello,[5,6] G. Leuchs,[1,5,6] and L. L. Sánchez-Soto[2,5,6]

[1]*Department of Physics, University of Ottawa, 150 Louis Pasteur, Ottawa, Ontario, Canada K1N 6N5*
[2]*Departamento de Óptica, Facultad de Física, Universidad Complutense, 28040 Madrid, Spain*
[3]*Department of Physics, Lakehead University, Thunder Bay, Ontario, Canada P7B 5E1*
[4]*Department of Optics, Palacký University, 17 listopadu 12, 746 01 Olomouc, Czech Republic*
[5]*Max-Planck-Institut für die Physik des Lichts, Günther-Scharowsky-Straße 1, Bau 24, 91058 Erlangen, Germany*
[6]*Department für Physik, Universität Erlangen-Nürnberg, Staudtstraße 7, Bau 2, 91058 Erlangen, Germany*

(Received 31 January 2014; published 16 June 2014)

We introduce an operator linked with the radial index in the Laguerre-Gauss modes of a two-dimensional harmonic oscillator in cylindrical coordinates. We discuss ladder operators for this variable, and confirm that they obey the commutation relations of the su(1,1) algebra. Using this fact, we examine how basic quantum optical concepts can be recast in terms of radial modes.

DOI: 10.1103/PhysRevA.89.063813 PACS number(s): 42.50.Tx, 03.67.Ac, 42.25.−p, 42.50.Dv

I. INTRODUCTION

An optical vortex is a light field exhibiting a pure screw phase dislocation along the propagation axis; i.e., an azimuthal phase dependence $\exp(i\ell\varphi)$. The integer ℓ plays the role of a topological charge: the phase changes its value by ℓ cycles of 2π in any closed circuit about the axis, while the amplitude is zero there [1].

One of the most intriguing properties of vortices is that they carry orbital angular momentum (OAM). This was first realized by Allen and co-workers [2] for the important instance of Laguerre-Gauss (LG) laser modes. Furthermore, they demonstrated that these modes carry an OAM of $\ell\hbar$ per photon along the propagation direction.

A useful feature of optical OAM is that it can be easily manipulated and transferred; this has opened new horizons in various fields, ranging from mechanical micromanipulation [3] to imaging sciences [4,5], as well as potential astronomical [6,7] and communication applications [8]. Beyond optical wavelengths, OAM now plays a major role in electron [9–12], x-ray [13–15], and radio-frequency engineering [16–18]. The core observation that individual photons also carry OAM brings the most exciting possibilities for employing this variable in the quantum regime, and a number of uses has already been demonstrated [19–24].

Despite this intense activity, very little attention has been paid thus far to the radial index p of the LG modes. Usually, it is stated that for $p > 0$, the modes are multiringed with $p + 1$ radial nodes. Beyond this short mention, no physical meaning is attached to this quantity. Two recent papers, however, have presented challenging and interesting insights into this issue [25,26]. Our purpose here is to present a simple comprehensive analysis of this variable.

The two aforementioned papers considered optical modes, governed by the paraxial wave equation. These modes are ultimately suitably rescaled wave functions of the stationary states of a two-dimensional quantum oscillator, under the Schrödinger equation [27]. Since this latter system can properly model other interesting vortices arising in different media (as in plasmas [28], superfluids [29], and Bose-Einstein condensates [29]), the oscillator will serve as our thread, bearing in mind that the results can be immediately translated to the optical case.

II. STATIONARY STATES OF A TWO-DIMENSIONAL OSCILLATOR

A. Cartesian coordinates

To be as self-contained as possible, we briefly review the example of an isotropic two-dimensional quantum harmonic oscillator of mass m and natural frequency ω, with coordinates in two orthogonal axes, say x and y [30,31]. The Hamiltonian can be compactly written as $\hat{H} = \hbar\omega(\hat{n} + \hat{\mathbb{1}})$, where the total number operator $\hat{n}$ is

$$\hat{n} = \hat{n}_x + \hat{n}_y = \hat{a}_x^\dagger \hat{a}_x + \hat{a}_y^\dagger \hat{a}_y \,, \tag{2.1}$$

and the annihilation and creation operators fulfill the canonical commutation relations $[\hat{a}_j, \hat{a}_k^\dagger] = \delta_{jk}\hat{\mathbb{1}}$, with $j,k \in \{x,y\}$. Since the spectrum of $\hat{n}_j$ is composed of all non-negative integers n_j, the energies are given by $E_{n_x,n_y} = \hbar\omega(n_x + n_y + 1)$ and these eigenvalues are $(n_x + n_y + 1)$-fold degenerate.

Elements of the Fock basis are the common eigenvectors of $\hat{n}_x$ and $\hat{n}_y$:

$$|n_x, n_y\rangle = \frac{1}{\sqrt{n_x! n_y!}} (\hat{a}_x^\dagger)^{n_x} (\hat{a}_y^\dagger)^{n_y} |0,0\rangle \,, \tag{2.2}$$

where $|0,0\rangle$ is the ground state. The stationary states of the oscillator are the product of Hermite-Gauss modes, as the oscillations in each axes are kinematically independent:

$$\Psi_{n_x n_y}(x,y) = \sqrt{\frac{\alpha^2}{\pi\ 2^{n_x+n_y} n_x! n_y!}} H_{n_x}(\alpha x) H_{n_y}(\alpha y) \times \exp[-\alpha^2(x^2 + y^2)/2] \,, \tag{2.3}$$

with $\alpha = \sqrt{m\omega/\hbar}$. To recover the equivalent beam solutions, one needs to take $\alpha = \sqrt{2}$, since the paraxial wave equation (in adimensional coordinates) coincides with the Schrödinger equation for the oscillator when $m = 2\hbar$ and $\omega = 1$.

For our purposes, the solution at $t = 0$ is enough. The wave function at any other time can be obtained in a simple way by using the explicit form of the propagator. For beams, where the role of time is played by the coordinate z along the symmetry axis, this propagation brings about additional interesting points, such as the Gouy phase.

B. Cylindrical coordinates

The axes x and y do not enjoy a privileged role in the problem. Since the energy is invariant under rotations in the xy plane, we could as well have chosen any other rotated reference frame. To take a better advantage of this symmetry, we consider the z component of the angular momentum, $\hat{L}_z = \hbar\hat{\ell}$, with $\hat{\ell} = i(\hat{a}_y^\dagger \hat{a}_x - \hat{a}_x^\dagger \hat{a}_y)$, and use the rotated bosonic operators [32]

$$\hat{a}_\pm = \frac{1}{\sqrt{2}}(\hat{a}_x \mp i\hat{a}_y)\,, \quad \hat{a}_\pm^\dagger = \frac{1}{\sqrt{2}}(\hat{a}_x^\dagger \pm i\hat{a}_y^\dagger)\,, \tag{2.4}$$

where $[\hat{a}_j,\hat{a}_k^\dagger] = \delta_{jk}\hat{\mathbb{1}}$, with $j,k \in \{+,-\}$. We can then check that

$$\hat{n} = \hat{n}_+ + \hat{n}_-\,, \quad \hat{\ell} = \hat{n}_+ - \hat{n}_-\,, \tag{2.5}$$

whose interpretation is direct: the system can be envisioned now as consisting of "quanta" with positive (counterclockwise rotation around z) and negative (clockwise rotation around z) orbital angular momentum.

The Fock basis $\{|n_+,n_-\rangle\}$ of the common eigenvectors of $\hat{n}_+$ and $\hat{n}_-$ can be constructed much in the same way as in Eq. (2.2). However, it will prove useful to consider instead the continuous set

$$|\eta\rangle = \exp\left(-\tfrac{1}{2}|\eta|^2 + \eta\hat{a}_+^\dagger - \eta^*\hat{a}_-^\dagger + \hat{a}_+^\dagger\hat{a}_-^\dagger\right)|0,0\rangle\,, \tag{2.6}$$

parametrized by the complex number $\eta = r\exp(-i\varphi)$. The states $|\eta\rangle$ constitute an orthonormal basis, whose properties have been reviewed in depth in Ref. [33]. In the representation they generate $[\psi(\eta) = \langle\eta|\psi\rangle]$, the action of the basic operators is

$$\begin{aligned} \hat{a}_+\psi(\eta) &= \left(\frac{\eta}{2} + \frac{\partial}{\partial\eta^*}\right)\psi(\eta)\,, \\ \hat{a}_-\psi(\eta) &= -\left(\frac{\eta^*}{2} + \frac{\partial}{\partial\eta}\right)\psi(\eta)\,, \end{aligned} \tag{2.7}$$

while for the adjoints we have

$$\hat{a}_+^\dagger = \hat{a}_- - \eta^*\,, \quad \hat{a}_-^\dagger = \hat{a}_+ - \eta\,. \tag{2.8}$$

Since the exponential acting on the vacuum in Eq. (2.6) is not unitary, the creation and destruction operators are not conjugates one of the other under the usual boson conjugation.

Given the above, $\hat{n}$ and $\hat{\ell}$ act in this space as

$$\begin{aligned} \hat{n} &\mapsto \frac{r^2}{2} - \frac{1}{2}\left(\frac{\partial^2}{\partial r^2} + \frac{1}{r}\frac{\partial}{\partial r} + \frac{1}{r^2}\frac{\partial^2}{\partial\varphi^2}\right) - 1\,, \\ \hat{\ell} &\mapsto -i\frac{\partial}{\partial\varphi}\,. \end{aligned} \tag{2.9}$$

As $[\hat{\ell},\hat{n}] = 0$, the basis $\{|n_+,n_-\rangle\}$ can be reinterpreted as common eigenvectors of $\hat{n}$ and $\hat{\ell}$, with eigenvalues $n = n_+ + n_-$ and $\ell = n_+ - n_-$, respectively. The stationary states in this basis can be readily obtained using Eqs. (2.9); the final result is

$$\Psi_{n\ell}(r,\varphi) = A_{n\ell}(r)\,e^{i\ell\varphi}\,, \tag{2.10}$$

where the normalized amplitude is

$$A_{n\ell}(r) = \frac{\sqrt{2\alpha^2 p!}}{\sqrt{(p+|\ell|)!}}\,e^{-\alpha^2r^2/2}(\alpha r)^{|\ell|}L_p^{|\ell|}(\alpha^2r^2)\,, \tag{2.11}$$

$L_p^\ell(x)$ are the generalized Laguerre polynomials and we have written $p = (n-|\ell|)/2$. The probability distribution $|\Psi_{n\ell}(r,\varphi)|^2$ shows p dark concentric rings.

III. QUANTUM OPTICS WITH RADIAL MODES

A. The radial number operator

Since the number of dark rings is $p = (n-|\ell|)/2$, the operator

$$\hat{p} = \frac{1}{2}(\hat{n} - |\hat{\ell}|) = \begin{cases} \hat{n}_- & \text{for} \quad \ell > 0\,, \\ \hat{n}_+ & \text{for} \quad \ell < 0\,, \end{cases} \tag{3.1}$$

seems to be a sensible definition for the radial-number operator of the Laguerre-Gauss modes. According to Eq. (2.9), in differential form it reads

$$\hat{p} \mapsto -\frac{1}{4}\left(\frac{\partial^2}{\partial r^2} + \frac{1}{r}\frac{\partial}{\partial r} + \frac{1}{r^2}\frac{\partial^2}{\partial\varphi^2}\right) + \frac{i}{2}\frac{\partial}{\partial\varphi} + \frac{1}{2}\frac{r^2}{2} - \frac{1}{2}\,. \tag{3.2}$$

Incidentally, it coincides with the operator found in Ref. [26] by setting $r \to \alpha r$.

To simplify the following discussion, let us, for the time being, relabel the stationary states $|n,\ell\rangle$ as $|p,\ell\rangle$, where p indicates the radial mode eigenvalue; i.e.,

$$\hat{p}|p,\ell\rangle = p|p,\ell\rangle\,. \tag{3.3}$$

As heralded in the Introduction, we are interested in exploring the Hilbert space associated with the radial number p, while keeping the OAM ℓ fixed. At first sight, one might look for the canonical conjugate variable to $\hat{p}$. Since, according to Eq. (3.1), $\hat{p} = \hat{n}_-$ or $\hat{n}_+$ (depending on the sign of ℓ), such a variable would be a phase $\hat{\phi}_-$ or $\hat{\phi}_+$. This means that if we denote by $\hat{e} = \exp(i\hat{\phi}_\pm)$ the exponential of such a putative phase, the corresponding commutation relation will read [34]

$$[\hat{e},\hat{p}] = \hat{e}\,. \tag{3.4}$$

This immediately implies

$$\hat{e} = \sum_{p=0}^{\infty} |p,\ell\rangle\langle p+1,\ell|\,, \tag{3.5}$$

so that

$$\hat{e}|p,\ell\rangle = |p-1,\ell\rangle\,, \quad \hat{e}^\dagger|p,\ell\rangle = |p+1,\ell\rangle\,. \tag{3.6}$$

Whereas the spectrum of $\hat{\ell}$ is unbounded, including all the integer numbers, the spectrum of $\hat{p}$ is semibounded, as it comprises only non-negative integers. This indicates that the action of $\hat{e}$ as a ladder operator fails at $p = 0$, and consequently it cannot be unitary:

$$\hat{e}\hat{e}^\dagger = \hat{\mathbb{1}}\,, \quad \hat{e}^\dagger\hat{e} = \hat{\mathbb{1}} - \hat{\mathscr{P}}_0, \tag{3.7}$$

where $\hat{\mathscr{P}}_0 = |0,\ell\rangle\langle 0,\ell|$ is the projector on the "vacuum."

All these problems thus place this interpretation on shaky grounds. For this reason, we prefer to follow an alternative route. To this end, we observe that to increase (decrease) the radial number by one unit, with ℓ unchanged, we need to create (annihilate) one positive quantum and one negative quantum, namely,

$$\begin{aligned} \hat{k}_+|p,\ell\rangle &= \hat{a}_-^\dagger\hat{a}_+^\dagger|p,\ell\rangle \propto |p+1,\ell\rangle\,, \\ \hat{k}_-|p,\ell\rangle &= \hat{a}_-\hat{a}_+|p,\ell\rangle \propto |p-1,\ell\rangle\,. \end{aligned} \tag{3.8}$$

One can check that

$$[\hat{k}_+,\hat{k}_-] = -2\hat{k}_z\,, \quad [\hat{k}_z,\hat{k}_+] = \hat{k}_+\,, \quad [\hat{k}_z,\hat{k}_-] = -\hat{k}_-\,, \tag{3.9}$$

with $\hat{k}_z = (\hat{n} + \hat{\mathbb{1}})/2$. This means that if we define $\hat{k}_\pm = \hat{k}_x \pm i\hat{k}_y$, we have

$$[\hat{k}_x,\hat{k}_y] = -i\hat{k}_z\,, \quad [\hat{k}_y,\hat{k}_z] = i\hat{k}_x\,, \quad [\hat{k}_z,\hat{k}_x] = i\hat{k}_y\,, \tag{3.10}$$

that is, they are the generators of the su(1, 1) algebra, as first noticed in Ref. [25].

B. Radial coherent states

To explore the issue in more detail, it is convenient to give some basic background on some well-known irreducible representations (irreps) of SU(1,1), which are excellently reviewed in Ref. [35] and whose role in quantum optics is difficult to underestimate [36–45]. The Casimir operator for this group is $\hat{K}^2 = \hat{k}_z^2 - \hat{k}_x^2 - \hat{k}_y^2$, which can be expressed as $\hat{K}^2 = k(k-1)\hat{\mathbb{1}}$, where the Bargmann index k labels the different irreps (this index plays the role of spin for rotations). In our case, a simple calculation shows that $k = (|\ell| + 1)/2$, so that $k = 1/2, 1, 3/2, \ldots$, which corresponds to the so-called positive discrete series, for which $\hat{k}_z$ is diagonal and has a discrete spectrum. In the Fock basis $\{|n_+,n_-\rangle\}$, the basis states of the irrep k are $\{|k,k+p\rangle\}$, with $p = 0, 1, \ldots$, and hence

$$\hat{k}_z|k,k+p\rangle = (k+p)|k,k+p\rangle\,, \tag{3.11}$$

while the ladder operators act as

$$\begin{aligned}\hat{k}_+|k,k+p\rangle &= \sqrt{(2k+p)(p+1)}|k,k+p+1\rangle\,,\\ \hat{k}_-|k,k+p\rangle &= \sqrt{p(2k+p-1)}|k,k+p-1\rangle\,.\end{aligned} \tag{3.12}$$

Note that we can make the identification $|p,\ell\rangle \leftrightarrow |k,k+p\rangle$, provided $k = (|\ell| + 1)/2$.

Since $\hat{k}_-|k,k\rangle = 0$, this state can be taken as the vacuum. Indeed, $\hat{D}(\xi) = \exp(\xi\hat{k}_+ - \xi^*\hat{k}_-)$ are truly displacement operators, so according to the Perelomov prescription [46], the set

$$|\zeta\rangle = \hat{D}(\xi)|k,k\rangle \tag{3.13}$$

constitutes a family of *bona fide* coherent states parametrized by the pseudo-Euclidean unit vector $\mathbf{n} = (\sinh\omega\cos\varphi, \sinh\omega\sin\varphi, \cosh\omega)$, with $\xi = (\omega/2)\exp(i\varphi)$ and $\zeta = \tanh(\omega/2)\exp(-i\varphi)$.

By expanding the exponential and employing the disentangling theorem, we get the decomposition

$$|\zeta\rangle = (1-|\zeta|^2)^k \sum_{p=0}^{\infty} \sqrt{\frac{\Gamma(2k+p)}{p!\Gamma(2k)}}\,\zeta^p |k,k+p\rangle\,, \tag{3.14}$$

and by projecting over the complete basis $|\eta\rangle$ we get the corresponding wave function $\Psi_\zeta(r,\varphi)$ in the transverse parameters. The expression can be simplified into an exponential form using the identity

$$\exp\left(\frac{\gamma x}{\gamma - 1}\right) = (1-\gamma)^{1+|\ell|} \sum_{p=0}^{\infty} \gamma^p L_p^{|\ell|}(x)\,, \tag{3.15}$$

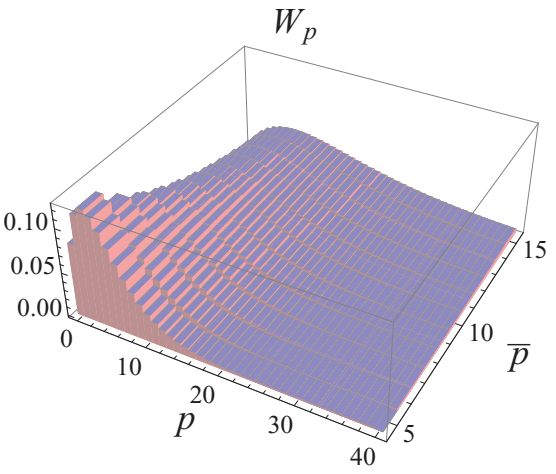

FIG. 1. (Color online) Probability distribution W_p for a coherent state $|\zeta\rangle$ with $\ell = 1$ as as a function of p and the ring average number $\bar{p}$.

so the final result is

$$\Psi_\zeta(r,\varphi) = \sqrt{\frac{\alpha^2}{\pi|\ell|!}}\left[\frac{1-|\zeta|^2}{(1-\zeta)^2}\right]^{(|\ell|+1)/2} \times e^{(\zeta+1)/(\zeta-1)\alpha^2 r^2/2}(\alpha r)^{|\ell|}e^{i\ell\varphi}\,. \tag{3.16}$$

We see that the Perelomov coherent states are polynomial-Gauss modes at $t = 0$; a subfamily of hypergeometric-Gauss modes upon evolution, as discussed in Ref. [47]. They are also eigenstates of the OAM and shape invariant in the time evolution.

The average number of sharp rings in the state $|\zeta\rangle$ is

$$\bar{p} = \frac{|\zeta|^2}{|\zeta|^2 - 1}(|\ell| + 1)\,, \tag{3.17}$$

and the statistical distribution of rings $W_p = |\langle p,\ell|\zeta\rangle|^2$ is

$$W_p = \frac{(|\ell|+1)^{|\ell|+1}(p+|\ell|)!}{p!|\ell|!}\,\frac{\bar{p}^p}{(\bar{p}+|\ell|+1)^{p+|\ell|+1}}\,. \tag{3.18}$$

In Fig. 1 we have plotted this distribution for a coherent state with $\ell = 1$ and different values of $\bar{p}$. In Fig. 2, we have plotted

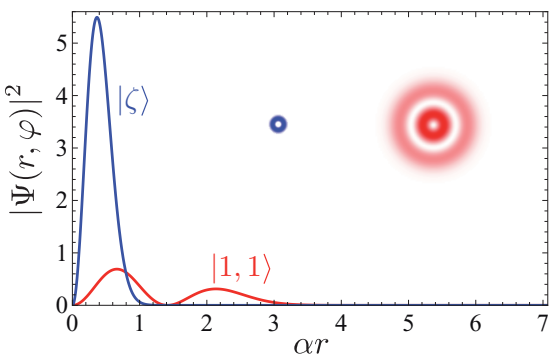

FIG. 2. (Color online) Intensity profiles $|\Psi(r,\phi)|^2$ for a radial coherent state $|\zeta\rangle$ written as in (3.16), with $\langle p\rangle = 1$ and for an eigenstate $|p,\ell\rangle$ with $p = 1$ and $\ell = 1$. In the inset, we show the corresponding density plots, in the same order.

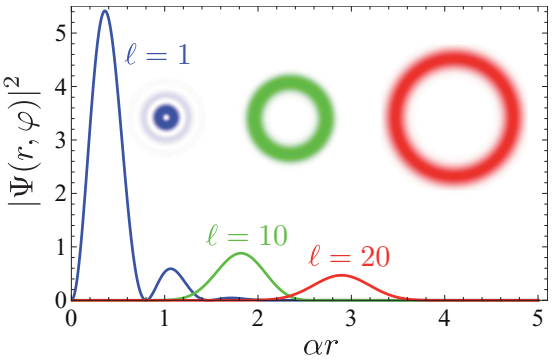

FIG. 3. (Color online) Intensity profiles $|\Psi(r,\varphi)|^2$ for intelligent states with $M = 10$ and $\tau = 1/2$ for several values of ℓ: $\ell = 1$, $\ell = 10$, and $\ell = 20$. The inset shows the corresponding density plots, in the same order.

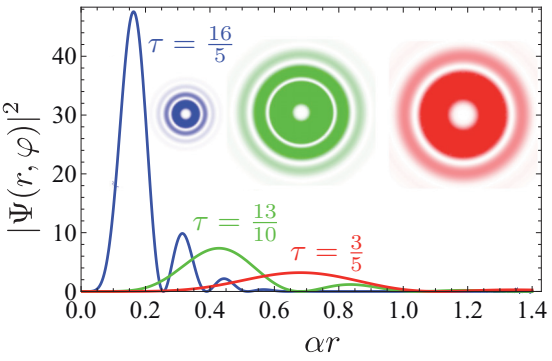

FIG. 4. (Color online) Intensity profiles $|\Psi(r,\varphi)|^2$ for intelligent states with $M = 11$ and $\ell = 3$ for several values of τ: $\tau = 16/5$, $\tau = 13/10$, and $\tau = 3/5$. The inset shows the corresponding density plots, in the same order.

$|\Psi_\zeta(r,\varphi)|^2$ for a coherent state with $\ell = 1$ and $\langle\hat{p}\rangle = 1$, and the corresponding distribution for the Laguerre-Gauss eigenstate with $p = 1$. The striking differences can be appreciated at a glance.

It is worth mentioning that there is an alternative definition of coherent states, due to Barut and Girardello [48]:

$$\hat{k}_-|\zeta\rangle_{\rm BG} = \zeta|\zeta\rangle_{\rm BG}\,, \tag{3.19}$$

which appears as a reasonable generalization of the standard coherent states as eigenstates of the annihilation operator. This equation can be solved in the $|p,\ell\rangle$ basis, yielding

$$|\zeta\rangle_{\rm BG} = \frac{|\zeta|^{\ell/2}}{\sqrt{I_\ell(2|\zeta|)}}\sum_{p=0}^{\infty}\frac{\zeta^p}{\sqrt{p!(p+|\ell|)!}}|p,\ell\rangle\,, \tag{3.20}$$

where $I_\ell(x)$ is the modified Bessel function. Projecting again in the transverse coordinates we get, after some calculations,

$$\Psi_{\zeta,{\rm BG}}(r,\varphi) = \sqrt{\frac{\alpha^2}{\pi\, I_{|\ell|}(2|\zeta|^2)}}\,e^{(\zeta^2-\alpha^2r^2/2)}J_{|\ell|}(2\zeta r)e^{i\ell\varphi}\,. \tag{3.21}$$

This set of coherent states are thus realized as Bessel-Gauss modes. However, these solutions are not shape invariant, which runs against the notion of coherence.

C. Radial intelligent and squeezed states

The commutation relations (3.9) imply that these operators cannot be measured simultaneously, which is reflected by the uncertainty relation

$$\Delta\hat{k}_x\,\Delta\hat{k}_y \geqslant \tfrac{1}{2}|\langle\hat{k}_z\rangle|\,, \tag{3.22}$$

where $\Delta\hat{A} = [\langle\hat{A}^2\rangle - \langle\hat{A}\rangle^2]^{1/2}$ stands for the variance. According to the standard definition, squeezing occurs whenever [49]

$$(\Delta\hat{k}_x)^2 \leqslant \tfrac{1}{2}|\langle\hat{k}_z\rangle| \quad\text{or}\quad (\Delta\hat{k}_y)^2 \leqslant \tfrac{1}{2}|\langle\hat{k}_z\rangle|\,. \tag{3.23}$$

Intelligent states are those for which (3.22) holds as an equality. The coherent states (3.16) and (3.21) are intelligent but not squeezed.

Indeed, these intelligent states are solutions of the eigenvalue problem [50]

$$(\hat{k}_x - i\lambda\hat{k}_y)|\Psi_\lambda\rangle = \Lambda|\Psi_\lambda\rangle\,,\quad \lambda\in\mathbb{R}\,. \tag{3.24}$$

Although they have been investigated from various perspectives [51–53], we follow here the comprehensive approach of Ref. [54], which starts by noting that the state $\exp(i\tau\hat{k}_y)|k,k\rangle$ is intelligent provided $\lambda = \cosh\tau$ [with eigenvalue $\Lambda = -(k+M)\sinh\tau$, and $M = 0,1,\ldots$ an integer number]. Then, the most general intelligent state can be written as

$$|\Psi_{\ell,M}(\tau)\rangle = \exp(i\tau\hat{k}_y)\big|\kappa_M^k(\tau)\big\rangle\,, \tag{3.25}$$

where τ is the squeezing parameter and the seed state $|\kappa_M^k\rangle$ can be expressed as

$$\big|\kappa_M^k(\tau)\big\rangle = \sum_{p=0}^{M}c_p^k(\tau)|k,k+p\rangle\,. \tag{3.26}$$

The coefficients c_p^k can be obtained as a recursion relation; the final result reads

$$c_p^k = \binom{M}{p}\frac{\tanh^p\tau}{\binom{2k+p-1}{p}^{1/2}}\,c_0^k\,, \tag{3.27}$$

and c_0^k is fixed by the normalization of the state. The infinite family (3.25) of states parametrized by k and M is actually squeezed.

Next we need to project $\exp(i\tau\hat{k}_y)|\kappa_M^k(\tau)\rangle$ on the basis $|k,k+p\rangle$. To this end, we recall that the action of $\exp(i\tau\hat{k}_y)$ on a basis state $|k,k+p\rangle$ is given in terms of SU(1,1) Wigner d functions [55]

$$\exp(i\tau\hat{k}_y)|k,k+p\rangle = \sum_{p'=0}^{\infty}d^k_{k+p,k+p'}(-\tau)\,|k,k+p'\rangle\,. \tag{3.28}$$

In this way, we get, expressed in transverse coordinates,

$$\Psi_{\ell M}(r,\varphi,\tau) = \sum_{p'=0}^{\infty}\sum_{p=0}^{M}d^k_{k+p',k+p}(-\tau)\,c_p^k(\tau)\,A_{p\;2k-1}(r)e^{i\ell\varphi}\,, \tag{3.29}$$

where $A_{p\ell}$ has been defined in Eq. (2.11). The effect of increasing ℓ, for fixed p and τ, is illustrated by plotting the intensity profile $|\Psi_{\ell,M}(r,\varphi,\tau)|^2$ as a function of r in Fig. 3: this intensity tends to a Gaussian-like shape. The effect of increasing τ for fixed ℓ and M is illustrated in Fig. 4, and leads to the appearance of rings as we increase τ.

For large values of ℓ (more concretely, for k and p large, but $p/k \ll 1$), one has at hand a compact asymptotic approximation to the d functions, namely [56],

$$d^k_{k+p,k}(\tau) \simeq \frac{1}{[(k+p)^2 - k^2]^{1/4}}\, e^{-k(\tau-\tau_p)^2/2}, \qquad (3.30)$$

with $\cosh\tau_p = (k+p)/k$, and whose Gaussian nature is evident.

IV. CONCLUDING REMARKS

In summary, we have provided a handy toolbox to deal with the radial index of Laguerre-Gauss modes and shown how it can be used to construct a consistent quantum theory of this variable. We stress that this is more than an academic curiosity, since recent experiments in our laboratory [57] have confirmed that the radial degree of freedom of single photons can be manipulated individually in a quantum regime. It is our hope that the results presented here will inspire novel quantum protocols and algorithms using such a "forgotten quantum number."

ACKNOWLEDGMENTS

E.K. and R.W.B. acknowledge the support of the Canada Excellence Research Chairs (CERC) Program. The work of H.G. is supported by the Natural Sciences and Engineering Research Council (NSERC) of Canada. J.R. and Z.H. are grateful for the financial assistance of the Technology Agency of the Czech Republic (Grant No. TE01020229) and the Czech Ministry of Industry and Trade (Grant No. FR-TI1/364). G.L. is partially funded by EU FP7 (Grant Q-ESSENCE). Finally, P.H. and L.L.S.S. acknowledge the support from the Spanish MINECO (Grant No. FIS2011-26786).

[1] *Twisted Photons: Applications of Light with Orbital Angular Momentum*, edited by J. Torres and L. Torner (Wiley-VCH, Weinheim, 2011).
[2] L. Allen, M. W. Beijersbergen, R. J. C. Spreeuw, and J. P. Woerdman, Phys. Rev. A **45**, 8185 (1992).
[3] *Optical Tweezers*, edited by M. J. Padgett, J. Molloy, and D. McGloin (Chapman and Hall, London, 2010).
[4] C. Maurer, A. Jesacher, S. Bernet, and M. Ritsch-Marte, Laser Photon. Rev. **5**, 81 (2011).
[5] N. Uribe-Patarroyo, A. Fraine, D. S. Simon, O. Minaeva, and A. V. Sergienko, Phys. Rev. Lett. **110**, 043601 (2013).
[6] N. M. Elias, II, Astron. Astrophys. **492**, 883 (2008).
[7] F. Tamburini, B. Thide, G. Molina-Terriza, and G. Anzolin, Nat. Phys. **7**, 195 (2011).
[8] J. Wang, J.-Y. Yang, I. M. Fazal, N. Ahmed, Y. Yan, H. Huang, Y. Ren, Y. Yue, S. Dolinar, M. Tur, and A. E. Willner, Nat. Photon. **6**, 488 (2012).
[9] M. Uchida and A. Tonomura, Nature (London) **464**, 737 (2010).
[10] J. Verbeeck, H. Tian, and P. Schattschneider, Nature (London) **467**, 301 (2010).
[11] B. J. McMorran, A. Agrawal, I. M. Anderson, A. A. Herzing, H. J. Lezec, J. J. McClelland, and J. Unguris, Science **331**, 192 (2011).
[12] E. Karimi, L. Marrucci, V. Grillo, and E. Santamato, Phys. Rev. Lett. **108**, 044801 (2012).
[13] A. G. Peele, P. J. McMahon, D. Paterson, C. Q. Tran, A. P. Mancuso, K. A. Nugent, J. P. Hayes, E. Harvey, B. Lai, and I. McNulty, Opt. Lett. **27**, 1752 (2002).
[14] K. A. Nugent, Adv. Phys. **59**, 1 (2009).
[15] E. Hemsing, A. Knyazik, M. Dunning, D. Xiang, A. Marinelli, C. Hast, and J. B. Rosenzweig, Nat. Phys. **9**, 549 (2013).
[16] B. Thidé, H. Then, J. Sjöholm, K. Palmer, J. Bergman, T. D. Carozzi, Y. N. Istomin, N. H. Ibragimov, and R. Khamitova, Phys. Rev. Lett. **99**, 087701 (2007).
[17] S. M. Mohammadi, L. K. S. Daldorff, K. Forozesh, B. Thidé, J. E. S. Bergman, B. Isham, R. Karlsson, and T. D. Carozzi, Radio Sci. **45**, RS4007 (2010).
[18] F. Tamburini, E. Mari, A. Sponselli, B. T. A. Bianchini, and F. Romanato, New J. Phys. **14**, 033001 (2012).
[19] A. Mair, A. Vaziri, G. Weihs, and A. Zeilinger, Nature (London) **412**, 313 (2001).
[20] G. Molina-Terriza, A. Vaziri, J. Řeháček, Z. Hradil, and A. Zeilinger, Phys. Rev. Lett. **92**, 167903 (2004).
[21] S. S. R. Oemrawsingh, A. Aiello, E. R. Eliel, G. Nienhuis, and J. P. Woerdman, Phys. Rev. Lett. **92**, 217901 (2004).
[22] L. Marrucci, E. Karimi, S. Slussarenko, B. Piccirillo, E. Santamato, E. Nagali, and F. Sciarrino, J. Opt. **13**, 064001 (2011).
[23] G. Molina-Terriza, L. Rebane, J. P. Torres, L. Torner, and S. Carrasco, J. Eur. Opt. Soc. **2**, 07014 (2007).
[24] R. Fickler, R. Lapkiewicz, W. N. Plick, M. Krenn, C. Schaeff, S. Ramelow, and A. Zeilinger, Science **338**, 640 (2012).
[25] E. Karimi and E. Santamato, Opt. Lett. **37**, 2484 (2012).
[26] W. N. Plick, R. Lapkiewicz, S. Ramelow, and A. Zeilinger, arXiv:1306.6517.
[27] G. Nienhuis and J. Visser, J. Opt. A **6**, S248 (2004).
[28] A. B. Mikhailovskii, V. P. Lakhin, G. D. Aburdzhaniya, L. A. Mikhailovskaya, O. G. Onishchenko, and A. I. Smolyakov, Plasma Phys. Controlled Fusion **29**, 1 (1987).
[29] M. M. Salomaa and G. E. Volovik, Rev. Mod. Phys. **59**, 533 (1987).
[30] V. V. Dodonov and V. I. Mank'o, *Invariants and the Evolution of Nonstationary Quantum Systems* (Nova Science, New York, 1989).
[31] C. Cohen-Tannoudji, B. Diu, and F. Laloë, *Quantum Mechanics* (Wiley, New York, 2006).
[32] L. L. Sánchez-Soto, A. B. Klimov, P. de la Hoz, I. Rigas, J. Řeháček, Z. Hradil, and G. Leuchs, Phys. Rev. A **88**, 053839 (2013).
[33] H. S. Yi, H. R. Lee, and K. S. Sohn, Phys. Rev. A **49**, 3277 (1994).
[34] R. Lynch, Phys. Rep. **256**, 367 (1995).
[35] L. C. Biedenharn, J. Nuyts, and N. Straumann, Ann. Inst. Henri Poincaré, Section A, tome **3**, 13 (1965).
[36] C. C. Gerry, Phys. Rev. A **31**, 2721 (1985).
[37] B. Yurke, S. L. McCall, and J. R. Klauder, Phys. Rev. A **33**, 4033 (1986).

[38] V. Bužek, Phys. Rev. A **39**, 3196 (1989).
[39] A. Vourdas, Phys. Rev. A **45**, 1943 (1992).
[40] M. Ban, Phys. Rev. A **47**, 5093 (1993).
[41] C. Brif and A. Mann, Phys. Rev. A **54**, 4505 (1996).
[42] C. C. Gerry, S. C. Gou, and J. Steinbach, Phys. Rev. A **55**, 630 (1997).
[43] G. S. Agarwal and J. Banerji, Phys. Rev. A **64**, 023815 (2001).
[44] G. I. Mias, N. R. Cooper, and S. M. Girvin, Phys. Rev. A **77**, 023616 (2008).
[45] A. M. Marino, N. V. Corzo Trejo, and P. D. Lett, Phys. Rev. A **86**, 023844 (2012).
[46] A. Perelomov, *Generalized Coherent States and their Applications* (Springer, Berlin, 1986).
[47] E. Karimi, G. Zito, B. Piccirillo, L. Marrucci, and E. Santamato, Opt. Lett. **32**, 3053 (2007).
[48] A. O. Barut and L. Girardello, Commun. Math. Phys. **21**, 41 (1971).
[49] K. Wódkiewicz and J. H. Eberly, J. Opt. Soc. Am. B **2**, 458 (1985).
[50] R. Jackiw, J. Math. Phys. **9**, 339 (1968).
[51] J. A. Bergou, M. Hillery, and D. Yu, Phys. Rev. A **43**, 515 (1991).
[52] C. C. Gerry and R. Grobe, Phys. Rev. A **51**, 4123 (1995).
[53] R. R. Puri and G. S. Agarwal, Int. J. Mod. Phys. B **10**, 1563 (1996).
[54] P. Joanis, D. H. Mahler, and H. de Guise, J. Phys. A **43**, 385304 (2010).
[55] H. Ui, Prog. Theor. Phys. **44**, 689 (1970).
[56] D. J. Rowe, H. de Guise, and B. C. Sanders, J. Math. Phys. **42**, 2315 (2001).
[57] E. Karimi, D. Giovannini, E. Bolduc, N. Bent, F. M. Miatto, M. J. Padgett, and R. W. Boyd, Phys. Rev. A **89**, 013829 (2014).

Paper 5

G. Björk, H. de Guise, A.B. Klimov, P. de la Hoz, L.L. Sánchez-Soto:

"Classical distinguishability as an operational measure of polarization",

Physical Review A **90**, 013830

Classical distinguishability as an operational measure of polarization

G. Björk,[1] H. de Guise,[2] A. B. Klimov,[3] P. de la Hoz,[4] and L. L. Sánchez-Soto[4]

[1]*Department of Applied Physics, Royal Institute of Technology (KTH), AlbaNova University Center, SE-106 91 Stockholm, Sweden*

[2]*Department of Physics, Lakehead University, Thunder Bay, Ontario, Canada P7B 5E1*

[3]*Departamento de Física, Universidad de Guadalajara, 44420 Guadalajara, Jalisco, Mexico*

[4]*Departamento de Óptica, Facultad de Física, Universidad Complutense, 28040 Madrid, Spain*

(Received 7 May 2014; published 23 July 2014)

We put forward an operational degree of polarization that can be extended in a natural way to fields whose wave fronts are not necessarily planar. This measure appears as a distance from a state to the set of all of its polarization-transformed counterparts. By using the Hilbert-Schmidt metric, the resulting degree is a sum of two terms: one is the purity of the state and the other can be interpreted as a classical distinguishability, which can be experimentally determined in an interferometric setup. For transverse fields, this reduces to the standard approach, whereas it allows one to get a straight expression for nonparaxial fields.

DOI: 10.1103/PhysRevA.90.013830 PACS number(s): 42.25.Ja, 05.40.−a

I. INTRODUCTION

Far from its source, any electromagnetic wave can be locally approximated by a plane wave, i.e., with a well-defined direction of propagation and thus a specific transverse plane. Such beamlike fields are described by two orthogonal electric-field components and, consequently, their polarization is characterized by a 2×2 correlation matrix, usually called the polarization matrix [1,2].

This polarization matrix can be uniquely decomposed as a sum of two matrices: one represents a fully polarized part and the other represents a completely unpolarized part. The ratio of the intensity of the polarized part to the total intensity is the degree of polarization.

Equivalently, one may resort to the Stokes parameters, which are the coefficients of the expansion of the polarization matrix onto the Pauli basis. These variables determine a locus on the Poincaré sphere, wherein the state of polarization is elegantly visualized: actually, the degree of polarization can be seen as the length of the Stokes vector.

This two-dimensional (2D) theory is the backbone of the standard polarization optics. However, the necessity of addressing new issues, such as highly nonparaxial fields [3], narrowband imaging systems [4], and the recognition of associated propagation questions [5], has revived interest in extending the 2D approach to fully three-dimensional (3D) field distributions. Although this question has been considered for many years, no satisfactory solution has thus far been found. Indeed, there are several contradictory claims made in the literature on this subject [6–15]. The divergences occur because notions that are equivalent for the 2D case lead to different definitions when extrapolated to the 3D limit. This diversity has prompted various authors to suggest alternative 3D measures of polarization based in, e.g., nonquantum entanglement [16], von Neumann entropy [17], the fully polarized field component [12], or the invariants of the rotational group [18]. All of these instances produce sensible computable magnitudes, but they are hardly measurable, which prevents a proper assessment of their merits.

In this paper, we revisit an operational measure introduced some time ago in the realm of quantum optics [19]: in 2D, the prescription is to look at the minimum overlap between a state and the set of its polarization-transformed [i.e., SU(2)-rotated] counterparts. The key point is that this magnitude, as discussed in Ref. [20], can be directly determined as the visibility of an interference experiment. Our main goal is to extend this notion to the 3D case.

To this end, we first reinterpret that measure as a distance between the state and its rotated partners. In this vein, it is worth stressing that distance measures have been successfully employed in assessing a number of disputed quantities, such as nonclassicality [21–23], entanglement [24–26], information [27–29], non-Gaussianity [30], and localization [31,32], to cite only a few examples.

Two main hurdles are usually faced when defining a distance-type measure: choosing a convenient metric and identifying a reference set of states. As to the first question, different candidates have been investigated, including, among others, relative entropy [33–35], Bures and related metrics [36–39], as well as Monge [40], trace [41,42], and Hilbert-Schmidt [43–45] distances, each having its own advantages for certain applications. In particular, the last one is probably the simplest from a computational viewpoint and will be adopted here.

In polarization, it has been suggested to take unpolarized states as the reference set, both in the quantum [46] and the classical domain [47]. Such a set is very well characterized [48–50] and this provides sensible results. However, as anticipated above, we prefer to consider the rotated versions of the original state. Going from the 2D to the 3D situation is just extending the SU(2)-rotated set to its SU(3) analog, and the resulting degrees have a clear physical interpretation.

The paper is arranged as follows. In Sec. II, we recall the basic tools used to describe the partial polarization of both 2D and 3D electromagnetic fields, emphasizing the similarities and differences between these two situations. In Sec. III, we introduce the general notion of degree of polarization as a distance, and work out the resulting expressions for both cases, comparing with previous proposed measures. Finally, we summarize our work in Sec. IV.

II. BASIC DESCRIPTION OF POLARIZATION

A pivotal quantity in the characterization of polarization of both 2D and 3D fields is the degree of polarization. It quantitatively captures the random character of the electric

field as a function of time. Such a behavior cannot be accounted for in terms of a deterministic description: we must, instead, adopt a statistical perspective. To be as self-contained as possible, we briefly review the essential ingredients needed for that purpose.

A. Two-dimensional fields

Consider a monochromatic beam propagating in the z direction. The electric field can be resolved in the transverse plane in terms of horizontal (x) and vertical (y) components, which are taken to be a probabilistic ensemble given by E_x and E_y. The corresponding 2×2 (equal-time) polarization matrix (also called the coherence matrix) is defined as [1,2]

$$\rho^{(2)}_{k\ell} = \langle E^*_k E_\ell \rangle, \quad k,\ell \in \{x,y\}. \tag{2.1}$$

Here, the brackets denote ensemble averaging over different realizations and the superscript indicates the dimensionality, although in the following we will suppress it when there is no risk of confusion.

The diagonal elements of the matrix ρ represent the energy distribution between the two components of the field: $I = \langle |E_x|^2 \rangle + \langle |E_y|^2 \rangle = \mathrm{Tr}(\rho)$, where Tr is the trace of the matrix. Without loss of generality, we henceforth normalize this intensity to unity. On the other hand, the off-diagonal elements describe the correlations between the field components. From its very definition, it follows that $\rho_{k\ell} = \rho^*_{\ell k}$, so ρ is Hermitian.

The matrix ρ can be conveniently decomposed in terms of the (Hermitian) Pauli matrices $\boldsymbol{\sigma}$; the result reads

$$\rho = \tfrac{1}{2}(\mathbb{1} + \mathbf{n} \cdot \boldsymbol{\sigma}). \tag{2.2}$$

The normalized coordinates n_r ($r = 1,2,3$) can be recovered as

$$n_r = \mathrm{Tr}(\rho \sigma_r), \tag{2.3}$$

and are nothing but the Stokes parameters. In other words, we can map each polarization matrix ρ into a Stokes vector $\rho \mapsto \mathbf{n} = (n_1,n_2,n_3)$. The length of $\mathbf{n}$ will be denoted as

$$\mathbb{P}^{(2)} = |\mathbf{n}| = \sqrt{n_1^2 + n_2^2 + n_3^2}, \tag{2.4}$$

and, as we shall justify soon, deserves the name of degree of polarization for 2D fields.

The Stokes parameters provide geometric information about the polarization ellipse, i.e., the ellipse that the electric-field tip traces out during one optical cycle. The parameters n_1 and n_2 carry information about the alignment of the ellipse axes, while πn_3 gives the ellipse area, signed according to polarization handedness.

If the relation between the E_x and E_y is completely deterministic, the field is fully polarized. For such a pure state (borrowing the terminology from quantum optics), the polarization matrix is idempotent, i.e.,

$$\rho^2_{\mathrm{pol}} = \rho_{\mathrm{pol}}, \tag{2.5}$$

and we get $\mathbb{P}^{(2)}_{\mathrm{pol}} = 1$. On the other hand, if the components of the field are fully uncorrelated, the off-diagonal elements are zero. If, in addition, the energy is distributed evenly between the x and y components,

$$\rho_{\mathrm{unpol}} = \tfrac{1}{2}\mathbb{1}, \tag{2.6}$$

and we have $\mathbb{P}^{(2)}_{\mathrm{unpol}} = 0$. This leads to the important decomposition of ρ into fully polarized and unpolarized parts, viz.,

$$\rho = [1 - \mathbb{P}^{(2)}]\rho_{\mathrm{unpol}} + \mathbb{P}^{(2)}\rho_{\mathrm{pol}}. \tag{2.7}$$

In this way, $\mathbb{P}^{(2)}$ appears as the proportion of the energy of the fully polarized part from the total energy, which gives a transparent physical meaning to the definition of $\mathbb{P}^{(2)}$.

Alternatively, $\mathbb{P}^{(2)}$ can be written in a slightly different yet equivalent way,

$$\mathbb{P}^{(2)} = \sqrt{2\,\mathrm{Tr}(\rho^2) - 1} = \sqrt{1 - 4\det(\rho)}, \tag{2.8}$$

as can be checked by a direct calculation. In the first form, the degree of polarization seems to be intimately linked to $\mathrm{Tr}(\rho^2)$, which, following again a quantum jargon, is called the purity. In the second form, it can be immediately related with the eigenvalues of ρ: if we denote them by λ_+ and λ_-, ($\lambda_+ > \lambda_-$), then $(\lambda_+ + \lambda_-)^2 = 1$ and $\det(\rho) = \lambda_+\lambda_-$, so that

$$\mathbb{P}^{(2)} = \lambda_+ - \lambda_-, \tag{2.9}$$

the importance of which will soon become apparent.

Polarization transformations are generated by wave plates and represented by 2×2 unitary matrices of SU(2) [51],

$$R_g \equiv R(\alpha,\beta,\gamma) = \begin{pmatrix} e^{-i(\alpha+\gamma)/2}\cos(\beta/2) & -e^{-i(\alpha-\gamma)/2}\sin(\beta/2) \\ e^{+i(\alpha-\gamma)/2}\sin(\beta/2) & e^{+i(\alpha+\gamma)/2}\cos(\beta/2) \end{pmatrix}, \tag{2.10}$$

where (α,β,γ) denote the Euler angles. The action of these transformations on the polarization matrix is via conjugation,

$$\rho_g = R_g\,\rho\,R_g^\dagger, \tag{2.11}$$

which, in turn, induces rotations on the Stokes vector $\mathbf{n}$, as confirmed by the well-known relation between SU(2) and the group of rotations SO(3) [52]. The essential point is that $\mathbb{P}^{(2)}$ is clearly unchanged by these transformations.

B. Three-dimensional fields

Next, we loosen the restriction to planar geometry and examine the behavior of electric fields having three nonvanishing components, in directions we denote as x, y, and z, respectively. Now, the vibrations of the field are not constrained to a plane and the polarization must be described by a 3×3 matrix,

$$\rho^{(3)}_{k\ell} = \langle E_k E_\ell \rangle, \quad k,\ell \in \{x,y,z\}. \tag{2.12}$$

The superscript 3 labels the 3D approach and will be dropped when the context is clear.

If all of the components are completely uncorrelated (and their energies are equal), the field is unpolarized and its direction is random. If one of the components has less energy than the other two, the vibrations are less random and, consequently, the field is more polarized than in the equal-energy case. This means that any field having only two nonvanishing components is never unpolarized in the 3D sense, regardless of the correlations between the components. Hence, a planar field, which is commonly called unpolarized in 2D, is not fully unpolarized but partially polarized in a 3D description.

As in 2D, the field is called fully polarized if all of the field components are completely correlated. Hence, in contrast to an unpolarized field, a planar field that is fully polarized is always fully polarized also in the 3D sense.

One of the most remarkable differences between 2D and 3D is that the 3×3 polarization matrix cannot be generally expressed as a sum of unpolarized and fully polarized parts [12]. Therefore, if one desires to define a degree of polarization for arbitrary electric fields, the approach taken in (2.7) must be abandoned.

In any event, the 3×3 polarization matrix can be expanded in a basis as

$$\rho = \tfrac{1}{3}(\mathbb{1} + \sqrt{3}\mathbf{n} \cdot \mathbf{\Lambda}), \tag{2.13}$$

where $\mathbf{\Lambda}$ are the Gell-Mann matrices (see details in the Appendix). The corresponding coordinates of the eight-dimensional Stokes vector can be obtained as

$$n_r = \frac{\sqrt{3}}{2} \operatorname{Tr}(\rho \Lambda_r). \tag{2.14}$$

We have introduced the factor $\sqrt{3}$ in such a way that for a pure state $\mathbf{n} \cdot \mathbf{n} = 1$ [53], although other choices can be found in the literature. One first option would be to define [9]

$$\mathbb{P}^{(3)} = |\mathbf{n}| = \sqrt{\sum_{r=1}^{8} n_r^2}, \tag{2.15}$$

i.e., again the length of the Stokes vector, which is readily shown to verify $0 \leqslant \mathbb{P}^{(3)} \leqslant 1$. Although this is mathematically correct, it is not clear physically what $\mathbb{P}^{(3)}$ represents. Unlike in 2D, where the Stokes vector represents the complete state of polarization and can be easily visualized, the generalized Stokes vector is eight dimensional and the geometrical space supporting this vector is not intuitive at all.

An alternative is to generalize (2.8) in a way so as to get the appropriate normalization; it reads [6,7]

$$\mathbb{P}^{(3)} = \sqrt{\frac{3 \operatorname{Tr}(\rho^2) - 1}{2}}. \tag{2.16}$$

The drawback of this definition is that it cannot be understood as a portion of the energy of the fully polarized part from the total energy and hence its physical properties need further examination.

Finally, the generalization of (2.9) seems even more dubious, since now we have three different eigenvalues. This reveals the major problem when extending 2D to 3D instances: while one parameter is enough to specify the degree of polarization in 2D, two independent parameters are, in general, needed when considering 3D, which makes the transition a tricky business.

We complete this section by describing the polarization transformations possible in the 3D case: they are represented by 3×3 matrices of SU(3), which we write as [54]

$$\begin{aligned} R_g =& R_g(\Omega) \equiv T_{23}(\alpha_1, \beta_1, -\alpha_1) T_{12}(\alpha_2, \beta_2, -\alpha_2) \\ & \times T_{23}(\alpha_3, \beta_3, -\alpha_3) \Phi(\gamma_1, \gamma_2), \end{aligned} \tag{2.17}$$

where Ω is an octuple of Euler-like angles $\Omega = (\alpha_1, \beta_1, \alpha_2, \beta_2, \alpha_3, \beta_3, \gamma_1, \gamma_2)$ and the set $\{T_{ij}\}$ comprises SU(2) subgroup matrices

$$T_{23} = \begin{pmatrix} 1 & 0 & 0 \\ 0 & e^{-i(\alpha+\gamma)/2} \cos(\beta/2) & -e^{-i(\alpha-\gamma)/2} \sin(\beta/2) \\ 0 & e^{+i(\alpha-\gamma)/2} \sin(\beta/2) & e^{+i(\alpha+\gamma)/2} \cos(\beta/2) \end{pmatrix}, \tag{2.18}$$

or

$$T_{12} = \begin{pmatrix} e^{-i(\alpha+\gamma)/2} \cos(\beta/2) & -e^{-i(\alpha-\gamma)/2} \sin(\beta/2) & 0 \\ e^{+i(\alpha-\gamma)/2} \sin(\beta/2) & e^{+i(\alpha+\gamma)/2} \cos(\beta/2) & 0 \\ 0 & 0 & 1 \end{pmatrix}, \tag{2.19}$$

depending on the values of (ij). Also,

$$\Phi(\gamma_1, \gamma_2) = \operatorname{diag}\left(e^{-2i\gamma_1}, e^{i(\gamma_1 - \gamma_2/2)}, e^{i(\gamma_1 + \gamma_2/2)}\right). \tag{2.20}$$

Equation (2.17) factorizes then into SU(2) submatrices, with parameters defined by the corresponding Euler angles.

The action of these transformations on ρ is via conjugation as in (2.11), which induces rotations on the vector $\mathbf{n}$. However, one word of caution seems pertinent here: there is no obvious physical interpretation via optical elements of SU(3) transformations, as now the plane waves averaging to the 3×3 polarization matrix do not share a common propagation direction, in general. Any physical device represented by a SU(3) transformation should be insensitive to the propagation directions of the separate members of the ensemble [55].

Despite the recent progress achieved in the control and manipulation of 3D polarization [56], we are still far from having at our disposal an SU(3) gadget, in sharp contrast with the simplicity of SU(2). Given these experimental difficulties, one might be tempted to consider invariance only under rotations and inversions; that is, a field is less polarized at a point if its behavior is fairly unchanged after we rotate it and reflect it around that point. Although attractive, this proposal does not allow us to find analytical results in what follows. Accordingly, we take SU(3) as the symmetry of the problem, even if its operational implementation may be elusive.

III. OPERATIONAL DEGREE OF POLARIZATION

As heralded in Sec. I, our proposal for the degree of polarization starts from the *ansatz*

$$\mathbb{P}^{(n)}(\rho) \propto \sup_{g \in \mathrm{SU}(n)} D(\rho, R_g \rho R_g^\dagger). \tag{3.1}$$

Here, the $\sup_g$ is taken over SU(2) or SU(3), depending on the appropriate situation. In addition, $D(\rho, \rho')$ stands for any measure of distance between the polarization matrices ρ and ρ'.

It is clear that there are numerous nontrivial choices for $D(\rho, \rho')$ (by nontrivial, we mean that the choice is not a simple scale transformation of any other distance). None of them could be said to be more important than any other *a priori*, but the significance of each candidate would have to be seen through physical assumptions. In our case, we take the Hilbert-Schmidt distance

$$\begin{aligned} D_{\mathrm{HS}}^2(\rho, \rho') &= \tfrac{1}{2} \operatorname{Tr}[(\rho - \rho')^2] \\ &= \tfrac{1}{2}[\operatorname{Tr}(\rho^2) + \operatorname{Tr}(\rho'^2) - 2 \operatorname{Tr}(\rho \rho')]. \end{aligned} \tag{3.2}$$

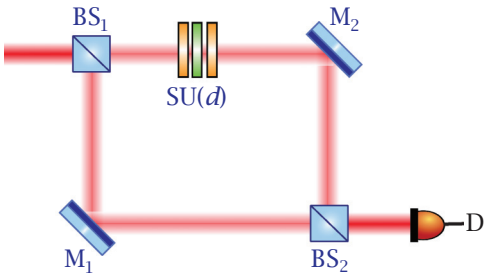

FIG. 1. (Color online) Mach-Zehnder setup to interfere the state ρ (lower arm) with its SU(n) transformed partners (upper arm). The distinguishability is related to the visibility of the interference pattern at the detector D.

Since $\rho' = \rho_g = R_g \rho R_g^\dagger$ and $\mathrm{Tr}(\rho^2) = \mathrm{Tr}(\rho_g^2)$, this distance reduces to

$$D^2_{\mathrm{HS}}(\rho, \rho_g) = \mathrm{Tr}(\rho^2) - \mathrm{Tr}(\rho\rho_g). \tag{3.3}$$

Consequently, we define a Hilbert-Schmidt degree of polarization as

$$\left[\mathbb{P}^{(n)}_{\mathrm{HS}}\right]^2 = \sup_{g\in \mathrm{SU(n)}} D^2_{\mathrm{HS}}(\rho, \rho_g) = \mathrm{Tr}(\rho^2) - \inf_{g\in \mathrm{SU(n)}} \mathrm{Tr}(\rho\rho_g). \tag{3.4}$$

The appealing point is that, formulated in this way, $\mathbb{P}^{(n)}_{\mathrm{HS}}$ depends on both the purity of the state and the distinguishability between the state and the set of all of its rotated counterparts. This later magnitude can be directly determined as the visibility of an interference experiment, as roughly schematized in Fig. 1. As unpolarized states are invariant under any SU(n) transformation, this visibility (which is a measure of the distinguishability between ρ and ρ_g) is zero for them.

A. Two-dimensional fields

Let us put the general definition to work for the 2D case. The state purity and the distinguishability can be expressed as

$$\mathrm{Tr}(\rho^2) = \tfrac{1}{2}(1 + |\mathbf{n}|^2), \quad \mathrm{Tr}(\rho\rho_g) = \tfrac{1}{2}(1 + \mathbf{n}_\rho \cdot \mathbf{n}_{\rho_g}), \tag{3.5}$$

where $\mathbf{n}_\rho$ and $\mathbf{n}_{\rho_g}$ are the Stokes vectors associated with ρ and ρ_g, respectively.

To find the minimum overlap, we follow a route that will be useful in extending this to the 3D case: one notices that any state ρ can be brought to a diagonal form $\rho = R_{g_0}\rho_0 R_{g_0}^\dagger$, with R_{g_0} being an SU(2) matrix and

$$\rho_0 = \frac{1}{2}\begin{pmatrix} 1+|\mathbf{n}| & 0 \\ 0 & 1-|\mathbf{n}| \end{pmatrix} = \begin{pmatrix} \lambda_+ & 0 \\ 0 & \lambda_- \end{pmatrix}. \tag{3.6}$$

As $\inf_g \mathrm{Tr}(\rho\rho_g) = \inf_g \mathrm{Tr}(\rho_0\rho_{0g})$, we get

$$\inf_{g\in \mathrm{SU(2)}} \mathrm{Tr}(\rho\rho_g) = \inf_{g\in \mathrm{SU(2)}} \tfrac{1}{2}(1 + |\mathbf{n}|^2\cos\beta) = \tfrac{1}{2}(1 - |\mathbf{n}|^2), \tag{3.7}$$

where β is the corresponding Euler angle in (2.10). The minimum corresponds when $\mathbf{n}_g$ is the antipodal vector $\mathbf{n}_g = -\mathbf{n}$, as one might have anticipated. We thus conclude that

$$\mathbb{P}^{(2)}_{\mathrm{HS}} = |\mathbf{n}| = \lambda_+ - \lambda_-, \tag{3.8}$$

which coincides with the standard definition (2.9).

Notice that in SU(2) we also have

$$\mathbb{P}^{(2)}_{\mathrm{HS}} = \tfrac{1}{2} \inf_{g\in \mathrm{SU(2)}} \mathrm{Tr}\,|\rho - \rho_g|, \tag{3.9}$$

which shows that the Hilbert-Schmidt $\mathbb{P}^{(2)}_{\mathrm{HS}}$ is proportional to the trace distance. This reinforces the connection to distinguishability as a measure of the degree of polarization, since the trace distance is a preferred metric to quantify the distinguishability between probability distributions [57].

B. Three-dimensional fields

Now, we have that

$$\mathrm{Tr}(\rho^2) = \tfrac{1}{3}(1 + 2|\mathbf{n}|^2), \quad \mathrm{Tr}(\rho\rho_g) = \tfrac{1}{3}(1 + 2\mathbf{n}_\rho \cdot \mathbf{n}_{\rho_g}). \tag{3.10}$$

This last equation is surprisingly simple, but due to restrictions imposed by the SU(3) algebra, $\mathbf{n}_\rho$ and $\mathbf{n}_{\rho_g}$ cannot be antiparallel. Thus, to optimize this distinguishability, we write again $\rho = R_{g_0}\rho_0 R_{g_0}^\dagger$, with

$$\rho_0 = \frac{1}{3}\begin{pmatrix} 1+\sqrt{3}n_3+n_8 & 0 & 0 \\ 0 & 1-\sqrt{3}n_3+n_8 & 0 \\ 0 & 0 & 1-2n_8 \end{pmatrix} = \begin{pmatrix} \lambda_1 & 0 & 0 \\ 0 & \lambda_2 & 0 \\ 0 & 0 & \lambda_3 \end{pmatrix}, \tag{3.11}$$

with the eigenvalues sorted in decreasing order: $\lambda_1 \geqslant \lambda_2 \geqslant \lambda_3$. The vector $\mathbf{n}_0$ associated with ρ_0 has two nonzero components, n_3 and n_8, and the minimum overlap depends now on these two parameters. In addition, positivity imposes

$$\max\left(-\frac{1+n_8}{\sqrt{3}}, -\frac{2-n_8}{\sqrt{3}}\right) \leqslant n_3 \leqslant \min\left(\frac{1+n_8}{\sqrt{3}}, \frac{2-n_8}{\sqrt{3}}\right), \qquad -1 \leqslant n_8 \leqslant \frac{1}{2}. \tag{3.12}$$

This defines a triangular region of the plane similar to the one investigated in Ref. [58]. The minimization is now more involved, and we distinguish two different situations as follows.

1. $n_3 = 0$.

This corresponds to a density matrix with two identical eigenvalues:

$$\rho_0 = \frac{1}{3}\begin{pmatrix} 1+n_8 & 0 & 0 \\ 0 & 1+n_8 & 0 \\ 0 & 0 & 1-2n_8 \end{pmatrix}. \tag{3.13}$$

A direct numerical search shows that the minimum is reached when $\mathbf{n}_g$ is obtained from $\mathbf{n}_0$ by the linear transformation

$$\begin{pmatrix} n_{3g} \\ n_{8g} \end{pmatrix} = \frac{1}{2}\begin{pmatrix} 1 & -\sqrt{3} \\ -\sqrt{3} & -1 \end{pmatrix}\begin{pmatrix} n_3 \\ n_8 \end{pmatrix}, \tag{3.14}$$

so we have $\mathbf{n}\cdot\mathbf{n}_g = |\mathbf{n}|^2\cos(2\pi/3) = -n_8^2/2$. As explained above, the optimal angle between $\mathbf{n}_0$ and $\mathbf{n}_{0_g}$ is not π because this angle lies outside the permitted range. That not all angles are permitted can be explained by the fact that ρ_0 and ρ_{0g} must have the same eigenvalues since they are unitarily related. One

can confirm that the rotated vector $\mathbf{n}_g$ corresponds to the largest eigenvalue being permuted with one of the smaller eigenvalues. Hence, we can recast the infimum as $\mathrm{Tr}(\rho\rho_g) = 2\lambda_1\lambda_3 + \lambda_3^2$, so the degree becomes

$$\mathbb{P}^{(3)}_{\mathrm{HS}} = \lambda_+ - \lambda_-, \tag{3.15}$$

where $\lambda_+ = \lambda_1$ and $\lambda_- = \lambda_3$ (here, $\lambda_2 = \lambda_3$). In this way, it appears as the natural generalization of the 2D version (2.9).

2. $n_3 \neq 0$.

The three eigenvalues are now different. We set $n_8 = X\, n_3$ and write

$$\begin{pmatrix} n_{3g} \\ n_{8g} \end{pmatrix} = \begin{pmatrix} \cos\theta & \sin\theta \\ \sin\theta & \cos\theta \end{pmatrix} \begin{pmatrix} -1 & 0 \\ 0 & 1 \end{pmatrix} \begin{pmatrix} n_3 \\ n_8 \end{pmatrix}. \tag{3.16}$$

We have to consider three different zones:

(1) $X > 1/\sqrt{3}$. The minimum is found when the angles β_1, β_2, and β_3 are, respectively, set to (π,π,π) in the SU(3) matrix (2.17) and the rest of the angles equal 0. Then, $\theta = 2\pi/3$ in (3.16) reproduces this minimum.

(2) $|X| < 1/\sqrt{3}$. The minimum is now found when the angles β_1,β_2, and β_3 take the values $(0,\pi,0)$ in (2.17). Here, $\theta = 0$ in (3.16) gives the correct result.

(3) $X < -1/\sqrt{3}$. Here, the minimum occurs for $(\beta_1,\beta_2,\beta_3) = (0,0,\pi)$, corresponding to the angle $\theta = -2\pi/3$ in (3.16).

The transformed density matrix accounts for a reshuffling of the eigenvalues and, by simple inspection, one can check that (3.15) holds for all three cases.

Additional insight can be gained by considering a three-dimensional plot illustrating the loci of the minima and a contour plot of these points, as shown in Fig. 2. The sixfold symmetry of the result (corresponding to the six possible permutations of $\lambda_1,\lambda_2,\lambda_3$, so they remain in decreasing order) is explicit and quite similar to the symmetry exploited in Ref. [15].

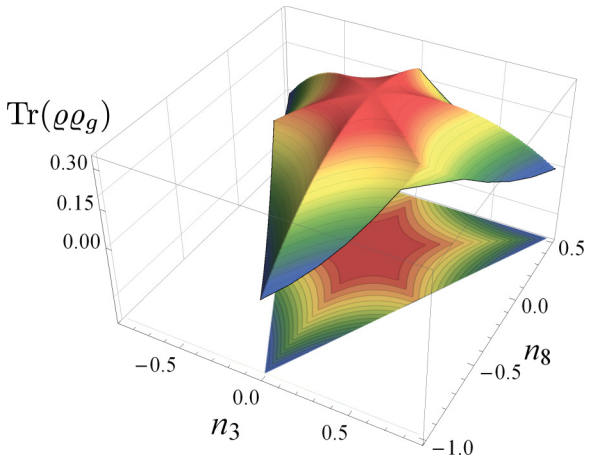

FIG. 2. (Color online) A 3D plot locating the overlap $\mathrm{Tr}(\rho\rho_g)$ as a function of the parameters n_3 and n_8. At the bottom, we show a contour plot of the surface.

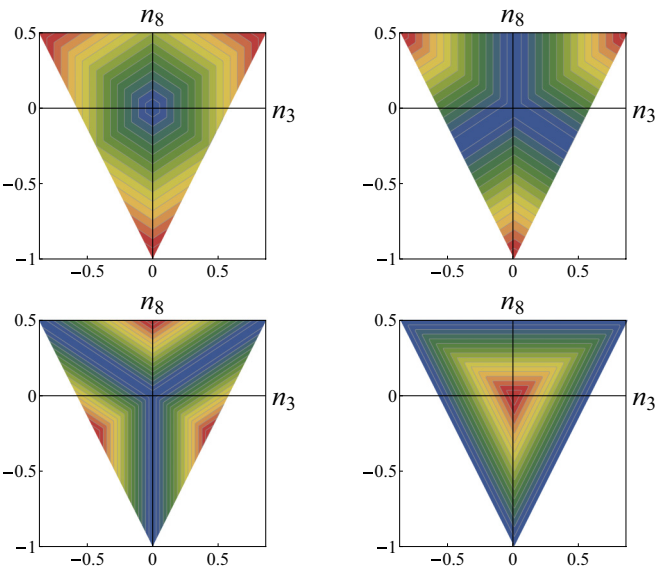

FIG. 3. (Color online) Isocontour lines (in the same color scale as in Fig. 2) of the different degrees of polarization as a function of the parameters n_3 and n_8. In the top panel, $\mathbb{P}^{(3)}_{\mathrm{HS}}$ (left) and $\mathbb{P}^{(3)}_{\mathrm{PP}}$ (right); in the bottom panel, $\mathbb{P}^{(3)}_{\mathrm{PU}}$ (left) and $\mathbb{P}^{(3)}_{\mathrm{U}}$ (right).

The Hilbert-Schmidt degree (3.9) admits a direct 3D translation, namely,

$$\mathbb{P}^{(3)}_{\mathrm{HS}} = \tfrac{1}{2} \inf_{g\in \mathrm{SU}(3)} \mathrm{Tr}\,|\rho - \rho_g|. \tag{3.17}$$

In this respect, it is worth stressing that several 3D measures have already been introduced in terms of the eigenvalues of the 3×3 polarization matrix. Relevant examples are [15]

$$\mathbb{P}^{(3)}_{\mathrm{PP}} = \lambda_1 - \lambda_2, \quad \mathbb{P}^{(3)}_{\mathrm{U}} = 3\lambda_3, \quad \mathbb{P}^{(3)}_{\mathrm{PU}} = 2(\lambda_2 - \lambda_3). \tag{3.18}$$

Here, $\mathbb{P}^{(3)}_{\mathrm{PP}}$ measures the strength of the pure polarized component, $\mathbb{P}^{(3)}_{\mathrm{U}}$ is the strength of the unpolarized component, and $\mathbb{P}^{(3)}_{\mathrm{PU}}$ is the strength of the component that is unpolarized within a plane. In Ref. [59], the method of majorization, previously used in quantum information, is applied to these measures to establish a partial ordering on the polarization state spaces.

For the sake of completeness, in Fig. 3 we have plotted the lines of constant degrees of polarization for $\mathbb{P}^{(3)}_{\mathrm{HS}}$ and the three alternatives in (3.18), again as a function of n_3 and n_8. The figure is so explicit that it does not deserve many additional comments. What is really remarkable is how differently these measures quantify the polarization at the apices of the triangle.

IV. CONCLUDING REMARKS

We have explored the use of a degree of polarization based on the distance of a state to the set of its rotated counterparts. Such a definition is closely related to other recent proposals in different areas of quantum optics and is well behaved in the classical domain, providing an operational approach that can be extended from the 2D formalism (where it reproduces the standard results) to the 3D case (where it gives a new measure).

The resulting degree is tightly linked to the notion of distinguishability, which can be experimentally determined as the visibility in a simple interference setup, which confirms previous contentions along the same lines [60].

We hope that our analysis adds to and clarifies the discussion on measures of higher-dimensional polarization in the literature.

ACKNOWLEDGMENTS

The work of G.B. is supported by the Swedish Foundation for International Cooperation in Research and Higher Education (STINT), and the Swedish Research Council (VR) through its Linnæus Center of Excellence ADOPT and Contract No. 621-2011-4575. H.d.G. is supported by the Natural Sciences and Engineering Research Council (NSERC) of Canada. A.K. is thankful for the financial assistance of the Mexican CONACyT (Grant No. 106525). Finally, P.H. and L.L.S.S. acknowledge the support from the Spanish MINECO (Grant No. FIS2011-26786). It is also a pleasure to thank I. Bengtsson, J. J. Monzón, and G. Leuchs for stimulating discussions.

APPENDIX: BASIC FACTS AND PARAMETRIZATION OF SU(3)

The SU(3) algebra is usually presented in terms of a set of Hermitian generators known as the Gell-Mann matrices [61], Λ_r ($r = 1, \ldots, 8$). They obey the commutation relations

$$[\Lambda_r, \Lambda_s] = 2i f_{rst} \Lambda_t, \tag{A1}$$

where, above and in the following, the summation over repeated indices applies. The structure constants f_{rst} are elements of a completely antisymmetric tensor spelled out explicitly in Ref. [53], whose notation we follow.

A particular feature of the generators of SU(3) in the defining 3×3 matrix representation is closure under anticommutation,

$$\{\Lambda_r, \Lambda_s\} = \tfrac{4}{3}\delta_{rs}\mathbb{1} + 2d_{rst}\Lambda_t, \tag{A2}$$

where δ_{rs} is the Kronecker symbol and d_{rst} form a totally symmetric tensor [61].

For the following, a vector-type notation is useful, based on the structure constants. The f and d symbols allow us to define both antisymmetric and symmetric products by

$$\begin{aligned}(\mathbf{A} \wedge \mathbf{B})_r &= f_{rst} A_s B_t = -(\mathbf{B} \wedge \mathbf{A})_r, \\ (\mathbf{A} \star \mathbf{B})_r &= \sqrt{3} d_{rst} A_s B_t = +(\mathbf{B} \star \mathbf{A})_r.\end{aligned} \tag{A3}$$

Given a density matrix ρ, we can expand it in terms of the unit matrix $\mathbb{1}$ and the Λ_r in the form

$$\rho = \tfrac{1}{3}(1 + \sqrt{3}\mathbf{n} \cdot \mathbf{\Lambda}). \tag{A4}$$

This is the equivalent to the Bloch ball for SU(3). For a pure state, the analogous Bloch sphere is defined by the condition

$$\mathbf{n} \cdot \mathbf{n} = 1, \quad \mathbf{n} \star \mathbf{n} = \mathbf{n}. \tag{A5}$$

Thus, each pure qutrit state corresponds to a unique unit vector $\mathbf{n} \in \mathscr{S}^7$, the seven-dimensional unit sphere. In addition, this vector must obey the condition $\mathbf{n} \star \mathbf{n} = \mathbf{n}$, which places three additional constraints, thus reducing the number of real parameters required to specify a pure state from seven to four.

[1] C. Brosseau, *Fundamentals of Polarized Light: A Statistical Optics Approach* (Wiley, New York, 1998).
[2] L. Mandel and E. Wolf, *Optical Coherence and Quantum Optics* (Cambridge University Press, Cambridge, 1995).
[3] E. A. Ash and G. Nicholls, Nature (London) **237**, 510 (1972).
[4] D. W. Pohl, W. Denk, and M. Lanz, Appl. Phys. Lett. **44**, 651 (1984).
[5] J. C. Petruccelli, N. J. Moore, and M. A. Alonso, Opt. Commun. **283**, 4457 (2010).
[6] J. C. Samson, Geophys. J. R. Astron. Soc. **34**, 403 (1973).
[7] R. Barakat, Opt. Commun. **23**, 147 (1977).
[8] T. Setälä, M. Kaivola, and A. T. Friberg, Phys. Rev. Lett. **88**, 123902 (2002).
[9] T. Setälä, A. Shevchenko, M. Kaivola, and A. T. Friberg, Phys. Rev. E **66**, 016615 (2002).
[10] O. Korotkova and E. Wolf, J. Opt. Soc. Am. A **21**, 2382 (2004).
[11] A. Luis, Opt. Commun. **253**, 10 (2005).
[12] J. Ellis, A. Dogariu, S. Ponomarenko, and E. Wolf, Opt. Commun. **248**, 333 (2005).
[13] P. Réfrégier and F. Goudail, J. Opt. Soc. Am. A **23**, 671 (2006).
[14] M. R. Dennis, J. Opt. Soc. Am. A **24**, 2065 (2007).
[15] C. J. R. Sheppard, J. Opt. Soc. Am. A **28**, 2655 (2011).
[16] X.-F. Qian and J. H. Eberly, Opt. Lett. **36**, 4110 (2011).
[17] J. J. Gil, Eur. Phys. J. Appl. Phys. **40**, 1 (2007).
[18] R. Barakat, J. Mod. Opt. **30**, 1171 (1983).
[19] G. Björk, J. Söderholm, A. Trifonov, P. Usachev, L. L. Sánchez-Soto, and A. B. Klimov, Proc. SPIE **4750**, 1 (2002).
[20] G. Björk, S. Inoue, and J. Söderholm, Phys. Rev. A **62**, 023817 (2000).
[21] M. Hillery, Phys. Rev. A **35**, 725 (1987).
[22] V. V. Dodonov, O. V. Manko, V. I. Manko, and A. Wünsche, J. Mod. Opt. **47**, 633 (2000).
[23] P. Marian, T. A. Marian, and H. Scutaru, Phys. Rev. Lett. **88**, 153601 (2002).
[24] V. Vedral, M. B. Plenio, M. A. Rippin, and P. L. Knight, Phys. Rev. Lett. **78**, 2275 (1997).
[25] P. Marian and T. A. Marian, Phys. Rev. A **77**, 062319 (2008).
[26] B. Bellomo, G. L. Giorgi, F. Galve, R. Lo Franco, G. Compagno, and R. Zambrini, Phys. Rev. A **85**, 032104 (2012).
[27] A. Gilchrist, N. K. Langford, and M. A. Nielsen, Phys. Rev. A **71**, 062310 (2005).
[28] Z. Ma, F.-L. Zhang, and J.-L. Chen, Phys. Lett. A **373**, 3407 (2009).
[29] A. Monras and F. Illuminati, Phys. Rev. A **81**, 062326 (2010).
[30] M. G. Genoni, M. G. A. Paris, and K. Banaszek, Phys. Rev. A **76**, 042327 (2007).
[31] B. Mirbach and H. J. Korsch, Ann. Phys. **265**, 80 (1998).
[32] S. Gnutzmann and K. Życzkowski, J. Phys. A **34**, 10123 (2001).
[33] A. Wehrl, Rev. Mod. Phys. **50**, 221 (1978).
[34] V. Vedral, Rev. Mod. Phys. **74**, 197 (2002).

[35] M. Ohya and D. Petz, *Quantum Entropy and Its Use*, 2nd ed. (Springer, Berlin, 2004).
[36] D. Bures, Trans. Amer. Math. Soc. **135**, 199 (1969).
[37] A. Uhlmann, Rep. Math. Phys. **9**, 273 (1976).
[38] W. K. Wootters, Phys. Rev. D **23**, 357 (1981).
[39] S. L. Braunstein and C. M. Caves, Phys. Rev. Lett. **72**, 3439 (1994).
[40] K. Życzkowski and W. Slomczyński, J. Phys. A **31**, 9095 (1998).
[41] V. P. Belavkin, G. M. D'Ariano, and M. Raginsky, J. Math. Phys. **46**, 062106 (2005).
[42] M. A. Nielsen and I. L. Chuang, *Quantum Computation and Quantum Information* (Cambridge University Press, Cambridge, 2010).
[43] C. Witte and M. Trucks, Phys. Lett. A **257**, 14 (1999).
[44] M. Ozawa, Phys. Lett. A **268**, 158 (2000).
[45] R. A. Bertlmann, H. Narnhofer, and W. Thirring, Phys. Rev. A **66**, 032319 (2002).
[46] A. B. Klimov, L. L. Sánchez-Soto, E. C. Yustas, J. Söderholm, and G. Björk, Phys. Rev. A **72**, 033813 (2005).
[47] A. Luis, J. Opt. Soc. Am. A **24**, 1063 (2007).
[48] H. Prakash and N. Chandra, Phys. Rev. A **4**, 796 (1971).
[49] G. S. Agarwal, Lett. Nuovo Cimento **1**, 53 (1971).
[50] J. Lehner, U. Leonhardt, and H. Paul, Phys. Rev. A **53**, 2727 (1996).
[51] R. Simon and N. Mukunda, Phys. Lett. A **138**, 474 (1989).
[52] J. F. Cornwell, *Group Theory in Physics* (Academic, San Diego, 1997), Vol. 1.
[53] Arvind, K. S. Mallesh, and N. Mukunda, J. Phys. A **30**, 2417 (1997).
[54] D. J. Rowe, B. C. Sanders, and H. de Guise, J. Math. Phys. **40**, 3604 (1999).
[55] M. R. Dennis, J. Opt. A **6**, S26 (2004).
[56] X. Li, T.-H. Lan, C.-H. Tien, and M. Gu, Nat. Commun. **3**, 998 (2012).
[57] I. Bengtsson and K. Życzkowski, *Geometry of Quantum States: An Introduction to Quantum Entanglement* (Cambridge University Press, Cambridge, 2008).
[58] T. Saastamoinen and J. Tervo, J. Mod. Opt. **51**, 2039 (2004).
[59] O. Gamel and D. F. V. James, J. Opt. Soc. Am. A **31**, 1620 (2014).
[60] D. N. Klyshko, Phys. Lett. A **163**, 349 (1992).
[61] S. Weigert, J. Phys. A **30**, 8739 (1997).

Paper 6

P. de la Hoz, G. Björk, A. B. Klimov, G. Leuchs, L. L. Sánchez-Soto:

"Unpolarized states and hidden polarization",

Physical Review A 90, 043826 (2014)

Unpolarized states and hidden polarization

P. de la Hoz,[1] G. Björk,[2] A. B. Klimov,[3] G. Leuchs,[4,5] and L. L. Sánchez-Soto[1,4,5]
[1]*Departamento de Óptica, Facultad de Física, Universidad Complutense, 28040 Madrid, Spain*
[2]*Department of Applied Physics, Royal Institute of Technology (KTH), AlbaNova, SE-106 91 Stockholm, Sweden*
[3]*Departamento de Física, Universidad de Guadalajara, 44420 Guadalajara, Jalisco, Mexico*
[4]*Max-Planck-Institut für die Physik des Lichts, Günther-Scharowsky-Straße 1, Bau 24, 91058 Erlangen, Germany*
[5]*Department für Physik, Universität Erlangen-Nürnberg, Staudtstraße 7, Bau 2, 91058 Erlangen, Germany*
(Received 6 July 2014; published 15 October 2014)

We capitalize on a multipolar expansion of the polarization density matrix, in which multipoles appear as successive moments of the Stokes variables. When all the multipoles up to a given order K vanish, we can properly say that the state is Kth-order unpolarized, as it lacks of polarization information to that order. First-order unpolarized states coincide with the corresponding classical ones, whereas unpolarized to any order tally with the quantum notion of fully invariant states. In between these two extreme cases, there is a rich variety of situations that are explored here. The existence of hidden polarization emerges in a natural way in this context.

DOI: 10.1103/PhysRevA.90.043826 PACS number(s): 42.25.Ja, 42.50.Dv, 42.50.Ar, 42.50.Lc

I. INTRODUCTION

Very often an involved physical concept can be better understood in terms of its opposite. Polarization is a pertinent example: perhaps the most sensible way to look at it is to explore unpolarized states, as one can make sense of them using exclusively invariance principles, a tool of paramount importance in physics.

The constitution of unpolarized light was investigated from the very beginning of modern optics. Indeed, already Stokes [1] and Verdet [2] offered a lucid characterization of what they called "natural" light by using the projections of the intensity onto the axes of a rotated Cartesian coordinate system. Unpolarized states are those that remain invariant under any rotation of that coordinate system and under any phase shift between its rectangular components.

In classical optics, the field components of unpolarized light are well modeled by zero-mean, uncorrelated, stationary Gaussian random process [3]. The previous invariance conditions thus determine the entire probabilistic structure of the projected intensities [4]. However, as the standard theory is limited to first-order moments, unpolarized light is presented as having zero-mean Stokes vector, which in geometrical terms means that it is just the origin of the Poincaré sphere [5]. We stress, though, that this is an incomplete characterization, for it safely overlooks higher-order moments [6].

At the quantum level, the invariance requirement fixes once and for all the structure of the density matrix, as first pointed out in Refs. [7,8]: unpolarized states are maximally mixed in each subspace with a given number of photons [9,10]. To put it in another way, it specifies the probability distribution and, as a result, all the moments of the Stokes variables.

Nowadays, there is a widespread belief that a thorough appreciation of the subtle effects arising in the quantum world requires a careful scrutiny of higher-order polarization fluctuations. We have been advocating the use of a hierarchy of correlation functions that take into account the successive moments of the Stokes variables [11–13]. The most systematic way to accomplish this is by expanding the density matrix in multipoles [14].

The idea of unpolarized states can be directly translated in this scenario: when all the multipoles up to a given order (say K) vanish, the state lacks of polarization information up to that order and hence will be called Kth-order unpolarized. The classical picture matches the first-order theory, whereas the quantum condition implies that all the multipoles are identically null. Our goal here is to explore the *terra incognita* between these two extreme cases. In this respect, we mention that, as we shall see, this is closely related with the so-called hidden polarization, introduced by Klychko [15,16].

Our paper is organized as follows: In Sec. II we concisely sketch the fundamentals needed to grasp the polarization hallmarks of quantum fields and introduce the multipoles. In Sec. III we revisit unpolarized states from the viewpoint of these multipoles, defining Kth unpolarized states. In Sec. IV we apply the formalism to some illuminating examples and, finally, our conclusions are briefly summarized in Sec. V.

II. POLARIZATION STRUCTURE OF QUANTUM FIELDS

A satisfactory description of the polarization structure of quantum fields is of utmost significance for our purposes. This is precisely the objective of this section.

A. Quantum polarization sector

Let us consider a monochromatic field specified by two operators $\hat{a}_H$ and $\hat{a}_V$, representing the complex amplitudes in two linearly polarized orthogonal modes, we indicate as horizontal (H) and vertical (V), respectively. The Stokes operators are [17]

$$\hat{S}_x = \frac{1}{2}(\hat{a}_H^\dagger \hat{a}_V + \hat{a}_V^\dagger \hat{a}_H), \quad \hat{S}_y = \frac{i}{2}(\hat{a}_H \hat{a}_V^\dagger - \hat{a}_H^\dagger \hat{a}_V),$$
$$\hat{S}_z = \frac{1}{2}(\hat{a}_H^\dagger \hat{a}_H - \hat{a}_V^\dagger \hat{a}_V), \tag{2.1}$$

together with the total photon number

$$\hat{N} = \hat{a}_H^\dagger \hat{a}_H + \hat{a}_V^\dagger \hat{a}_V. \tag{2.2}$$

The superscript † stands for the Hermitian adjoint. In this Schwinger representation [18], these operators differ by a

factor 1/2 from the common Stokes parameters [5], but in this way the components of the Stokes vector $\hat{\mathbf{S}} = (\hat{S}_x, \hat{S}_y, \hat{S}_z)$ satisfy the commutation relations of the SU(2) algebra:

$$[\hat{S}_x, \hat{S}_y] = i\,\hat{S}_z, \tag{2.3}$$

and cyclic permutations (we use $\hbar = 1$ throughout).

The noncommutability of these operators precludes the simultaneous sharp measurement of the corresponding quantities. Among other consequences, this implies that no field state (apart from the two-mode vacuum) can have definite nonfluctuating values of all the Stokes operators simultaneously. This is quantified by the uncertainty relation

$$\Delta^2\hat{\mathbf{S}} = \Delta^2\hat{S}_x + \Delta^2\hat{S}_y + \Delta^2\hat{S}_z \geqslant \tfrac{1}{2}\langle\hat{N}\rangle, \tag{2.4}$$

where $\Delta^2\hat{S}_j = \langle\hat{S}_j^2\rangle - \langle\hat{S}_j\rangle^2$ are the variances. In this vein, one can say that the electric vector of a monochromatic quantum field never describes a definite ellipse.

Moreover, while the Stokes operators are all Hermitian, the noncommutability makes mixed, nonsymmetric products (such as $\hat{S}_x\hat{S}_y$) non-Hermitian, also precluding their direct measurement.

In classical optics, the total intensity is a well-defined quantity and the Poincaré sphere appears then as a smooth surface with radius equal to that intensity. In contradistinction, in quantum optics we have

$$\hat{\mathbf{S}}^2 = \hat{S}_x^2 + \hat{S}_y^2 + \hat{S}_z^2 = S(S+1)\hat{\mathbb{1}}, \tag{2.5}$$

where $S = N/2$ plays the role of the spin (N being the photon number). As fluctuations in N are unavoidable (leaving aside photon-number states), we are forced to talk of a three-dimensional Poincaré space (with axis S_x, S_y, and S_z) that can be envisioned as a set of nested spheres with radii proportional to the different photon numbers that contribute significantly to the state.

We next make the important observation that

$$[\hat{N}, \hat{\mathbf{S}}] = 0. \tag{2.6}$$

This expresses in the quantum language the fact that polarization and intensity are separate concepts: the form of the ellipse described by the electric field (polarization) does not depend on its size (intensity).

This fact brings about remarkable simplifications. First, it means that each subspace with a fixed number of photons must be handled separately. Equivalently, in the previous onionlike picture of the Poincaré space, each shell has to be addressed independently. This can be emphasized if instead of the Fock states $\{|n_H, n_V\rangle\}$, which are an orthonormal basis of the Hilbert space of these two-mode fields, we employ the relabeling

$$|S,m\rangle \equiv |n_H = S + m, n_V = S - m\rangle, \tag{2.7}$$

which can be seen as the common eigenstates of $\hat{S}^2$ and $\hat{S}_z$. For each fixed S, m runs from $-S$ to S and these states span a $(2S+1)$-dimensional invariant subspace, wherein the operators $\hat{\mathbf{S}}$ act in the standard form

$$\begin{aligned} \hat{S}_\pm\,|S,m\rangle &= \sqrt{S(S+1) - m(m\pm 1)}\,|S,m\pm 1\rangle, \\ \hat{S}_z\,|S,m\rangle &= m|S,m\rangle. \end{aligned} \tag{2.8}$$

Second, from (2.6) it follows that any function of the Stokes operators $f(\hat{\mathbf{S}})$ commutes with $\hat{N}$. Therefore, the matrix elements of the density matrix $\hat{\varrho}$ (which describes the state) connecting subspaces with different values of S do not contribute to $\langle f(\hat{\mathbf{S}})\rangle$. Put differently, the only accessible polarization information from any state $\hat{\varrho}$ is its block-diagonal form

$$\hat{\varrho}_{\rm pol} = \bigoplus_S P_S\,\hat{\varrho}^{(S)}, \tag{2.9}$$

where P_S is the photon-number distribution ($S = 0, 1/2, 1, \ldots$) and $P_S\,\hat{\varrho}^{(S)}$ is the reduced density matrix in the subspace with spin S. This $\hat{\varrho}_{\rm pol}$ has been termed the polarization sector [19] or the polarization density matrix [20]. What matters for our purposes is that any $\hat{\varrho}$ and its associated $\hat{\varrho}_{\rm pol}$ cannot be distinguished in polarization measurements and, accordingly, we shall be using the block-diagonal form (2.9) and drop henceforth the subscript pol.

B. Polarization multipoles

Instead of using directly the states $\{|S,m\rangle\}$, it is more convenient to expand each component $\hat{\varrho}^{(S)}$ in (2.9) as

$$\hat{\varrho}^{(S)} = \sum_{K=0}^{2S}\sum_{q=-K}^{K} \varrho_{Kq}^{(S)}\,\hat{T}_{Kq}^{(S)}. \tag{2.10}$$

The irreducible tensor operators $T_{Kq}^{(S)}$ are [21]

$$\hat{T}_{Kq}^{(S)} = \sqrt{\frac{2K+1}{2S+1}}\sum_{m,m'=-S}^{S} C_{Sm,Kq}^{Sm'}\,|S,m'\rangle\langle S,m|, \tag{2.11}$$

with $C_{Sm,Kq}^{Sm'}$ being the Clebsch-Gordan coefficients that couple a spin S and a spin K ($0 \leqslant K \leqslant 2S$) to a total spin S. These tensors are an orthonormal basis

$$\mathrm{Tr}\left[\hat{T}_{Kq}^{(S)}\,\hat{T}_{K'q'}^{(S')\dagger}\right] = \delta_{SS'}\delta_{KK'}\delta_{qq'}, \tag{2.12}$$

and they have the right transformation properties: under a rotation parametrized by the Euler angles (α,β,γ), we have

$$\hat{R}(\alpha,\beta,\gamma)\,\hat{T}_{Kq}^{(S)}\,\hat{R}^\dagger(\alpha,\beta,\gamma) = \sum_{q'} D_{q'q}^{S}(\alpha,\beta,\gamma)\,\hat{T}_{Kq'}^{(S)}, \tag{2.13}$$

where the $D_{q'q}^{S}(\alpha,\beta,\gamma)$ stands for the matrix elements of the rotation operator $\hat{R}(\alpha,\beta,\gamma)$ in the basis $|S,m\rangle$ [21].

Although at first sight they might look a bit intimidating, they are nothing but the multipoles used in atomic physics [14]. After some calculations, one can recast Eq. (2.11) as

$$\begin{aligned} &\hat{T}_{00}^{(S)} = \frac{1}{\sqrt{2S+1}}\hat{\mathbb{1}}, \\ &\hat{T}_{10}^{(S)} = \sqrt{\frac{3}{(2S+1)(S+1)S}}\,\hat{S}_z,\ \hat{T}_{1\mp1}^{(S)} = \sqrt{\frac{3}{(2S+1)(S+1)S}}\,\hat{S}_\pm, \\ &\hat{T}_{20}^{(S)} = \sqrt{\frac{C}{6}}\left(3\hat{S}_z^2 - \hat{S}^2\right),\ \hat{T}_{2\mp1}^{(S)} = \sqrt{\frac{C}{2}}\,\{\hat{S}_z, \hat{S}_\pm\},\ \hat{T}_{1\mp2}^{(S)} = \sqrt{\frac{C}{2}}\,\hat{S}_\pm^2, \end{aligned} \tag{2.14}$$

where $C = 30/[(2S+3)(2S+1)(2S-1)(S+1)]$ and $\{,\}$ is the anticommutator. In consequence, we conclude that $\hat{T}_{Kq}^{(S)}$ can be related to the Kth power of the Stokes operators (2.1).

The corresponding expansion coefficients

$$\varrho_{Kq}^{(S)} = \mathrm{Tr}\left[\hat{\varrho}^{(S)}\,\hat{T}_{Kq}^{(S)\dagger}\right] \tag{2.15}$$

are known as state multipoles. The hermiticity imposes the symmetry condition

$$\varrho_{K-q}^{(S)} = (-1)^q\,\varrho_{Kq}^{(S)}, \tag{2.16}$$

and the positive semidefiniteness of $\hat{\varrho}^{(S)}$ forces the bound

$$\mathcal{W}_K^{(S)} \equiv \sum_{q=-K}^{K} \left|\varrho_{Kq}^{(S)}\right|^2 \leqslant C_K^{(S)}, \tag{2.17}$$

for every $K > 1$ and $C_K^{(S)}$ a positive constant. The quantity $\mathcal{W}_K^{(S)}$ is just the strength of the Kth multipole in the state $\hat{\varrho}^{(S)}$.

Finally, we turn to the important class of axially symmetric states [14]. They are invariant under rotations about an axis that we take as the z axis. Since $D_{qq'}^{S}(0,0,\gamma) = \exp(-iq\gamma)\delta_{qq'}$, this implies

$$\hat{\varrho}_{\mathrm{axsym}}^{(S)} = \sum_{K=0}^{2S} \varrho_{K0}^{(S)}\,\hat{T}_{K0}^{(S)}. \tag{2.18}$$

Thus, they are characterized exclusively by the multipole components ϱ_{K0}. Any density operator that can be obtained from $\hat{\varrho}_{\mathrm{axsym}}$ via an SU(2) transformation, represents as well an axial symmetric state, as a rotation only change the direction of the symmetry axis of the state.

Some axially symmetric systems are also invariant under the reversal of the symmetry axis (i.e., $z \to -z$). As this corresponds to a rotation around the y axis by an angle π and $D_{qq'}^{S}(0,\pi,0) = (-1)^{K+q}\delta_{q\,-q'}$, we get from (2.13)

$$\varrho_{K0}^{(S)} = (-1)^K \varrho_{K0}^{(S)}, \tag{2.19}$$

so only multipoles of even rank K contribute.

III. *K*TH-ORDER UNPOLARIZED STATES

From now on, we restrict ourselves to a single component $\hat{\varrho}^{(S)}$ (i.e., a fixed number of photons). This is by no means a restriction, as the discussion can be extended in a natural way to the complete polarization density matrix in (2.9).

The full polarization information is encoded in the complete multipole distribution $\{\mathcal{W}_K^{(S)}\}$. However, for most of the states, only a limited number of multipoles play a substantive role and the rest of them have a small contribution. As a consequence, gaining a good feeling of the corresponding behavior may be tricky.

A way to bypass this disadvantage is to look at the cumulative distribution

$$\mathcal{A}_K^{(S)} = \sum_{\ell=1}^{K} \mathcal{W}_\ell^{(S)}. \tag{3.1}$$

Please, note carefully that the monopolar term has been excluded, as it is trivially isotropic for all the states. The quantity $\mathcal{A}_K^{(S)}$ conveys whole information up to order K. We know from probability that it has remarkable properties [22].

To get extra insights into this subject, let us focus, for the time being, on the key example of SU(2) coherent states (also known as spin or atomic coherent states), which can be written down as the superposition [23,24]

$$|\theta,\phi\rangle = \sum_{m=-S}^{S} C_{Sm}(\theta,\phi)\,|S,m\rangle, \tag{3.2}$$

with coefficients

$$C_{Sm}(\theta,\phi) = \binom{2S}{S+m}^{1/2} \left(\sin\frac{\theta}{2}\right)^{S+m} \left(\cos\frac{\theta}{2}\right)^{S-m} e^{-i(S+m)\phi}, \tag{3.3}$$

and θ and ϕ are the polar and azimuthal angles on the sphere, respectively. If $\mathbf{n}$ is the unit vector in the direction (θ,ϕ), the operator $\hat{S}_{\mathbf{n}} = \mathbf{n}\cdot\hat{\mathbf{S}}$ is the observable measured in polarization experiments [25]: coherent states can be alternatively interpreted as eigenstates of $\hat{S}_{\mathbf{n}}$

$$\hat{S}_{\mathbf{n}}|\theta,\phi\rangle = S|\theta,\phi\rangle, \tag{3.4}$$

from which one can confirm that they saturate the uncertainty relation (2.4) and so they are the minimum uncertainty states in polarization optics.

For these states, one can immediately find

$$\mathcal{A}_{K,\mathrm{SU(2)}}^{(S)} = \frac{2S}{2S+1} - \frac{[\Gamma(2S+1)]^2}{\Gamma(2S-K)\Gamma(2S+K+2)}. \tag{3.5}$$

As conjectured in Ref. [13], this is the maximal value attainable for any K in each subspace S. This nicely corroborates the amazing properties of SU(2) coherent states: they are maximally polarized states to any order, as one would expect from a pure state that corresponds as nearly as possible to a classical spin vector pointing in a given direction.

This maximality property suggests at once a hierarchy of degrees of polarization

$$\mathbb{P}_K^{(S)} = \sqrt{\frac{\mathcal{A}_K^{(S)}}{\mathcal{A}_{K,\mathrm{SU(2)}}^{(S)}}}, \tag{3.6}$$

which sort the relevant polarization information *up* to order K ($K = 1,\ldots,S$). The experimental reconstruction reported in Ref. [13] reveals that by performing a Stokes measurement in $2K+1$ independent directions, one can actually determine $\mathcal{A}_K^{(S)}$ and hence all the degrees $\mathbb{P}_K^{(S)}$.

We will say that a state is Kth-order unpolarized when $\mathbb{P}_K^{(S)} = 0$ (which obviously implies $\mathcal{A}_K^{(S)} = 0$; i.e., all the multipoles up to order K vanish) and we will denote these states as $\hat{\varrho}_{\mathrm{unpol},K}^{(S)}$. Note, though, that Kth-order unpolarized states do carry polarization information when one looks at higher-order moments. This is referred to as hidden polarization, according to the terminology coined by Klyshko [15,16], albeit it would be better to say that such states display higher-order polarization [26].

In more physical terms, the condition of Kth-order unpolarization amounts to imposing that the moments $\langle\hat{\mathbf{S}}_{\mathbf{n}}^{\ell}\rangle$ are independent of the direction $\mathbf{n}$ for $\ell = 1,\ldots,K$ (i.e., they are isotropic). Therefore, all the moments up to order K do not show any angular structure, whereas higher-order ones do. Notice, in passing, that this is the logic beyond the recent

proposal of anticoherent states [27]: such states point nowhere (to a given order), and this is certainly one way to serve as the opposite of a state that points, as much as possible, somewhere. From this perspective, these unpolarized states are exhibits the most nonclassical features [28,29].

For the particular case of the dipole ($K = 1$), Eq. (3.6) reduces to

$$\mathbb{P}_1^{(S)} = \frac{\sqrt{\langle \hat{S}_x\rangle^2 + \langle \hat{S}_y\rangle^2 + \langle \hat{S}_z\rangle^2}}{S}, \tag{3.7}$$

which coincides with the standard definition [30]. First-order unpolarized states verify $\mathbb{P}_1^{(S)} = 0$, so $\langle \hat{\mathbf{S}}\rangle = 0$. This goes to the classical notion of random states, as it involves exclusively first-order moments.

When the state is unpolarized to any order, only the monopole contributes:

$$\hat{\varrho}_{\rm unpol}^{(S)} = \frac{1}{2S+1}\,\mathbb{1}_{2S+1}, \tag{3.8}$$

so it is a random state within each invariant subspace. This is the quantum definition, which demands that the whole probability distribution to be SU(2) invariant [7,8]; that is,

$$[\hat{\varrho}, \hat{\mathbf{S}}] = 0, \tag{3.9}$$

wherefrom Eq. (3.8) follows [10]. The vacuum state is the only pure state that is unpolarized according to this definition, and unpolarized mixed states are maximally mixed in each subspace S. Any two-mode thermal state is hence unpolarized.

IV. MENAGERIE OF UNPOLARIZED STATES

A. Single-photon unpolarized states

Single-photon states ($S = 1/2$) are fairly special: they can only be first-order unpolarized. The multipole expansion of a general single-photon state reads

$$\hat{\varrho}^{(1/2)} = \varrho_{00}^{(1/2)}\,\hat{T}_{00}^{(1/2)} + \sum_q \varrho_{1q}^{(1/2)}\hat{T}_{1q}^{(1/2)}. \tag{4.1}$$

Since the state has only dipolar component, quantum and classical descriptions coincide. Positivity constraints the possible values of the dipole to the range $0 \leqslant \mathcal{A}_1^{(1/2)} \leqslant 1/2$. The condition $\mathcal{A}_1^{1/2} = 0$ fixes at once unpolarized states; viz,

$$\varrho_{\rm unpol,1}^{(1/2)} = \frac{1}{2}\begin{pmatrix} 1 & 0 \\ 0 & 1 \end{pmatrix}. \tag{4.2}$$

These states are both classically and quantum unpolarized, but, like all quantum objects, can only be considered as elements of an ensemble [31].

B. Two-photon unpolarized states

For two-photon states, there are first-order (or classical) and second-order (or quantum) unpolarized states. The general condition for first-order unpolarization is

$$\hat{\varrho}_{\rm unpol,1}^{(1)} = \varrho_{00}^{(1)}\,\hat{T}_{00}^{(1)} + \sum_q \varrho_{2q}^{(1)}\,\hat{T}_{2q}^{(1)}, \tag{4.3}$$

with the extra constraint of positivity.

The case of axially symmetric states deserves special attention as they can always be diagonalized via SU(2) rotations; viz, $\hat{\rho}_{\rm assym}^{(1)} = \hat{R}(\alpha,\beta,\gamma)\,\hat{\varrho}_d^{(1)}\,\hat{R}^\dagger(\alpha,\beta,\gamma)$, with

$$\hat{\varrho}_d^{(1)} = \begin{pmatrix} \lambda_1 & 0 & 0 \\ 0 & \lambda_2 & 0 \\ 0 & 0 & \lambda_3 \end{pmatrix} = \frac{1}{\sqrt{3}}\hat{T}_{00}^{(1)} + \frac{\lambda_1-\lambda_3}{\sqrt{2}}\hat{T}_{10}^{(1)} + \frac{1-3\lambda_2}{\sqrt{6}}\hat{T}_{20}^{(1)}. \tag{4.4}$$

The state is first-order unpolarized when $\lambda_1 = \lambda_3$. Since $\mathrm{Tr}(\hat{\varrho}_d) = 1$, we can write

$$\hat{\varrho}_{\rm unpol,1}^{(1)} = \begin{pmatrix} \lambda & 0 & 0 \\ 0 & 1-2\lambda & 0 \\ 0 & 0 & \lambda \end{pmatrix}, \tag{4.5}$$

and positivity enforces $0 \leqslant \lambda \leqslant 1/2$, i.e., $0 \leqslant \mathcal{A}_2^{(1)} \leqslant 2/3$. Both the purity $\mathcal{P}^{(1)} = \mathrm{Tr}\{[\hat{\varrho}_d^{(1)}]^2\}$ and the second-order degree $\mathbb{P}_2^{(1)}$ depend on λ

$$\mathcal{P}^{(1)} = 6\lambda^2 - 4\lambda + 1, \quad \mathbb{P}_2^{(1)} = \sqrt{(3\lambda-1)^2}, \tag{4.6}$$

while $\mathbb{P}_1^{(1)} = 0$ as anticipated. This can be recast as

$$\mathbb{P}_2^{(1)} = \sqrt{[3\mathcal{P}^{(1)} - 1]/2}. \tag{4.7}$$

In Fig. 1 we have plotted $\mathbb{P}_2^{(1)}$ as a function of the purity. The maximum degree $\mathbb{P}_2^{(1)}$ is attained for the pure states

$$\left|\Psi_{\rm unpol,1}^{(1)}\right\rangle = \frac{1}{\sqrt{2}}\sin\beta[e^{i\alpha}|1,1\rangle - e^{-i\alpha}|1,-1\rangle] + \cos\beta|1,0\rangle, \tag{4.8}$$

and they are the transformed of the state $|1,0\rangle$ under SU(2) rotations $\hat{R}(\alpha,\beta,\gamma)$. Incidentally, these states have served as the thread to experimentally verify the existence of hidden polarization [32,33]. They coincide with the anticoherent states introduced in Ref. [27] and worked out using the Majorana representation [34,35]. Unfortunately, their nice geometric properties cannot be extended to mixed states (4.5).

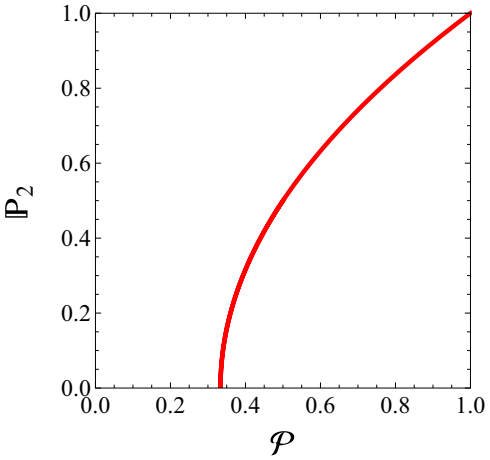

FIG. 1. (Color online) Second-order degree of polarization as a function of the purity, for the first-order unpolarized states (4.5).

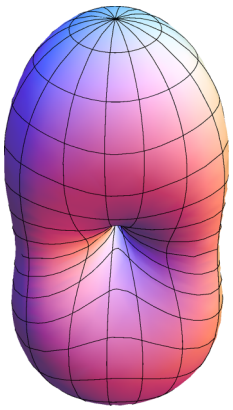

FIG. 2. (Color online) Q function for three-photon first-order pure unpolarized states (4.13).

C. Three-photon unpolarized states

For three-photon states we have first- (classical), second-, and third-order (quantum) unpolarized states.

The diagonalizable states can be brought to the form

$$\begin{aligned}\hat{\varrho}_d^{(3/2)} &= \begin{pmatrix} \lambda_1 & 0 & 0 & 0 \\ 0 & \lambda_2 & 0 & 0 \\ 0 & 0 & \lambda_3 & 0 \\ 0 & 0 & 0 & \lambda_4 \end{pmatrix} = \frac{1}{2}\hat{T}_{00}^{(3/2)} \\ &- \left(\frac{2\lambda_2 + 4\lambda_3 + 6\lambda_4 - 3}{2\sqrt{5}}\right)\hat{T}_{10}^{(3/2)} \\ &+ \left(\frac{1}{2} - \lambda_2 - \lambda_3\right)\hat{T}_{20}^{(3/2)} \\ &+ \left(\frac{-4\lambda_2 + 2\lambda_3 - 2\lambda_4 + 1}{2\sqrt{5}}\right)\hat{T}_{30}^{(3/2)}. \end{aligned} \quad (4.9)$$

The condition for first-order unpolarization is

$$2\lambda_2 + 4\lambda_3 + 6\lambda_4 - 3 = 0, \quad (4.10)$$

and the dipole is absent. Now there are not axially symmetric first-order unpolarized states, because when S is a half integer, no state of the basis lacks first-order polarization.

The diagonal operator of a three-photon first-order unpolarized state reads

$$\hat{\varrho}_{\mathrm{unpol},1}^{(3/2)} = \begin{pmatrix} \lambda_3 + 2\lambda_4 - 1/2 & 0 & 0 & 0 \\ 0 & -2\lambda_3 - 3\lambda_4 + 3/2 & 0 & 0 \\ 0 & 0 & \lambda_3 & 0 \\ 0 & 0 & 0 & \lambda_4 \end{pmatrix}, \quad (4.11)$$

and positivity translates into $0 \leqslant \lambda_3 + 2\lambda_4 - 1/2 \leqslant 1$ and $0 \leqslant -2\lambda_3 - 3\lambda_4 + 3/2 \leqslant 1$, $0 \leqslant \lambda_3, \lambda_4 \leqslant 1$. The purity $\mathcal{P}$ is

$$\mathcal{P} = \tfrac{1}{4} + \tfrac{5}{4}(2\lambda_3 + 2\lambda_4 - 1)^2 + (\lambda_3 + 3\lambda_4 - 1)^2. \quad (4.12)$$

with the bounds $1/4 \leqslant \mathcal{P} \leqslant 5/8$.

We remark that by using the Majorana representation mentioned above, one can check that the SU(2) transformed of

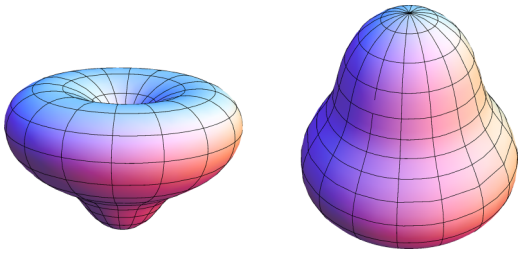

FIG. 3. (Color online) Q function for axially symmetric three-photon second-order unpolarized states with maximal purity. In the left, we represent the state $3/4|3/2,1/2\rangle\langle 3/2,1/2| + 1/4|3/2,-3/2\rangle\langle 3/2,-3/2|$, while in the right the state $1/3|3/2,3/2\rangle\langle 3/2,3/2| + 1/2|3/2,-1/2\rangle\langle 3/2,-1/2| + 1/6|3/2,-3/2\rangle\langle 3/2,-3/2|$ is plotted.

$$|\Psi_{\mathrm{unpol},1}^{(3/2)}\rangle = \frac{1}{\sqrt{2}}|3/2,-3/2\rangle + \frac{1}{\sqrt{2}}|3/2,3/2\rangle, \quad (4.13)$$

are first-order unpolarized, although they do not fall in the class of states defined by (4.11). To better appreciate these states, one can work out the SU(2) Q function, which is defined as [36,37]

$$Q^{(S)}(\theta,\phi) = \langle\theta,\phi|\hat{\varrho}^{(S)}|\theta,\phi\rangle, \quad (4.14)$$

where $|\theta,\phi\rangle$ are SU(2) coherent states. In Fig. 2 we plot this Q function for the state (4.13).

To get a second-order unpolarized state, we need the additional condition: $\lambda_3 + 3\lambda_4 - 1 = 0$ and, the diagonal form for these states is

$$\hat{\varrho}_{\mathrm{unpol},2}^{(3/2)} = \begin{pmatrix} \frac{1}{2} - \lambda_4 & 0 & 0 & 0 \\ 0 & 3\lambda_4 - \frac{1}{2} & 0 & 0 \\ 0 & 0 & 1 - 3\lambda_4 & 0 \\ 0 & 0 & 0 & \lambda_4 \end{pmatrix}. \quad (4.15)$$

The maximal purity of a second-order unpolarized axially symmetric three-photon state is $\mathcal{P} = 7/18$. In Fig. 3, we represent the Q function for second-order unpolarized states maximizing the purity.

V. CONCLUDING REMARKS

Multipolar expansions are a powerful machinery. We have applied such an expansion to the polarization density matrix, showing how the multipoles quantify higher-order fluctuations in the Stokes variables. In this way, we have provided a systematic characterization of unpolarized states as those states whose multipoles up to a given order vanish.

The formalism can be extended to systems in which SU(2) symmetry plays a crucial role (such as Bose-Einstein condensates, spin chains, etc.) and to other unitary symmetries, such as SU(3) (which is pivotal to understanding the polarization of the near field).

ACKNOWLEDGMENTS

Financial support from the Swedish Foundation for International Cooperation in Research and Higher Education

(STINT), the Swedish Research Council (VR) through its Linnæus Center of Excellence ADOPT and Contract No. 621-2011-4575, the Mexican CONACyT (Grant No. 106525), the EU FP7 (Grant Q-ESSENCE), and the Spanish MINECO (Grant No. FIS2011-26786) is gratefully acknowledged.

[1] G. G. Stokes, Trans. Cambridge Phil. Soc. **9**, 399 (1852).
[2] E. Verdet, *Leçons d' Optique Physique*, edited by A. Levistal, Vol. 2 (Imprimerie Impériale, Paris, 1869), pp. 78–98.
[3] N. G. van Kampen, *Stochastic Processes in Physics and Chemistry*, 2nd ed. (Elsevier, Amsterdam, 2007).
[4] R. Barakat, J. Opt. Soc. Am. A **6**, 649 (1989).
[5] M. Born and E. Wolf, *Principles of Optics*, 7th ed. (Cambridge University Press, Cambridge, 1999).
[6] H. Paul and J. Wegmann, Opt. Commun. **112**, 85 (1994).
[7] H. Prakash and N. Chandra, Phys. Rev. A **4**, 796 (1971).
[8] G. S. Agarwal, Lett. Nuovo Cimento **1**, 53 (1971).
[9] J. Lehner, U. Leonhardt, and H. Paul, Phys. Rev. A **53**, 2727 (1996).
[10] J. Söderholm, G. Björk, and A. Trifonov, Opt. Spectrosc. **91**, 532 (2014).
[11] C. R. Müller, B. Stoklasa, C. Peuntinger, C. Gabriel, J. Řeháček, Z. Hradil, A. B. Klimov, G. Leuchs, C. Marquardt, and L. L. Sánchez-Soto, New J. Phys. **14**, 085002 (2012).
[12] L. L. Sánchez-Soto, A. B. Klimov, P. de la Hoz, and G. Leuchs, J. Phys. B **46**, 104011 (2013).
[13] P. de la Hoz, A. B. Klimov, G. Björk, Y. H. Kim, C. Müller, C. Marquardt, G. Leuchs, and L. L. Sánchez-Soto, Phys. Rev. A **88**, 063803 (2013).
[14] K. Blum, *Density Matrix Theory and Applications* (Plenum, New York, 1981).
[15] D. N. Klyshko, Phys. Lett. A **163**, 349 (1992).
[16] D. M. Klyshko, JETP **84**, 1065 (1997).
[17] A. Luis and L. L. Sánchez-Soto, Prog. Opt. **41**, 421 (2000).
[18] J. Schwinger, in *Quantum Theory of Angular Momentum*, edited by L. C. Biedenharn and H. Dam (Academic, New York, 1965).
[19] M. G. Raymer, D. F. McAlister, and A. Funk, in *Quantum Communication, Computing, and Measurement 2*, edited by P. Kumar (Plenum, New York, 2000).
[20] V. P. Karassiov and A. V. Masalov, JETP **99**, 51 (2004).
[21] D. A. Varshalovich, A. N. Moskalev, and V. K. Khersonskii, *Quantum Theory of Angular Momentum* (World Scientific, Singapore, 1988).
[22] E. T. Jaynes, *Probability Theory: The Logic of Science* (Cambridge University Press, Cambridge, 2003).
[23] F. T. Arecchi, E. Courtens, R. Gilmore, and H. Thomas, Phys. Rev. A **6**, 2211 (1972).
[24] A. Perelomov, *Generalized Coherent States and their Applications* (Springer, Berlin, 1986).
[25] C. Marquardt, J. Heersink, R. Dong, M. V. Chekhova, A. B. Klimov, L. L. Sánchez-Soto, U. L. Andersen, and G. Leuchs, Phys. Rev. Lett. **99**, 220401 (2007).
[26] G. K. Gupta, A. Kumar, and R. S. Singh, Opt. Commun. **284**, 4951 (2011).
[27] J. Zimba, EJTP **3**, 143 (2006).
[28] O. Giraud, P. Braun, and D. Braun, New J. Phys. **12**, 063005 (2010).
[29] D. Baguette, T. Bastin, and J. Martin, Phys. Rev. A **90**, 032314 (2014).
[30] G. Björk, J. Söderholm, L. L. Sánchez-Soto, A. B. Klimov, I. Ghiu, P. Marian, and T. A. Marian, Opt. Commun. **283**, 4440 (2010).
[31] A. Peres, *Quantum Theory: Concepts and Methods* (Kluwer, New York, 2002).
[32] P. Usachev, J. Söderholm, G. Björk, and A. Trifonov, Opt. Commun. **193**, 161 (2001).
[33] A. Sehat, J. Söderholm, G. Björk, P. Espinoza, A. B. Klimov, and L. L. Sánchez-Soto, Phys. Rev. A **71**, 033818 (2005).
[34] J. Crann, R. Pereira, and D. W. Kribs, J. Phys. A **43**, 255307 (2010).
[35] E. Bannai and M. Tagami, J. Phys. A **44**, 342002 (2011).
[36] R. L. Stratonovich, Zh. Eksp. Teor. Fiz. **31**, 1012 (1956) [Sov. Phys. JETP **4**, 891 (1957)].
[37] F. A. Berezin, Commun. Math. Phys. **40**, 153 (1975).

Paper 7

Z. Hradil, J. Rehacek, P. de la Hoz, G. Leuchs, L. L. Sánchez-Soto:

"Extremal states for photon number and quadratures as gauges for nonclassicality",

Physical Review A **91**, 042128 (2015)

Extremal states for photon number and quadratures as gauges for nonclassicality

Z. Hradil,[1] J. Řeháček,[1] P. de la Hoz,[2] G. Leuchs,[3,4] and L. L. Sánchez-Soto[2,3,4]

[1]*Department of Optics, Palacký University, 17. listopadu 12, 771 46 Olomouc, Czech Republic*

[2]*Departamento de Óptica, Facultad de Física, Universidad Complutense, 28040 Madrid, Spain*

[3]*Max-Planck-Institut für die Physik des Lichts, Günther-Scharowsky-Straße 1, Bau 24, 91058 Erlangen, Germany*

[4]*Department für Physik, Universität Erlangen-Nürnberg, Staudtstraße 7, Bau 2, 91058 Erlangen, Germany*

(Received 17 December 2014; published 27 April 2015)

Rotated quadratures carry the phase-dependent information of the electromagnetic field, so they are somehow conjugate to the photon number. We analyze this noncanonical pair, finding an exact uncertainty relation, as well as a couple of weaker inequalities obtained by relaxing some restrictions of the problem. We also find the intelligent states saturating that relation and complete their characterization by considering extra constraints on the second-order moments of the variables involved. Using these moments, we construct performance measures tailored to diagnose photon-added and Schrödinger-cat-like states, among others.

DOI: 10.1103/PhysRevA.91.042128 PACS number(s): 03.65.Fd, 42.50.Dv

I. INTRODUCTION

Leaving aside interpretational issues [1–3], the quantum state is an essential ingredient of quantum theory: once it is known, the probabilities of the outcomes of any possible measurement may be predicted. Unfortunately, this elusive object cannot be directly determined and must be inferred from a suitable set of measurements, which constitutes the province of quantum tomography [4]. Although this might superficially appear to be a mere statistical estimation, the positivity of the reconstructed state imposes stringent quantum constraints.

Indeed, these constraints endow the set of admissible states with a rich geometry, the boundaries of which somehow establish the realm of the quantum world. Delimiting these borders is, in general, a difficult conundrum. One way to ease these complications is to look at the problem using moments of the relevant quantities, with the hope that only a few of them will be important enough. As a simple yet illustrative example of this, let us examine a single-mode quantum field, which will serve as a thread in this work. The complex amplitude $\hat{a}$ and the photon number $\hat{n} = \hat{a}^\dagger \hat{a}$ for this system must obey $\langle \hat{n} \rangle \geqslant |\langle \hat{a} \rangle|^2$, which can be readily obtained by a simple application of the Cauchy-Schwarz inequality [5]. The extremal states (i.e., those saturating the inequality) turn out to be coherent states. Hence, the difference between the average photon number and the square of the absolute value of the complex amplitude, which must be always positive, can be taken, up to second order, as a reliable indicator of the "quality" of a coherent state.

In classical signal processing, intensity and phase are the basic magnitudes specifying the field. At the quantum level, they translate into photon number and phase. However, the definition of a *bona fide* phase operator is beset by difficulties that have been the object of a heated debate [6–10]. Here, we choose a surrogate approach that considers the phase properly encoded in the field quadratures, as is routinely done in the theory of quantum nondemolition measurements [11–13]. While photon number lies at the heart of the discrete-variable quantum information, quadratures are the primary tool in the continuous-variable domain. Photon number and quadratures bridge these two complementary worlds in a natural way.

Extremal states for these variables were investigated some years ago, fueled by the search for noise minimum states [14,15]. More recently, the quite similar question of the uncertainty relation for the number and the annihilation operator was addressed [16]. Our aim here is to push this research further and explore how these extremal states can be used for the diagnostics of nonclassicality.

The plan of this paper is as follows. In Sec. II we revisit the uncertainty relations for photon number and rotated quadratures, as well as loose approximations thereof. Section III rounds off this discussion by looking at the extra restrictions that quantum theory imposes on the second-order moments of those variables and by looking at the properties of intelligent states, which obey the equality in the previous uncertainty relations. Based on those states, we tailor performance measures especially germane to verify photon-added and Schrödinger-cat-like states, among others. Finally, our conclusions are summarized in Sec. IV.

II. UNCERTAINTY RELATIONS FOR PHOTON NUMBER AND QUADRATURES

A. Tight uncertainty relations

The system we are interested in is a single-mode electromagnetic field, which can be formally deemed a harmonic oscillator. Classically, it is characterized by a complex amplitude that contains information about both the magnitude and the phase of the field. In the quantum formalism, the mode is specified by the action of annihilation ($\hat{a}$) and creation ($\hat{a}^\dagger$) operators satisfying the basic bosonic commutation relation [17]

$$[\hat{a}, \hat{a}^\dagger] = \hat{\mathbb{1}} \,. \tag{2.1}$$

At optical frequencies, the common way of measuring the field is with homodyne detection [18]. The readout in this scheme involves moments of the rotated quadratures

$$\hat{x}_\theta = \frac{1}{\sqrt{2}} (\hat{a}\, e^{+i\theta} + \hat{a}^\dagger\, e^{-i\theta}) \,, \quad \hat{p}_\theta = \frac{1}{\sqrt{2}i} (\hat{a} e^{+i\theta} - \hat{a}^\dagger e^{-i\theta}) \,, \tag{2.2}$$

where θ is the phase of the local oscillator that can be externally varied. The reader should be careful about comparing results

on quadrature, as there are a variety of normalizations used in the literature. Notice that $\hat{p}_\theta = -\hat{x}_{\theta+\pi/2}$ and that, for $\theta = 0$, they reduce to the canonical variables $\hat{x}$ and $\hat{p}$. They satisfy the canonical commutation relation (in units $\hbar = 1$ throughout)

$$[\hat{x}_\theta, \hat{p}_\theta] = i\hat{\mathbb{1}}\,. \tag{2.3}$$

Since $\hat{x}_\theta^2 + \hat{p}_\theta^2 = \hat{n} + \hat{\mathbb{1}}/2$, where $\hat{n} = \hat{a}^\dagger\hat{a}$ is the number operator, precise knowledge of the eigenvalue of $\hat{n}$ restricts the possible knowledge about the quadratures. This is quantified by the commutation

$$[\hat{n}, \hat{x}_\theta] = -i\,\hat{p}_\theta\,, \tag{2.4}$$

which, in turn, implies the uncertainty relation

$$V(\hat{n})\,V(\hat{x}_\theta) \geqslant \tfrac{1}{4}|\langle\hat{p}_\theta\rangle|^2\,. \tag{2.5}$$

Here, $V(\hat{A}) = \langle\hat{A}^2\rangle - \langle\hat{A}\rangle^2$ denotes the variance of $\hat{A}$, and the angular brackets $\langle\cdot\rangle$ mean averaging over the state of the system (either pure or mixed).

Equation (2.5) is an exact relation but depends on the local oscillator phase. Differentiation with respect to θ leads to the extremal values $\lambda_\pm$ of $V(\hat{x}_\theta)$; they can be written as [19]

$$\lambda_\pm^2 = C(\hat{a}^\dagger, \hat{a}) \pm |V(\hat{a})|\,, \tag{2.6}$$

where the (symmetrized) covariance is $C(\hat{A}, \hat{B}) = \langle\{\hat{A}, \hat{B}\}/2\rangle - \langle\hat{A}\rangle\langle\hat{B}\rangle$. It is convenient to introduce the quantity λ by

$$\lambda^2(\varphi) = \lambda_+^2 \sin^2\varphi + \lambda_-^2 \cos^2\varphi\,, \tag{2.7}$$

with $\varphi = \arg[V(\hat{a})/2] - \arg[\langle\hat{a}\rangle]$, in terms of which Eq. (2.5) takes the form

$$V(\hat{n})\left[\frac{\lambda_+\lambda_-}{\lambda(\varphi)}\right]^2 \geqslant |\langle\hat{a}\rangle|^2\,. \tag{2.8}$$

Apart from the invariant parameters $\lambda_\pm$, this expression also depends on the phase φ. However, this alternative presentation will allow us in the following to devise remarkable simplifications. In addition, it is closely related to the customary ball-and-stick representation of quantum states in phase space [20], where the quadratures $\hat{x}$ and $\hat{p}$ are taken as coordinates. In this picture, sketched in Fig. 1, the stick corresponds to the average value of the field $\langle\hat{a}\rangle$, and the ball corresponds to the fluctuations around the mean value. We display this area as a noise ellipse whose semiaxes are precisely the invariant parameters $\lambda_\pm$. In this way, $\lambda_\pm$, which are eigenvalues of the covariance matrix and related to the universal quantum invariants [21], play a key role in picturing the noise properties of the state [22,23]. The meaning of $\lambda(\varphi)$ can be gathered at once from Fig. 1.

As a final remark, we mention that inequality (2.8) formally makes it possible to introduce a quantity like phase variance $V(\hat{\phi})$, fulfilling a standard uncertainty relation with $V(\hat{n})$, namely,

$$V(\hat{\phi}) = \left[\frac{\lambda_+\lambda_-}{\lambda(\varphi)}\right]^2 \frac{1}{|\langle\hat{a}\rangle|^2}\,. \tag{2.9}$$

Interestingly enough, an explicit calculation shows that this variance of the putative operator $\hat{\phi}$ tallies with the smallest possible phase resolution in the Shapiro-Wagner phase concept [24] if both quadrature operators are measured simultaneously.

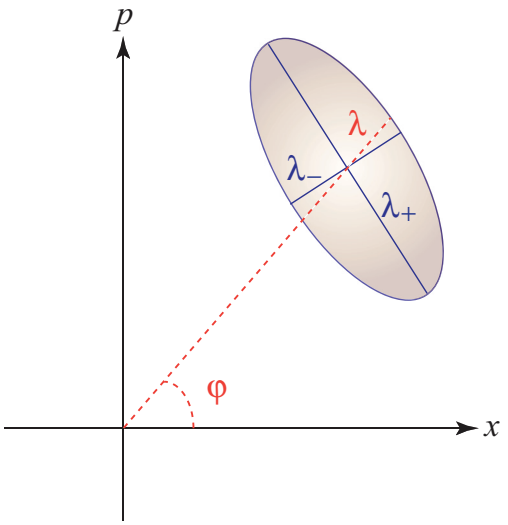

FIG. 1. (Color online) Ball-and-stick diagram in phase space. $\langle a\rangle$ is the complex amplitude of the field, and $\lambda_\pm$ are the semiaxes of the uncertainty ellipse. The variable $\lambda(\varphi)$ has been defined in Eq. (2.7).

B. Relaxing the bounds

The tight uncertainty relation (2.5) and its equivalent (2.8) convey complete information, but they provide phase-dependent bounds. It might be interesting to work out weaker inequalities, which are independent of the orientation of the noise ellipse.

A first option stems from the trivial observation that, according to (2.7), $\inf_\varphi \lambda(\varphi) = \lambda_-$, so (2.8) can be relaxed to

$$V(\hat{n})\,\lambda_+^2 \geqslant |\langle\hat{a}\rangle|^2\,, \tag{2.10}$$

or, using $C(\hat{a}^\dagger, \hat{a})$,

$$V(\hat{n})\,[C(\hat{a}^\dagger, \hat{a}) + |V(\hat{a})|] \geqslant |\langle\hat{a}\rangle|^2\,. \tag{2.11}$$

The second possibility comes from the estimate $[\lambda_+\lambda_-/\lambda(\varphi)]^2 \leqslant \lambda_+^2 + \lambda_-^2$. Now, we can write down

$$V(\hat{n})\,(\lambda_+^2 + \lambda_-^2) \geqslant |\langle\hat{a}\rangle|^2\,, \tag{2.12}$$

which, using again $C(\hat{a}^\dagger, \hat{a})$, reads as

$$V(\hat{n})\,C(\hat{a}^\dagger, \hat{a}) \geqslant |\langle\hat{a}\rangle|^2\,. \tag{2.13}$$

This coincides with the expression obtained in Ref. [16]. In spite of its simplicity, this inequality has a drawback: it cannot be exactly saturated (but see the solution worked out in Ref. [25]). This can be confirmed by noticing that Eq. (2.13) is just the sum of

$$V(\hat{n})\,V(\hat{x}) \geqslant \tfrac{1}{4}|\langle\hat{p}\rangle|^2\,, \quad V(\hat{n})\,V(\hat{p}) \geqslant \tfrac{1}{4}|\langle\hat{x}\rangle|^2 \tag{2.14}$$

since $|\langle\hat{x}\rangle|^2 + |\langle\hat{p}\rangle|^2 = 2|\langle\hat{a}\rangle|^2$. But these two relations cannot be saturated simultaneously [26,27], and as consequence, Eq. (2.13) is not tight.

In Fig. 2 we have plotted both approximate inequalities (2.11) and (2.13) in a three-dimensional space, with the moments $V(\hat{a})$, $C(\hat{a}^\dagger, \hat{a})$, and $V(\hat{n})$ as axes. The region above

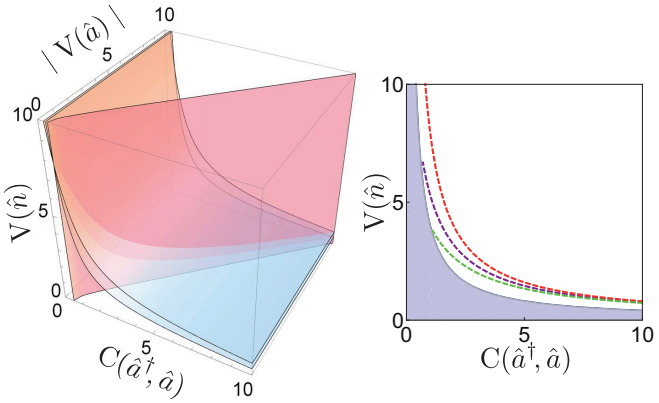

FIG. 2. (Color online) Uncertainty relations (2.8) and (2.11) as a function of the second-order moments of the variables involved. The plane along the diagonal corresponds to the constraint (3.2). In the right panel, we plot sections of the previous figure for several values of $|V(\hat{a})|$ [up to the value permitted by (3.3)]. The solid line represents the bound (2.13), and the shaded region designates the forbidden states.

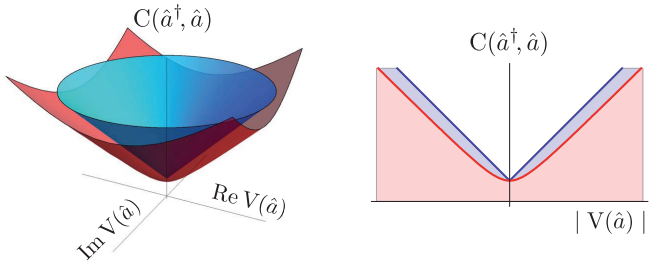

FIG. 3. (Color online) Three-dimensional subspace of all the possible second-order moments for a fixed value of $\langle\hat{a}\rangle$, ranged by the red hyperboloid. The blue cone is the boundary for moments representing squeezed light. On the right, we present a section of that plot; the red (light gray) shaded region represents the forbidden states, while the blue (dark gray) shaded one gives the squeezed states.

these surfaces is the allowed states. We have also plotted several two-dimensional sections for different values of $|V(\hat{a})|$. It is evident that (2.11) is tighter than (2.13), which actually is independent of $|V(\hat{a})|$.

In summary, the exact uncertainty relation (2.8) and its two weaker approximations (2.10) and (2.13) fully specify the complementary nature of photon number and quadratures. They can be regarded as a sensible alternative to the more controversial uncertainty relations for number-phase observables [28,29] and their entropic counterparts [30–32].

III. EXTREMAL STATES

A. Additional restrictions on the moments

The discussion thus far has capitalized on the variances as the proper estimator of quantum uncertainties, as is generally accepted. To have a complete grasp of the problem, we have to assess also the constraints arising in the second-order moments involved in the problem, as they are not independent.

As heralded in the Introduction, an appropriate tool to delimit these moments is the generalized Cauchy-Schwarz inequality, which can be jotted down as [14]

$$|\langle\hat{A}^\dagger\hat{B}\rangle|^2 \leqslant \langle\hat{A}^\dagger\hat{A}\rangle\,\langle\hat{B}^\dagger\hat{B}\rangle\,. \tag{3.1}$$

The equality occurs only for states where $\langle\hat{A}^\dagger\hat{A}\rangle = 0$, $\langle\hat{B}^\dagger\hat{B}\rangle = 0$, or $(\hat{A} - ir\hat{B})\,\hat{\rho} = 0$ for some real scalar r and with $\hat{\rho}$ being the density operator of the state.

A first application of Eq. (3.1), with $\hat{A} = \hat{a}$ and $\hat{B} = \hat{\mathbb{I}}$, gives $\langle\hat{a}^\dagger\hat{a}\rangle \geqslant \langle\hat{a}^\dagger\rangle\langle\hat{a}\rangle$. As a result, from its very definition, the covariance fulfills

$$C(\hat{a}^\dagger,\hat{a}) \geqslant \tfrac{1}{2}\,, \tag{3.2}$$

which is saturated by the coherent states. Repeating the same procedure, but now with $\hat{A}^\dagger = \hat{B} = \hat{a} - \langle\hat{a}\rangle$, we get

$$|V(\hat{a})|^2 \leqslant C(\hat{a}^\dagger,\hat{a})^2 - \tfrac{1}{4}\,. \tag{3.3}$$

This condition is equivalent to requiring $\lambda_+^2\lambda_-^2 \geqslant 1/4$, which has a direct physical interpretation in the ball-and-stick diagram analyzed before: for any physical state, the uncertainty area (in quadrature units) must be greater than or equal to $1/4$. For coherent states the noise is equally distributed in both quadratures, $\lambda_-^2 = \lambda_+^2 = 1/2$, so they are depicted by a minimal circle. In squeezed states, the fluctuations in one quadrature are reduced below the value $1/2$, at the expense of the corresponding increased fluctuations in the other quadrature, such that they preserve the minimum area. Consequently, (3.3) is saturated by squeezed states.

In this regard, the condition of squeezing is just $\lambda_-^2 \leqslant 1/2$, which translates into

$$|V(\hat{a})| \geqslant C(\hat{a}^\dagger,\hat{a}) - 1/2\,, \tag{3.4}$$

which completes (3.3).

Inequalities (3.3) and (3.4) can be represented in a very appealing way if we plot $C(\hat{a}^\dagger,\hat{a})$ as a function of the real and imaginary parts of $V(\hat{a})$, as done in Fig. 3. In these variables, the equality in (3.3) defines a hyperboloid with the vertex in the point $(0,0,1/2)$, and all the moments about that hyperboloid are then possible. On the other hand, (3.4) defines a cone with the vertex in the same point $(0,0,1/2)$: all points below the cone are squeezed.

Finally, we use once more Eq. (3.1), with $\hat{A} = \hat{a}^2$ and $\hat{B} = \hat{\mathbb{I}}$, to get $\langle\hat{a}^{\dagger 2}\hat{a}^2\rangle \geqslant \langle\hat{a}^{\dagger 2}\rangle\langle\hat{a}^2\rangle$. Assuming further the condition of zero complex amplitude, $\langle\hat{a}\rangle = 0$, we have

$$C(\hat{a}^{\dagger 2},\hat{a}^2) \geqslant 2\langle\hat{a}^\dagger\hat{a}\rangle + 1\,, \tag{3.5}$$

which is saturated by the states spanned on the Hilbert subspace of the superposition of coherent states $|\pm\alpha\rangle$, a general solution of the eigenvalue problem $a^2|\psi\rangle = \alpha^2|\psi\rangle$.

B. Intelligent states

We have been using the term extremal to loosely refer to those states for which the inequalities analyzed so far hold as equalities.

If the lower bound in an uncertainty relation is state dependent, states satisfying the equality in the uncertainty relation need not give a minimum in the uncertainty product. This is the case with our fundamental relation (2.4), so

it requires a distinction between intelligent states [33] and minimum uncertainty product states [34].

The intelligent states are solutions of the non-Hermitian eigenvalue problem [35]

$$(\hat{n} - ir\,\hat{x}_\theta)|\Psi_r\rangle = \Omega|\Psi_r\rangle\,, \quad r \in \mathbb{R}\,, \tag{3.6}$$

where Ω is the eigenvalue. Although the solution to this equation has already been discussed in Ref. [15], we provide here a simplified alternative derivation. By introducing the complex parameter $\alpha = -ir/\sqrt{2}\,\exp(-i\theta)$, where θ is the phase of the quadrature $\hat{x}_\theta$, (3.6) reads

$$(\hat{a}^\dagger + \alpha^*)(\hat{a} - \alpha)|\Psi_\alpha\rangle = (\Omega - |\alpha|^2)|\Psi_\alpha\rangle\,. \tag{3.7}$$

Since $[\hat{a} - \alpha, (\hat{a}^\dagger + \alpha^*)^M] = M(\hat{a}^\dagger + \alpha^*)^{M-1}$ for every integer M, one quickly guesses that the intelligent states we are looking for are

$$|\Psi_\alpha\rangle = \mathcal{N}(a^\dagger + \alpha^*)^M|\alpha\rangle\,, \tag{3.8}$$

where $\mathcal{N}$ is a normalization constant and $|\alpha\rangle$ is a coherent state. We can also expand this expression in the Fock basis: using the generating function of the generalized Laguerre polynomials $L_m^a(x)$ [36],

$$(1+t)^M e^{-xt} = \sum_{n=0}^{\infty} \frac{t^n}{\Gamma(1+M)} L_n^{M-n}(x)\,, \tag{3.9}$$

we get

$$|\Psi_\alpha\rangle = \mathcal{N}\exp(-|\alpha|^2/2)\sum_{n=0}^{\infty} \frac{\sqrt{n!}}{M!}(\alpha)^{*M-n} L_n^{M-n}(-|\alpha|^2)\,|n\rangle\,. \tag{3.10}$$

These states were found in a different context by Yuen [37], who called them near-photon-number eigenstates. They are also called crescent states [38] because the contours of their Wigner function are sheared due typically to a Kerr nonlinearity [39,40]. It is worth stressing the close similarity of these states, written as in Eq. (3.10), with the expansion for Fock-displaced states [41], although their arguments differ in the sign, which introduces remarkable differences in the photon-number distribution.

For weak fields $|\alpha| \ll 1$, the crescent states reduce to the so-called M-photon-added coherent states [42]

$$|\Psi_\alpha\rangle \simeq \mathcal{N}\hat{a}^{M\dagger}|\alpha\rangle\,, \tag{3.11}$$

while in the strong-field limit $|\alpha| \gg 1$ they can be well approximated by the superposition of coherent and single-photon-added coherent states

$$|\Psi_\alpha\rangle \simeq \mathcal{N}(|\alpha\rangle + \gamma\hat{a}^\dagger|\alpha\rangle)\,, \tag{3.12}$$

with $\gamma = M/\alpha^*$. For this particular case, we get

$$\begin{aligned} \langle\hat{a}\rangle &= \alpha + \mathcal{N}(\gamma + |\gamma|^2\alpha)\,, \\ \langle\hat{n}\rangle &= 1 + |\alpha|^2 + \mathcal{N}(|\gamma|^2|\alpha|^2 - 1)\,, \end{aligned} \tag{3.13}$$

and the normalization constant is $\mathcal{N}^{-1} = 1 + \gamma^*\alpha + \gamma\alpha^* + |\gamma|^2(1 + |\alpha|^2)$. The second-order moments can be analytically computed, although the expression is a bit involved and of no interest for our purposes here. In Fig. 4 we have plotted $V(\hat{n})$ versus $C(\hat{a}^\dagger,\hat{a})$, as we did in Fig. 2, for these states with varying values of γ. For comparison, we have included also

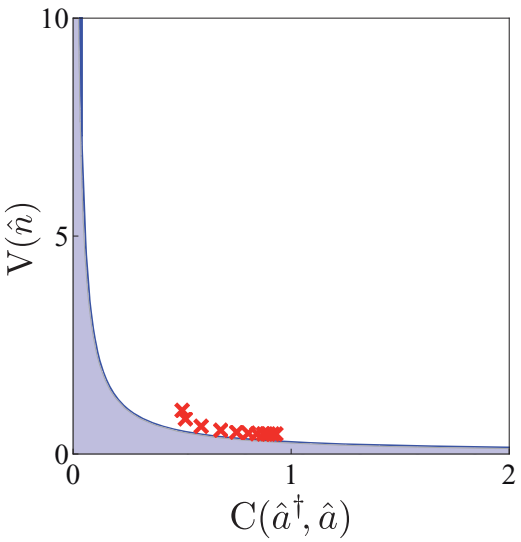

FIG. 4. (Color online) Same plot as in the right panel of Fig. 2. The solid line indicates the weak bound (2.13), while the crosses represent the approximate intelligent states (3.12) for several values of γ.

the bound imposed by the weak uncertainty relation (2.13). As we can appreciate, the intelligent states are always very close to that bound.

The final idea we wish to stress is that all these extremal states can be used as powerful tools to pinpoint important classes of states. Let us look at the crescent states (or the approximation of M-photon-added coherent states treated before). Since they are intelligent states for (2.4), the coefficient

$$G_1 := \frac{V(\hat{n})}{|\langle\hat{a}\rangle|^2}\left[\frac{\lambda_+\lambda_-}{\lambda(\varphi)}\right]^2 \geqslant 1 \tag{3.14}$$

quantifies how far a given state is from being intelligent.

Inequality (2.8) becomes trivial in the case of zero amplitude. In that case, however, inequality (3.5) provides a saturable bound. As discussed before, the extremal states are given by the linear superposition of coherent states $|\pm\alpha\rangle$, including Schrödinger-cat-like states $|\alpha\rangle + |-\alpha\rangle$. The performance measure suitable to check these states is

$$G_2 := \frac{C(\hat{a}^{\dagger 2},\hat{a}^2)}{2\langle\hat{n}\rangle + 1} = \frac{V(\hat{n}) + 4(\lambda_+^2 - 1/2)(\lambda_-^2 + 1/2)}{\langle\hat{n}\rangle} \geqslant 1\,, \tag{3.15}$$

which again provides a robust and simple alternative to more sophisticated methods. It is obvious that equivalent measures can be employed for the other extremal states explored here.

Although the inequalities reported above are fairly simple, they have interesting and not-yet-recognized consequences for quantum information processing. Actually, photon-added and catlike states are archetypes of non-Gaussian nonclassical feasible states [43,44]. Homodyne detection has been the only tool employed thus far to certify these states. However, the dimension of the reconstruction subspace predetermines the accuracy of the result.

The inequalities for G_1 and G_2 offer an intriguing alternative free from any assumptions of this kind: measuring

the lower-order moments suffices to quantify how far the experimental data are from the ideal prediction. We emphasize that this really makes sense from an experimental viewpoint and concurs with previous achievements in quantum optics: photon-number states were characterized by sub-Poissonian noise, and squeezed states were characterized by quadrature-noise reduction.

The proposed benchmarking for photon-added and catlike states is more demanding, for it requires the control of both photon number and quadrature variances. It is probably not by chance that all interesting and feasible quantum states are in some sense extremal.

Finally, we mention that a complete test along these lines would require addressing all the moments [45], which is much more demanding than our simple procedure.

IV. CONCLUDING REMARKS

In short, we have formulated a tight uncertainty relation for photon number and rotated quadratures, which can be considered a sensible and timely approach to the canonical pair number phase. We have also constructed intelligent states for this uncertainty relation, retrieving the well-known crescent states. This saturable inequality, along with some other obtained from a systematic application of the Cauchy-Schwarz inequalities to all the second-order moments of the variables involved, can serve as a handy toolbox for nonclassical state diagnosis, an alternative to the more onerous and laborious quantum tomography.

ACKNOWLEDGMENTS

We thank G. Tóth, H. de Guise, and B.-G. Englert for fruitful discussions. Z.H. and J.R. are thankful for the financial assistance of the Grant Agency of the Czech Republic (Grant No. 15-031945) and the IGA Project of the Palacký University (Grant No. PrF_2015_002). G.L. is partially funded by EU FP7 (Grant No. Q-ESSENCE). Finally, P.H. and L.L.S.-S. acknowledge the support from the Spanish MINECO (Grant No. FIS2011-26786) and UCM-Banco Santander Program (Grant No. GR3/14).

[1] C. M. Caves, C. A. Fuchs, and R. Schack, Quantum probabilities as Bayesian probabilities, Phys. Rev. A **65**, 022305 (2002).

[2] R. W. Spekkens, Evidence for the epistemic view of quantum states: A toy theory, Phys. Rev. A **75**, 032110 (2007).

[3] M. F. Pusey, J. Barrett, and T. Rudolph, On the reality of the quantum state, Nat. Phys. **8**, 475 (2012).

[4] *Quantum State Estimation*, edited by M. G. A. Paris and J. Řeháček, Lectures Notes in Physics Vol. 649 (Springer, Berlin, 2004).

[5] U. M. Titulaer and R. J. Glauber, Correlation functions for coherent fields, Phys. Rev. **140**, B676 (1965).

[6] P. Carruthers and M. M. Nieto, Phase and angle variables in quantum mechanics, Rev. Mod. Phys. **40**, 411 (1968).

[7] R. Lynch, The quantum phase problem: A critical review, Phys. Rep. **256**, 367 (1995).

[8] S. M. Barnett and P. M. Radmore, *Methods in Theoretical Quantum Optics* (Oxford University Press, Oxford, 1997).

[9] V. Peřinova, A. Lukš, and J. Peřina, *Phase in Optics* (World Scientific, Singapore, 1998).

[10] A. Luis and L. L. Sánchez-Soto, Quantum phase difference, phase measurements and quantum Stokes parameters, Prog. Opt. **41**, 421 (2000).

[11] N. Imoto, H. A. Haus, and Y. Yamamoto, Quantum nondemolition measurement of the photon number via the optical Kerr effect, Phys. Rev. A **32**, 2287 (1985).

[12] M. D. Levenson, R. M. Shelby, M. Reid, and D. F. Walls, Quantum nondemolition detection of optical quadrature amplitudes, Phys. Rev. Lett. **57**, 2473 (1986).

[13] H. F. Hofmann, T. Kobayashi, and A. Furusawa, Nonclassical correlations of photon number and field components in the vacuum state, Phys. Rev. A **62**, 013806 (2000).

[14] Z. Hradil, Noise minimum states and the squeezing and antibunching of light, Phys. Rev. A **41**, 400 (1990).

[15] Z. Hradil, Extremal properties of near-photon-number eigenstate fields, Phys. Rev. A **44**, 792 (1991).

[16] I. Urizar-Lanz and G. Tóth, Number-operator–annihilation-operator uncertainty as an alternative for the number-phase uncertainty relation, Phys. Rev. A **81**, 052108 (2010).

[17] C. Cohen-Tannoudji, B. Diu, and F. Laloë, *Quantum Mechanics* (Wiley, New York, 2006).

[18] U. Leonhardt, *Measuring the Quantum State of Light* (Cambridge University Press, Cambridge, 2005).

[19] A. Lukš, V. Peřinova, and J. Peřina, Principal squeezing of vacuum fluctuations, Opt. Commun. **67**, 149 (1988).

[20] H.-A. Bachor and T. C. Ralph, *A Guide to Experiments in Quantum Optics*, 2nd ed. (Wiley-VCH, Weinheim, 2004).

[21] V. V. Dodonov, Universal integrals of motion and universal invariants of quantum systems, J. Phys. A **33**, 7721 (2000).

[22] R. Loudon, Graphical representation of squeezed-state variances, Opt. Commun. **70**, 109 (1989).

[23] R. Tanaś, A. Miranowicz, and S. Kielich, Squeezing and its graphical representations in the anharmonic oscillator model, Phys. Rev. A **43**, 4014 (1991).

[24] J. H. Shapiro and S. S. Wagner, Phase and amplitude uncertainties in heterodyne detection, IEEE J. Quantum Electron. **20**, 803 (1984).

[25] P. Adam, M. Mechler, V. Szalay, and M. Koniorczyk, Intelligent states for a number-operator–annihilation-operator uncertainty relation, Phys. Rev. A **89**, 062108 (2014).

[26] J. Řeháček, Z. Bouchal, R. Čelechovský, Z. Hradil, and L. L. Sánchez-Soto, Experimental test of uncertainty relations for quantum mechanics on a circle, Phys. Rev. A **77**, 032110 (2008).

[27] Z. Hradil, J. Řeháček, A. B. Klimov, I. Rigas, and L. L. Sánchez-Soto, Angular performance measure for tighter uncertainty relations, Phys. Rev. A **81**, 014103 (2010).

[28] D. T. Pegg and S. M. Barnett, Phase properties of the quantized single-mode electromagnetic field, Phys. Rev. A **39**, 1665 (1989).
[29] I. Bialynicki-Birula, M. Freyberger, and W. Schleich, Various measures of quantum phase uncertainty: A comparative study, Phys. Scr. **T48**, 113 (1993).
[30] A. Rojas González, J. A. Vaccaro, and S. M. Barnett, Entropic uncertainty relations for canonically conjugate operators, Phys. Lett. A **205**, 247 (1995).
[31] A. E. Rastegin, Entropic formulation of the uncertainty principle for the number and annihilation operators, Phys. Scr. **84**, 057001 (2011).
[32] A. E. Rastegin, Number-phase uncertainty relations in terms of generalized entropies, Quantum Inf. Comput. **12**, 0743 (2012).
[33] C. Aragone, G. Guerri, S. Salamo, and J. L. Tani, Intelligent spin states, J. Phys. A **7**, L149 (1974).
[34] D. T. Pegg, S. M. Barnett, R. Zambrini, S. Franke-Arnold, and M. Padgett, Minimum uncertainty states of angular momentum and angular position, New J. Phys. **7**, 62 (2005).
[35] R. Jackiw, Minimum uncertainty product, number–phase uncertainty product, and coherent states, J. Math. Phys. **9**, 339 (1968).
[36] P. M. Morse and H. Feshbach, *Methods of Theoretical Physics* (McGraw-Hill, New York, 1953), Vol. 1.
[37] H. Yuen, Generation, detection, and application of high-intensity photon-number-eigenstate fields, Phys. Rev. Lett. **56**, 2176 (1986).
[38] C. Gerry and P. Knight, *Introductory Quantum Optics* (Cambridge University Press, Cambridge, 2005).
[39] M. Kitagawa and Y. Yamamoto, Number-phase minimum-uncertainty state with reduced number uncertainty in a Kerr nonlinear interferometerr, Phys. Rev. A **34**, 3974 (1986).
[40] I. Rigas, A. B. Klimov, L. L. Sánchez-Soto, and G. Leuchs, Nonlinear cross-Kerr quasiclassical dynamics, New J. Phys. **15**, 043038 (2013).
[41] A. Wünsche, Displaced Fock states and their connection to quasiprobabilities, Quantum Opt. **3**, 359 (1991).
[42] G. S. Agarwal and K. Tara, Nonclassical properties of states generated by the excitations on a coherent state, Phys. Rev. A **43**, 492 (1991).
[43] A. Zavatta, S. Viciani, and M. Bellini, Quantum-to-classical transition with single-photon-added coherent states of light, Science **306**, 660 (2004).
[44] A. Ourjoumtsev, H. Jeong, R. Tualle-Brouri, and P. Grangier, Generation of optical 'Schrödinger cats' from photon number states, Nature (London) **448**, 784 (2007).
[45] E. V. Shchukin and W. Vogel, Nonclassicality moments and their measurements, Phys. Rev. A **72**, 043808 (2005).

Paper 8

P. de la Hoz, G. Björk, H. de Guise, A. B. Klimov, G. Leuchs, L. L. Sánchez-Soto:

"Classical polarization multipoles: paraxial versus nonparaxial",

Physica Scripta **90**, 074030 (2015)

IOP Publishing | Royal Swedish Academy of Sciences Physica Scripta

Phys. Scr. **90** (2015) 074030 (7pp) doi:10.1088/0031-8949/90/7/074030

Classical polarization multipoles: paraxial versus nonparaxial

P de la Hoz[1], G Björk[2], H de Guise[3], A B Klimov[4], G Leuchs[5,6] and L L Sánchez-Soto[1,5]

[1] Departamento de Óptica, Facultad de Física, Universidad Complutense, E-28040 Madrid, Spain
[2] Department of Applied Physics, Royal Institute of Technology (KTH), AlbaNova University Center, SE-106 91 Stockholm, Sweden
[3] Department of Physics, Lakehead University, Thunder Bay, ON P7B 5E1, Canada
[4] Departamento de Física, Universidad de Guadalajara, 44420 Guadalajara, Jalisco, Mexico
[5] Max-Planck-Institut für die Physik des Lichts, Günther-Scharowsky-Straße 1, Bau 24, D-91058 Erlangen, Germany
[6] Department für Physik, Universität Erlangen-Nürnberg, Staudtstraße 7, Bau 2, D-91058 Erlangen, Germany

E-mail: lsanchez@fis.ucm.es

Received 12 November 2014, revised 21 January 2015
Accepted for publication 9 February 2015
Published 18 June 2015

Abstract

We discuss the polarization of paraxial and nonparaxial classical light fields by resorting to a multipole expansion of the corresponding polarization matrix. It turns out that only a dipolar term contributes when one considers SU(2) (paraxial) or SU(3) (nonparaxial) as fundamental symmetries. In this latter case, one can alternatively expand in SU(2) multipoles, and then both a dipolar and a quadrupolar component contribute, which explains the richer structure of this nonparaxial instance. These multipoles uniquely determine Wigner functions, in terms of which we examine some intriguing hallmarks arising in this classical scenario.

Keywords: polarisation, multipolar expansion, near fields

(Some figures may appear in colour only in the online journal)

1. Introduction

The standard theory of polarization optics deals with paraxial fields with a well-defined direction of propagation and thus a specific transverse plane. Such beamlike fields are described by two orthogonal electric field components and, consequently, their polarization is characterized by a 2×2 correlation matrix, usually called the polarization matrix (Mandel and Wolf 1995). When we expand this matrix onto the Pauli basis, the corresponding coefficients are nothing but the time honored Stokes parameters. They determine a locus on the Poincaré sphere, wherein the state of polarization is elegantly visualized; actually, the degree of paraxial polarization can be seen as the length of the Stokes vector.

The necessity of addressing new issues, such as highly nonparaxial fields (Ash and Nicholls 1972), narrow-band imaging systems (Pohl *et al* 1984), and the recognition of associated propagation questions (Petruccelli *et al* 2010), has fuelled interest in extending this two-dimensional (2D) approach to fully three-dimensional (3D) field distributions, where, in general, there is no well-defined propagation direction, and the Hermitian coherence matrix is 3×3 (Roman 1959, Brosseau 1998). However, when discussing the corresponding degree of polarization, some discrepancies occur (Samson 1973, Barakat 1977, Setälä *et al* 2002, Korotkova and Wolf 2004, Ellis *et al* 2005, Luis 2005, Dennis 2007, Moya-Cessa *et al* 2008, Sheppard 2011), mainly because notions that are equivalent in a 2D world lead to different definitions when extended to the 3D domain.

In this paper, we look at this problem from the perspective of a multipolar expansion that has been successfully employed in quantum optics (de la Hoz *et al* 2013, 2014, Sánchez-Soto *et al* 2013). For the 2D case, SU(2) is the natural symmetry group of the problem and the corresponding expansion of the polarization matrix contains only a dipolar term. The 3D polarization can be treated in quite a similar

way by taking now SU(3) as the symmetry group; again, only the SU(3) dipole contributes. Yet we can also expand the 3×3 polarization matrix in SU(2) tensors, getting an SU(2) dipole and a quadrupole. We discuss the role of these multipoles and construct Wigner functions that can be very useful in appreciating the substantial differences between paraxial and nonparaxial polarization.

2. 2D polarization

2.1. SU(2) polarization structure

We briefly review here the ingredients we shall need later for a proper understanding of the 3D polarization. We consider a monochromatic beam propagating in the z direction. The electric field can be resolved in the transverse plane in terms of horizontal (x) and vertical (y) components, which are taken to be a probabilistic ensemble given by E_x and E_y. The corresponding 2×2 (equal-time) polarization matrix (also called the coherence matrix) is defined as (Mandel and Wolf 1995)

$$\mathbf{C} = \begin{pmatrix} \langle E_x E_x^* \rangle & \langle E_x E_y^* \rangle \\ \langle E_y E_x^* \rangle & \langle E_y E_y^* \rangle \end{pmatrix}. \tag{2.1}$$

Here, the brackets denote ensemble averaging over different realizations. The diagonal elements of the Hermitian matrix $\mathbf{C}$ represent the energy distribution between the two components of the field: $I = \langle |E_x|^2 \rangle + \langle |E_y|^2 \rangle = \mathrm{Tr}\,(\mathbf{C})$, where Tr is the trace of the matrix. Without loss of generality, we henceforth normalize this intensity to unity. On the other hand, the off-diagonal elements describe the correlations between the field components.

Sometimes, the polarization matrix is interpreted as a classical counterpart of the density operator. Nonetheless, we emphasize that while the latter carries complete information of a quantum system, the former specifies only first-order classical correlations.

Polarization transformations are generated by wave plates and represented by 2×2 unitary matrices of SU(2) (Simon and Mukunda 1989)

$$\mathbf{R}_g \equiv \mathbf{R}(\alpha, \beta, \gamma) = \begin{pmatrix} \mathrm{e}^{-\mathrm{i}(\alpha+\gamma)/2} \cos(\beta/2) & -\mathrm{e}^{-\mathrm{i}(\alpha-\gamma)/2} \sin(\beta/2) \\ \mathrm{e}^{+\mathrm{i}(\alpha-\gamma)/2} \sin(\beta/2) & \mathrm{e}^{+\mathrm{i}(\alpha+\gamma)/2} \cos(\beta/2) \end{pmatrix}, \tag{2.2}$$

where (α, β, γ) denote the Euler angles. The action of these transformations on the polarization matrix is via conjugation

$$\mathbf{C}_g = \mathbf{R}_g\, \mathbf{C}\, \mathbf{R}_g^\dagger. \tag{2.3}$$

This symmetry seems to call for an SU(2)-covariant formulation of the problem. To this end, we recall that any matrix $\mathbf{O}$ acting in the $(2S+1)$-dimensional Hilbert space $\mathcal{H}_S$, which carries the irreducible representation (irrep) with spin S of SU(2), can be expanded as

$$\mathbf{O}^{(S)} = \sum_{K=0}^{2S} \sum_{q=-K}^{K} O_{Kq}^{(S)}\, \hat{T}_{Kq}^{(S)}. \tag{2.4}$$

Here, the irreducible tensor (or multipole) operators $\hat{T}_{Kq}^{(S)}$ constitute an orthonormal basis

$$\mathrm{Tr}\left[\hat{T}_{Kq}^{(S)}\, \hat{T}_{K'q'}^{(S')\,\dagger} \right] = \delta_{SS'} \delta_{KK'} \delta_{qq'}, \tag{2.5}$$

and have the right transformation properties under SU(2)

$$\mathbf{R}(\alpha, \beta, \gamma)\, \hat{T}_{Kq}^{(S)}\, \mathbf{R}^\dagger(\alpha, \beta, \gamma) = \sum_{q'} D_{q'q}^{S}(\alpha, \beta, \gamma)\, \hat{T}_{Kq'}^{(S)}, \tag{2.6}$$

where $D_{q'q}^{S}(\alpha, \beta, \gamma)$ stands for the Wigner D-function (Varshalovich *et al* 1988). The reader is referred to the abundant literature (Fano and Racah 1963, Blum 1981, Varshalovich *et al* 1988) to learn more about the amazing properties of these tensors. The point we wish to stress for our purposes here is that $\hat{T}_{Kq}^{(S)}$ is expressible as the Kth power of the SU(2) generators.

The corresponding expansion coefficients

$$O_{Kq}^{(S)} = \mathrm{Tr}\left[\mathbf{O}^{(S)}\, \hat{T}_{Kq}^{(S)\,\dagger} \right] \tag{2.7}$$

are known as state multipoles. The hermiticity imposes the symmetry condition

$$O_{K-q}^{(S)} = (-1)^q\, O_{Kq}^{(S)}. \tag{2.8}$$

For the case at hand in (2.1), we are dealing with the fundamental irrep of spin $S = 1/2$. Accordingly, the expansion (2.4) reduces to (we drop the superscript 1/2 henceforth, as there is no risk of confusion)

$$\mathbf{C} = C_{00} \hat{T}_{00} + \sum_{q=-1}^{+1} C_{1q} \hat{T}_{1q}, \tag{2.9}$$

and one can check that

$$\hat{T}_{00} = \frac{1}{\sqrt{2}}\, \mathbb{1}_2, \qquad \hat{T}_{1q} = \frac{1}{\sqrt{2}}\, \sigma_q, \tag{2.10}$$

where $\mathbb{1}_2$ is the identity matrix and $q = 0, \pm 1$ runs over the spherical basis. The unit vectors in that basis $(\mathfrak{e}_{-1}, \mathfrak{e}_0, \mathfrak{e}_{+1},)$ are related to the Cartesian ones $(\mathbf{e}_1, \mathbf{e}_2, \mathbf{e}_3)$ by

$$\mathfrak{e}_{\pm 1} = \mp \frac{1}{\sqrt{2}} \left(\mathbf{e}_1 \pm \mathrm{i}\, \mathbf{e}_2 \right), \qquad \mathfrak{e}_0 = \mathbf{e}_3, \tag{2.11}$$

and $(\sigma_1, \sigma_2, \sigma_3)$ is the standard Pauli basis.

Obviously, $C_{00} = 1/\sqrt{2}$ and the physical relevant information comes from the dipole C_{1q}. In fact,

$$n_q \equiv \sqrt{2}\, C_{1q} = \mathrm{Tr}\left(\mathbf{C} \sigma_q \right), \qquad q = 0, \pm 1, \tag{2.12}$$

are nothing but the components of the Stokes vector, which in Cartesian coordinates $\mathbf{n} = (n_1, n_2, n_3)$ provides geometric information about the polarization ellipse: n_1 and n_3 carry information about the alignment of the ellipse axes, while πn_2 gives the ellipse area, signed according to polarization handedness.

With this notation, (2.9) can be recast as

$$\mathbf{C} = \frac{1}{2}\begin{pmatrix} 1 + n_3 & n_1 - \mathrm{i}n_2 \\ n_1 + \mathrm{i}n_2 & 1 - n_3 \end{pmatrix}. \tag{2.13}$$

so that for each polarization matrix $\mathbf{C}$ we have a natural map onto a dipole $\mathbf{C} \mapsto \mathbf{n} = (n_1, n_2, n_3)$. This is consistent with the fact that at the classical level only first-order moments of the Stokes variables are taken into consideration.

The length of $\mathbf{n}$ will be denoted as

$$\mathbb{P}^{(2)} = |\mathbf{n}| = \sqrt{n_1^2 + n_2^2 + n_3^2}, \tag{2.14}$$

and is the conventional degree of polarization for classical 2D fields. If the relation between the E_x and E_y is completely deterministic, the field is fully polarized. For such a pure state (borrowing the terminology from quantum optics), the polarization matrix is idempotent, i.e.,

$$\mathbf{C}_{\mathrm{pol}}^2 = \mathbf{C}_{\mathrm{pol}}, \tag{2.15}$$

and we get $\mathbb{P}_{\mathrm{pol}}^{(2)} = 1$. On the other hand, if the components of the field are fully uncorrelated, the off-diagonal elements are zero. If, in addition, the energy is distributed evenly between the x and y components,

$$\mathbf{C}_{\mathrm{unpol}} = \frac{1}{2}\,\mathbb{1}_2, \tag{2.16}$$

and we have $\mathbb{P}_{\mathrm{unpol}}^{(2)} = 0$.

Note that the SU(2) polarization transformations (2.3) induce rotations on the Stokes vector $\mathbf{n}$, as confirmed by the well-known relation between SU(2) and the group of rotations SO(3) (Cornwell 1997). Therefore, $\mathbb{P}^{(2)}$ is clearly unchanged by these transformations.

Finally, we stress that for quantum fields with N photons, the spin of the associated irrep is $S = N/2$, so classical polarization is formally identical with single-photon quantum polarization, which, in turn, is the prototype of a qubit.

2.2. Wigner function on the Poincaré sphere

In signal processing, the Wigner representation yields a description displaying both the time and frequency features, which are related via the Fourier transform. This arises naturally in music, for instance, where a signal is usually described not by a time function nor by the Fourier transform of that function, but by its musical score (i.e., a prescription of the frequencies of the tones that should be present at a certain moment). It arises also in mechanics, where the position and the momentum of a particle are given simultaneously, leading to a simple interpretation in phase space.

Although originally introduced to represent quantum mechanical phenomena in phase space (Wigner 1932), the Wigner distribution function was established in optics (Walther 1968) to relate partial coherence with radiometry. Since then, a great number of applications of this function have been reported (Dragoman 1997, Mecklenbraüker and Hlawatsch 1997, Galleani and Cohen 2002, Bastiaans 2009, Alonso 2011).

With regard to polarization, the SU(2) symmetry discussed earlier allows us to take advantage of the pioneering papers by Stratonovich (1956) and Berezin (1975), who worked out *bona fide* Wigner distributions on the sphere. This construction was later generalized by others (Agarwal 1981, Brif and Mann 1998, Heiss and Weigert 2000, Klimov and Chumakov 2000, Klimov and Romero 2008) and has proved to be very useful in visualizing properties of spinlike systems (Dowling *et al* 1994, Chumakov *et al* 1999, Klimov 2002).

The Wigner function associated to the operator $\mathbf{O}^{(S)}$ is uniquely defined as (Dowling *et al* 1994)

$$W_{\mathbf{O}}^{(S)}(\theta, \phi) = \sum_{K=0}^{2S} \sum_{q=-K}^{K} O_{Kq}^{(S)}\, Y_{Kq}(\theta, \phi), \tag{2.17}$$

where $Y_{Kq}(\theta, \phi)$ are the standard spherical harmonics. In quantum optics, $\mathbf{O}$ is most often taken as the density operator. One can check that, in this way, the function $W_{\mathbf{O}}^{(S)}(\theta, \phi)$ satisfies all the pertinent requirements. We have the normalization

$$\mathrm{Tr}\left[\mathbf{O}^{(S)}\right] = \sqrt{\frac{2S+1}{4\pi}} \int_{S_2} W_{\mathbf{O}}^{(S)}(\theta, \phi)\, \mathrm{d}\Omega, \tag{2.18}$$

where $\mathrm{d}\Omega = \sin\theta\, \mathrm{d}\theta \mathrm{d}\phi$ is the invariant measure on the unit sphere $\mathcal{S}_2$.

Besides, $W_{\mathbf{O}}^{(S)}(\theta, \phi)$ is covariant under rotations, which means that for a rotated operator $\mathbf{O}_g^{(S)} = \mathbf{R}_g \mathbf{O}^{(S)}\, \mathbf{R}_g^{\dagger}$ one has

$$W_{\mathbf{O}_g}^{(S)}(\Omega) = W_{\mathbf{O}}^{(S)}\left(\mathbf{R}_g^{-1}\Omega\right), \tag{2.19}$$

where $\Omega = (\theta, \phi)$ parametrizes the points in $\mathcal{S}_2$. The Wigner function of the rotated state follows thus the rotation rigidly without deformation, reflecting the fact that physics should not depend on the orientation of the reference frame.

For the classical polarization matrix $\mathbf{C}$, the associated Wigner function reads (we also omit the superscript 1/2)

$$W_{\mathbf{n}}(\theta, \phi) = \frac{1}{\sqrt{2}}\left[Y_{00} + \sum_{q=-1}^{+1} n_q\, Y_{1q}(\theta, \phi) \right]. \tag{2.20}$$

In figure 1 we plot this Wigner function for a fully polarized field with $\mathbf{n} = (0, 0, 1)$. The covariance under rotations guarantees that this is indeed the form (apart from trivial rotations) for any other polarized state.

In the opposite instance of unpolarized states only the monopole term contribute: the resulting Wigner function is just an isotropic sphere. Partially polarized states smoothly interpolate In between these two limiting cases.

As we can appreciate, the Wigner distribution is not a delta-like function, as one would expect from the accepted practice of picturing the state by the point determined by $\mathbf{n}$. This would be compatible with the assumption that classically, since there are no fluctuations, the polarization direction can be measured in a single-shot measurement. Instead, the Wigner function has some width because if one measures a classically polarized state in a rotated Stokes basis, then one will only detect part of the intensity. This means that the detected fraction of the polarization correspond to the overlap

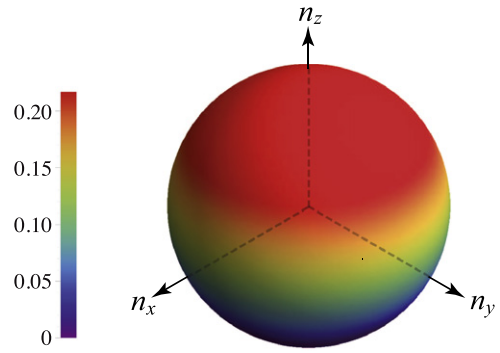

Figure 1. Density plot over the unit sphere (the scale is indicated on the left) of the Wigner distribution for a 2D polarization state with $n = (0, 0, 1)$.

of the Wigner function for the state and the corresponding one for the detection direction on the Poincaré sphere. In fact, if we denote by $W_{\mathbf{n}}$ and $W_{\mathbf{n}'}$ these two Wigner functions, then

$$\int W_{\mathbf{n}}(\theta, \phi) W_{\mathbf{n}'}(\theta, \phi)\, \mathrm{d}\Omega = \cos^2\left(\frac{\chi}{2}\right), \tag{2.21}$$

where $\mathbf{n} \cdot \mathbf{n}' = \cos\chi$ is the angle between the two vectors. This is just another way to look at the Malus law from a phase-space perspective (Wódkiewicz 1995).

3. 3D polarization

3.1. SU(3) polarization structure

Next, we loosen the restriction of planar geometry and examine the behavior of electric fields having three non-vanishing components, in directions we denote as x, y, and z, respectively. Now, the vibrations of the field are no longer constrained to a plane and the polarization must be described by a 3×3 matrix

$$C = \begin{pmatrix} \langle E_x E_x^* \rangle & \langle E_x E_y^* \rangle & \langle E_x E_z^* \rangle \\ \langle E_y E_x^* \rangle & \langle E_y E_y^* \rangle & \langle E_y E_z^* \rangle \\ \langle E_z E_x^* \rangle & \langle E_z E_y^* \rangle & \langle E_z E_z^* \rangle \end{pmatrix}. \tag{3.1}$$

Once more, we normalize the total intensity $I = \langle |E_x|^2 \rangle + \langle |E_y|^2 \rangle + \langle |E_z|^2 \rangle = \mathrm{Tr}\,(C)$, to unity. If all of the components are completely uncorrelated (and their energies are equal) the field is unpolarized and its direction is random. If one of the components has less energy than the other two, the vibrations are less random and, consequently, the field is more polarized than in the equal-energy case. Any field having only two non-vanishing components is thus never unpolarized in the 3D sense, regardless of the correlations between the components. Hence, a planar field, which is commonly called unpolarized in 2D, is not fully unpolarized but partially polarized in a 3D description.

As in 2D, the field is called fully polarized if all of the field components are completely correlated. Hence, in contrast to an unpolarized field, a planar field that is fully polarized is always fully polarized also in the 3D sense. One of the most remarkable differences between 2D and 3D is that the 3×3 polarization matrix cannot be generally expressed as a sum of unpolarized and fully polarized parts (Ellis *et al* 2005).

The 3D polarization transformations are represented by 3×3 matrices of SU(3), which we write as (Rowe *et al* 1999)

$$\begin{aligned} \mathbf{R}_g = \mathbf{R}_g(\omega) \equiv \mathbf{T}_{23}\left(\alpha_1, \beta_1, -\alpha_1\right)\mathbf{T}_{12}\left(\alpha_2, \beta_2, -\alpha_2\right) \\ \times \mathbf{T}_{23}\left(\alpha_3, \beta_3, -\alpha_3\right)\boldsymbol{\Phi}(\gamma_1, \gamma_2), \end{aligned} \tag{3.2}$$

where ω is an octuple of Euler-like angles $\omega = (\alpha_1, \beta_1, \alpha_2, \beta_2, \alpha_3, \beta_3, \gamma_1, \gamma_2)$ and the set $\{\mathbf{T}_{ij}\}$ comprises SU(2) subgroup matrices

$$\mathbf{T}_{23} = \begin{pmatrix} 1 & 0 & 0 \\ 0 & \mathrm{e}^{-\mathrm{i}(\alpha+\gamma)/2}\cos(\beta/2) & -\mathrm{e}^{-\mathrm{i}(\alpha-\gamma)/2}\sin(\beta/2) \\ 0 & \mathrm{e}^{+\mathrm{i}(\alpha-\gamma)/2}\sin(\beta/2) & \mathrm{e}^{+\mathrm{i}(\alpha+\gamma)/2}\cos(\beta/2) \end{pmatrix}, \tag{3.3}$$

or

$$\mathbf{T}_{12} = \begin{pmatrix} \mathrm{e}^{-\mathrm{i}(\alpha+\gamma)/2}\cos(\beta/2) & -\mathrm{e}^{-\mathrm{i}(\alpha-\gamma)/2}\sin(\beta/2) & 0 \\ \mathrm{e}^{+\mathrm{i}(\alpha-\gamma)/2}\sin(\beta/2) & \mathrm{e}^{+\mathrm{i}(\alpha+\gamma)/2}\cos(\beta/2) & 0 \\ 0 & 0 & 1 \end{pmatrix}, \tag{3.4}$$

depending on the values of (ij). Also,

$$\boldsymbol{\Phi}(\gamma_1, \gamma_2) = \mathrm{diag}\left(\mathrm{e}^{-2\mathrm{i}\gamma_1}, \mathrm{e}^{\mathrm{i}(\gamma_1-\gamma_2/2)}, \mathrm{e}^{\mathrm{i}(\gamma_1+\gamma_2/2)}\right). \tag{3.5}$$

Equation (3.2) factorizes then into SU(2) submatrices, with parameters defined by the corresponding Euler angles.

The action of these transformations on C is via conjugation, as in (2.3), and induces rotations of the vector $\mathbf{n}$. However, one word of caution seems pertinent here: there is no obvious physical interpretation via optical elements of SU(3) transformations, as now the plane waves averaging to the 3×3 polarization matrix do not share a common propagation direction, in general. Any physical device represented by a SU(3) transformation should be insensitive to the propagation directions of the separate members of the ensemble (Dennis 2004).

After our discussion in section 2, one might be tempted to look for an expansion of C in SU(3) irreducible tensors. The corresponding formalism is now much more involved than for SU(2), and we refer the reader to (Banyai *et al* 1966) for a full account. Without going into inessential details, such an expansion reads

$$C = C_{00}\hat{\mathcal{T}}_{00} + \sum_{\nu=1}^{8} C_{1\nu}\hat{\mathcal{T}}_{1\nu}, \tag{3.6}$$

where the relevant SU(3) tensors are

$$\hat{\mathcal{T}}_{00} = \frac{1}{\sqrt{3}}\mathbb{1}_3, \qquad \hat{\mathcal{T}}_{1\nu} = \frac{1}{\sqrt{2}}\lambda_\nu, \tag{3.7}$$

and $\{\lambda_\nu\}$ (the ν index running from 1 to 8) are the Gell-Mann matrices, whose properties are discussed in detail e.g., in (Cornwell 1997).

Therefore, $C_{00} = 1/\sqrt{3}$ and the SU(3) dipole is $C_{1\nu}$. Actually, if we define

$$n_\nu \equiv \sqrt{3}\, C_{1\nu} = \frac{\sqrt{3}}{2}\,\mathrm{Tr}\left(C\lambda_\nu\right), \tag{3.8}$$

then we have

$$C = \frac{1}{3}\left(\mathbb{1}_3 + \sqrt{3}\,\mathbf{n}\cdot\boldsymbol{\lambda}\right) = \frac{1}{3} \times \begin{pmatrix} 1+\sqrt{3}n_3+n_8 & \sqrt{3}\left(n_1 - \mathrm{i}n_2\right) & \sqrt{3}\left(n_4 - \mathrm{i}n_5\right) \\ \sqrt{3}\left(n_1 + \mathrm{i}n_2\right) & 1-\sqrt{3}n_3+n_8 & \sqrt{3}\left(n_6 - \mathrm{i}n_7\right) \\ \sqrt{3}\left(n_4 + \mathrm{i}n_5\right) & \sqrt{3}\left(n_6 + \mathrm{i}n_7\right) & 1-2n_8 \end{pmatrix}. \tag{3.9}$$

This is the SU(3)-equivalent version of (2.13). Consequently, the SU(3) symmetry gives a natural degree of polarization as

$$\mathbb{P}^{(3)} = |\mathbf{n}| = \sqrt{\sum_{\nu=1}^{8} n_\nu^2}, \tag{3.10}$$

i.e., again the length of the Stokes vector, which is readily shown to verify $0 \leqslant \mathbb{P}^{(3)} \leqslant 1$.

3.2. Picturing multipoles on the Poincaré sphere

Although the previous SU(3) approach is mathematically correct, it is not clear physically what $\mathbb{P}^{(3)}$ represents. Unlike in 2D, where the Stokes vector represents the complete state of polarization and can be easily visualized, the generalized Stokes vector is eight-dimensional and the geometrical space supporting this vector is not intuitive at all.

To proceed further, we note that the 3×3 matrix C acts also in the carrier space of the irrep $S = 1$ of SU(2). In consequence, we can alternatively expand C following the general prescription (2.4). Omitting for simplicity the superscript 1, we get

$$C = C_{00}\hat{T}_{00} + \sum_{q=-1}^{+1} C_{1q}\hat{T}_{1q} + \sum_{q=-2}^{+2} C_{2q}\hat{T}_{2q}, \tag{3.11}$$

where now the SU(2) tensors are (Varshalovich *et al* 1988)

$$\begin{aligned} \hat{T}_{00} &= \frac{1}{\sqrt{3}}\mathbb{1}_3, \\ \hat{T}_{1q} &= \frac{1}{\sqrt{2}}S_q, \qquad q = 0, \pm 1, \\ \hat{T}_{2q} &= \sum_{r,r'=-1}^{+1} C^{2q}_{1r,1r'}\, S_r S_{r'}, \qquad q = 0, \pm 1, \pm 2. \end{aligned} \tag{3.12}$$

Here, $C^{2q}_{1r,1r'}$ is the corresponding Clebsch–Gordan coefficient and S_q stands for the spherical components of the su(2) sub algebra generated by $\mathbf{S} = (\lambda_2, -\lambda_5, \lambda_7)$.

The resulting multipoles can be expressed as

$$\begin{aligned} C_{00} &= 1/\sqrt{3}\,, \\ D_q &\equiv \sqrt{3}\, C_{1q} = \sqrt{3}\ \mathrm{Tr}\left(C\hat{T}_{1q}\right), \\ Q_q &\equiv C_{2q} = \sqrt{3}\ \mathrm{Tr}\left(C\hat{T}_{2q}\right). \end{aligned} \tag{3.13}$$

As a consequence, this leads naturally to an SU(2) Wigner function:

$$W(\theta, \phi) = \frac{1}{\sqrt{3}}\left[Y_{00} + \sum_{q=-1}^{+1} D_q\, Y_{1q}(\theta, \phi) + \sum_{q=-2}^{+2} Q_q\, Y_{2q}(\theta, \phi) \right]. \tag{3.14}$$

What it is remarkable is that, in this way, we can picture the 3D polarization state in the sphere S_2 associated to SU(2). In figure 2 we have plotted this Wigner function for the state with eight-dimensional Stokes vector $\mathbf{n} = (0, 0, \sqrt{3}/2, 0, 0, 0, 0, 1/2)$, which is 3D fully polarized, as $\mathbb{P}^{(3)} = 1$. However, this state has $\mathbf{D} = (0, 0, 1/2)$, so is not SU(2) polarized and presents a quadrupole contribution along the z axis. Note that the different multipolar contributions can be plotted separately, as in the figure. Unpolarized states have only monopole contribution, so their Wigner function is isotropic.

To investigate this point, we recall that it is conventional to use a quadrupolar tensor, with Cartesian components

$$\hat{Q}_{ik} = \frac{1}{2}\left(S_i S_k + S_k S_i - \frac{4}{3}\delta_{jk}\right), \qquad i, k \in \{1, 2, 3\}, \tag{3.15}$$

which are related with $\hat{T}_{2q}$ in the form

$$\begin{aligned} \hat{T}_{2\pm 2} &= \frac{1}{2}\left(\hat{Q}_{11} - \hat{Q}_{22} \pm 2\mathrm{i}\hat{Q}_{12}\right), \\ \hat{T}_{2\pm 1} &= \mp\left(\hat{Q}_{13} \pm \mathrm{i}\hat{Q}_{23}\right), \\ \hat{T}_{20} &= \sqrt{\frac{3}{2}}\,\hat{Q}_{33}. \end{aligned} \tag{3.16}$$

In this case, the nondiagonal elements of this symmetric tensor are $\hat{Q}_{12} = \lambda_6$, $\hat{Q}_{13} = \lambda_1$ and $\hat{Q}_{23} = \lambda_4$, whereas the diagonal ones can be expressed as

$$\hat{Q}_{11} - \hat{Q}_{22} = 2\lambda_3, \qquad 2\hat{Q}_{23} - \hat{Q}_{11} - \hat{Q}_{33} = 2\sqrt{3}\,\lambda_8, \tag{3.17}$$

where (λ_3, λ_8) is just the Cartan subalgebra (Rowe *et al* 1989).

The decomposition in terms of SU(2) multipoles is known as the irreducible embedding of SU(2) in SU(3) and has been widely employed in nuclear physics (Dalitz 1952, Ward 1982). In optics, this was first noticed by (Carozzi *et al* 2000) and later on its physical meaning was elucidated from different perspectives (Dennis 2004, Petrov 2008, Sheppard 2014). The dipole terms are precisely Im $\langle E_i E_j^* \rangle$, so they measure the strength of two of the oscillating fields in antiphase, as two distinguishable sources in antiphase constitute a dipole. The three components (n_6, n_4, n_1) of the quadrupole correspond to Re $\langle E_i E_j^* \rangle$ and measure the strength of two of the oscillating fields in phase: now two distinguishable sources oscillating in phase generate a field with a quadropole component.

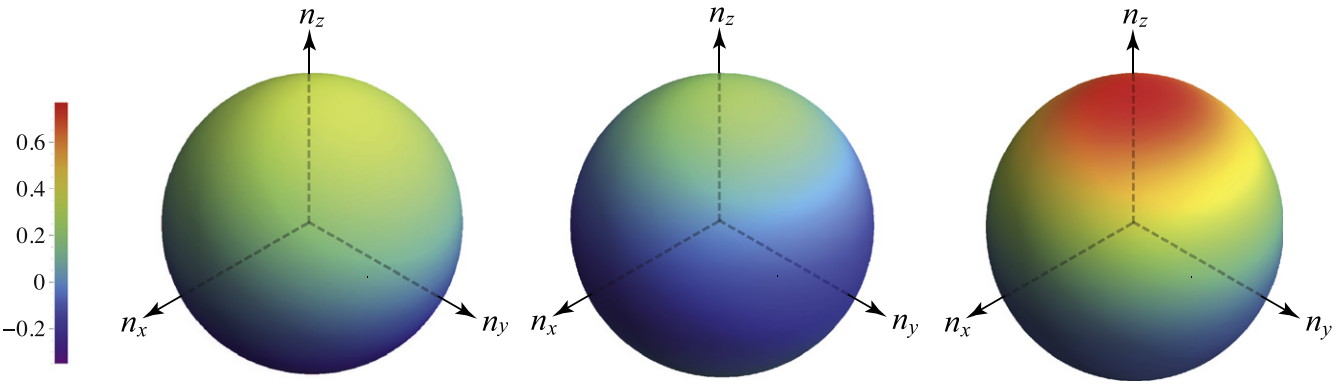

Figure 2. From left to right, density plots (the scale is included) for the Wigner function associated with the dipolar component, the quadrupolar component, and total one for the state $\mathbf{n} = (0, 0, \sqrt{3}/2, 0, 0, 0, 0, 1/2)$.

4. Concluding remarks

We have explored the use of Wigner functions to depict the behavior of 2D and 3D polarizations. Although this has been mostly considered as a quantum tool, it has proven to be also quite an efficient approach to deal with classical fields. Especially, in the 3D case, we have tailored an efficient procedure to represent state on the sphere. We hope that this analysis clarifies the discussion on 3D polarization in the literature.

Acknowledgments

Financial support from the Swedish Foundation for International Cooperation in Research and Higher Education (STINT), the Swedish Research Council (VR) through its Linnaeus Center of Excellence ADOPT and Contract No. 621-2011-4575, the CONACyT (Grant 106525), Canadian NSERC, the European Union FP7 (Grant Q-ESSENCE), the Spanish MINECO (Grant FIS2011-26786) and the Program UCM-Banco Santander (Grant GR3/14) is gratefully acknowledged. GB thanks the Max-Planck-Institut für die Physik des Lichts for hosting him during the fall 2014 and the Wenner-Gren Foundation for economic support.

References

Agarwal G S 1981 *Phys. Rev.* A **24** 2889–96
Alonso M A 2011 *Adv. Opt. Photon.* **3** 272–365
Ash E A and Nicholls G 1972 *Nature* **237** 510–2
Banyai L, Marinescu N, Raszilier I and Rittenberg V 1966 *Commun. Math. Phys.* **2** 121–32
Barakat R 1977 *Opt. Commun.* **23** 147–50
Bastiaans M J 2009 *Wigner Distribution in Optics* (New York: McGraw-Hill) pp 1–44
Berezin F A 1975 *Commun. Math. Phys.* **40** 153–74
Blum K 1981 *Density Matrix Theory and Applications* (New York: Plenum)
Brif C and Mann A 1998 *J. Phys. A: Math. Gen.* **31** 9–17
Brosseau C 1998 *Fundamentals of Polarized Light: A Statistical Optics Approach* (New York: Wiley)
Carozzi T, Karlsson R and Bergmank J 2000 *Phys. Rev.* E **61** 2024–8
Chumakov S M, Frank A and Wolf K B 1999 *Phys. Rev.* A **60** 1817–22
Cornwell J F 1997 *Group Theory in Physics* vol 1 (San Diego, CA: Academic)
Dalitz R H 1952 *Proc. Phys. Soc. Sect.* A **65** 175–8
de la Hoz P, Björk G, Klimov A B, Leuchs G and Sánchez-Soto L L 2014 *Phys. Rev.* A **90** 043826
de la Hoz P, Klimov A B, Björk G, Kim Y H, Müller C, Marquardt C, Leuchs G and Sánchez-Soto L L 2013 *Phys. Rev.* A **88** 063803
Dennis M R 2004 *J. Opt.* A **6** S26–31
Dennis M R 2007 *J. Opt. Soc. Am.* A **24** 2065–9
Dowling J P, Agarwal G S and Schleich W P 1994 *Phys. Rev.* A **49** 4101–9
Dragoman D 1997 *Progress in Optics* ed E Wolf vol 37 (Amsterdam: Elsevier)
Ellis J, Dogariu A, Ponomarenko S and Wolf E 2005 *Opt. Commun.* **248** 333–7
Fano U and Racah G 1963 *Irreducible Tensorial Sets* (New York: Academic)
Galleani L and Cohen L 2002 *Phys. Lett.* A **302** 149–55
Heiss S and Weigert S 2000 *Phys. Rev.* A **63** 012105
Klimov A B 2002 *J. Math. Phys* **43** 2202–13
Klimov A B and Chumakov S M 2000 *J. Opt. Soc. Am.* A **17** 2315–8
Klimov A B and Romero J L 2008 *J. Phys. A: Math. Theor.* **41** 055303
Korotkova O and Wolf E 2004 *J. Opt. Soc. Am.* A **21** 2382–5
Luis A 2005 *Opt. Commun.* **253** 10–4
Mandel L and Wolf E 1995 *Optical Coherence and Quantum Optics* (Cambridge: Cambridge University Press)
Mecklenbraüker W and Hlawatsch F 1997 *The Wigner Distribution: Theory and Applications in Signal Processing* (Amsterdam: Elsevier)
Moya-Cessa H, Moya-Cessa J R, Landgrave J, Martínez-Niconoff G, abd A T and Friberg A P L 2008 *J. Eur. Opt. Soc. Rapid Publ.* **3** 08014
Petrov N I 2008 *Laser Phys.* **18** 522–5
Petruccelli J C, Moore N J and Alonso M A 2010 *Opt. Commun.* **283** 4457–66
Pohl D W, Denk W and Lanz M 1984 *Appl. Phys. Lett.* **44** 651–3
Roman P 1959 *Nuovo Cimento* **13** 2546–54
Rowe D J, Blanc R L and Repka J 1989 *J. Phys. A: Math. Gen.* **22** 309–16
Rowe D J, Sanders B C and de Guise H 1999 *J. Math. Phys.* **40** 3604–15
Samson J C 1973 *Geophys. J. R. Astron. Soc.* **34** 403–19
Sánchez-Soto L L, Klimov A B, de la Hoz P and Leuchs G 2013 *J. Phys. B: At. Mol. Opt. Phys.* **46** 104011

Setälä T, Kaivola M and Friberg A T 2002 *Phys. Rev. Lett.* **88** 123902
Sheppard C J R 2011 *J. Opt. Soc. Am.* A **28** 2655–9
Sheppard C J R 2014 *Phys. Rev.* A **90** 023809
Simon R and Mukunda N 1989 *Phys. Lett.* A **138** 474–80
Stratonovich R L 1956 *Sov. Phys. JETP*-USSR **31** 1012–20
Varshalovich D A, Moskalev A N and Khersonskii V K 1988 *Quantum Theory of Angular Momentum* (Singapore: World Scientific)
Walther A 1968 *J. Opt. Soc. Am.* **58** 1256–9
Ward R S 1982 *Commun. Math. Phys.* **86** 437–48
Wigner E 1932 *Phys. Rev.* **40** 749–59
Wódkiewicz K 1995 *Phys. Rev.* A **51** 2785–8

Paper 9

G. Björk, M. Grassl, P. de la Hoz, G. Leuchs, L. L. Sánchez-Soto:
"Stars of the quantum universe: extremal constellations on the Poincaré sphere",
Physica Scripta **90**, 108008 (2015)

OPEN ACCESS
IOP Publishing | Royal Swedish Academy of Sciences Physica Scripta
Phys. Scr. **90** (2015) 108008 (9pp) doi:10.1088/0031-8949/90/10/108008

Invited Comment

Stars of the quantum Universe: extremal constellations on the Poincaré sphere

Gunnar Björk[1], Markus Grassl[2,3], Pablo de la Hoz[4], Gerd Leuchs[2,3] and Luis L Sánchez-Soto[2,3,4]

[1] Department of Applied Physics, Royal Institute of Technology (KTH), AlbaNova University Center, SE-106 91 Stockholm, Sweden
[2] Max-Planck-Institut für die Physik des Lichts, Günther-Scharowsky-Straße 1, Bau 24, D-91058 Erlangen, Germany
[3] Institut für Optik, Information und Photonik, Universität Erlangen-Nürnberg, Staudtstraße 7/B2, D-91058 Erlangen, Germany
[4] Departamento de Óptica, Facultad de Física, Universidad Complutense, E-28040 Madrid, Spain

E-mail: gbjork@kth.se

Received 8 May 2015, revised 7 July 2015
Accepted for publication 6 August 2015
Published 18 September 2015

Abstract

The characterization of the polarization properties of a quantum state requires the knowledge of the joint probability distribution of the Stokes variables. This amounts to assessing all the moments of these variables, which are aptly encoded in a multipole expansion of the density matrix. The cumulative distribution of these multipoles encapsulates in a handy manner the polarization content of the state. We work out the extremal states for that distribution, finding that SU(2) coherent states are maximal to any order, so they are the most polarized allowed by quantum theory. The converse case of pure states minimizing that distribution, which can be seen as the most quantum ones, is investigated for a diverse range of number of photons. Exploiting the Majorana representation, the problem appears to be closely related to distributing a number of points uniformly over the surface of the Poincaré sphere.

S Online supplementary data available from stacks.iop.org/ps/90/108008/mmedia

Keywords: polarization, quantum optics, fluctuations, anti-coherence, Majorana representation, spherical t-design

(Some figures may appear in colour only in the online journal)

1. Introduction

In this focus issue, celebrating the International Year of Light, we wish to discuss one of the fundamental properties of a beam of light: its polarization [1]; which can be roughly defined as the figure traced out by the tip of the electric field vector during one optical cycle.

In classical optics, if the field is fully polarized, this figure is an ellipse, which can degenerate into a line or a circle. If the field is completely unpolarized, then the figure is erratic and can only be described in statistical terms. This statistical description must be invariant under any change of the polarization basis: in operational terms, this means that unpolarized light remains invariant under any polarization transformation.

At the quantum level, this picture becomes too simplistic. There are, for example, states that classically are unpolarized, but which do carry a quantum polarization structure. These

are called states with 'hidden polarization' [2, 3]. What we will show here is that this is just the first level of a hierarchy of states that at first glance look unpolarized, but are in fact polarized when one looks at higher-order fluctuations.

In order to systematically derive this hierarchy, we shall use the Majorana representation [4], which maps any N-photon state onto N points on the Poincaré sphere. We will subsequently show that the problem we consider, quantum optical states with peculiar polarization properties, is connected to several other seemingly unrelated problems in physics and computational science. We do not yet understand either why or to what extent the problems are related, but intuitively they all boil down to a geometrical problem, namely: what is the optimal configuration if one wishes to place N points on the unit sphere in the 'most symmetric fashion' possible? [5–7].

This paper is organized as follows. In section 2 we review some of the required mathematical concepts. In section 3 we state the problem in more precise terms and in section 4 we present some of the stars of the quantum Universe, i.e. the most unpolarized and therefore the most nonclassical states in a polarization context. Subsequently, in section 5, we discuss several related problems and compare the solutions. In section 6 we speculate about the potential use our stars may have. Finally, in section 7 we make some concluding remarks and explore ideas for the future directions of this research.

2. Basic polarization tools and concepts

We consider a monochromatic, plane field, described by two amplitudes $\hat{a}_+$ and $\hat{a}_-$, representing the annihilation operators of two circularly polarized orthogonal modes, right-handed (+) and left-handed (−), respectively. They obey the bosonic commutation relations $[\hat{a}_j, \hat{a}_k^\dagger] = \delta_{jk}$ ($j, k \in \{+, -\}$) and the superscript † stands for the Hermitian conjugate.

The Stokes operators are [8]:

$$\hat{S}_0 = \tfrac{1}{2}\left(\hat{a}_+^\dagger \hat{a}_+ + \hat{a}_-^\dagger \hat{a}_-\right), \qquad \hat{S}_1 = \tfrac{1}{2}\left(\hat{a}_+ \hat{a}_-^\dagger + \hat{a}_+^\dagger \hat{a}_-\right),$$
$$\hat{S}_2 = \tfrac{\mathrm{i}}{2}\left(\hat{a}_+ \hat{a}_-^\dagger - \hat{a}_+^\dagger \hat{a}_-\right), \qquad \hat{S}_3 = \tfrac{1}{2}\left(\hat{a}_+^\dagger \hat{a}_+ - \hat{a}_-^\dagger \hat{a}_-\right), \quad (1)$$

and bear a very simple operational interpretation: $\hat{S}_0$ represents the intensity, $\hat{S}_1$ the intensity difference between horizontal and vertical linear polarizations, $\hat{S}_2$ the intensity difference between linear polarizations at $+45^\circ$ and -45°, and $\hat{S}_3$ the intensity difference between right- and left-handed circular polarizations. While the last assertion is rather obvious, it is less obvious that $\hat{S}_1$ indeed is the the intensity difference between horizontal (H) and vertical (V) linear polarizations. However, expressing $\hat{a}_\mathrm{H} = (\hat{a}_+ + \hat{a}_-)/\sqrt{2}$ and $\hat{a}_\mathrm{V} = (\hat{a}_+ - \hat{a}_-)/\sqrt{2}$ it is straightforward to derive that $\hat{S}_1$ indeed equals $\hat{a}_\mathrm{H}^\dagger \hat{a}_\mathrm{H} - \hat{a}_\mathrm{V}^\dagger \hat{a}_\mathrm{V}$.

As written in equation (1), they differ by a factor $1/2$ from the conventional definition [9], but in this way they satisfy the commutation relations of the $\mathfrak{su}(2)$ algebra (in units $\hbar = 1$ throughout)

$$[\hat{S}_1, \hat{S}_2] = \mathrm{i}\hat{S}_3, \quad (2)$$

and cyclic permutations. This noncommutability precludes the simultaneous sharp measurement of the quantities they represent. Among other consequences, this implies that no field state (apart from the vacuum) can have sharp nonfluctuating values of all the operators $\hat{\mathbf{S}} = (\hat{S}_1, \hat{S}_2, \hat{S}_3)$ simultaneously. This is expressed by the uncertainty relation

$$\langle \hat{S}_0 \rangle \leqslant \Delta^2 \hat{S}_1 + \Delta^2 \hat{S}_2 + \Delta^2 \hat{S}_3 \leqslant \langle \hat{S}_0 (\hat{S}_0 + 1) \rangle, \quad (3)$$

where the variances are given by $\Delta^2 \hat{S}_i = \langle \hat{S}_i^2 \rangle - \langle \hat{S}_i \rangle^2$. In other words, the electric field of a quantum state never traces out a definite ellipse. Note that there is a complete formal equivalence between the space of fixed total photon number N with a spin $S \equiv S_0 = N/2$.

In addition, we have

$$[\hat{\mathbf{S}}, \hat{S}_0] = 0, \quad (4)$$

and one must therefore address each subspace with a fixed number of photons N separately. This can be emphasized if instead of the two-mode Fock basis $|n_+, n_-\rangle$, we employ the relabeling

$$|S, m\rangle \equiv |n_+ = S + m, n_- = S - m\rangle. \quad (5)$$

In this way, for each fixed S (i.e., fixed number of photons N), m runs in unit steps from $-S$ to S and these states span a $(2S+1)$-dimensional subspace wherein $\hat{\mathbf{S}}$ acts in the usual way.

In classical optics the total intensity is a well-defined quantity. In consequence, normalizing the Stokes variables by the intensity determines the unit Poincaré sphere. At the quantum level, as fluctuations in the number of photons are unavoidable, one should talk of a three-dimensional Poincaré space (with axes S_1, S_2 and S_3) that can be envisioned as foliated in a set of nested spheres with radii proportional to the different photon numbers that contribute significantly to the state. But if one limits oneself to a single spin component S and picks one of those nested spheres, we can rightly speak about the unit Poincaré sphere as in the classical world.

The Stokes operators are also the infinitesimal generators of SU(2) polarization transformations; that is

$$\hat{U}(\mathbf{n}, \theta) = \exp(-\mathrm{i}\theta \hat{\mathbf{S}} \cdot \mathbf{n}/2), \quad (6)$$

with θ a real parameter, and $\mathbf{n}$ a normalized, three-dimensional, real vector. These are all linear energy-preserving transformations of the field amplitudes, embracing every optical operation of phase plates and rotators. It can be seen that the action of $\hat{U}(\mathbf{n}, \theta)$ on $\hat{\mathbf{S}}$ is a rotation of angle θ around an axis $\mathbf{n}$:

$$\hat{U}(\mathbf{n}, \theta)\, \hat{\mathbf{S}}\, \hat{U}^\dagger(\mathbf{n}, \theta) = \mathcal{R}(\mathbf{n}, \theta)\, \hat{\mathbf{S}}. \quad (7)$$

Observe that given the rotation $\mathcal{R}(\mathbf{n}, \theta)$, with $0 \leqslant \theta \leqslant \pi$, both $\hat{U}(\mathbf{n}, \theta)$ and $\hat{U}(\mathbf{n}, \theta + 2\pi) = -\hat{U}(\mathbf{n}, \theta)$ lead to $\mathcal{R}(\mathbf{n}, \theta)$.

The relation (4) implies that the polarization properties of any quantum state can be analyzed by splitting its density matrix into a direct sum of finite-dimensional components

$$\hat{\varrho}_{\rm pol} = \bigoplus_S \hat{\varrho}^{(S)}, \qquad S = 0, \tfrac{1}{2}, 1, \tfrac{3}{2}, \ldots, \tag{8}$$

where $\hat{\varrho}^{(S)}$ is the density matrix in the subspace of spin S. This $\hat{\varrho}_{\rm pol}$ has been termed the polarization sector [10] or the polarization density matrix [11].

Instead of using the states $\{|S, m\rangle\}$, in the following we will expand $\hat{\varrho}^{(S)}$ as

$$\hat{\varrho}^{(S)} = \sum_{K=0}^{2S} \sum_{q=-K}^{K} \varrho_{Kq}^{(S)} \hat{T}_{Kq}^{(S)}. \tag{9}$$

The irreducible tensor operators $\hat{T}_{Kq}^{(S)}$ are [12, 13]

$$\hat{T}_{Kq}^{(S)} = \sqrt{\frac{2K+1}{2S+1}} \sum_{m,m'=-S}^{S} C_{Sm,Kq}^{Sm'} |S, m'\rangle \langle S, m|, \tag{10}$$

with $C_{Sm,Kq}^{Sm'}$ being the Clebsch–Gordan coefficients that couple a spin S and a spin K ($0 \leqslant K \leqslant 2S$) to a total spin S. The tensors $\hat{T}_{Kq}^{(S)}$ constitute an orthonormal basis and have desirable properties under SU(2) transformations. An important property is that $\hat{T}_{Kq}^{(S)}$ can be written down in terms of the Kth powers of the Stokes operators (1). In particular, if for a given pair of S and M all coefficients $\varrho_{Kq}^{(S)}$ vanish for $K = 1, 2, \ldots, M$, irrespective of q, then the moment $\langle \hat{S}_{\mathbf{n}}^{M} \rangle$ (with $\hat{S}_{\mathbf{n}} = \hat{\mathbf{S}} \cdot \mathbf{n}$) will be isotropic and independent of $\mathbf{n}$. Clearly, this then also holds for all moments $\langle \hat{S}_{\mathbf{n}}^{\ell} \rangle$ where $\ell < M$.

The expansion coefficients $\varrho_{Kq}^{(S)}$ are known as state multipoles. Hence, $\sum_{q=-K}^{K} |\varrho_{Kq}^{(S)}|^2$ is just the square of the overlap of the state with the Kth multipole pattern in the Sth subspace. For most states only a limited number of multipoles play a substantive role and the rest of them have quite a small contribution. Therefore, it seems that a convenient way to quantify the polarization information is to look at the cumulative distribution

$$\mathcal{A}_M^{(S)} = \sum_{K=1}^{M} \sum_{q=-K}^{K} \left| \varrho_{Kq}^{(S)} \right|^2, \tag{11}$$

which conveys all the information *up* to order M. Note that the monopole term $|\varrho_{00}^{(S)}|^2$ is excluded, as it is just a constant term. As with any cumulative distribution, $\mathcal{A}_M^{(S)}$ is a monotone, nondecreasing function of the multipole order. Using (9) and the fact that the tensor operators are orhonormal we see that

$$\mathrm{Tr}\left([\hat{\varrho}^{(S)}]^2\right) = \sum_{K=0}^{2S} \sum_{q=-K}^{K} |\varrho_{Kq}^{(S)}|^2 = \mathcal{A}_{2S}^{(S)} + |\varrho_{00}^{(S)}|^2, \tag{12}$$

so for a state with a fixed S, $\mathcal{A}_{2S}^{(S)}$ is equal to the state's purity [14–16] (minus the monopole contribution $|\varrho_{00}^{(S)}|^2 = (2S+1)^{-1}$).

We shall be mainly interested in dealing with pure states belonging to a specific excitation manifold S. Accordingly, if we expand the state as $|\Psi^{(S)}\rangle = \sum_{m=-S}^{S} \Psi_m |S, m\rangle$, with coefficients $\Psi_m = \langle S, m|\Psi\rangle$, we can then recast (11) as

$$\mathcal{A}_M^{(S)} = \sum_{K=1}^{M} \sum_{q=-K}^{K} \frac{2K+1}{2S+1} \left| \sum_{m,m'=-S}^{S} C_{Sm,Kq}^{Sm'} \Psi_{m'} \Psi_m^* \right|^2. \tag{13}$$

3. Classical versus quantum polarization states

Given a fixed spin S, the classical configuration space is the unit sphere associated with the SU(2) symmetry. The SU(2) coherent states in this case can be identified with a point on the sphere obtained by a rotation of the North pole $|S, S\rangle$ [17, 18]. There is a consensus that they are the most classical states, as they have all their polarization aligned in one direction. Besides, they have nice extremal properties, such as minimal total variance of $\hat{\mathbf{S}}$ [19] or minimal Wehrl entropy [20].

In our context, it is remarkable that they have maximal aggregated multipole strength $\mathcal{A}_M^{(S)}$ for any order M [15, 21]. It is irresistible to ask which states attain the minimum of this magnitude, as they can be considered in a sense as 'the opposite' of SU(2) coherent states and so the most nonclassical ones. This appears to be closely related with a proposal that has met with considerable interest: anti-coherent states, defined as the states that have a vanishing Stokes vector as well as isotropic Stokes variances [22].

A useful tool in this context is the Majorana representation of a pure N-photon state [4], which is based on the fact that any such state $|\Psi^{(S)}\rangle$ (where the reader is reminded that $N = 2S$) can be written as [23]

$$\left|\Psi^{(S)}\right\rangle = \frac{1}{\sqrt{\mathcal{N}}} \prod_{m=1}^{2S} \left[\cos\left(\frac{\theta_m}{2}\right) \hat{a}_+^\dagger + \mathrm{e}^{\mathrm{i}\varphi_m} \sin\left(\frac{\theta_m}{2}\right) \hat{a}_-^\dagger \right] |0, 0\rangle, \tag{14}$$

where $\mathcal{N}$ is a normalization factor, and the angles θ_m and φ_m satisfy the natural constraints $0 \leqslant \theta_m \leqslant \pi$ and $0 \leqslant \varphi_m < 2\pi$. Thus, each factor in (14) can be pictured as a point on the unit Poincaré sphere. Since the operators $\hat{a}_+^\dagger$ and $\hat{a}_-^\dagger$ create an excitation in right- and left-hand circularly polarized modes, respectively, each of the factors in (14) can also naively be thought of as creating an 'excitation component' with a polarization state corresponding to its position on the sphere. The resulting configuration of points is called the Majorana constellation associated to the state $|\Psi^{(S)}\rangle$. An illustration of these ideas is schematized in figure 1.

We associate the North (South) pole with right- (left-) handed circular polarization and thus the equator represents different linear polarization excitations. For example, the N-photon SU(2) coherent state $|S, S\rangle = (N!)^{-1/2} (\hat{a}_+^\dagger)^N |0, 0\rangle$ is represented by N points at the North pole of the sphere so that all 'excitation components' have identical (right-handed) circular polarization.

An SU(2) rotation simply corresponds to a solid rotation of the Majorana constellation. Thus, states with the same constellation, irrespective of its relative orientation, have the

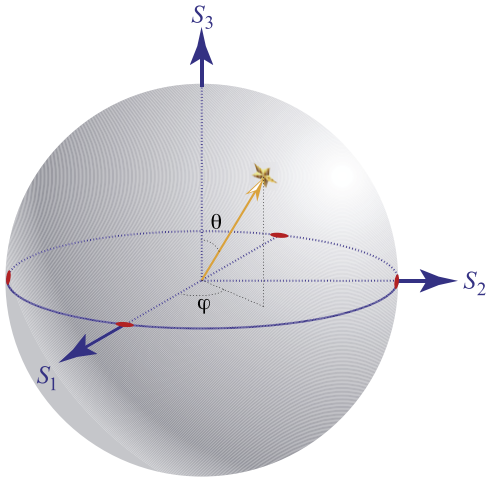

Figure 1. The star denotes the Majorana constellation of the state $\cos(\theta/2)\,|1/2,\,1/2\rangle + \exp(\mathrm{i}\varphi)\sin(\theta/2)|1/2,\,-1/2\rangle$. The four red dots give the constellation for the $S = 2$ N00N state in equation (17).

same polarization invariants. Intuitively, one would guess that states with polarization as isotropic as possible would have a constellation as symmetric as possible.

To place this guess in a more rigorous mathematical frame, one can go beyond the variance, and look for the states that have isotropic polarization properties for *all* the moments $\{\langle\hat{S}_{\mathbf{n}}\rangle, \langle\hat{S}_n^2\rangle, \ldots, \langle\hat{S}_{\mathbf{n}}^M\rangle\}$ [22, 24, 25]. For a given S, one cannot find pure states that have isotropic moments up to order $M = 2S$: only completely mixed states have this property [26, 27]. Thus, for each S there exists a set of pure states that are unpolarized up to a maximal degree M. These Mth-order unpolarized states are the stars of the quantum Universe. Below we shall sometimes be a bit imprecise and speak about a constellation as a state, which is evident from (14).

4. Stars of the quantum Universe

To find the Mth-order unpolarized states for a given S, we start from a set of $2S + 1$ amplitudes $\Psi_m = a_m + \mathrm{i}b_m$, where a_m, b_m are real numbers, as in equation (13). Since the orientation of the constellation is irrelevant we can reduce the number of variables by fixing one of the points to be at, say, the North pole and another to lie in the the S_2–S_3 plane. We subsequently try to get $\mathcal{A}_M^{(S)} = 0$ for the highest possible M, which amounts to setting the state multipoles $\varrho_{Kq}^{(S)}$ to zero. This leads to a system of polynomial equations of degree two for a_m and b_m, which we solve using Gröbner bases [28] implemented in the computer algebra system MAGMA [29, 30]. In this way, we get exact algebraic expressions, and we can detect when no feasible solution exists.

Our results can be summarized as follows. For small values, $1/2 \leqslant S \leqslant 3/2$, the parameter space is simply too small even to allow for states with isotropic variance. For $S = 1$ and $S = 3/2$ one can find states with vanishing Stokes vector, but all such pure states have non-isotropic variance [21] and so they present hidden polarization [2]. The $S = 2$ excitation manifold is the first allowing a second-order unpolarized state. However, the space is still so small that the solution is unique. For $S = 5/2$ no second-order unpolarized state exists. For larger numbers, $S > 3$, there exist several different constellations that all are unpolarized to the same order M, but that are not simply connected by a unitary polarization transformation. We have not yet found a way of assuring that we find all constellations for a given S, nor have we found a general way of asserting with certainty that for a given S we have found the constellations that maximize M. This is related to the fact that with growing S, the number of different maximally unpolarized constellations grows and it becomes more difficult to show that the corresponding system of polynomial equations has no solution over the real numbers. The same kind of difficulties appear in several related problems such as spherical t-designs, the Thomson problem, and the Queens of quantumness that will be discussed in the next section. However, after spending considerable time on computer searches, we are fairly confident that the constellations we present are indeed optimal.

Let us now look at some of the stars of the quantum Universe. A list of star states having $S = 1$ to 10 can be found in the Supplementary material file, available at stacks.iop.org/ps/90/108008/mmedia. Note that for most values of S, except for the smallest, there exist many inequivalent star states. As exemplified in figure 3, below, in general they have different cumulative multipole distributions $\mathcal{A}_M^{(S)}$. For more complete information and lists over inequivalent star states for different values of S, the reader is referred to [31].

$\mathbf{S = 2}$. The least excited second-order unpolarized state is the four-photon state. Its Majorana constellation is a regular tetrahedron and this configuration is unique. The corresponding state is $\left(|2,-1\rangle + \sqrt{2}\,|2,2\rangle\right)/\sqrt{3}$ (and, of course, all states on its SU(2) orbit).

$\mathbf{S = 5/2}$. Five is a number that does not allow a high degree of spherical symmetry. Based on an elementary counting, it was conjectured in [22] that five-photon anticoherent states would exist. However, some time later it was proven that one can only find first-order, but no second-order unpolarized states [32]. The constellation consists of the vertices of an equilateral triangle inscribed in the equator, plus the two poles.

$\mathbf{S = 3}$. Now another Platonic solid appears, the regular octahedron. The corresponding state, which is unique up to SU(2) transformations, is $(|3,-2\rangle + |3,2\rangle)/\sqrt{2}$. This is the least excited state that is third-order unpolarized. Since $\langle\hat{S}_{\mathbf{n}}^M\rangle = -\langle\hat{S}_{-\mathbf{n}}^M\rangle$ for odd M, all odd order Stokes operator moments must vanish for them to be isotropic (irrespective of S). This state, like all states that have isotropic variance, has the maximum sum of Stokes operator variances. Since for any unpolarized state $\langle\hat{\mathbf{S}}\rangle = 0$, the relation (3) imposes the bound

$$\langle\hat{S}_0\rangle \leqslant \langle\hat{S}_1^2\rangle + \langle\hat{S}_2^2\rangle + \langle\hat{S}_3^2\rangle \leqslant \langle\hat{S}_0(\hat{S}_0+1)\rangle. \qquad (15)$$

All second-order unpolarized states saturate the upper bound in the inequality above [22]. Thus, all maximally unpolarized states with $N \geqslant 6$ fulfill $\langle\hat{S}_{\mathbf{n}}^2\rangle = S(S+1)/3$ in any direction $\mathbf{n}$ on the Poincaré sphere. In figure 2 we plot the Majorana constellation, the Q-function, and the first non-isotropic

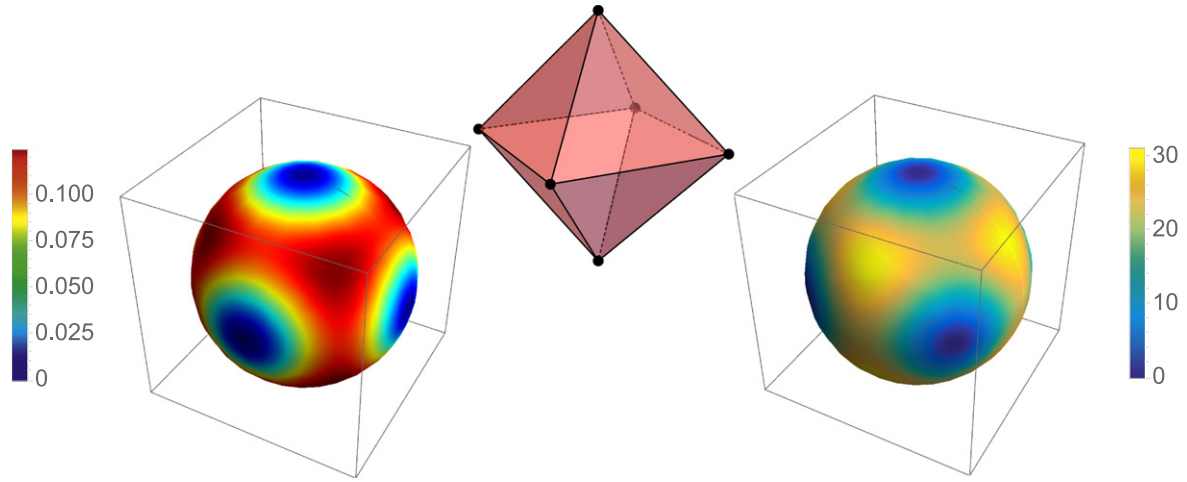

Figure 2. Density plots of the SU(2) Q-function (left) and the first non-isotropic moments $\langle \hat{S}^4_{\mathbf{n}} \rangle$ (right) for the maximally unpolarized state $(|3,-2\rangle + |3,2\rangle)/\sqrt{2}$ in the excitation manifold $S = 3$. In both cases, we have used a pseudo-color map with the indicated scales. On top, we have given the Majorana constellation of the state, which is a regular octahedron inscribed in the Poincaré sphere. Note that the vertices coincide with the zeros of the Q function, but not with the zeros of $\langle \hat{S}^4_{\mathbf{n}} \rangle$.

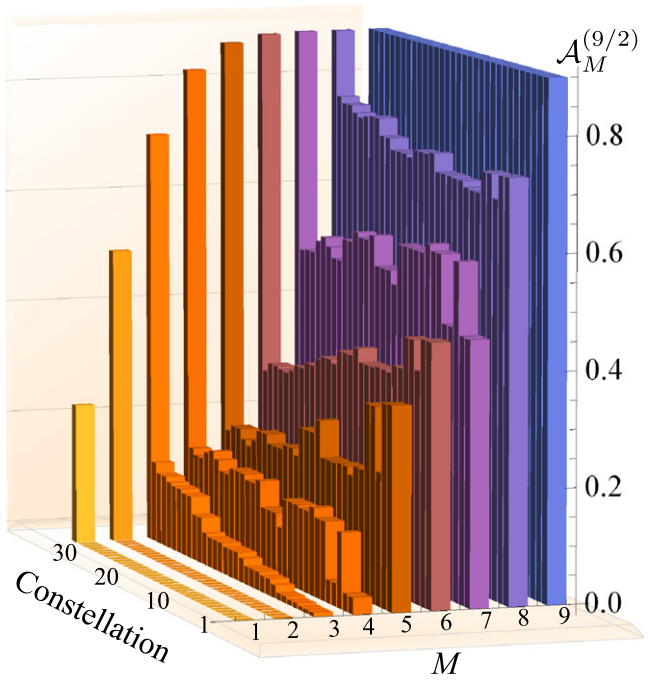

Figure 3. The multipole cumulative distribution $\mathcal{A}_M^{(9/2)}$ as a function of the multipole order M for all the 31 maximally unpolarized constellations we have found for $S = 9/2$. The last constellation, number 32, corresponds to an SU(2) coherent state, taken as a reference.

moments ($M = 4$) as a function of the direction on the Poincaré sphere for this state.

$\mathbf{S = 9/2}$. In this space there are at least 31 different constellations with six different abstract symmetry groups that are second-order unpolarized, but we conjecture that no third-order unpolarized constellations exist. The constellations differ in how the aggregated multipole strength $\mathcal{A}_M^{(9/2)}$ increases with M. We have found 20 different such functions and they are plotted in figure 3. The constellation with the smallest third-order multipole strength has $\mathcal{A}_3^{(9/2)} \approx 0.00642$, and the one with the largest has $\mathcal{A}_3^{(9/2)} \approx 0.141$. The former case is generated by three equilateral triangles: one inscribed in the equator and the other in two rings symmetrically placed above and below the equator. The middle triangle is rotated 60° around the polar axis with respect to the other two. The corresponding state is

$$(\sqrt{6}\,|9/2,-9/2\rangle - 2\sqrt{3}\,|9/2,-3/2\rangle - 2\sqrt{3}\,|9/2,3/2\rangle + \sqrt{6}\,|9/2,9/2\rangle)/6.$$

The $S = 9/2$ case is rather typical for $S > 4$: several different constellations unpolarized to the same (maximal) order exist. Different constellations may have the same or different accumulated multipole strength $\mathcal{A}_M^{(S)}$ as a function of M.

For some values of S, such as 4, 6, 8, 12 and 20, one can guess a maximally unpolarized constellation, in each case corresponding to the vertices of a Platonic solid. For other numbers such as $S = 17/2$ it is not easy to guess an optimal, 'exact' constellation, but solving the system of polynomial equations, as described at the beginning of this section, yields exact algebraic expressions for the coefficients Ψ_n, from which one can easily compute the points of the Majorana constellation with arbitrary numerical precision.

5. Other spherical configuration problems

The problem of distributing N points on a sphere in the 'most symmetric' fashion has a long history and many different solutions depending on the cost function one tries to optimize [5, 6]. Here, we shall only discuss a few of the formulations: spherical t-designs [33–35], the Thomson problem [36–39] and the Queens of quantumness [40]. We leave out the connections to other intriguing problems, such as as maximally

Table 1. Some designs on a sphere and their respective degrees of unpolarization M. 'same' and 'similar' always refer to the closest description column to the left. Explicit expressions for the stars of the quantum Universe for several values of S can be found in [31].

S	Quantum stars	M	t-design	t	M	Thomson	M	Queens	M
1	Radial line	1	same	1	1	same	1	same	1
3/2	Equatorial triangle	1	same	1	1	same	1	same	1
2	Tetrahedron	2	same	2	2	same	2	same	2
5/2	Equatorial triangle + poles	1	same	1	1	same	1	same	1
3	Octahedron	3	same	3	3	same	3	same	3
7/2	Two triangles + pole	2	similar	2	0	equatorial pentagon + poles	1	same	1
4	Cube	3	same	3	3	square antiprism	1	see [40]	1
9/2	Three triangles	2	similar	2	1	three staggered triangles	1	similar	1
5	Pentagonal prism	3	similar	3	1	two staggered squares + poles	1	same	1
6	Icosahedron	5	same	5	5	same	5	NA	—
7	Four triangles + poles	4	same	4	1	two hexagonal rings + poles	1	NA	—
10	Dodecahedron	5	same	5	3	see [38]	?	NA	—

entangled symmetric states [41, 42], k-maximally mixed states [43], and states with maximal Wehrl–Lieb entropy [44].

Spherical t-designs are configurations of N points on a sphere such that the average value of any polynomial of degree at most t has the same average over the N points as over the sphere. Thus, the N points can be seen to give a representative average value of any polynomial of degree t or lower. Such designs can be found for (hyper)spheres of higher dimensions, but to connect to the stars we will only consider t-designs on the three-dimensional sphere. It has been conjectured that a state is t-order unpolarized if and only if its Majorana constellation is a spherical t-design [24]. However, although the statement is true for some t-designs, such as those represented by the Platonic solids, the conjecture is not true in general [25].

It is clear that there must be some connection between the number of points that are at one's disposal and the maximal degree t for which an N point configuration allows for a spherical t-design. The configurations that maximize t for a given N are called optimal designs, and in the following t will denote the degree of an optimal N-point design. No analytical expression is known between N and t: it is known that for a t-design in three-dimensional space, the number of points N is at least proportional to t^2, whereas for some orders t only constructions are known for which N scales proportionally to t^3. As a function of N, the order t is non-monotonic. The current state of knowledge is summarized for $1 \leqslant N \leqslant 100$ in [35]. In table 1 we list some maximally unpolarized constellations and their corresponding optimal t-designs.

Several interesting conclusions can be drawn from table 1. First, the maximum M and t coincide. In fact, this has been the case for any excitation manifold we have studied, and these include all S up to 24, with some omissions. We therefore conjecture that if an optimal spherical design of order t exists for some N, then one can find an Mth-order unpolarized N-photon state with $M = t$.

The next thing one can note is that an optimal t-design does not necessarily give a tth-order unpolarized state. Quite often the configurations are similar, e.g. regular polygons with their surface normals along the polar axis, but displaced from each other along the axis by certain distances. However, these distances need often be fine-tuned for an optimal t-design to become a star. The Platonic solids are exceptions to this observation. That the optimal configurations for t-designs and maximally unpolarized states do not coincide underscores the 'mystery' that the optimal t and maximal M always seem to be equal for any N (or equivalently, for any S).

Another similarity between optimal spherical t-designs and the stars of the quantum Universe is that the configurations typically are not unique, aside from the smallest dimensions.

The Thomson problem consists of arranging N identical point charges on the surface of a sphere so that the electrostatic potential energy of the configuration is minimized. For $N = 2$ the solution is easily visualized: the repelling force tends to place the charges on antipodal points of the sphere, thereby maximizing the distance between them. The problem can be generalized to potential energies of the form r^{-d}, where r is the Euclidian distance between the charges. The choice $d = 1$ is the Thomson problem, corresponding to the usual Coulomb potential and it is the one we will focus on in this work. The case $d \to \infty$ is called Tammes problem [45].

In table 1 we have listed the optimal Thomson configurations and the degree of unpolarization of the corresponding state. We see that for small S, up to 3, the configurations are identical to the optimal spherical t-design and to the stars. For larger S, they differ in general and the degree of unpolarization of the 'Thomson' states is lower than the maximum. Different from the two previous cases, the solution of the Thomson problem appears to be unique for every S [46].

The Queens of quantumness are the states that maximize the Hilbert–Schmidt distance to the closest point of the convex hull of the mixed SU(2) coherent states [40]. This convex hull defines the subspace of classical states. Therefore, the states maximizing the distance to the nearest point on this hull can be thought of as having maximally quantum characteristics. In [40] it is claimed that the Queens can be seen as the least classical (or most quantum) of all states given this metric. Although we have used another figure of merit, our

approach and that in [40] share the view that the states 'most different' from SU(2) coherent states are the most nonclassical.

It is not surprising that the Queens turn out to be anti-coherent (second-order unpolarized) when possible, since they should be as 'far away' from the SU(2) coherent state as possible. In table 1 we have also listed the configurations and the degree of unpolarization for these states. These configurations also seems to be unique, contrary to the maximally unpolarized states and the optimal spherical t-designs. We also see that the Queens are not maximally unpolarized except when $S < 3$.

6. What are the applications?

In deriving the maximally unpolarized states we have simply been driven by the quest for the most nonclassical states from a polarization perspective. Yet, the remarkable properties of such states make them potential candidates to outperform classical states in certain tasks.

The salient feature of the stars is their ability to signal small, but arbitrary SU(2) transformations with optimal resolution. This has already been anticipated in [32], where the authors specifically found that for photon numbers 4, 6, 8, 12 and 20, the states corresponding to regular polyhedra Majorana constellations best signal misalignments between two Cartesian reference frames. To understand this, it is instructive to look at related states, namely the N00N states

$$|\mathrm{N00N}\rangle = \frac{1}{\sqrt{2}}(|S, S\rangle - |S, -S\rangle). \tag{16}$$

Such N00N states are known to have the highest sensitivity for a fixed excitation S to small rotations about the $\hat{S}_3$-axis [47]. Their Majorana constellation consists of $2S$ equidistantly placed points around the Poincaré sphere equator. For example, the state $|\Psi\rangle = (|2, 2\rangle - |2, -2\rangle)/\sqrt{2}$ can be written

$$|\Psi\rangle = \frac{\left(\hat{a}_+^\dagger + \hat{a}_-^\dagger\right)\left(\hat{a}_+^\dagger - \hat{a}_-^\dagger\right)\left(\hat{a}_+^\dagger + \mathrm{i}\hat{a}_-^\dagger\right)\left(\hat{a}_+^\dagger - \mathrm{i}\hat{a}_-^\dagger\right)}{4\sqrt{3}}|0, 0\rangle. \tag{17}$$

That is, the four Majorana points are $(1, 0, 0)$, $(-1, 0, 0)$, $(0, 1, 0)$ and $(0, -1, 0)$, as sketched in figure 1. The angle between any two adjacent points is $\pi/2$, while for a general N00N state of the form (16), this angle is π/S.

A rotation around the $\hat{S}_3$-axis is described by the unitary operator $\hat{U}(\vartheta) = \exp(-\mathrm{i}\vartheta\hat{S}_3/2)$. We have that for $\vartheta = \pi/(2S)$ the states $|\mathrm{N00N}\rangle$ and $\hat{U}(\vartheta)|\mathrm{N00N}\rangle$ are orthogonal, whereas for $\vartheta = q\pi/S$ they are parallel, where q is an integer. Thus, it should not come as a surprise that N00N states are optimal for detecting small rotations around the $\hat{S}_3$ -axis, in the interval $0 \leqslant \vartheta \leqslant \pi/(2S)$. However, as soon as the rotation exceeds the upper bound in this inequality, one will have difficulties in resolving the rotation angle, as two or more rotation angles will result in the very same rotated state. If the rotation axis lies in the equatorial plane, then a rotation of π is needed to get a parallel state, irrespective of S. This happens only if the axis intersects one of the Majorana points when S is a half integer, or if the axis intersects either a point or is the intersector between two points if S is an integer. Thus, the rotation resolution is highly directional for a N00N state.

The situation is to some extent similar and to some extent different for the stars of the quantum Universe. It may not be obvious from their appearance that they have high sensitivity to small rotations around an arbitrary axis. To substantiate this claim, recall that the action τ needed to make a state $|\psi\rangle$ evolve so that $|\langle\psi|\exp(\mathrm{i}\hat{A}\tau)|\psi\rangle|^2 = 1 - \epsilon$ where ϵ is a small, positive, real number, and $\hat{A}$ is Hermitian, is inversely proportional to the state's variance $\Delta^2\hat{A}$ [48]. The relation connecting the evolution speed $\mathrm{d}\epsilon/\mathrm{d}\tau$ and the variance is sometimes called the 'quantum speed limit' [49, 50]. A N00N state in the $\hat{S}_3$ basis has maximal variance $\Delta^2\hat{S}_3 = S^2$ for a fixed S and thus is the state with maximal sensitivity for a rotation around the $\hat{S}_3$ axis. However, the state's $\hat{S}_1$ and $\hat{S}_2$ variances are only $S/2$ and thus the state is rather insensitive for rotations around those axes (or to any rotation axis in the $\hat{S}_1$–$\hat{S}_2$ plane). However, all the star states have isotropic variances equal to $S(S+1)/3$, that is, close to the maximum. The proof of this statement is as follows:

$$\begin{aligned}&\Delta^2\hat{S}_1 + \Delta^2\hat{S}_2 + \Delta^2\hat{S}_3\\ &\quad = \langle\hat{S}_1^2\rangle + \langle\hat{S}_2^2\rangle + \langle\hat{S}_3^2\rangle = \langle\hat{S}_0^2\rangle = S(S+1).\end{aligned} \tag{18}$$

The second expression from the left follows from the fact that the star states have vanishing mean first order moments $\langle\hat{S}_{\mathbf{n}}\rangle$. Since their variance per definition is isotropic, we also have that $\langle\hat{S}_{\mathbf{n}}^2\rangle = \langle\hat{S}_1^2\rangle = \langle\hat{S}_2^2\rangle = \langle\hat{S}_3^2\rangle$. Having a large, and isotropic variance of the Stokes operator, the quantum speed limit theorem thus asserts that these states are rather sensitive to rotations around any axis $\hat{S}_{\mathbf{n}}$.

Another way of explaning the star states' sensitivity to a rotation around an arbitrary axis is to observe that, since these states have 'maximal' spherical symmetry, they become parallel, or almost parallel, for relatively small rotations around several axes. For example, for the Platonic solids, rotations around all the facets normal axes map the Majorana constellation onto itself (resulting in a parallel state) for rotations of $2\pi/3$ (tetrahedron, octahedron and icosahedron), $\pi/2$ (cube), or $2\pi/5$ (dodecahedron). For other constellations and other rotation axes the Majorana constellation will only become approximately identical, but the problem with resolution of large rotations will predominantly remain. However, having a high degree of spherical symmetry, the maximally unpolarized states will resolve rotations around any axis approximately equally well. To quantify this statement one could use the Fisher information and the Cramér–Rao bound to assess the uncertainty in estimating the rotation direction and the rotation angle [49, 50]. Such an investigation lies outside the scope for this paper, but work along this direction is in progress.

To conclude, we stress that there is also some structural similarity between the stars of the quantum Universe and

quantum error correcting codes. In both cases, low-order terms in the expansion of the density matrices vanish. The putative application of the stars for error correction constitutes an important goal for our future research.

7. Conclusions

We have derived a class of pure states that lack polarization properties to the lowest orders. They can be seen as generalizations of states with hidden polarization and the anticoherent states. We call them stars of the quantum Universe and they are Mth-order unpolarized: the moments $\langle \hat{S}_{\mathbf{n}}^{\ell} \rangle$ are isotropic for $1 \leqslant \ell \leqslant M$. We find, so far to our surprise, that although their respective Majorana constellations do not necessarily coincide, we always find that for a pure N-photon state, the highest possible degree of unpolarization is $M = t$, where t is the maximal degree for an N-point spherical t-design. Our conjecture is that this is indeed true for any N.

We have also discussed the possible connections between the Majorana constellations for the stars and some other problems involving symmetry of points on a sphere, namely the Thomson problem and the Queens of quantumness. The conclusion is that although the problems are related, the fact that the solutions coincide for small dimensions is surely due to the limited degrees of freedom low-dimensional systems offer. When the dimension becomes larger, say involving more than ten points, the solutions are no longer identical except perhaps for when 'exact' symmetry is possible, as is the case for the Platonic solid constellations.

The maximally unpolarized states are an academic curiosity in that they can be said to be the most nonclassical polarization states. In a more practical setting, they seem to be the optimal states for detecting small SU(2) rotations around an arbitrary unknown axis. However, there are still many things to explore: for example, what is the significance of the strength of the first nonzero multipole of a maximally unpolarized state? The cumulative distribution $\mathcal{A}_M^{(S)}$ may increase in different ways as seen in figure 3, but since $\mathcal{A}_{2S}^{(S)} = 2S/(2S+1)$ for any pure state, a slower growth for small M must be compensated by a faster growth for larger M. What difference do different constellations make on the fundamental and on the application level?

It is also still unclear why there seems to be such a strong connection between spherical t-designs and maximally unpolarized states. In particular, this connection seems unjustified, as the optimal Majorana constellations do not coincide.

In summary, one can use the example of maximally unpolarized states to marvel about the connections between different branches of science, and on how some seemingly simple problems—distributing points in the most symmetric manner on a sphere—can illuminate such complicated optimization problems that we have just described. The science of light is fantastic!

Acknowledgments

The authors acknowledge interesting discussions with Daniel Braun, Olivia di Matteo and Juan J Monzón. Financial support was obtained from the Swedish Research Council (VR) through its support of Linnaeus Center of Excellence ADOPT and by Grant No. 621-2011-4575. We also thank the European Union FP7 (Grant Q-ESSENCE), the Spanish MINECO (Grant FIS2011-26786) and the Program UCM-BSCH (Grant GR3/14). GB thanks the MPL for hosting him and the Wenner-Gren Foundation for economic support during the autumn of 2014.

References

[1] Stokes G G 1852 On the composition and resolution of streams of polarized light from different sources *Trans. Camb. Phil. Soc.* **9** 399–416
[2] Klyshko D N 1992 Multiphoton interference and polarization effects *Phys. Lett.* A **163** 349–55
[3] Bushev P A, Karassiov V P, Masalov A V and Putilin A A 2001 Biphoton light with hidden polarization and its polarization tomography *Opt. Spectrosc.* **91** 526–31
[4] Majorana E 1932 Atomi orientati in campo magnetico variabile *Nuovo Cimento* **9** 43–50
[5] Conway J H, Hardin R H and Sloane N J A 1996 Packing lines, planes, etc: packings in Grassmannian spaces *Exp. Math.* **5** 139–59
[6] Saff E B and Kuijlaars A B J 1997 Distributing many points on a sphere *Math. Intell.* **19** 5–11
[7] Conway J H and Sloane N J A 1998 *Sphere Packings: Lattices and Groups* 3rd edn (Berlin: Springer)
[8] Collett E 1970 Stokes parameters for quantum systems *Am. J. Phys.* **38** 563–74
[9] Born M and Wolf E 1999 *Principles of Optics* 7th edn (Cambridge: Cambridge University Press)
[10] Raymer M G, McAlister D F and Funk A 2000 Measuring the quantum polarization state of light *Quantum Communication, Computing, and Measurement 2* ed P Kumar (New York: Plenum)
[11] Karassiov V P and Masalov A V 2004 The method of polarization tomography of radiation in quantum optics *JETP* **99** 51–60
[12] Fano U and Racah G 1959 *Irreducible Tensorial Sets* (New York: Academic)
[13] Blum K 1981 *Density Matrix Theory and Applications* (New York: Plenum)
[14] Sánchez-Soto L L, Klimov A B, de la Hoz P and Leuchs G 2013 Quantum versus classical polarization states: when multipoles count *J. Phys. B: At. Mol. Opt. Phys.* **46** 104011
[15] de la Hoz P, Klimov A B, Björk G, Kim Y H, Müller C, Marquardt Ch, Leuchs G and Sánchez-Soto L L 2013 Multipolar hierarchy of efficient quantum polarization measures *Phys. Rev.* A **88** 063803
[16] de la Hoz P, Björk G, Klimov A B, Leuchs G and Sánchez-Soto L L 2014 Unpolarized states and hidden polarization *Phys. Rev.* A **90** 043826
[17] Arecchi F T, Courtens E, Gilmore R and Thomas H 1972 Atomic coherent states in quantum optics *Phys. Rev.* A **6** 2211–37
[18] Perelomov A 1986 *Generalized Coherent States and their Applications* (Berlin: Springer)

[19] Delbourgo R and Fox J R 1977 Maximum weight vectors possess minimal uncertainty *J. Phys. A: Math. Gen.* **10** 233–5

[20] Lee C T 1988 Wehrl's entropy of spin states and Lieb's conjecture *J. Phys. A: Math. Gen.* **21** 3749–56

[21] Björk G, Klimov A B, de la Hoz P, Grassl M, Leuchs G and Sánchez-Soto L L 2015 Extremal quantum states and their Majorana constellations *Phys. Rev.* A **92** 031801(R)

[22] Zimba J 2006 Anticoherent spin states via the Majorana representation *EJTP* **3** 143–56

[23] Hofmann H F 2004 Generation of highly nonclassical n-photon polarization states by superbunching at a photon bottleneck *Phys. Rev.* A **70** 023812

[24] Crann J, Pereira R and Kribs D W 2010 Spherical designs and anticoherent spin states *J. Phys. A: Math. Theor.* **43** 255307

[25] Bannai E and Tagami M 2011 A note on anticoherent spin states *J. Phys. A: Math. Theor.* **44** 342002

[26] Prakash H and Chandra N 1971 Density operator of unpolarized radiation *Phys. Rev.* A **4** 796–9

[27] Agarwal G S 1971 On the state of unpolarized radiation *Lett. Nuovo Cimento* **1** 53–56

[28] Adams W W and Loustaunau P 1994 *An Introduction to Gröbner Bases* (Providence, RI: American Mathematical Society)

[29] http://magma.maths.usyd.edu.au/magma/

[30] Bosma W, Cannon J and Playoust C 1997 The Magma algebra system: I. The user language *J. Symb. Comput.* **24** 235–65

[31] http://polarization.markus-grassl.de/

[32] Kolenderski P and Demkowicz-Dobrzanski R 2008 Optimal state for keeping reference frames aligned and the platonic solids *Phys. Rev.* A **78** 052333

[33] Delsarte P, Goethals J M and Seidel J J 1977 Spherical codes and designs *Geom. Dedicata* **6** 363–88

[34] Hardin R H and Sloane N J A 1992 New spherical 4-designs *Discrete Math.* **106/107** 255–64

[35] Hardin R H and Sloane N J A 1996 Mclaren's improved snub cube and other new spherical designs in three-dimensions *Discrete Comput. Geom.* **15** 429–41

[36] Thomson J J 1904 On the structure of the atom: an investigation of the stability and periods of oscillation of a number of corpuscles arranged at equal intervals around the circumference of a circle; with application of the results to the theory of atomic structure *Phil. Mag. Ser. 6* **7** 37265

[37] Ashby N and Brittin W E 1986 Thomson's problem *Am. J. Phys.* **54** 776–7

[38] Edmundson J R 1992 The distribution of point charges on the surface of a sphere *Acta Crystallogr.* A **48** 46–60

[39] Melnyk T H, Knop O and Smith W R 1977 Extremal arrangements of points and unit charges on a sphere: equilibrium configurations revisited *Can. J. Chem.* **55** 1745–61

[40] Giraud O, Braun P and Braun D 2010 Quantifying quantumness and the quest for queens of quantum *New J. Phys.* **12** 063005

[41] Aulbach M, Markham D and Murao M 2010 The maximally entangled symmetric state in terms of the geometric measure *New J. Phys* **12** 073025

[42] Giraud O, Braun D, Baguette D, Bastin T and Martin J 2015 Tensor representation of spin states *Phys. Rev. Lett.* **114** 080401

[43] Arnaud L and Cerf N J 2013 Exploring pure quantum states with maximally mixed reductions *Phys. Rev.* A **87** 012319

[44] Baecklund A and Bengtsson I 2014 Four remarks on spin coherent states *Phys. Scr.* T **163** 014012

[45] Tammes P M L 1930 On the origin of number and arrangement of places of exit on the surface of pollen grains *Recueil Trav. Bot. Néerl.* **27** 1–84

[46] Erber T and Hockney G M 1991 Equilibrium configurations of *n* equal charges on a sphere *J. Phys. A: Math. Gen.* **24** L1369–74

[47] Bollinger J J, Itano W M, Wineland D J and Heinzen D J 1996 Optimal frequency measurements with maximally correlated states *Phys. Rev.* A **54** 4649–52

[48] Mandelstam L and Tamm I 1945 The uncertainty relation between energy and time in nonrelativistic quantum mechanics *J. Phys. USSR* **9** 249–54

[49] Taddei M M, Escher B M, Davidovich L and de Matos Filho R L 2013 Quantum speed limit for physical processes *Phys. Rev. Lett.* **110** 050402

[50] del Campo A, Egusquiza I L, Plenio M B and Huelga S F 2013 Quantum speed limits in open system dynamics *Phys. Rev. Lett.* **110** 050403

Paper 10

G. Björk, A. B. Klimov, M. Grassl, P. de la Hoz, G. Leuchs, L. L. Sánchez-Soto:

"Extremal quantum states and their Majorana constellations",

Physical Review A **92**, 031801(R) (2015)

PHYSICAL REVIEW A **92**, 031801(R) (2015)

Extremal quantum states and their Majorana constellations

G. Björk,[1] A. B. Klimov,[2] P. de la Hoz,[3] M. Grassl,[4,5] G. Leuchs,[4,5] and L. L. Sánchez-Soto[3,4,5]

[1]*Department of Applied Physics, Royal Institute of Technology (KTH), AlbaNova, SE-106 91 Stockholm, Sweden*

[2]*Departamento de Física, Universidad de Guadalajara, 44420 Guadalajara, Jalisco, Mexico*

[3]*Departamento de Óptica, Facultad de Física, Universidad Complutense, E-28040 Madrid, Spain*

[4]*Max-Planck-Institut für die Physik des Lichts, Günther-Scharowsky-Straße 1, Bau 24, D-91058 Erlangen, Germany*

[5]*Institut für Optik, Information und Photonik, Universität Erlangen-Nürnberg, Staudtstraße 7/B2, D-91058 Erlangen, Germany*

(Received 26 March 2015; revised manuscript received 11 June 2015; published 1 September 2015)

The characterization of quantum polarization of light requires knowledge of all the moments of the Stokes variables, which are appropriately encoded in the multipole expansion of the density matrix. We look into the cumulative distribution of those multipoles and work out the corresponding extremal pure states. We find that SU(2) coherent states are maximal to any order whereas the converse case of minimal states (which can be seen as the most quantum ones) is investigated for a diverse range of the number of photons. Taking advantage of the Majorana representation, we recast the problem as that of distributing a number of points uniformly over the surface of the Poincaré sphere.

DOI: 10.1103/PhysRevA.92.031801 PACS number(s): 42.50.Ar, 42.25.Ja, 42.50.Dv, 42.50.Lc

Introduction. Stokes variables constitute an invaluable tool for assessing light polarization, both in the classical and quantum domains. They can be efficiently measured and lead to an elegant geometric representation, the Poincaré sphere, which not only provides remarkable insights, but also greatly simplifies otherwise complex problems.

Classical polarization is chiefly built on the first-order moments of the Stokes parameters: states are pictured as points on the Poincaré sphere (i.e., neglecting fluctuations altogether). Nowadays, however, there is a general agreement that a thorough understanding of the effects arising in the realm of the quantum world calls for an analysis of higher-order polarization fluctuations [1–7]. In fact, this is what comes up in coherence theory, where, in general, one needs a hierarchy of correlation functions to specify a field.

Recently, we have laid the foundations for a systematic solution to this fundamental and longstanding question [8–10]. The backbone of our proposal is a multipole expansion of the density matrix, which naturally sorts successive moments of the Stokes variables. The dipole term, being just the first-order moment, renders the classical picture, while the other multipoles account for the fluctuations we wish to scrutinize. Consequently, the cumulative distribution for these multipoles yields complete information about the polarization properties.

This Rapid Communication represents a substantial step ahead in this program, as we elaborate on the extremal states for the aforementioned multipole distribution. We find that the SU(2) coherent states maximize it to any order, so they are the most polarized allowed by quantum theory. We determine as well the states that kill the cumulative distribution up to a given order M: they serve precisely as the opposite of SU(2) coherent states and hence can be considered as the kings of quantumness. Furthermore, employing the striking advantages of the Majorana representation [11], these kings appear naturally related to the problem of distributing N points on the Poincaré sphere in the "most symmetric" fashion, a problem with a long history and many different solutions depending on the cost function one tries to optimize [12,13].

Polarization multipoles. The quantum Stokes operators are defined as [14]

$$\hat{S}_x = \frac{1}{2}(\hat{a}_+^\dagger \hat{a}_- + \hat{a}_-^\dagger \hat{a}_+), \quad \hat{S}_y = \frac{i}{2}(\hat{a}_+ \hat{a}_-^\dagger - \hat{a}_+^\dagger \hat{a}_-),$$
$$\hat{S}_z = \frac{1}{2}(\hat{a}_+^\dagger \hat{a}_+ - \hat{a}_-^\dagger \hat{a}_-), \tag{1}$$

together with the total photon number $\hat{N} = \hat{a}_+^\dagger \hat{a}_+ + \hat{a}_-^\dagger \hat{a}_-$. Here, $\hat{a}_+$ and $\hat{a}_-$ represent the amplitudes in two circularly polarized orthogonal modes. We have that $[\hat{a}_k, \hat{a}_\ell^\dagger] = \delta_{k\ell}$, $k,\ell \in \{+,-\}$, with $\hbar = 1$ throughout and the superscript $\dagger$ stands for the Hermitian conjugate. The definition (1) differs by a factor $1/2$ from its classical counterpart [15], but in this way the components of the vector $\hat{\mathbf{S}} = (\hat{S}_x, \hat{S}_y, \hat{S}_z)$ satisfy the su(2) commutation relations: $[\hat{S}_x, \hat{S}_y] = i\hat{S}_z$ and cyclic permutations. For an N-photon state, $\hat{\mathbf{S}}^2 = S(S+1)\hat{\mathbb{1}}$, where $S = N/2$, so the number of photons fixes the effective spin.

Put in a different way, (1) is nothing but the Schwinger representation of the su(2) algebra. Consequently, the ideas to be explored here are by no means restricted to polarization, but concern numerous instances wherein su(2) is the fundamental symmetry [16].

In our case, $[\hat{N}, \hat{\mathbf{S}}] = 0$, so each subspace with a fixed number of photons ought to be addressed separately. To bring out this fact more prominently, instead of the Fock states $\{|n_+, n_-\rangle\}$, we employ the relabeling $|S,m\rangle \equiv |n_+ = S+m, n_- = S-m\rangle$, which can be thought of as the common eigenstates of $\hat{\mathbf{S}}^2$ and $\hat{S}_z$. For each fixed S, m runs from $-S$ to S, and the states $\{|S,m\rangle\}$ span a $(2S+1)$-dimensional invariant subspace [17].

As a result, the only accessible information from any density matrix $\hat{\rho}$ is its block-diagonal form $\hat{\rho}_{\rm pol} = \bigoplus_S \hat{\rho}^{(S)}$, where $\hat{\rho}^{(S)}$ is the density matrix in the subspace of spin S. This $\hat{\rho}_{\rm pol}$ has been termed the polarization sector [18] or the polarization density matrix [19]. It is advantageous to expand each $\hat{\rho}^{(S)}$ as

$$\hat{\rho}^{(S)} = \sum_{K=0}^{2S} \sum_{q=-K}^{K} \rho_{Kq}^{(S)} \hat{T}_{Kq}^{(S)}, \tag{2}$$

rather than using directly the basis $\{|S,m\rangle\}$. The irreducible tensor operators $\hat{T}^{(S)}_{Kq}$ are [20,21]

$$\hat{T}^{(S)}_{Kq} = \sqrt{\frac{2K+1}{2S+1}} \sum_{m,m'=-S}^{S} C^{Sm'}_{Sm,Kq}\, |S,m'\rangle\langle S,m|, \qquad (3)$$

with $C^{Sm'}_{Sm,Kq}$ being Clebsch-Gordan coefficients ($0 \leqslant K \leqslant 2S$). These tensors form an orthonormal basis and have the right properties under SU(2) transformations. The crucial point is that $\hat{T}^{(S)}_{Kq}$ can be jotted down in terms of the Kth power of the Stokes operators.

The expansion coefficients $\rho^{(S)}_{Kq} = \mathrm{Tr}\,[\hat{\rho}^{(S)}\hat{T}^{(S)\dagger}_{Kq}]$ are known as state multipoles. The quantity $\sum_q |\rho^{(S)}_{Kq}|^2$ gauges the state overlapping with the Kth multipole pattern. For most states, only a limited number of multipoles play a substantive role and the rest of them have an exceedingly small contribution. Therefore, it seems more convenient to look at the cumulative distribution [9]

$$\mathcal{A}^{(S)}_M = \sum_{K=1}^{M} \sum_{q=-K}^{K} \left|\rho^{(S)}_{Kq}\right|^2, \qquad (4)$$

which sums polarization information up to order M ($1 \leqslant M \leqslant 2S$). Note that the monopole $K = 0$ is omitted, as it is just a constant term. As with any cumulative distribution, $\mathcal{A}^{(S)}_M$ is a monotonically nondecreasing function of the multipole order.

Maximal states. The distribution $\mathcal{A}^{(S)}_M$ can be regarded as a nonlinear functional of the density matrix $\hat{\rho}^{(S)}$. On that account, one can try to ascertain the states that maximize $\mathcal{A}^{(S)}_M$ for each order M. We shall be considering only pure states, which we expand as $|\Psi\rangle = \sum_{m=-S}^{S} \Psi_m\, |S,m\rangle$, with coefficients $\Psi_m = \langle S,m|\Psi\rangle$. We easily get

$$\mathcal{A}^{(S)}_M = \sum_{K=1}^{M} \sum_{q=-K}^{K} \frac{2K+1}{2S+1} \left| \sum_{m,m'=-S}^{S} C^{Sm'}_{Sm,Kq}\, \Psi_{m'} \Psi^*_m \right|^2. \qquad (5)$$

The details of the calculation are presented in the Appendix. We content ourselves with the final result: the maximum value is

$$\mathcal{A}^{(S)}_M = \frac{2S}{2S+1} - \frac{[\Gamma(2S+1)]^2}{\Gamma(2S-M)\Gamma(2S+M+2)}, \qquad (6)$$

and this happens for the state $|S,\pm S\rangle$, irrespective of M. Here, $\Gamma(x)$ stands for the Gamma function. Since $\mathcal{A}^{(S)}_M$ is invariant under polarization transformations, all the displaced versions $|\theta,\phi\rangle = (1+|\alpha|^2)^{-S} \exp(\alpha \hat{S}_+)|S,-S\rangle$ [with $\hat{S}_\pm = \hat{S}_x \pm i\hat{S}_y$ and the stereographic projection $\alpha = \tan(\theta/2)e^{-i\phi}$] also maximize $\mathcal{A}^{(S)}_M$. In other words, SU(2) coherent states $|\theta,\phi\rangle$ [22] maximize $\mathcal{A}^{(S)}_M$ for all orders M.

It will be useful in the following to exploit the Majorana representation [11], which maps every $(2S+1)$-dimensional pure state $|\Psi\rangle$ into the polynomial

$$\Psi(\alpha) = \sum_{m=-S}^{S} \sqrt{\frac{(2S)!}{(S-m)!(S+m)!}}\, \Psi_m \alpha^{S+m}. \qquad (7)$$

Up to a global unphysical factor, $|\Psi\rangle$ is determined by the set $\{\alpha_i\}$ of the $2S$ complex zeros of $\Psi(\alpha)$, suitably completed by points at infinity if the degree of $\Psi(\alpha)$ is less than $2S$. A nice geometrical representation of $|\Psi\rangle$ by $2S$ points on the unit sphere (often called the constellation) is obtained by an inverse stereographic map of $\{\alpha_i\} \mapsto \{\theta_i,\phi_i\}$. For SU(2) coherent states, the Majorana constellation collapses to a single point. States with the same Majorana constellation, irrespective of its relative orientation, share the same polarization properties.

The SU(2) Q function, defined as $Q(\theta,\phi) = |\langle\theta,\phi|\Psi\rangle|^2$, is an alternative way to depict the state. Although $Q(\theta,\phi)$ can be expressed in terms of the Majorana polynomial [and so $\{\alpha_i\}$ are also the zeros of $Q(\theta,\phi)$], sometimes the symmetry group of $|\Psi\rangle$ can be better appreciated with this function, which can be very valuable.

Minimal states. Next, we concentrate on minimizing $\mathcal{A}^{(S)}_M$. Obviously, the maximally mixed state $\hat{\rho}^{(S)} = \frac{1}{2S+1}\hat{\mathbb{1}}_{2S+1}$ kills all the multipoles and so indeed causes (4) to vanish for all M, being fully unpolarized [23,24]. Nonetheless, we are interested in pure Mth-order unpolarized states. The strategy we adopt is thus very simple to state: starting from a set of unknown normalized state amplitudes in Eq. (5), which we write as $\Psi_m = a_m + ib_m$ ($a_m,b_m \in \mathbb{R}$), we try to get $\mathcal{A}^{(S)}_M = 0$ for the highest possible M. This yields a system of polynomial equations of degree two for a_m and b_m, which we solve using Gröbner bases implemented in the computer algebra system MAGMA [25]. In this way, we get exact algebraic expressions and we can detect when there is no feasible solution.

Table I lists the resulting states (which, in some cases, are not unique) for different selected values of S [26]. We also indicate the associated Majorana constellations. For completeness, in Fig. 1 we also plot the constellations as well as the Q functions for some of these states.

Intuitively, one would expect that these constellations should have the points as symmetrically placed on the unit sphere as possible. This fits well with the notion of states of maximal Wehrl-Lieb entropy [27]. In more precise mathematical terms, such points may be generated via optimization with respect to a suitable criterion [13]. Here, we explore the connection with spherical t-designs [28], which are patterns of N points on a sphere such that every polynomial of degree at most t has the same average over the N points as over the sphere. Thus, the N points mimic a flat distribution up to order t, which obviously implies a fairly symmetric distribution.

For a given S, the maximal order of M for which we can cancel out $\mathcal{A}^{(S)}_M$ does not follow a clear pattern. The numerical evidence suggests that $M_{\max}$ coincides with $t_{\max}$ in the corresponding spherical design, but further work is needed to support this conjecture.

The simplest nontrivial example is that of two-photon states, $S = 1$. We find only first-order unpolarized states: these are biphotons generated in spontaneous parametric down-conversion, which were the first known to have hidden polarization [30].

With three photons, $S = 3/2$, we have again only first-order unpolarized states: the constellation is an equilateral triangle inscribed in a great circle, which can be taken as the equator. This coincides with the three-point spherical 1-design.

For $S = 2$, the Majorana constellation is a regular tetrahedron: it is the least-excited second-order unpolarized state. It

TABLE I. States that kill $\mathcal{A}_M^{(S)}$ for the indicated values of S. In the second column, we indicate the order M, which we conjecture is the highest possible. We give the nonzero state components Ψ_m ($m = -S, \ldots, S$) and the Majorana constellation. We include the associated spherical t-design (with the maximal t value) and the queens of quantumness (with their unpolarization degree). "Same", "Similar," and "Different" always refer to the closest description column to the left.

S	M	State	Constellation	Design	t	Queens	M
1	1	$\Psi_0 = 1$	Radial line	Same	1	Same	1
$\frac{3}{2}$	1	$\Psi_{-\frac{3}{2}} = \Psi_{\frac{3}{2}} = \frac{1}{\sqrt{2}}$	Equatorial triangle	Same	1	Same	1
2	2	$\Psi_{-1} = \frac{1}{\sqrt{3}}$, $\Psi_2 = \sqrt{\frac{2}{3}}$	Tetrahedron	Same	2	Same	2
$\frac{5}{2}$	1	$\Psi_{-\frac{5}{2}} = \Psi_{\frac{5}{2}} = \frac{1}{\sqrt{2}}$	Equatorial triangle + poles	Same	1	Same	1
3	3	$\Psi_{-2} = \Psi_2 = \frac{1}{\sqrt{2}}$	Octahedron	Same	3	Same	3
$\frac{7}{2}$	2	$\Psi_{-\frac{5}{2}} = \Psi_{\frac{1}{2}} = \sqrt{\frac{7}{18}}$, $\Psi_{\frac{7}{2}} = \sqrt{\frac{2}{9}}$	Two triangles + pole	Similar	2	Equatorial pentagon + poles	1
4	3	$\Psi_{-4} = \Psi_4 = \sqrt{\frac{5}{24}}$, $\Psi_0 = \sqrt{\frac{7}{12}}$	Cube	Same	3	See Ref. [29]	1
$\frac{9}{2}$	2	$\Psi_{-\frac{9}{2}} = \Psi_{\frac{9}{2}} = \frac{1}{\sqrt{6}}$, $\Psi_{-\frac{3}{2}} = \Psi_{\frac{3}{2}} = \frac{1}{\sqrt{3}}$	Three triangles	Similar	2	Similar	1
5	3	$\Psi_{-5} = \Psi_5 = \frac{1}{\sqrt{3}}$, $\Psi_0 = \frac{1}{\sqrt{5}}$	Pentagonal prism	Similar	3	Two staggered squares + poles	1
$\frac{11}{2}$	3	$\Psi_{-\frac{11}{2}} = \Psi_{\frac{11}{2}} = \frac{\sqrt{17}}{12}$, $\Psi_{-\frac{5}{2}} = \Psi_{\frac{5}{2}} = i\frac{\sqrt{55}}{12}$	Pentagon + two triangles	Similar	3	Similar	1
6	5	$\Psi_{-5} = -\Psi_5 = \frac{\sqrt{7}}{5}$, $\Psi_0 = -\frac{\sqrt{11}}{5}$	Icosahedron	Same	5	Same	5
7	4	$\Psi_{-6} = \Psi_6 = \sqrt{\frac{854}{3645}}$, $\Psi_{-3} = \Psi_3 = \sqrt{\frac{637}{13\,420}} + i\sqrt{\frac{512\,603}{9\,783\,180}}$, $\Psi_0 = \sqrt{\frac{12\,561\,757}{163\,053\,000}} - i\sqrt{\frac{512\,603}{2\,013\,000}}$	Three squares + poles	Different	4	–	–
10	5	$\Psi_{-10} = \Psi_{10} = \sqrt{\frac{187}{1875}}$, $\Psi_{-5} = -\Psi_5 = \sqrt{\frac{209}{625}}$, $\Psi_0 = \sqrt{\frac{247}{1875}}$	Deformed dodecahedron	Similar	5	–	–

is not surprising that the tetrahedron is the 2-design with the lowest number of points.

The case $S = 5/2$ does not admit a high degree of spherical symmetry: only first-order unpolarized states exist. There are neither five-photon $M = 2$ unpolarized states [31,32] nor five-point 2-designs [33].

When increasing the number of photons to six, $S = 3$, another Platonic solid appears: the regular octahedron. Now, we have the least-excited third-order unpolarized states, which, in addition, take on the maximum sum of the Stokes variances.

For $S = 7/2$, an $M = 2$ constellation consists of the north pole, an equilateral triangle inscribed at the $z = 0.2424$ plane, and another equilateral triangle, with the same orientation (e.g., one vertex on the x axis) at the $z = -0.5816$ plane. The spherical t-design has a larger separation between the triangles, but the corresponding Stokes vector does not vanish, so the t-design does not coincide with any unpolarized state.

The next Platonic solid, the cube, appears when $S = 4$. The state is third-order unpolarized and its Majorana constellation coincides with the eight-point spherical 3-design, which is the tightest for this number of points.

A nine-photon second-order unpolarized state, $S = 9/2$, is generated by three equilateral triangles with the same orientation inscribed in the equator and in two symmetric rings. The highest nine-point spherical t-design has $t = 2$ and a similar, but not identical, configuration because the two smaller triangles are displaced by a larger distance from the equator than the previous constellation. As a consequence, the nine-point spherical 2-design is only first-order unpolarized.

The Majorana constellation for a maximally unpolarized 10-photon state ($S = 5$) is similar to the matching spherical t-design and consists of two identical regular pentagons inscribed in rings symmetrically displaced from the equator. The maximally unpolarized state has the two pentagons a bit

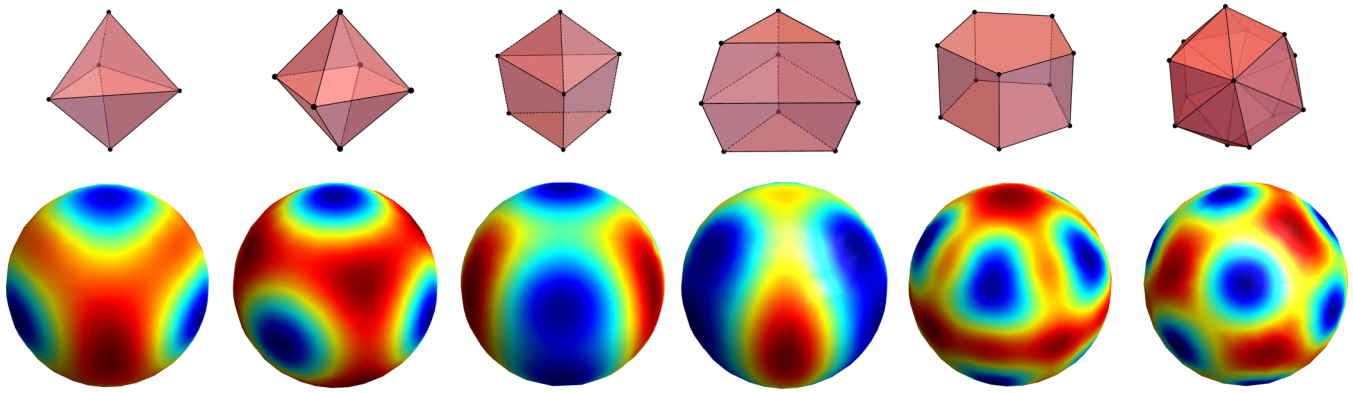

FIG. 1. (Color online) Density plots of the SU(2) Q functions for the optimal states in Table I for the cases $S = 5/2$, 3, $7/2$, $9/2$, 5, and 7 (from left to right, blue indicates the zero values and red maximal ones). On top, we sketch the Majorana constellation for each of them.

closer to the equator than the spherical 3-design (that has $M = 1$).

For larger photon numbers, the computational complexity of finding optimal designs becomes a real hurdle. The t-designs have been investigated in the range 2–100 and numerical evidence suggests that the optimal designs (in some instances, they are not unique) have been found [34]. However, for some dimensions, e.g., 12 ($S = 6$) and 20 ($S = 10$), one would naively guess that the optimal designs fit with the icosahedron and the dodecahedron. For $S = 6$ this turns out to be a correct guess, the corresponding state is unpolarized to the same order as the spherical 5-design formed by the icosahedron. For $S = 10$ this intuition fails: the optimal t-design is indeed a dodecahedron, but this Majorana constellation is third-order unpolarized, whereas this is a spherical 5-design. If the dodecahedron is stretched (i.e., the four pentagonal rings that define its vertices are displaced against the pole), one can find a 20-photon fifth-order unpolarized state.

To check the correspondence between unpolarized states and optimal t-designs we look at dimension 14, which is the smallest number of points for which a spherical 4-design, but not a 5-design, exists. This consists of four equilateral triangles that are pairwise similar in size, displaced from the equator by the same distance, and rotated an angle $\pm\alpha$ or $\pm\beta$ around their surface normal, plus the two poles. The t-design state is only first-order unpolarized, but if the spacing and triangle orientation is optimized, the design can be made third-order unpolarized. There is indeed a 14-photon state that is fourth-order unpolarized: its Majorana constellation is made of three quadrangles and the poles, but this is only a 1-design.

To round up, it is worth commenting on the connections that our theory shares with two recently introduced notions: anticoherent states [35] and queens of quantumness [29]. For completeness, in Table I we have also listed the configurations and the degree of unpolarization for these queens. Anticoherent states are in a sense "the opposite" of SU(2) coherent states: while the latter correspond as nearly as possible to a classical spin vector pointing in a given direction, the former "point nowhere," i.e., the average Stokes vector vanishes and the fluctuations up to order M are isotropic. The queens of quantumness are the most distant states (in the sense of a Hilbert-Schmidt distance) to the classical ones (states than can be written as a convex sum of projectors onto coherent states). In particular low-dimensional cases, these two instances coincide with our optimal states. However, we stress that our theory is built from first principles, starting from magnitudes that are routinely determined in the laboratory. Besides, we have an algebraic criterion, namely, the vanishing of the cumulative multipole distribution, that can be handled in a clear and compact manner.

When we interpret our $(2S + 1)$-dimensional subspace as the symmetric subspace of a system of S qubits, the kings appear also closely linked to other intriguing problems, such as maximally entangled symmetric states [36,37] and k-maximally mixed states [38,39].

Applications. The main goal of quantum metrology is to measure a physical magnitude with surprising precision by exploiting quantum resources. In particular, tailoring polarization states to better detect SU(2) rotations is quite a relevant problem with direct applications to magnetometry, polarimetry, and metrology, in general [40].

In this respect, NOON states [defined as $|N00N\rangle = (|S,S\rangle - |S,-S\rangle)/\sqrt{2}$] are known to be maximally sensitive to small phase shifts (i.e., to small rotations about the S_z axis) for a fixed excitation S [41]. This can be easily understood by looking at their Majorana constellation, which consists in just $2S$ equidistantly placed points around the Poincaré sphere equator. Since a rotation around the S_z axis is described by the unitary operator $\hat{U}(\vartheta) = \exp(-i\vartheta\hat{S}_z/2)$, the states $|N00N\rangle$ and $\hat{U}(\vartheta)|N00N\rangle$ are orthogonal for $\pi/(2S)$. However, to make optimal use of a NOON state it is essential to know the rotation axis so as to ensure that the state is aligned with the axis to achieve its best sensitivity: the rotation resolution is thus highly directional for a NOON state.

This is precisely the advantage of maximally unpolarized states: Having a high degree of spherical symmetry, they resolve rotations around any axis approximately equally well. This has been confirmed for the Platonic solids [31]: Platonic states saturate the optimal average sensitivity to rotations about any axis; NOON states outperform these states about one specific axis [42]. Indeed, for the Platonic solids, rotations around all the facets normal axes map the Majorana constellation onto itself for rotations of $2\pi/3$ (tetrahedron, octahedron, and icosahedron), $\pi/2$ (cube), or $2\pi/5$ (dodecahedron). It is clear that for other constellations and other rotation axes the Majorana constellation will only become approximately identical, but the statement is more likely to hold true.

In a different vein, we draw attention to the structural similarity between the kings of quantumness and quantum error correcting codes: in both cases, low-order terms in the expansion of the density matrices are required to vanish.

As a final but relevant remark, we stress that all the basic tools needed for our treatment (Schwinger representation, multipole expansion, and constellations) have been extended in a direct way to other symmetries, such as SU(3) [43] or Heisenberg-Weyl [44]. Therefore, the notion of kings of quantumness can be easily developed for other systems. Work along these lines is already in progress in our group.

Concluding remarks. In short, we have consistently reaped the benefits of the cumulative distribution of polarization multipoles, which is a sensible and experimentally realizable quantity. We have proven that SU(2) coherent states maximize that quantity to all orders: in this way, they manifest their classical virtues. Their opposite counterparts, minimizing that quantity, are certainly the kings of quantumness.

Apart from their indisputable geometrical beauty, there surely is plenty of room for the application of these states, whose generation has started to be seriously considered in several groups.

Acknowledgments. The authors acknowledge interesting discussions with Professor Daniel Braun and Olivia di Matteo. Financial support from the Swedish Research Council (VR) through its Linnaeus Center of Excellence ADOPT and Contract No. 621-2011-4575, the CONACyT (Grant No. 106525), the European Union FP7 (Grant Q-ESSENCE), and

the Program UCM-Banco Santander (Grant No. GR3/14) is gratefully acknowledged. G.B. thanks the MPL for hosting him and the Wenner-Gren Foundation for economic support.

Appendix: Optimal states. We have to maximize the cumulative multipole distribution (4) for a pure state $|\Psi\rangle = \sum_{m=-S}^{S} \Psi_m |S,m\rangle$, which takes the form (5). If we use an integral representation for the product of two Clebsch-Gordan coefficients [17], we get

$$\mathcal{A}_M^{(S)} = \sum_{m,m'=-S}^{S} \sum_{n,n'=-S}^{S} \frac{2S+1}{8\pi^2} \sum_{K=0}^{M} \sum_{q=-K}^{K} \frac{2K+1}{2S+1} \Psi_{m'} \Psi_m^* \Psi_n \Psi_{n'}^* \times \int dR\, D_{mn}^{S}(R) D_{m'n'}^{S*}(R) D_{qq}^{K}(R), \tag{A1}$$

where D_{mn}^{S} are the Wigner D functions and R refers to the three Euler angles (α,β,γ) and the integration is on the group manifold

$$\int dR\ f(R) \equiv \int_0^{2\pi} d\alpha \int_0^{\pi} d\beta \sin\beta \int_0^{2\pi} d\gamma f(\alpha,\beta,\gamma). \tag{A2}$$

Since

$$\sum_{q=-K}^{K} D_{qq}^{K}(R) = \chi_K(\omega), \tag{A3}$$

where $\chi_K(\omega)$ is a SU(2) generalized character and $\cos(\omega/2) = \cos(\beta/2)\cos[(\alpha+\gamma)/2]$, we rewrite $\mathcal{A}_M^{(S)}$ as

$$\mathcal{A}_M^{(S)} = \sum_{K=0}^{M} \frac{2K+1}{8\pi^2} \int dR\, \chi_K(\omega) \left|\langle\Psi|\hat{T}_g^S|\Psi\rangle\right|^2, \tag{A4}$$

and $\hat{T}_g$ is the group action. Then, we observe that the above is

$$\mathcal{A}_M^{(S)} = \mathrm{Tr}\left[|\Psi\rangle\langle\Psi| \otimes |\tilde{\Psi}\rangle\langle\tilde{\Psi}| \times \sum_{K=0}^{M} \frac{2K+1}{8\pi^2} \int dR\, \chi_K(\omega) \hat{T}_g^S \otimes \hat{T}_g^S \right], \tag{A5}$$

with

$$|\tilde{\Psi}\rangle = \sum_{m=-S}^{S} (-1)^m\, \Psi_{-m}^* |S,m\rangle. \tag{A6}$$

Because the integral

$$\frac{1}{4\pi^2} \int dR\, \chi_K(\omega) \hat{T}_g^S \otimes \hat{T}_g^{S\dagger} = c_K \Pi_K, \tag{A7}$$

where Π_K is the identity on the $(2K+1)$-dimensional irreducible SU(2) subspace which appear in the tensor product of $\mathcal{H}_S \otimes \mathcal{H}_S$ [i.e., $\mathrm{Tr}(\Pi_K) = 2K+1$], then

$$\mathcal{A}_M^{(S)} = \sum_{K=1}^{M} \langle\tilde{\Psi}|\langle\Psi|\Pi_K|\Psi\rangle|\tilde{\Psi}\rangle. \tag{A8}$$

Such an overlap is maximized (all coefficients are the same) whenever in every subspace of dim $2K+1$ there is only one element from the decomposition $|\Psi\rangle|\tilde{\Psi}\rangle$, which is consistent with (A6). The only states that produce a single state in each invariant subspace are the basis states $|S,m\rangle$, so that $|\tilde{\Psi}\rangle = (-1)^m |S,-m\rangle$, then

$$\mathcal{A}_M^{(S)} = \sum_{K=1}^{M} \frac{2K+1}{2S+1} \left|C_{SS,K0}^{SS}\right|^2. \tag{A9}$$

Since the maximum value of $C_{Sm,K0}^{Sm}$ is $C_{SS,K0}^{SS}$, the states $|S,\pm S\rangle$ maximize $\mathcal{A}_M^{(S)}$, as heralded before.

[1] A. B. Klimov, L. L. Sánchez-Soto, E. C. Yustas, J. Söderholm, and G. Björk, Distance-based degrees of polarization for a quantum field, Phys. Rev. A **72**, 033813 (2005).

[2] A. Sehat, J. Söderholm, G. Björk, P. Espinoza, A. B. Klimov, and L. L. Sánchez-Soto, Quantum polarization properties of two-mode energy eigenstates, Phys. Rev. A **71**, 033818 (2005).

[3] C. Marquardt, J. Heersink, R. Dong, M. V. Chekhova, A. B. Klimov, L. L. Sánchez-Soto, U. L. Andersen, and G. Leuchs, Quantum Reconstruction of an Intense Polarization Squeezed Optical State, Phys. Rev. Lett. **99**, 220401 (2007).

[4] A. B. Klimov, G. Björk, J. Söderholm, L. S. Madsen, M. Lassen, U. L. Andersen, J. Heersink, R. Dong, C. Marquardt, G. Leuchs, and L. L. Sánchez-Soto, Assessing the Polarization of a Quantum Field from Stokes Fluctuations, Phys. Rev. Lett. **105**, 153602 (2010).

[5] C. R. Müller, B. Stoklasa, C. Peuntinger, C. Gabriel, J. Řeháček, Z. Hradil, A. B. Klimov, G. Leuchs, C. Marquardt, and L. L. Sánchez-Soto, Quantum polarization tomography of bright squeezed light, New J. Phys. **14**, 085002 (2012).

[6] G. Björk, J. Söderholm, Y. S. Kim, Y. S. Ra, H. T. Lim, C. Kothe, Y. H. Kim, L. L. Sánchez-Soto, and A. B. Klimov, Central-moment description of polarization for quantum states of light, Phys. Rev. A **85**, 053835 (2012).

[7] R. S. Singh and H. Prakash, Degree of polarization in quantum optics through the second generalization of intensity, Phys. Rev. A **87**, 025802 (2013).

[8] L. L. Sánchez-Soto, A. B. Klimov, P. de la Hoz, and G. Leuchs, Quantum versus classical polarization states: When multipoles count, J. Phys. B **46**, 104011 (2013).

[9] P. de la Hoz, A. B. Klimov, G. Björk, Y. H. Kim, C. Müller, C. Marquardt, G. Leuchs, and L. L. Sánchez-Soto, Multipolar hierarchy of efficient quantum polarization measures, Phys. Rev. A **88**, 063803 (2013).

[10] P. de la Hoz, G. Björk, A. B. Klimov, G. Leuchs, and L. L. Sánchez-Soto, Unpolarized states and hidden polarization, Phys. Rev. A **90**, 043826 (2014).

[11] E. Majorana, Atomi orientati in campo magnetico variabile, Nuovo Cimento **9**, 43 (1932).

[12] J. H. Conway, R. H. Hardin, and N. J. A. Sloane, Packing lines, planes, etc.: Packings in Grassmannian spaces, Exp. Math. **5**, 139 (1996).

[13] E. B. Saff and A. B. J. Kuijlaars, Distributing many points on a sphere, Math. Intell. **19**, 5 (1997).

[14] A. Luis and L. L. Sánchez-Soto, Quantum phase difference, phase measurements and Stokes operators, Prog. Opt. **41**, 421 (2000).
[15] M. Born and E. Wolf, *Principles of Optics*, 7th ed. (Cambridge University Press, Cambridge, UK, 1999).
[16] S. Chaturvedi, G. Marmo, and N. Mukunda, The Schwinger representation of a group: Concept and applications, Rev. Math. Phys. **18**, 887 (2006).
[17] D. A. Varshalovich, A. N. Moskalev, and V. K. Khersonskii, *Quantum Theory of Angular Momentum* (World Scientific, Singapore, 1988).
[18] M. G. Raymer, D. F. McAlister, and A. Funk, in *Quantum Communication, Computing, and Measurement 2*, edited by P. Kumar (Plenum, New York, 2000).
[19] V. P. Karassiov and A. V. Masalov, The method of polarization tomography of radiation in quantum optics, JETP **99**, 51 (2004).
[20] U. Fano and G. Racah, *Irreducible Tensorial Sets* (Academic Press, New York, 1959).
[21] K. Blum, *Density Matrix Theory and Applications* (Plenum, New York, 1981).
[22] A. Perelomov, *Generalized Coherent States and their Applications* (Springer, Berlin, 1986).
[23] H. Prakash and N. Chandra, Density operator of unpolarized radiation, Phys. Rev. A **4**, 796 (1971).
[24] G. S. Agarwal, On the state of unpolarized radiation, Lett. Nuovo Cimento **1**, 53 (1971).
[25] W. Bosma, J. Cannon, and C. Playoust, The Magma algebra system. I. the user language, J. Symbolic Comput. **24**, 235 (1997).
[26] A more detailed list of minimal states can be found at http://polarization.markus-grassl.de.
[27] A. Baecklund and I. Bengtsson, Four remarks on spin coherent states, Phys. Scr. **T163**, 014012 (2014).
[28] P. Delsarte, J. M. Goethals, and J. J. Seidel, Spherical codes and designs, Geom. Dedicata **6**, 363 (1977).
[29] O. Giraud, P. Braun, and D. Braun, Quantifying quantumness and the quest for queens of quantumness, New J. Phys. **12**, 063005 (2010).
[30] D. M. Klyshko, Polarization of light: Fourth-order effects and polarization-squeezed states, JETP **84**, 1065 (1997).
[31] P. Kolenderski and R. Demkowicz-Dobrzanski, Optimal state for keeping reference frames aligned and the platonic solids, Phys. Rev. A **78**, 052333 (2008).
[32] J. Crann, R. Pereira, and D. W. Kribs, Spherical designs and anticoherent spin states, J. Phys. A **43**, 255307 (2010).
[33] Y. Mimura, A construction of spherical 2-design, Graphs Combinator. **6**, 369 (1990).
[34] For a complete account, see http://neilsloane.com/sphdesigns/.
[35] J. Zimba, "Anticoherent" spin states via the Majorana representation, Electron. J. Theor. Phys. **3**, 143 (2006).
[36] M. Aulbach, D. Markham, and M. Murao, The maximally entangled symmetric state in terms of the geometric measure, New J. Phys. **12**, 073025 (2010).
[37] O. Giraud, D. Braun, D. Baguette, T. Bastin, and J. Martin, Tensor Representation of Spin States, Phys. Rev. Lett. **114**, 080401 (2015).
[38] L. Arnaud and N. J. Cerf, Exploring pure quantum states with maximally mixed reductions, Phys. Rev. A **87**, 012319 (2013).
[39] D. Goyeneche and K. Życzkowski, Genuinely multipartite entangled states and orthogonal arrays, Phys. Rev. A **90**, 022316 (2014).
[40] L. A. Rozema, D. H. Mahler, R. Blume-Kohout, and A. M. Steinberg, Optimizing the Choice of Spin-Squeezed States for Detecting and Characterizing Quantum Processes, Phys. Rev. X **4**, 041025 (2014).
[41] J. J. Bollinger, W. M. Itano, D. J. Wineland, and D. J. Heinzen, Optimal frequency measurements with maximally correlated states, Phys. Rev. A **54**, R4649 (1996).
[42] L. A. Rozema, Experimental quantum measurement with a few photons, Ph.D. thesis, University of Toronto, 2014.
[43] L. Bányai, N. Marinescu, I. Raszillier, and V. Rittenberg, Irreducible tensors for the group su(3), Commun. Math. Phys. **2**, 121 (1966).
[44] J. S. Ivan, N. Mukunda, and R. Simon, Moments of non-Gaussian Wigner distributions and a generalized uncertainty principle: I. the single-mode case, J. Phys. A: Math. Theor. **45**, 195305 (2012).

Paper 11

A. Aiello, G. S. Agarwal, M. Paur, B. Stoklasa, Z. Hradil, J. Rehacek,

P. de la Hoz, G. Leuchs, L. L. Sánchez Soto:

"Unraveling beam self-healing",

Optics Express **25**, 19147 (2017)

Research Article | Vol. 25, No. 16 | 7 Aug 2017 | OPTICS EXPRESS 19147
Optics EXPRESS

Unraveling beam self-healing

ANDREA AIELLO,[1,2] GIRISH S. AGARWAL,[3,4] MARTIN PAÚR,[5] BOHUMIL STOKLASA,[5] ZDENĚK HRADIL,[5] JAROSLAV ŘEHÁČEK,[5] PABLO DE LA HOZ,[6] GERD LEUCHS,[1] AND LUIS L. SÁNCHEZ-SOTO[1,6,*]

[1]*Max Planck Institut für die Physik des Lichts, Staudtstraße 2, 91058 Erlangen, Germany*
[2]*Institut für Theoretische Physik II, Friedrich-Alexander Universität Erlangen-Nürnberg, Staudtstraße 2, 91058 Erlangen, Germany*
[3]*Institute for Quantum Science and Engineering and Department of Biological and Agricultural Engineering, Texas A&M University, College Station, TX 77845, USA*
[4]*Department of Physics, Oklahoma State University, Stillwater, OK 74078, USA*
[5]*Department of Optics, Palacký University, 17. listopadu 12, 771 46 Olomouc, Czech Republic*
[6]*Departamento de Óptica, Facultad de Física, Universidad Complutense, 28040 Madrid, Spain*
[*]*lsanchez@fis.ucm.es*

Abstract: We show that, contrary to popular belief, diffraction-free beams not only may reconstruct themselves after hitting an opaque obstacle but also, for example, Gaussian beams. We unravel the mathematics and the physics underlying the self-reconstruction mechanism and we provide for a novel definition for the minimum reconstruction distance beyond geometric optics, which is in principle applicable to any optical beam that admits an angular spectrum representation. Moreover, we propose to quantify the self-reconstruction ability of a beam via a newly established degree of self-healing. This is defined via a comparison between the amplitudes, as opposite to intensities, of the original beam and the obstructed one. Such comparison is experimentally accomplished by tailoring an innovative experimental technique based upon Shack-Hartmann wave front reconstruction. We believe that these results can open new avenues in this field.

OCIS codes: (050.1940) Diffraction; (070.7345) Wave propagation; (260.1960) Diffraction theory.

References and links

1. Z. Bouchal, J. Wagner, M. Chlup, "Self-reconstruction of a distorted nondiffracting beam," Opt. Commun. **151**, 207–211 (1998).
2. M. V. Vasnetsov, I. G. Marienko, and M. S. Soskin, "Self-reconstruction of an optical vortex," JETP Lett. **71**, 130–133 (2000).
3. V. Garcés-Chávez, D. McGloin, M. D. Summers, A. Fernandez-Nieves, G. C. Splading, G. Cristobal, and K. Dholakia, "The reconstruction of optical angular momentum after distortion in amplitude, phase and polarization," J. Opt. A: Pure Appl. Opt. **6**, S235–S238 (2004).
4. J. Arlt, V. Garcés-Chávez, W. Sibbett, and K. Dholakia, "Optical micromanipulation using a Bessel light beam," Opt. Commun. **197**, 239–245 (2001).
5. V. Garcés-Chávez, D. McGloin, H. Melville, W. Sibbett, and K. Dholakia, "Simultaneous micromanipulation in multiple planes using a self-reconstructing light beam," Nature **419**, 145–147 (2002).
6. F. O. Fahrbach, P. Simon, and A. Rohrbach, "Microscopy with self-reconstructing beams," Nat. Phot. **4**, 780–785 (2010).
7. F. O. Fahrbach, and A. Rohrbach, "Propagation stability of self-reconstructing Bessel beams enables contrast-enhanced imaging in thick media," Nat. Commun. **3**, 632 (2012).
8. M. McLaren, T. Mhlanga, M. J. Padgett, F. S. Roux, and A. Forbes, "Self-healing of quantum entanglement after an obstruction," Nat. Commun. **5**, 3248 (2014).
9. J. Durnin, J. J. Miceli, Jr. and J. H. Eberly, "Diffraction-free beams," Phys. Rev. Lett. **58**, 1499–1501 (1987).
10. Z. Bouchal, "Resistance of nondiffracting vortex beams to amplitude and phase perturbations," Opt. Commun. **210**, 155–164 (2002).
11. S. H. Tao and X. Yuan, "Self-reconstruction property of fractional Bessel beams," J. Opt. Soc. Am. A **21**, 1192–1197 (2004).
12. P. Fischer, H. Little, R. L. Smith, C. Lopez-Mariscal, C. T. A. Brown, W. Sibbett and K. Dholakia, "Wavelength dependent propagation and reconstruction of white light Bessel beams," J. Opt. A **8**, 477–482 (2006).

#297092 https://doi.org/10.1364/OE.25.019147
Journal © 2017 Received 31 May 2017; revised 14 Jul 2017; accepted 15 Jul 2017; published 31 Jul 2017

Optics EXPRESS

13. X. Chu, "Analytical study on the self-healing property of Bessel beam," Eur. Phys. J. D **66**, 259 (2012).
14. J. Broky, G. A. Siviloglou, A. Dogariu, and D. N. Christodoulides, "Self-healing properties of optical Airy beams," Opt. Express **16**, 12880–12891 (2008).
15. M. Anguiano-Morales, A. Martínez, M. D. Iturbe-Castillo, S. Chávez-Cerda, and N. Alcalá-Ochoa, "Self-healing property of a caustic optical beam," Appl. Opt. **46**, 8284–8290 (2007).
16. P. Zhang, Y. Hu, T. Li, D. Cannan, X. Yin, R. Morandotti, Z. Chen, and X. Zhang, "Nonparaxial Mathieu and Weber accelerating beams," Phys. Rev. Lett. **109**, 193901 (2012).
17. V. Arrizón, D. Aguirre-Olivas, G. Mellado-Villaseñor, and S. Chávez-Cerda, "Self-healing in scaled propagation invariant beams," arXiv:1503.03125 (2015).
18. P. Vainty and R. P. Singh, "Self-healing property of optical ring lattice," Opt. Lett. **36**, 2994–2996 (2011).
19. J. D. Ring, J. Lindberg, A. Mourka, M. Mazilu, K. Dholakia, and M. R. Dennis, "Autofocusing and self-healing of Pearcey beams," Opt. Express **20**, 18955–18966 (2012).
20. S. Vyas, Y. Kozawa, and S. Sato, "Self-healing of tightly focused scalar and vector Bessel-Gauss beams at the focal plane," J. Opt. Soc. Am. A **28**, 837–843 (2011).
21. G. Wu, F. Wang, and Y. Cai, "Generation and self-healing of a radially polarized Bessel-Gauss beam," Phys. Rev. A **89**, 043807 (2014).
22. F. Wang, Y. Chen, X. Liu, Y. Cai, and S. A. Ponomarenko, "Self-reconstruction of partially coherent light beams scattered by opaque obstacles," Opt. Express **24**, 23735–23746 (2016).
23. A. Aiello, and G. S. Agarwal, "Wave-optics description of self-healing mechanism in Bessel beams," Opt. Lett. **39**, 6819–6822 (2014).
24. D. McGloin and K. Dholakia, "Bessel beams: Diffraction in a new light," Contemp. Phys. **46**, 15–28 (2005).
25. I. A. Litvin, M. G. Mclaren, and A. Forbes, "A conical wave approach to calculating suggBessel-Gauss beam reconstruction after complex obstacles," Opt. Commun. **282**, 1078–1082 (2009).
26. D. L. Andrews (Ed.), *Structured Light and Its Applications: An Introduction to Phase-Structured Beams and Nanoscale Optical Forces*, (Academic, 2008).
27. L. Mandel and E. Wolf, *Optical Coherence and Quantum Optics* (Cambridge University, 1995).
28. M. Born and E. Wolf, *Principles of Optics* (Cambridge University, 1999).
29. R. Kress, *Linear Integral Equations* (Springer, 1999).
30. K. Ball, "Ellipsoids of maximal volume in convex bodies," Geom. Dedic. **41**, 241–250 (1992).
31. M. A. Nielsen and I. L. Chuang, "Quantum Computation and Quantum Information," (Cambridge University, 2000).
32. X. Chu, and W. Wen, "Quantitative description of the self-healing ability of a beam," Opt. Express **22**, 6899–6904 (2012).
33. A. N. Kolmogorov and S. V. Fomin, *Elements of the Theory of Functions and Functional Analysis* (Dover, 1999).
34. M. Hillery, "Nonclassical distance in quantum optics," Phys. Rev. A **35**, 725–732 (1987).
35. V. Vedral, M. B. Plenio, M. A. Rippin, and P. L. Knight, "Quantifying entanglement," Phys. Rev. Lett. **78**, 2275–2278 (1997).
36. A. B. Klimov, L. L. Sánchez-Soto, E. C. Yustas, J. Söderholm, and G. Björk, "Distance-based degrees of polarization for a quantum field," Phys. Rev. A **72**, 033813 (2005).
37. S. Gnutzmann and K. Życzkowski, "Rényi–Wehrl entropies as measures of localization in phase space," J. Phys. A **34**, 10123 (2001).

1. Introduction

In recent years, the remarkable capacity of a beam to reconstruct itself after encountering an obstacle (frequently called self-healing) has attracted a good deal of attention [1–3] and has already found applications in diverse areas [4–8].

Self-healing has been long time considered as a distinctive feature of nondiffracting beams [9]; most prominently of Bessel beams [10–13], although also Airy [14], caustic [15], and Mathieu and Weber [16] beams have been examined.

It was subsequently realized that some diffracting beams, including the whole family of scaled propagation invariant beams [17] optical ring lattices [18], Pearcey beams [19], and tightly focused [20] and radially polarized [21] Bessel-Gauss beams, can self-reconstruct. However, there is still the widespread perception that the self-reconstruction hinges on engineering special beam profiles and, in many instances, it is sensitive to the obstruction size and shape, thereby limiting applications of this phenomenon [22].

Recently, a complete account of self-healing for Bessel beams has been given in terms of wave optics [23]. The basic mechanism can be entirely explained in terms of the propagation of plane waves with radial wave vectors lying on a ring. The results obtained are in agreement with the standard ones established from a geometrical approach [24, 25], yet they open a new

Optics EXPRESS

scope.

In this paper, still using a wave-optics methodology, we come to the conclusion that self-healingmay occur, potentially, for almost any kind of beam. Note, though, that it is outside the scope of most self-healing researches, and the present work is not an exception, the study of self-reconstruction capabilities of structured optical beams, as multiple-beam assemblies and, more generally, beams with complex and intricate intensity, polarization, frequency and temporal structures [26].

Furthermore, we introduce an appropriate degree that quantifies the similarity between the field of the unperturbed beam (namely, the beam that would propagate as if the obstacle were not present) and the field of the perturbed one (that is, the beam that propagates behind the obstruction). In this way, we put in evidence that self-healing is a property of both the intensity and the phase of the spatial distribution of the beam. We experimentally test these issues with a Gaussian beam, whose intensity and phase are measured by means of a CCD camera and a Shack-Hartman wavefront sensor, finding an outstanding agreement with our theoretical predictions.

2. Self-healing as an eigenvalue problem

Let us first set the stage for our construction. We consider a scalar field $\Psi(x, y, z)$ propagating along the z-axis. An obstruction, characterized by an amplitude transmission function $t_O(x, y)$, is placed in the plane $z = 0$. Here and hereafter with obstruction we denote any physical object that decreases the intensity of a light beam, possibly in a space-dependent manner, without changing directly phase and polarization of light. The amplitude $\Psi_O(x, y, 0)$ of the obstructed field at the plane $z = 0$ is

$$\Psi_O(x, y, 0) = t_O(x, y)\, \Psi(x, y, 0)\,. \tag{1}$$

The angular spectrum representation [27] is probably the most germane method to deal with the field propagation. Accordingly, the amplitude $\Psi_O(x, y, z)$ of the field transmitted at a distance z from the obstruction can be expressed as the plane-wave superposition

$$\Psi_O(x, y, z) = \frac{1}{(2\pi)^2} \iint_{-\infty}^{\infty} \exp(i\boldsymbol{\rho}\cdot\boldsymbol{\kappa}) \exp(izk_z) \left[\iint_{-\infty}^{\infty} \widehat{t_O}(\boldsymbol{\kappa} - \boldsymbol{\kappa}')\widehat{\Psi}(\boldsymbol{\kappa}')\, d^2\boldsymbol{\kappa}' \right] d^2\boldsymbol{\kappa}\,. \tag{2}$$

The wide hat (not to be confused with the small hat marking unit vectors) will denote throughout the spatial Fourier transform of the corresponding function evaluated at $z = 0$; i.e., its angular spectrum. Two-dimensional transverse vectors, in either real and Fourier space, are denoted with Greek letters: $\boldsymbol{\rho} = x\hat{x} + y\hat{y}$ and $\boldsymbol{\kappa} = k_x\hat{x} + k_y\hat{y}$. In addition, $k_z = (k^2 - \kappa^2)^{1/2}$, with $\kappa^2 = k_x^2 + k_y^2$.

Given the function $t_O(x, y)$, one can always define the transmission function $t_A(x, y)$ of an aperture complementary to the obstruction [28] via the Babinet principle $t_A(x, y) + t_O(x, y) = 1$. Therefore, (1) yields

$$\Psi_O(x, y, 0) = [1 - t_A(x, y)]\Psi(x, y, 0) \equiv \Psi(x, y, 0) - \Psi_A(x, y, 0). \tag{3}$$

Taking the absolute value squared of both sides of this equation and integrating over the whole xy-plane, we obtain

$$\mathcal{I}[\Psi_O] = \mathcal{I}[\Psi] + \mathcal{I}[\Psi_A] - 2\,\mathrm{Re} \iint_{-\infty}^{\infty} \Psi^*(x, y, 0)\Psi_A(x, y, 0)\, dxdy, \tag{4}$$

where $\mathcal{I}[h] = \iint_{-\infty}^{\infty} h^*(x, y, z)h(x, y, z)\, dxdy$ is the average beam intensity at the plane z.

Optics EXPRESS

Conventionally, a beam is dubbed self-healing when it has the ability to recover its amplitude or intensity profile after being obscured by an obstacle. Quite obviously, perfect self-reconstruction is impossible, even in principle, because, as Eq. (4) distinctly shows, the intensity of the transmitted field is unavoidably reduced unless $\mathcal{I}[\Psi_A] = 0$. We thus content ourselves with the condition

$$\Psi_O(x, y, z) \approx \lambda_0 \Psi(x, y, z)\,, \qquad \forall z \geq z_0\,, \tag{5}$$

where z_0 denotes the so-called minimum reconstruction distance and the scaling factor $\lambda_0 = \{\mathcal{I}[\Psi_O]/\mathcal{I}[\Psi]\}^{1/2}$ accounts for the average intensity reduction caused by the obstruction.

The left-hand side of (5) is given by (2), while the field in the right-hand side can be jotted down as

$$\Psi(x, y, z) = \frac{1}{2\pi} \iint_{-\infty}^{\infty} \exp(i\boldsymbol{\rho} \cdot \boldsymbol{\kappa}) \exp(izk_z) \widehat{\Psi}(\boldsymbol{\kappa})\, d^2\kappa. \tag{6}$$

Consequently, (5) can be equivalently recast as

$$\widehat{\Psi}_O(\boldsymbol{\kappa}) \approx \lambda_0 \widehat{\Psi}(\boldsymbol{\kappa})\,. \tag{7}$$

Notice carefully, though, that (7) does not contain the variable z, whereas the relation (5) is supposed to be valid only for $z \geq z_0$. The latter requirement cannot be ignored because (5) cannot be satisfied at $z = 0$, where instead (3) must be fulfilled. Of course, in (3) we are implicitly excluding the trivial case of a spatially-uniform semi-transparent intensity obstruction (think of, e.g., a neutral-density filter) such that $\Psi_A(x, y, 0) = (1 - \lambda_0)\Psi(x, y, 0)$.

Hence, we are apparently faced with a contradiction here. In fact, (7) constitutes more a statement about the obstruction rather than the field. This can be seen by rewriting (7) in the more enlightening form

$$\frac{1}{2\pi} \iint_{-\infty}^{\infty} \widehat{t}_O(\boldsymbol{\kappa} - \boldsymbol{\kappa}') \widehat{\Psi}(\boldsymbol{\kappa}')\, d^2\kappa' \approx \lambda_0 \widehat{\Psi}(\boldsymbol{\kappa})\,. \tag{8}$$

With the equality sign, this is a homogeneous Fredholm integral equation [29] for the function $\widehat{\Psi}(\boldsymbol{\kappa})$, which has to be an eigenfunction with eigenvalue $2\pi\lambda_0$, of the integral kernel $\widehat{t}_O(\boldsymbol{\kappa} - \boldsymbol{\kappa}')$ describing the obstruction. This means that the requirement (5) is indeed too much restrictive because it can be satisfied only by those beams whose angular spectrum (the eigenfunction) is unaffected by the interaction with the obstruction, apart from a trivial proportionality factor (the eigenvalue), as shown in (8).

3. Minimum reconstruction distance

Let us have a closer look at the minimum reconstruction distance z_0, after which a self-reconstructing beam is supposed to restore its profile. For a single plane wave $\exp(i\mathbf{k} \cdot \mathbf{r})$, with wave vector $\mathbf{k} = k(\hat{x} \sin\theta \cos\phi + \hat{y} \sin\theta \sin\phi + \hat{z} \cos\theta)$, this parameter can be straightforwardly estimated in the context of either geometrical and wave optics [23].

Actually, let us consider an arbitrary obstruction on the xy-plane with an area O. As sketched in Fig. 1, for a simply connected region O, we can always find the incircle (the largest circle inscribed in O) and the excircle (the smallest circumscribed circle), both centered on the beam axis [30]. The respective radii are b (inradius) and a (exradius). Then, elementary considerations lead us to [24,25]

$$z_0 \propto \frac{a}{\tan\theta}, \tag{9}$$

where the proportionality factor essentially depends on the shape of the obstruction.

Optics EXPRESS

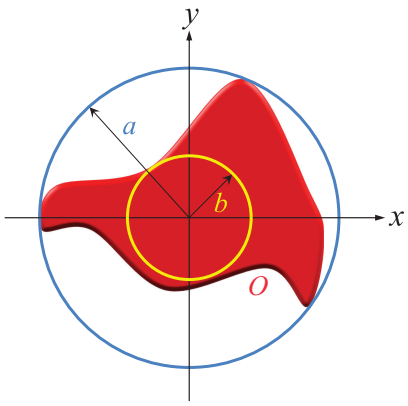

Fig. 1. Obstruction of area O represented in red. This region is circumscribed by the blue circle of radius a (exradius) and it inscribes the yellow circle of radius b (inradius). Both circles are centered along the z-axis of the beam at $x = y = 0$.

Next, notice that for our single plane wave

$$\frac{1}{\tan\theta} = \frac{k_z}{(k_x^2 + k_y^2)^{1/2}} = \frac{(k^2 - k_x^2 - k_y^2)^{1/2}}{(k_x^2 + k_y^2)^{1/2}}, \tag{10}$$

provided that $k_x^2 + k_y^2 \leq k^2$. This condition is necessary to maintain k_z real-valued and it limits the applicability of the equation above to beams whose angular spectrum does not contain evanescent waves [27]. We can thus regard z_0 as a function of $\kappa = (k_x^2 + k_y^2)^{1/2}$ in the k-space, namely

$$z_0 \sim a\, Z(\kappa) := a\, \frac{\left(k^2 - \kappa^2\right)^{1/2}}{\kappa}. \tag{11}$$

For an arbitrary beam, the transverse wave vector $\boldsymbol{\kappa}$ has a density distribution function given by $|\widehat{\Psi}(\boldsymbol{\kappa})|^2$. So, we can define the minimum reconstruction distance z_0 as the expected value of the function $a\, Z(\kappa)$; namely,

$$\frac{z_0}{a} = \langle Z(\kappa) \rangle = \frac{\displaystyle\iint \frac{\left(k^2 - \kappa^2\right)^{1/2}}{\kappa} |\widehat{\Psi}(\boldsymbol{\kappa})|^2\, d^2\kappa}{\displaystyle\iint |\widehat{\Psi}(\boldsymbol{\kappa})|^2\, d^2\kappa}, \tag{12}$$

where both integrals are limited to the disk $k_x^2 + k_y^2 \leq k^2$. We stress that this formula assigns a definite value of z_0 to any density $|\widehat{\Psi}(\boldsymbol{\kappa})|^2$: self-healing does occur for any beam.

4. Gaussian beams

As the Gaussian beam is the simplest example of a transversally unbounded diffracting beam, we shall use it as our thread to test the proposed concepts. We take it to be a Gaussian of waist w_0, so it can be written as

$$\Psi(x, y, z) = \exp(ikz)\psi(x, y, z)\,, \tag{13}$$

with $\psi(x, y, z)$ being the fundamental solution of the paraxial wave equation:

$$\psi(x, y, z) = \frac{1}{z - iz_R} \exp\left[i\frac{k}{2}\left(\frac{x^2 + y^2}{z - iz_R}\right)\right], \tag{14}$$

Optics EXPRESS

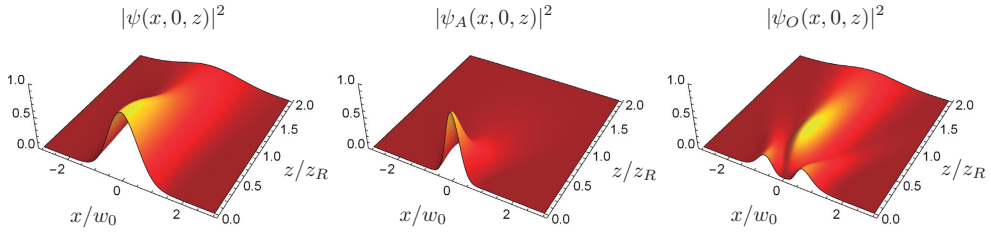

Fig. 2. Intensity distributions (evaluated at $y = 0$), of (from left to right): the incident field $\psi(x, 0, z)$, the "virtual" field transmitted by the aperture complementary to the obstruction $\psi_A(x, 0, z)$, and the field transmitted behind the obstacle $\psi_O(x, 0, z)$. The plots correspond to a Gaussian beam $w_0 = 0.26$ mm and a soft-edge Gaussian obstruction with full width $a/w_0 = 0.28$. At $z/z_R = 2$, the intensity profiles of $\psi(x, 0, z)$ and $\psi_O(x, 0, z)$ appear very similar.

and $z_R = kw_0^2/2$ denotes the Rayleigh range.

To facilitate the calculations, the obstruction is taken as a soft-edge Gaussian obstacle of full width $2a$ located along the axis of the beam at $z = 0$. This is described by the transmission function

$$t_O(x, y) = 1 - \exp\left(-\frac{|\boldsymbol{\rho} - \boldsymbol{\rho}_0|^2}{2a^2}\right), \tag{15}$$

where $\boldsymbol{\rho}_0 = \hat{x}x_0 + \hat{y}y_0$ represents the displacement of the obstacle with respect to the beam propagation axis. The Fourier transformations are straightforward and we finally get the following expression for the beam transmitted by the virtual aperture complementary to the obstruction:

$$\psi_A(x, y, z) = \frac{a_R}{z_R}\frac{1}{z - ia_R}\exp\left[i\frac{k}{2}\left(\frac{x^2 + y^2}{z - ia_R}\right)\right], \tag{16}$$

where, for the sake of clarity, we have chosen $\boldsymbol{\rho}_0 = 0$ and we have defined the modified Rayleigh range a_R as

$$a_R = \frac{z_R}{1 + \dfrac{z_R}{ka^2}} \leq z_R. \tag{17}$$

The self-healing mechanism of the Gaussian beam is vividly illustrated in Fig. 2. A close inspection of this figure reveals how the self-reconstruction works. From (17) it follows that $a_R \leq z_R$. Therefore, the "virtual" field $\psi_A(x, y, z)$ transmitted by the complementary aperture spreads in the xy-plane, while propagating along the z-axis, much more rapidly than the unperturbed field $\psi(x, y, z)$ and then for $z/z_R \gtrsim 2$ the intensity profile of the obstructed beam almost coincides with the profile of the unperturbed one.

The integrals in (12) can be evaluated analytically; the final result is

$$\frac{z_0}{a} = \frac{\pi}{2\theta_0^2}\frac{I_0(1/\theta_0^2) + I_1(1/\theta_0^2)}{\sinh(1/\theta_0^2)}, \tag{18}$$

where $\theta_0 = 2/(kw_0)$ is the angular spread of the Gaussian beam [27] and $I_\nu(z)$ is the modified

Optics EXPRESS

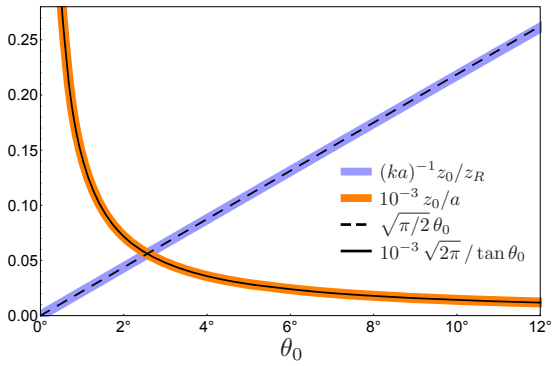

Fig. 3. Minimum reconstruction distance z_0/a as a function of θ_0 as well as the paraxial approximation. We also plot z_0/z_R, which shows a perfect linear behavior. The numerical factor 10^{-3} is introduced to fit both curves in the same scale.

Bessel function of the first kind of order ν. In the paraxial regime, $\theta_0 \ll 1$ and then

$$\frac{z_0}{a} \approx \frac{\sqrt{2\pi}}{\tan\theta_0}\,, \tag{19}$$

which is consistent with the expected geometrical optics result. A plot of z_0/a is given in Fig. 3, as well as the paraxial approximation, which works pretty well. Notice that z_0 is larger for smaller θ_0, which might appear counterintuitive. The reason is that for smaller θ_0, z_R becomes larger. To bypass this drawback, we have also plotted z_0/z_R, which can be easily obtained from (18). For $\theta_0 \ll 1$, we get

$$\frac{z_0}{z_R} \approx ka\sqrt{\frac{\pi}{2}}\,\theta_0\,. \tag{20}$$

The goodness of this linear approximation can be appreciated in Fig. 3.

5. Quantifying self-healing

We still have a conundrum pending from the end of Sec. 2: how is it possible to obtain the simultaneous validity of both (1) and (5)?

Indeed, what one really needs is simply to satisfy (5) on the xy-plane in the neighborhood of the propagation axis z. This statement may be formalized as follows. Consider again the obstruction represented in Fig. 1 that occupies the region O in the xy-plane. Let E be an arbitrary area in the xy-plane *strictly* contained within O. For example, E can be the region confined by the inner circle of radius b, although different symmetries in the problem may dictate different choices. Then, as a necessary condition for self-healing, we require that the amplitude $\Psi_O(x,y,z)$ of the obstructed beam is proportional to the amplitude $\Psi(x,y,z)$ of the unperturbed beam *only* within E; viz,

$$\Psi_O(x,y,z)\Big|_{(x,y)\in E} \approx \lambda_0 \Psi(x,y,z)\Big|_{(x,y)\in E} \qquad \forall z \geq z_0\,. \tag{21}$$

From a mathematical point of view, (21) makes much more sense than (5). In fact, the field configuration at $z = 0$ completely determines the field distribution at $z > 0$. Then, if at a certain distance z, (5) were satisfied upon *all* the xy-plane, then it should be also valid at $z = 0$. But the latter statement is clearly false because at $z = 0$ one has, by definition, $\Psi_O(x,y,0) = t_O(x,y)\Psi(x,y,0) \neq \Psi(x,y,0)$. Therefore, the *desideratum* of satisfying both equations (1) and (5) over all the xy-plane cannot be true.

Optics EXPRESS

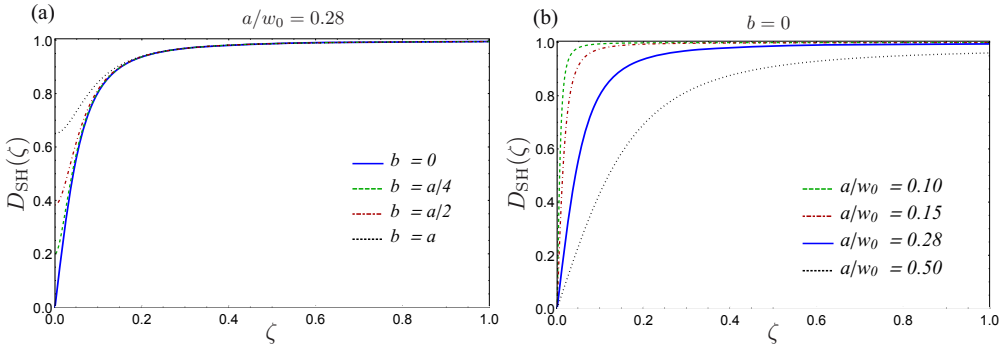

Fig. 4. (*a*) Plots of the degree of self-healing $D_{\mathrm{SH}}(z)$ for a Gaussian field of waist w_0 and different radii b of the integration region E. The continuous blue line represents the limit value for $b \to 0$. (*b*) The limit value of $D_{\mathrm{SH}}(z)$ for $b \to 0$, given in (26), for several values of the width a of the soft-edge Gaussian obstruction.

To circumvent this difficulty, we first define a scalar product in the space of functions $L_2(E)$ as

$$\langle f|g\rangle := \int_E f^*(x,y,z)g(x,y,z)\,dxdy\,. \tag{22}$$

With this definition, the scalar product $\langle f|g\rangle$ naturally becomes a function of z. Of course, the choice of the integration domain E is partially discretionary (the only constraint is to be entirely contained within O). However, it is useful to remind here that the concept of self-healing and minimum reconstruction distance suffer from the same kind of arbitrariness. In other words, since both (1) and (5) are impossible to satisfy over the whole xy-plane, one is forced to chose *where* these equations should be satisfied. This is because in the total average the field does not heal. This follows from Babinet's principle, the perturbation is somewhere. The beam shape becomes more similar to what it would have been without obstruction because the effect of the obstruction is spread out. To some extent this is the core of any self-healing claim and defining the healing locally at the position of the obstruction bypasses the problem.

The scalar product (22) allows us to introduce in a natural way the corresponding distance $\mathbb{D}(f,g)$ between two functions in $L_2(E)$ as $\mathbb{D}(f,g) = \|f-g\|$, where $\|f\| = \langle f|f\rangle^{1/2}$. This distance somehow quantifies the similarity between the obstructed and the unobstructed field. In quantum information [31] there are many measures of the "closeness" of two (normalized) states we want to compare. Probably, one of the most popular one is the fidelity, a modified version thereof has been proposed in this context by Chu and Wen [32]. However, the standard fidelity fails to furnish a quantitative description of self-healing because it is defined in terms of a scalar product resulting from integration upon the whole xy-plane and this erases any z-dependence.

In this paper, we shall use instead the notion of relative distance, which we define as

$$\mathbb{D}_r(\Psi,\Psi_O) = \frac{\|\Psi-\Psi_O\|}{\|\Psi+\Psi_O\|} = \frac{\langle\Psi_A|\Psi_A\rangle^{1/2}}{[\langle\Psi_A|\Psi_A\rangle + 4\langle\Psi|\Psi\rangle - 4\,\mathrm{Re}\langle\Psi|\Psi_A\rangle]^{1/2}}\,, \tag{23}$$

where the scalar products are defined as in (22). A direct application of the parallelogram law [33] $[\|f-g\|^2 + \|f+g\|^2 = 2(\|f\|^2 + \|g\|^2)]$ immediately confirms that $0 \le \mathbb{D}_r^2 \le 1$. If $\Psi_O \simeq \lambda_0\Psi$, with $0 \le \lambda_0 \le 1$, then

$$\mathbb{D}_r(\Psi,\Psi_O) \simeq \frac{1-\lambda_0}{1+\lambda_0}\,. \tag{24}$$

Optics EXPRESS

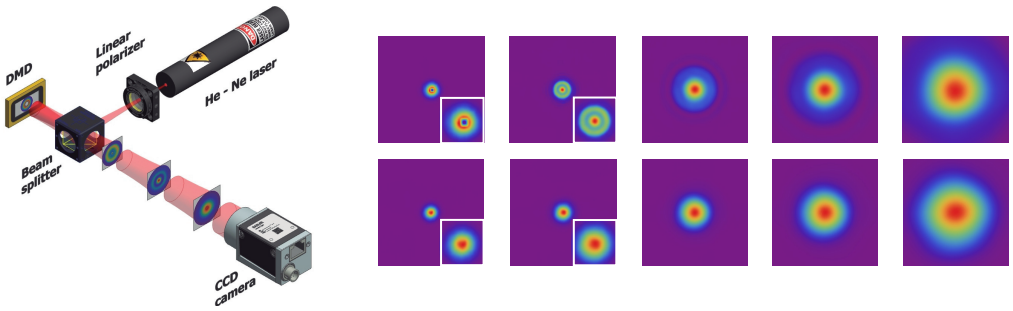

Fig. 5. (Left panel) Experimental setup used to check the self-healing of a fundamental Gaussian beam created by the He-Ne laser. (Right panel) Intensity scans recorded by the CCD camera at increasing distances $\zeta = 0, 0.5, 1.5, 4$ and 6.5 (from left to the right). The beam has a waist $w_0 = 0.24$ mm, divergence $\theta_0 = 0.84$ mrad, and Rayleigh range $z_R = 285$ mm. The upper row corresponds to the obstructed beam (with $\alpha = 0.206$), whereas the lower row is for the unobstructed beam. In the first two scans, the images are very small, so we have included insets (in white frames) with enlarged pictures to better appreciate the patterns.

On that account, we find it convenient to introduce a z-dependent degree of self-healing:

$$D_{\rm SH}(z) = \sqrt{1 - \mathbb{D}_r^2(\Psi, \Psi_O)}\,, \tag{25}$$

and one can check that $0 \leq D_{\rm SH}(z) \leq 1$. We underline that this concept of distance measure has been successfully used in assessing a number of key concepts in quantum optics. In general, a distance measure quantifies the extent to which two physical states behave in the same way. While these distance measures are usually given by certain mathematical expressions, they often possess a simple operational meaning, i.e., they are related to the problem of distinguishing the two states. The notions of nonclassicality [34], entanglement [35], polarization [36], and localization [37], to cite only a few relevant examples, have been systematically formulated within this framework.

For a Gaussian beam, with cylindrical symmetry about the propagation axis z, we can choose for E a disk of radius $b \leq a$. The function $D_{\rm SH}(z)$ can be calculated analytically, although the final expression is complicated and of little use for our purposes. When b goes to zero, we obtain the asymptotic form

$$D_{\rm SH}(\zeta) = \zeta \sqrt{\frac{1-\beta^2}{\beta^2 + \zeta^2}}\,, \tag{26}$$

where we have used the dimensionless variables

$$\zeta = \frac{z}{z_R}\,, \qquad \alpha = \frac{a}{w_0}\,, \tag{27}$$

and $\beta = \alpha^2/(1+\alpha^2)$. It is interesting to notice that this function does not depend explicitly on the angular spread θ_0 of the Gaussian beam.

In Fig. 4(a) we plot $D_{\rm SH}(\zeta)$, for a fixed value of α, and different radii b of the integration region E. When b increases, the dependence of $D_{\rm SH}(\zeta)$ with ζ becomes weaker. In Fig. 4(b) we plot the limit form of $D_{\rm SH}(\zeta)$, given in (26), for different values of α. When α goes to zero, $D_{\rm SH}(\zeta)$ tends to the unity, as expected from physical considerations.

Optics EXPRESS

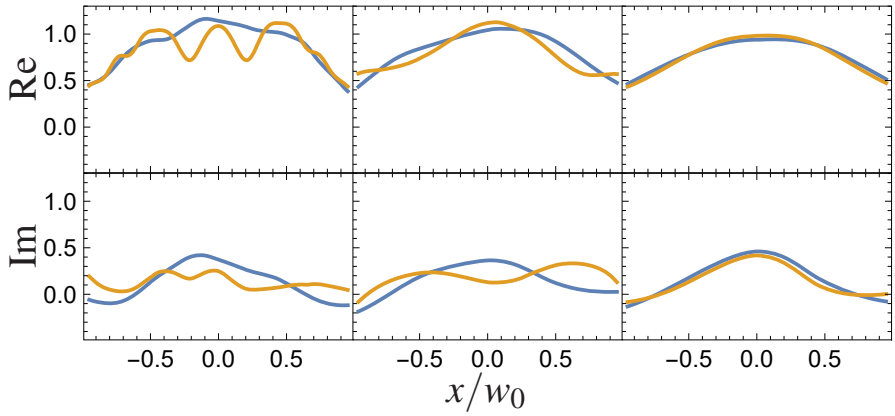

Fig. 6. Real and imaginary parts of the energy-normalized field amplitudes at the positions $\zeta = 0.05, 0.28$, and 0.56 (from left to right). The obstructed field is represented in orange, while the unobstructed is in blue. The obstruction is characterized by $\alpha = 0.14$.

6. Experiment

We have checked these predictions in the laboratory. To build up a Gaussian beam with a central obstruction, a He-Ne laser beam (633 nm, Thorlabs) was used. The beam impinges on a digital micromirror device (DMD) chip (Texas Instrument), with square micromirrors of 7.6 μm size each. The obstruction was generated as an off-state region on this chip. A sketch of the setup is presented in Fig. 5. All the previous treatment can be directly applied to this reflection mode.

First, we observed the intensity self-reconstruction of a Gaussian beam of waist $w_0 = 0.24$ mm, divergence $\theta_0 = 0.84$ mrad, and Rayleigh range $z_R = 285$ mm. The beam was propagated a distance $z = z_R$, where the half-width is $w_{z_R} = 0.34$ mm. Then, the DMD is inserted at this position where we generate a centered obstruction of either circular or square shape of half-widths a of 0.09 mm. For both shapes of the obstruction the results are much the same. Then, the intensity scans are captured in several positions by a CCD camera (Basler) with 5.5 μm pixel size. Some of these intensity profiles (for the case of a square obstruction) are depicted in Fig. 5 for different propagating distances from the obstruction.

To experimentally assess the degree of self-healing $D_{\mathrm{SH}}(\zeta)$ we must be able to measure the

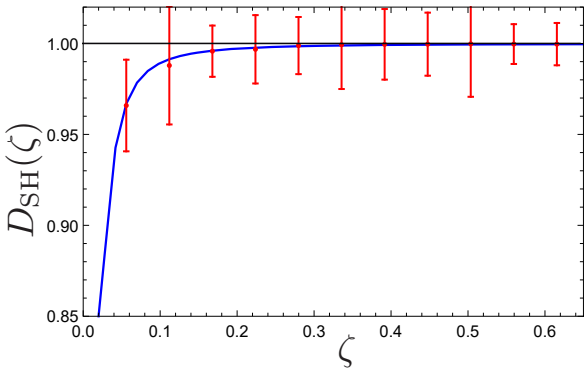

Fig. 7. Experimentally determined degree of self-healing $D_{\mathrm{SH}}(\zeta)$ obtained from the field measurements shown in Fig. 6. The integration region E is a dist of radius $b = a = 0.07$ mm. The error bars represent standard deviations.

Optics EXPRESS

whole complex amplitude for both the obstructed and the unobstructed fields, as it is apparent from (23). To facilitate the measurement, a calibrated beam expander was used, so the new waist was $w_0 = 0.6$ mm and the Rayleigh range $z_R = 1787$ mm. Then we place alternatively the CCD camera and a Shack-Hartmann wavefront sensor (consisting of a microlens array with 150 μm lens pitch) to the same distance from the DMD and measure the intensity and the wavefront profile of the beam. To increase the wavefront measurement resolution, we used another beam expander coupled directly to the wavefront sensor.

The field complex amplitude was then reconstructed from these measurements that were interpolated to the same resolution. The DMD was positioned now at a distance of 560 mm from the waist with half-width $w_z = 0.635$ mm. For this measurement, we use the obscuration with $\alpha = 0.14$, and detection planes at ζ in the range 0.05–0.61. Some of the resulting amplitudes are shown in Fig. 6, where the real and imaginary parts are plotted.

Once the complex amplitudes are experimentally determined, we can compute the degree $D_{\mathrm{SH}}(\zeta)$. For this purpose, we take the integration region E as a disk of radius $b = a = 0.09$ mm, which is the size of the obstruction. Our experimental results are presented in Fig. 7. For each distance, the measurements have been repeated over 100 times, so we can assign error bars. The agreement with the theory is pretty good.

7. Concluding remarks

In summary, we have presented a general theory of the so-called self-healing process occurring in diverse partially obstructed optical beams, whose validity is not limited to diffractionless beams as, e.g., Bessel beams. From a careful analysis of the physical mechanisms involved, we could ascertain the minimum propagation distance from the obstacle after which an optical beam recovers its original intensity profile. Our results, obtained within the framework of wave optics, confirm and extend the traditional ones based on purely geometrical arguments.

We have quantified self-healing as the closeness between the obstructed and unobstructed beams, proposing a suitable measure that has been experimentally tested for Gaussian beams, getting a beautiful agreement with the proposed theory.

Funding

Technology Agency of the Czech Republic (TE01020229); Grant Agency of the Czech Republic (15-03194S); IGA Palacký University (IGA PrF 2016-005); MINECO (FIS2015-67963-P).

Acknowledgments

We thank Miguel Alonso for comments that greatly improved the manuscript. G. S. A. thanks the BioPhotonics Initiative of the Texas A&M University.

Paper 12

F. Bouchard, P. de la Hoz, G. Björk, R. W. Boyd, M. Grassl, Z. Hradil, E. Karimi, A. Klimov, G. Leuchs, J. Rehacek, L. L. Sánchez-Soto

"Quantum metrology at the limit with extremal Majorana constellations"

Optica **4**, 1429 (2017)

Letter Vol. 4, No. 11 / November 2017 / Optica 1429

optica

Quantum metrology at the limit with extremal Majorana constellations

F. Bouchard,[1] P. de la Hoz,[2] G. Björk,[3] R. W. Boyd,[1,4] M. Grassl,[5] Z. Hradil,[6] E. Karimi,[1,7,*] A. B. Klimov,[8] G. Leuchs,[5,1] J. Řeháček,[6] and L. L. Sánchez-Soto[2,5]

[1]Department of Physics, University of Ottawa, 150 Louis Pasteur, Ottawa, Ontario K1N 6N5, Canada
[2]Department of Optics, Faculty of Physics, Universidad Complutense, 28040 Madrid, Spain
[3]Department of Applied Physics, Royal Institute of Technology (KTH), AlbaNova, SE-106 91 Stockholm, Sweden
[4]Institute of Optics, University of Rochester, Rochester, New York 14627, USA
[5]Max Planck Institute for the Science of Light, Staudtstraß e 2, 91058 Erlangen, Germany
[6]Department of Optics, Palacký University, 17. listopadu 12, 771 46 Olomouc, Czech Republic
[7]Department of Physics, Institute for Advanced Studies in Basic Sciences, 45137-66731 Zanjan, Iran
[8]Department of Physics, Universidad de Guadalajara, 44420 Guadalajara, Jalisco, Mexico
*Corresponding author: ekarimi@uottawa.ca

Received 30 June 2017; revised 2 October 2017; accepted 21 October 2017 (Doc. ID 301465); published 17 November 2017

Quantum metrology allows for a tremendous boost in the accuracy of measurement of diverse physical parameters. The estimation of a rotation constitutes a remarkable example of this quantum-enhanced precision. The recently introduced Kings of Quantumness are especially germane for this task when the rotation axis is unknown, as they have a sensitivity independent of that axis and they achieve a Heisenberg-limit scaling. Here, we report the experimental realization of these states by generating up to 21-dimensional orbital angular momentum states of single photons, and confirm their high metrological abilities.

OCIS codes: (270.0270) Quantum optics; (270.5585) Quantum information and processing; (120.3940) Metrology.

https://doi.org/10.1364/OPTICA.4.001429

The conventional description of the quantum world involves a key mathematical object—the quantum state—that conveys complete information about the system under study; once it is known, the probabilities of the outcomes of any measurement can be predicted. This statistical description entails counterintuitive effects that have prompted several notions of quantumness, yet no single one captures the whole breadth of the physics.

There are, however, instances of quantum states that behave in an almost classical way. The paradigm of such a behavior is that of coherent states of light [1]; they are as much localized as possible in phase space, a property that is preserved under free evolution.

The concept of coherent states has been extended to other physical systems [2]. The case of spin is of paramount importance. The corresponding spin coherent states have minimal uncertainty and they are conserved under rotations. So, in the usual way of speaking, they mimic a classical angular momentum as much as possible. One could rightly wonder what kind of state might serve as the opposite of a coherent state. The answer will depend on the ways to formalize the idea of being "the opposite" [3]. Here, we take advantage of the Majorana representation, which maps a pure spin S into $2S$ points on the Bloch sphere [4].

It turns out that the Majorana representation of a coherent state consists of a single point (with multiplicity $2S$). At the opposite extreme, we can imagine states whose Majorana representations are spread uniformly over the sphere. The resulting states are precisely the Kings of Quantumness [5,6]. With such symmetric spreadings, the constellations essentially map onto themselves for relatively small rotations around arbitrary axes. This means that they resolve rotations around any axis approximately equally well. We emphasize that the problem of estimating a rotation is of utmost interest in magnetometry [7–9], polarimetry [10,11], and metrology in general [12]. In this work, we experimentally demonstrate the generation of these states and certify their potential for quantum metrology [13].

Let us first set the stage for our experiment. We consider a system that can be described in terms of two independent bosonic modes with creation operators $\hat{a}_\alpha^\dagger$, with $\alpha \in \{+,-\}$. This encompasses many different instances, such as strongly correlated systems, light polarization, Bose–Einstein condensates, and Gaussian–Schell beams, to mention only a few [14]. The Stokes operators for these two-mode systems can be compactly expressed as [15] $\hat{\mathbf{S}} = \frac{1}{2}\hat{a}_\alpha^\dagger \boldsymbol{\sigma}_{\alpha\beta}\hat{a}_\beta$, where $\boldsymbol{\sigma}$ denotes the Pauli matrices, and summation over repeated indices is assumed. One can verify that $\hat{\mathbf{S}}^2 = \hat{S}_0(\hat{S}_0+1)$ with $\hat{S}_0 = \hat{N}/2$, and $\hat{N} = \hat{a}_\alpha^\dagger \delta_{\alpha\beta}\hat{a}_\beta = \hat{N}_+ + \hat{N}_-$ being the total number of excitations.

From now on, we restrict our attention to the case where N is fixed. This corresponds to working in a $(2S+1)$-dimensional Hilbert space $\mathcal{H}_S$ of spin S (with $N = 2S$). This space $\mathcal{H}_S$ is spanned by the Dicke basis $|S, m\rangle$, wherein the action of $\hat{\mathbf{S}}$ operators is the standard for an angular momentum. Sometimes, it is preferable to use the two-mode Fock basis $|N_+, N_-\rangle$, related to the Dicke basis by $N_+ = S + m$ and $N_- = S - m$.

Spin coherent states are constructed much in the same way as in the canonical case [2]: they are displaced versions of the north pole of the Bloch unit sphere $\mathcal{S}_2$. If $\mathbf{n}$ is a unit vector in the direction of the spherical angles (θ, ϕ), they can be defined as $|\mathbf{n}\rangle = e^{i\phi\hat{S}_z}e^{i\theta\hat{S}_y}|S, S\rangle$. They are not orthogonal, but one can still decompose an arbitrary state $|\Psi\rangle$ using this overcomplete set. The associated coherent-state wave function is $\Psi(\mathbf{n}) = \langle\mathbf{n}|\Psi\rangle$, and the corresponding probability distribution, $Q(\mathbf{n}) = |\Psi(\mathbf{n})|^2$, is nothing but the Husimi function.

The wave function $\Psi(\mathbf{n})$ can be expanded in terms of the Dicke basis $|S, m\rangle$. If the corresponding coefficients are $\Psi_m = \langle S, m|\Psi\rangle$, we obtain $\Psi(\mathbf{n}) = (1+|z|^2)^{-S}\sum_{m=-S}^{S} c_m \Psi_m z^{S+m}$, where $c_m = \sqrt{(2S)!/[(S-m)!(S+m)!]}$, and $z = \tan(\theta/2)e^{-i\phi}$ is the complex number derived by the stereographic projection of (θ, ϕ). Apart from the unessential positive prefactor, this is a polynomial of order $2S$; thus, $|\Psi\rangle$ is determined by the set $\{z_i\}$ of the $2S$ complex zeros of $\Psi(\mathbf{n})$. These zeros, which are also the zeros of $Q(\mathbf{n})$, specify the so-called constellation by an inverse stereographic map of $\{z_i\} \mapsto (\theta_i, \phi_i)$.

Since the spherical harmonics $Y_{\mathrm{Kq}}(\mathbf{n})$ are a complete set of orthonormal functions on $\mathcal{S}_2$, they may be used to expand the Husimi function $Q(\mathbf{n})$. The resulting coefficients, ϱ_{Kq}, are nothing but the standard state multipoles [16], and there are $2S + 1$ of them (see Supplement 1). The monopole is trivial, as it is just a constant term. The dipole indicates the position of the state in the Bloch sphere. When it vanishes, the state has vanishing (first-order) polarization and points nowhere in the mean. If the quadrupole also vanishes, the variance of the state is uniform; i.e., no directional signature can be observed in its second-order fluctuations, and we say that it is second-order unpolarized. Similar interpretation holds for higher-order multipoles. One can also look at these multipoles as the Kth directional moments of the state constellation and, therefore, these terms resolve progressively finer angular features.

The quantity $\sum_q |\varrho_{\mathrm{Kq}}|^2$ gauges the overlap of the state with the Kth multipole pattern. It seems thus suitable to look at the cumulative distribution [17] $\mathcal{A}_M = \sum_{K=1}^{M}\sum_{q=-K}^{K}|\varrho_{\mathrm{Kq}}|^2$, which concisely condenses the state angular capacity up to order M $(1 \le M \le 2S)$. Observe that the monopole is omitted, as it is just a constant term.

The spin coherent states $|\mathbf{n}\rangle$ have remarkably simple constellations, just the point $-\mathbf{n}$, and they maximize $\mathcal{A}_M$ for all orders M, confirming yet from another perspective the outstanding properties of these states [5].

In contradistinction, the Kings are those pure states that make $\mathcal{A}_M \equiv 0$ for the highest possible value of M. This means that they convey the relevant information in higher-order fluctuations. The search for these states has been systematically undertaken recently in Ref. [5], where the interested reader can check the details (see also Supplement 1, where one can find the nonzero components Ψ_m of the Kings). The resulting Majorana constellations for some values of S are depicted in Fig. 1. For $S = 3$, the constellation is a regular octahedron and the state is third-order unpolarized $(M = 3)$. For $S = 5$, it consists of two pentagons. For $S = 6$ we have the icosahedron, and the corresponding state is fifth-order unpolarized. For $S = 10$ we have a slightly stretched dodecahedron (i.e., the four pentagonal rings that define its vertices are displaced against the pole), and it is fifth-order unpolarized. As we can appreciate, the Kings have the points very symmetrically placed on the unit sphere, so their constellations possess many axes along which they return to themselves after a rotation. Consequently, they can resolve relatively small angles around a large number of axes.

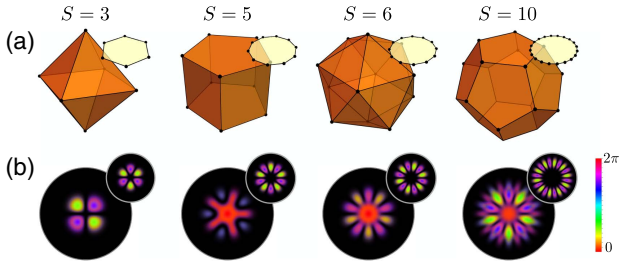

Fig. 1. (a) The Majorana constellations in the Bloch sphere for the Kings (orange) and the NOON states (yellow) corresponding to spin $S = 3$, 5, 6, and 10. (b) The Laguerre–Gauss representation of the same Kings and NOON states, shown in (a), where the azimuthal index ℓ corresponds to m in the Dicke basis. We consider the fundamental radial mode, i.e., $p = 0$, where p is the radial index of the Laguerre–Gauss modes.

Other states with a high degree of angular resolution are the NOON states, given by $|\mathrm{NOON}\rangle = \frac{1}{\sqrt{2}}(|N, 0\rangle - |0, N\rangle)$ in the two-mode Fock basis and $\frac{1}{\sqrt{2}}(|S, S\rangle - |S, -S\rangle)$ in the Dicke basis. As shown in Fig. 1, their Majorana constellation consists of $2S$ equidistantly placed points around the equator of $\mathcal{S}_2$. A rotation around the z axis of angle $\pi/(2S)$ makes $|\mathrm{NOON}\rangle$ orthogonal to itself, whereas for π/S it returns to itself. This nicely supports the ability of NOON states to detect small rotations.

To compare the performance of these two classes of states, let us assume we have to estimate a rotation $R(\omega, \mathbf{u})$ of angle ω around an axis $\mathbf{u}$ of spherical angles (Θ, Φ). We consider only small rotations and take the measurement to be a projection of the rotated state onto the original one; i.e., it can be represented by $\hat{P} = |\Psi\rangle\langle\Psi|$. As discussed in Supplement 1, the respective sensitivities (defined as the ratio $\Delta\omega = \Delta\hat{P}/|\partial\langle\hat{P}\rangle/\partial\omega|$, the variance being $\Delta\hat{P} = [\langle\hat{P}^2\rangle - \langle\hat{P}\rangle^2]^{1/2}$) are

$$\Delta\omega_{\mathrm{Kings}} = \frac{\sqrt{3}}{2}\frac{1}{\sqrt{S(S+1)}},$$
$$\Delta\omega_{\mathrm{NOON}} = \frac{1}{\sqrt{2}}\frac{1}{\sqrt{2S^2\cos^2\Theta + S\sin^2\Theta}}. \quad (1)$$

The sensitivity of the Kings is completely independent of the rotation axis and with a Heisenberg-limit scaling $1/S$ for large S. For the NOON states, the sensitivity scales as $1/S$ when $\Theta = 0$, but can be as bad as $1/\sqrt{S}$ when $\Theta = \pi/2$. In short, it is essential to know the rotation axis to ensure that the NOON state is aligned to achieve its best sensitivity.

We stress that the measurement scheme for $\Delta\omega$ involves only second-order moments of $\hat{\mathbf{S}}$. Given their properties, one could expect that detecting higher-order moments will bring out even more advantages of the Kings.

To check these issues, we have generated these extremal states for the cases of $S = 3$, 5, 6, and 10 using orbital angular momentum (OAM) states of single photons [18], which has already proven fruitful in quantum metrology [19]. Working at the single-photon regime is not essential, but it highlights the potential implications for quantum information processing [20]. Therefore, the index m in the Dicke basis is identified with the OAM eigenvalue ℓ of a single photon along its propagation

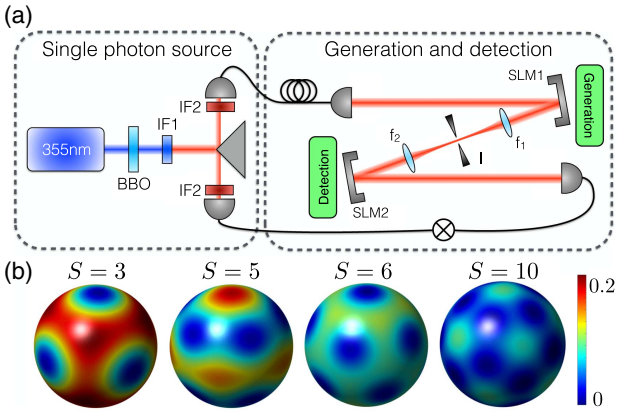

Fig. 2. (a) Sketch of the experimental setup and (b) density plots of the experimentally reconstructed Husimi Q functions for the same King states as in Fig. 1. The fidelities of these reconstructed states are (from left to right) 0.94, 0.87, 0.91, and 0.93. The differences with the theoretical Q functions cannot be visually noticed.

direction. In general, there exist many families of optical modes carrying OAM, but we choose the Laguerre–Gauss basis $\mathrm{LG}_{\ell,p}$, where p is the radial index. Since the radial profile is irrelevant to the experimental realization of the Kings states, for the sake of simplicity, we always set the radial index to its fundamental value, i.e., $p = 0$. The resulting transverse profiles of both the Kings and the NOON states are as in Fig. 1(b).

We experimentally create the Kings by means of spontaneous parametric downconversion. A sketch of the experimental setup is shown in Fig. 2(a). A quasi-continuous wave ultraviolet (UV) laser operating with a repetition rate of 100 MHz and an average power of 150 mW at a wavelength of 355 nm is used to pump a type-I β-barium borate crystal. The single photons, signal and idler, are subsequently coupled to single-mode fibers to filter their spatial mode. One of the photons, the idler, is used as a trigger. The other photon, the signal, is made incident on a first spatial light modulator (SLM1), where the desired quantum states were imprinted on the signal photon holographically [21]. The generated photonic Kings are subsequently imaged onto a second spatial light modulator (SLM2) by a $4f$ system. The second SLM possessing the desired hologram followed by a single-mode optical fiber perform the projective measurement on the state of the signal photon. Both photons are sent to avalanche photodiode detectors (APD), and coincidence counts are recorded by a coincidence box with a coincidence time window of 3 ns [22].

To verify the accurate experimental generation of these states, we perform quantum state tomography to reconstruct the Husimi Q function, as shown in Fig. 2(b). The average fidelity of the resulting states is around 90%; i.e., 94%, 87%, 91%, and 93%, respectively (see Supplement 1).

We now study the behavior of such states under rotations in the sphere $\mathcal{S}_2$. This is experimentally realized by projective measurements of the Kings onto themselves after a rotation ω around several axes (see Fig. 3). To demonstrate the high sensitivity to rotation of these states along arbitrary axes, we perform such rotations around each axis passing through the Majorana points and facets of the Kings constellations. For the cases of $S = 3$, 6, and 10, we find four-, five-, and three-fold symmetry axes passing through their Majorana points and three-, three-, and five-fold symmetry axes passing through the normals to the facets of their constellations, respectively. Note that, since we are dealing with OAM, these rotations correspond to rather abstract mode transformations, although the polar axis still represents a physical real-space rotation around the optical axis.

Finally, in Fig. 4 we experimentally check the sensitivity of the Kings and NOON states. As we can see, the experimental

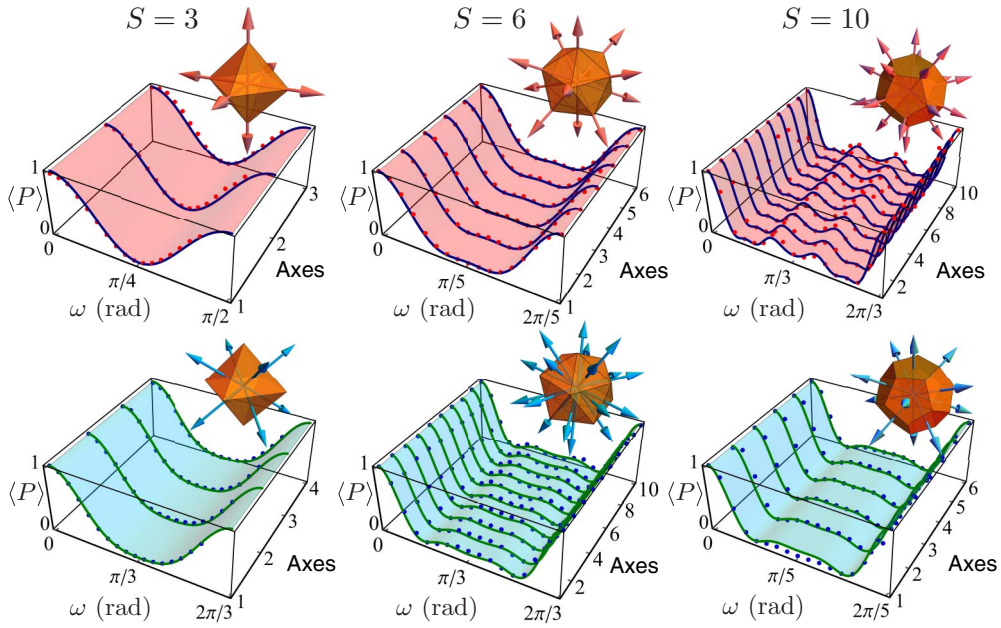

Fig. 3. Experimental results of the projection of the $S = 3$, 6, and 10 (first, second, and third column, respectively) Kings states, $|\Psi^{(S)}\rangle$, onto themselves after a rotation of ω around the axis $\mathbf{u}$, $\hat{R}(\omega, \mathbf{u})$, i.e., $\langle\hat{P}\rangle = |\langle\Psi^{(S)}|\hat{R}(\omega, \mathbf{u})|\Psi^{(S)}\rangle|^2$. The axes are presented graphically along with the associated constellations. The first row corresponds to rotations along the axes passing through the Majorana points (pink arrows), and the second row corresponds to rotations along the axes normal to the facets of the constellations (blue arrows). The experimental results (red and blue dots) are shown along with the theoretical results (blue and green curves) for all rotation axes.

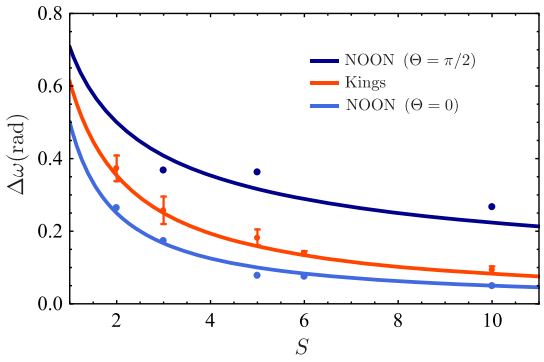

Fig. 4. Rotational sensitivity $\Delta\omega$ for the Kings (red) and NOON states (blue). The solid curves correspond to the theory predicted in Eq. (1), and the points correspond to experimental results. In the case of the Kings, we show the mean rotational sensitivity over all axes presented in Fig. 3, where the error bars correspond to variation in sensitivity from axes to axes. For the NOON states, we show the rotational sensitivity for rotation axes with $\Theta = 0$ and $\Theta = \pi/2$.

sensitivity of the Kings is completely independent of the orientation of the rotation axes (within the error bars). In the limit of small rotation angles, the NOON states overcome the Kings all the way up to $\cos\Theta = 1/\sqrt{3}$. Nonetheless, since the Kings achieve the ideal sensitivity irrespectively of the axis, they are the most appropriate to detect rotation around arbitrary axes.

The problem of the Kings is closely related to other notions as states of maximal Wehrl–Lieb entropy [23], Platonic states [24], the Queens of Quantumness [25], or the Thomson problem [26]. However, there are still many things to elucidate concerning these links. They are, however, a nice illustration of the connections between different branches of science, and on how some seemingly simple problems—distributing points in the most symmetric manner on a sphere—can illuminate such complicated optimization problems that we have just described.

Thus far, efforts were concentrated in estimating the rotation angle, which in terms of magnetometry means that we only want to know the magnetic field magnitude. The Kings will allow for a simultaneous precise determination of the rotation axis (i.e., the magnetic field direction). Our experimental results corroborate that this extra advantage can pave the way to much more refined measurement schemes.

Funding. Natural Sciences and Engineering Research Council of Canada (NSERC); Canada Foundation for Innovation (CFI); Technologická Agentura České Republiky (TAČR) (TE01020229); Grantová Agentura České Republiky (GACR) (15-03194S); Ministerio de Economía y Competitividad (MINECO) (FIS2015-67963-P).

Acknowledgment. F. B. acknowledges the support of the Vanier Canada Graduate Scholarships Program of the Natural Sciences and Engineering Research Council of Canada (NSERC). E. K. acknowledges the support of the Canada Research Chairs (CRC), and Canada Foundation for Innovation (CFI) Programs. F. B., R. W. B., and E. K. acknowledge the support of the Max Planck–University of Ottawa Centre for Extreme and Quantum Photonics. G. B. acknowledges the support of the Wenner–Gren Foundation and the Swedish Research Council (VR) through the Linnaeus Center of Excellence ADOPT.

See Supplement 1 for supporting content.

REFERENCES

1. R. J. Glauber, Phys. Rev. **131**, 2766 (1963).
2. A. Perelomov, *Generalized Coherent States and Their Applications* (Springer, 1986).
3. J. Zimba, Electron. J. Theor. Phys. **3**, 143 (2006).
4. E. Majorana, Nuovo Cimento **9**, 43 (1932).
5. G. Björk, A. B. Klimov, P. de la Hoz, M. Grassl, G. Leuchs, and L. L. Sánchez-Soto, Phys. Rev. A **92**, 031801 (2015).
6. G. Björk, M. Grassl, P. de la Hoz, G. Leuchs, and L. L. Sánchez-Soto, Phys. Scripta **90**, 108008 (2015).
7. W. Wasilewski, K. Jensen, H. Krauter, J. J. Renema, M. V. Balabas, and E. S. Polzik, Phys. Rev. Lett. **104**, 133601 (2010).
8. R. J. Sewell, M. Koschorreck, M. Napolitano, B. Dubost, N. Behbood, and M. W. Mitchell, Phys. Rev. Lett. **109**, 253605 (2012).
9. W. Muessel, H. Strobel, D. Linnemann, D. B. Hume, and M. K. Oberthaler, Phys. Rev. Lett. **113**, 103004 (2014).
10. V. Meyer, M. A. Rowe, D. Kielpinski, C. A. Sackett, W. M. Itano, C. Monroe, and D. J. Wineland, Phys. Rev. Lett. **86**, 5870 (2001).
11. V. D'Ambrosio, N. Spagnolo, L. Del Re, S. Slussarenko, Y. Li, L. C. Kwek, L. Marrucci, S. P. Walborn, L. Aolita, and F. Sciarrino, Nat. Commun. **4**, 2432 (2013).
12. L. A. Rozema, D. H. Mahler, R. Blume-Kohout, and A. M. Steinberg, Phys. Rev. X **4**, 041025 (2014).
13. V. Giovannetti, S. Lloyd, and L. Maccone, Nat. Photonics **5**, 222 (2011).
14. S. Chaturvedi, G. Marmo, and N. Mukunda, Rev. Math. Phys. **18**, 887 (2006).
15. A. Luis and L. L. Sánchez-Soto, Prog. Opt. **41**, 421 (2000).
16. K. Blum, *Density Matrix Theory and Applications* (Plenum, 1981).
17. P. de la Hoz, A. B. Klimov, G. Björk, Y. H. Kim, C. Müller, C. Marquardt, G. Leuchs, and L. L. Sánchez-Soto, Phys. Rev. A **88**, 063803 (2013).
18. L. Allen, S. M. Barnett, and M. J. Padgett, *Optical Angular Momentum* (Institute of Physics, 2003).
19. D. S. Simon, G. Jaeger, and A. V. Sergienko, *Quantum Metrology, Imaging, and Communication* (Springer, 2017).
20. J. Leach, M. J. Padgett, S. M. Barnett, S. Franke-Arnold, and J. Courtial, Phys. Rev. Lett. **88**, 257901 (2002).
21. E. Bolduc, N. Bent, E. Santamato, E. Karimi, and R. W. Boyd, Opt. Lett. **38**, 3546 (2013).
22. H. Qassim, F. M. Miatto, J. P. Torres, M. J. Padgett, E. Karimi, and R. W. Boyd, J. Opt. Soc. Am. B **31**, A20 (2014).
23. A. Baecklund and I. Bengtsson, Phys. Scripta **T163**, 014012 (2014).
24. P. Kolenderski and R. Demkowicz-Dobrzanski, Phys. Rev. A **78**, 052333 (2008).
25. O. Giraud, P. Braun, and D. Braun, New J. Phys. **12**, 063005 (2010).
26. J. J. Thomson, Philos. Mag. **7**(39), 237 (1904).